



*Luisa Alterio*

SEISMIC VULNERABILITY REDUCTION OF  
MONUMENTAL BUILDING BY SOILS TREATMENTS

*Tesi di Dottorato*  
*XXIV ciclo*

*Il Coordinatore*  
*Prof. Ing. Federico M. MAZZOLANI*

*Il Tutore*  
*Prof. Ing. Federico M. MAZZOLANI*

*I Co-tutori*  
*Prof. Ing. Gianpiero RUSSO*  
*Prof. Ing. Francesco SILVESTRI*



Alla mia famiglia,  
perché nessun albero  
senza salde radici  
in un terreno fertile  
e senza la giusta cura  
potrà mai dare frutto.

A Luigi,  
perché in te  
trovo il senso ultimo  
di ogni mio lavoro.





## ANKNOWLEDGEMENTS

Dutiful thanks goes first to my tutor Prof. Mazzolani for giving me the opportunity to work on a very interesting topic of great relevance. Thanks a lot to Prof. Russo for helping me during job setup, although leaving me full autonomy. Reserve an immense gratitude to Prof. Silvestri for always addressed me and encouraged in every part of the thesis.

I also thank Antonio Formisano for the essential support offered me during the survey and investigation on the structure of study. In this regard I thank the Ente per le Ville Vesuviane for having made available, without reservation, all the archive material and the availability offerer to open the villa and the park during the investigation phase.

I thank Prof. D'Onofrio for his suggestions and bibliographical material given me. A special thank goes to the laboratory of dynamic of geotechnical and hydraulic engineering department of the University for making available the staff and equipment needed to MASW tests carried out on site. Special thanks in this regard, Lorenza Evangelista for carrying out the tests and results processing and preparation.

A huge thank you goes to the "dynamic" Giuseppe Tropeano and Luigi Landolfi for the continued suggestions related to various aspects of the work and the implementation of lines of code that allowed me to accelerate and automate the analysis work. I thank more, Luigi, who supported me and endured every step of the work until the last moment.

I thank again, Carmine Castaldo, Vincenzo Macillo and Tony de Lucia for made me, constantly, suggestions and support.

Special thanks again to Roberta Fonti for help in understanding, modeling and calculation of the masonry walls and vaults.

I want to thank also Daniele Lombardi for sharing all that the bibliographic material in his possession.

I thank finally, Rianna Guido, Marianna Pirone, Raffaele Papa, Anna Scotto di Santolo and all the "inhabitants" of the second floor of the DIGA for the precious little aid of any kind that, each of them, has been able to give me from time to time.







## SUMMARY

<b>INTRODUCTION .....</b>	<b>I</b>
<b>CHAPTER 1 .....</b>	<b>1</b>
1.1 INTRODUCTION .....	1
1.2 HISTORICAL EXCURSUS .....	2
1.3 FUNDAMENTAL CONCEPTS .....	5
1.4 MONUMENTAL BUILDINGS IN SEISMIC AREAS: ADAPTATION OR IMPROVEMENT .....	8
1.5 PASSIVE SEISMIC PROTECTION OF CULTURAL HERITAGE .....	11
1.5.1 Energy dissipation .....	12
1.5.2 Base isolation .....	15
1.5.3 Passive protection application to cultural heritage in the World 20	
1.5.4 Passive protection application to cultural heritage in Italy ...	25
BIBLIOGRAPHY .....	31
<b>CHAPTER 2 .....</b>	<b>35</b>
2.1 INTRODUCTION .....	35
2.2 STRATIGRAPHIC EFFETC (1D) .....	39
2.3 EDGE EFFETCS (OR DOWNSTREAM) .....	48
2.4 TOPOGRAPHIC EFFETC (2D OR 3D) .....	51
2.4.1 Isolated relief .....	52
2.4.2 Slopes .....	54
BIBLIOGRAPHY .....	56
<b>CHAPTER 3 .....</b>	<b>61</b>
3.1 INTRODUCTION .....	61
3.2 ACCELEROGRAMS .....	62
3.3 SEISMIC HAZARD ANALYSIS .....	63
3.3.1 Deterministic Seismic Hazard Analysis .....	65
3.3.2 Probabilistic Seismic Hazard Analysis .....	67

3.4 PARAMETERS USEFUL FOR STRONG-MOTION RECORDS SELECTION.....	71
3.4.1 Ground motion parameters.....	71
3.4.2 Seismological parameters related to the source .....	75
3.4.3 Seismological parameters related to propagation-path .....	81
3.5 CRITERIA FOR SELECTING STRONG-MOTION RECORDS.....	83
3.6 CRITERIA FOR MATCHING PROCEDURE OF SELECTED RECORDS.....	87
BIBLIOGRAPHY .....	89
<b>CHAPTER 4.....</b>	<b>93</b>
4.1 INTRODUCTION.....	93
4.2 SOIL TREATMENTS CLASSIFICATION .....	94
4.3 SOIL TREATMENTS DESCRIPTION.....	96
4.3.1 Injective treatments .....	97
Compaction grouting.....	99
Jet grouting.....	104
BIBLIOGRAPHY .....	107
<b>CHAPTER 5.....</b>	<b>109</b>
5.1 DESCRIPTION .....	109
5.2 GEOLOGICAL FRAMEWORK .....	111
5.3 LITHOLOGY .....	118
5.4 THE GROUNDWATER.....	122
5.5 AVAILABLE IN SITU SOIL TEST (VELOTTI A. 1983) .....	123
5.6 AD HOC IN SITU MASW TEST (EVANGELISTA L. ET AL., 2007; EVANGELISTA L., 2010).....	125
5.6.1 Introduction.....	125
5.6.2 Field Equipment.....	127
5.6.3 Testing configuration .....	133
5.6.4 Experimental results.....	136
BIBLIOGRAPHY .....	138
<b>CHAPTER 6.....</b>	<b>141</b>
6.1 INTRODUCTION.....	141
6.2 SEISMIC HAZARD AND RESPONSE SPECTRA OF STUDY CASE	142

6.3	DISAGGREGATION MAGNITUDO-DISTANCE.....	146
6.4	RESEARCH OF REAL ACCELEROGRAMS .....	153
6.5	RESULTANT HORIZONTAL ACCELERATION .....	156
6.6	SELECTING AN ACCELEROMETRIC SET OF SEVEN RECORDS .....	161
6.6.1	Selection criteria adopted.....	161
6.6.2	Reference response spectra .....	162
6.6.3	Spectrum-compatibility and scale factors .....	164
6.6.4	Real accelerograms selected .....	176
	BIBLIOGRAPHY .....	180
<b>CHAPTER 7</b>	.....	<b>181</b>
7.1	INTRODUCTION.....	181
7.2	ONE-DIMENSIONAL GROUND RESPONSE ANALYSIS OF A LAYERED SOIL DEPOSIT (LANZO, SILVESTRI 1999) .....	185
7.3	EERA (BARDET ET.AL 2000).....	189
7.4	STUDY CASE MODEL .....	194
7.5	ANALYZED CASES .....	199
7.6	ANALYSIS RESULTS .....	202
7.6.1	Reference case before soil treatment :case 0 .....	202
7.6.2	Treated soil cases .....	206
	BIBLIOGRAPHY .....	227
<b>CHAPTER 8</b>	.....	<b>229</b>
8.1	INTRODUCTION.....	229
8.2	HISTORICAL BACKGROUND: GOLDEN MILE VILLAS ...	230
8.3	TERRITORIAL DISTRIBUTION OF THE VILLAS.....	232
8.4	FEATURES AND ARCHITECTURAL STYLES OF THE VILLAS	234
8.5	SEA PARK OF VILLA FAVORITA .....	239
8.5.1	Villa Favorita: historical background .....	239
8.5.2	The House of mosaics: architectural, dimensional and structural characteristics .....	245
8.5.3	Palazzina Mosaic's condition at the time of restoration in 1990	257
8.5.4	Palazzina Mosaic's consolidation intervention in 1990.....	260
8.5.5	Palazzina Mosaic's recent survey activities.....	267

BIBLIOGRAPHY .....	273
<b>CHAPTER 9.....</b>	<b>275</b>
9.1 INTRODUCTION .....	275
9.2 KNOWLEDGE OF THE STRUCTURE .....	276
9.2.1 Knowledge level and confidence factor .....	277
9.3 TREMURI® SOFTWARE (GALASCO ET AL 2002).....	280
9.3.1 Non-linear macro-element model .....	280
9.3.2 Crushing and compressive damage model .....	283
9.3.3 Three-dimensional masonry building model .....	283
9.4 HOUSE OF MOSAICS MODEL.....	287
9.5 STATIC NON LINEAR ANALYSIS (PUSHOVER) .....	289
BIBLIOGRAPHY .....	299
<b>CONCLUSIONS.....</b>	<b>301</b>



---

## INTRODUCTION

Great efforts are being devoted in several countries to the development and application of passive vibrations control systems for the seismic protection of cultural heritage. Italy, can, certainly, be said, in the world, the country with the biggest and most significant cultural and historical heritage built, and despite having made significant progress in recent decades in seismic research applied to our heritage, in relation to the theoretical and methodological study in the applicative field still has much margin for development. In all concerned countries application includes the seismic rehabilitation or improvement of some important monumental structures. The systems developed and devices used, in order to realize energy dissipation and seismic base-isolation, are many. With regard to seismic isolation, it is noted that this concept dates back to a long time ago. However, similar to other antiseismic techniques, the problem of the aforesaid systems (in particular, that of seismic base-solation) is now the need for respecting the conservation requirements, which are very strict in some countries, like, for instance, Italy.

The installation of devices dissipation, infact, is, often, incompatible with the requirements of the recovery, because they can be unaesthetic. Furthermore these devices, on the contrary of a base-isolation concept, don't reduce interstorey drifts, not increasing the fundamental vibration period of the structure, reducing of the action on the structure, acting, prior, on the stresses transmitted by the earthquake, but simply to reduce the consequences of such transmission. Base isolation system presents many important advantages, infact, it can limit the intervention only in foundation, avoiding

the traditional interventions that probably would require reinforcement of structural elements or the introduction of new elements which the what, is expressly prohibited by the Code. It should be, also, considered that the design and calculation of an isolated structure are easier than those of conventional earthquake-resistant structure. Finally, it should be emphasized that a base isolated building has a more simple dynamic behaviour. The only drawback is the need to create a joint around the building. Hence the use of this type of intervention is possible only for buildings that are not bound laterally by the presence of other buildings. At the present base isolation is usually obtained for buildings through cuts of the foundations or load-bearing structures (columns and walls) positioned at the lower floor, or by excavating a new underground floor and inserting the isolators there but, in Italy, the conservation requirements do not allow it. Based on the above, recovering the original idea of isolation, i.e. creating a disconnect in the structure, and inspired by various studies (Tashkov et al. 2009; David Muir Wood, 2006), the present work investigates the possibility of obtaining an attenuation of the seismic signal by means of the surface soil treatment interventions, coupled or not with structural elements. In dealing with a problem typically multidisciplinary, requiring the integration of different competences, in particular, restoration engineering, geotechnical engineering and seismology, particularly important and space was for the analysis work of literature. The references cover both theoretical aspects related to the issues of restoration and the behavior of soils in the dynamic field, the issues so local seismic response, the assessment of seismic risk and the theory of propagation of seismic waves to which it is closely linked and ultimately possible to existing technologies for the soil treatment.

The study of site effects related to the stratigraphy was then carried out numerically on a site: the park on the sea of Villa Favorita. After the definition of the geotechnical characteristics of the subsurface and seismic input we have defined a one-dimensional model and examined different cases in which were modified, from time to time, the characteristics of one layer, in relation to the hypothesis of a treatment of the same. Analyses were carried out assuming three different values of shear velocity and three different positions of the layer treated. It was then conducted a careful historical and geometric relief of a villa located within the park. It was made a three-dimensional numerical

model of the structure, using commercial software and through non-linear static analysis was assessed the capacity of the structure. The results of the seismic response analysis for the site, in terms of displacements and acceleration, for different stratigraphic hypotheses tested, were then compared with those offered by the hotel. The thesis, besides the introduction and conclusions, it consists of nine chapters.

The first chapter presents a brief historical evolution of the concept of restoration, and then moved to define its fundamental principles. In the following is then presented a more detailed overview on the techniques of passive protection by the earthquake (dissipation and seismic isolation) and their application on historical-monumental buildings in Italy and worldwide, highlighting the propriety or not of each technique.

The second chapter provides a general overview of the problem of local seismic response mainly with reference to the effects of site type stratigraphic (1D), ie connected to the impedance contrast between bedrock and soil deposits under conditions of essentially horizontal stratification and those more complex, affecting the seismic motion at the alluvial valleys. For each class of site effects are called the physical phenomena involved and the main geometrical factors and physical-mechanical influence are also reported and commented on some significant case studies.

In the third chapter, are provided the theoretical basis of a correct selection of the input earthquake: shows the different types of accelerograms used for dynamic analysis, assessing the adequacy of either. We then give useful hints for hazard analysis and finally we analyze all physical parameters and not useful for the selection of a record of strong motion. In the same chapter the identification of parameters that characterize the strong ground motion is carried out. Are discussed many factors that influence strong ground motions which effects are complex and often interrelated: ground motion parameters; seismological parameters and propagation parameters, indicating the definition and meaning, considering for each link with the physical phenomenon of earthquake event and the relationship with the record of the

same. Finally, the criteria have been shown to be able to select between different accelerometric records set more appropriate.

The fourth chapter provides a quick view of the soil treatment techniques: a first paragraph that makes a general classification of all possible treatments techniques, followed by a more detailed description only relatively techniques considered most appropriate in the case of interventions on existing buildings and in particular monuments and for which it was pointed out the possibility of obtaining an attenuation of the seismic signal at the surface. In particular are described the injective treatments.

In the fifth chapter investigated the site under study: it identifies the location on the slopes of Somma-Vesuvius volcanic complex, very interesting, for consequences on its geo-lithological characteristics, closely linked to the eruptions occurred over the centuries. The stratigraphy is characterized by the alternation of flow products, such as lava and fall products (pyroclastic): resulting 3 layer on the lava-bedrock: a top layer of pozzolana thickness, a layer of fractured lava (corresponding to the eruption of 1631), a thin layer of sand resting on compact lava, dating from the eruption of 79 a.C., considered as bed-rock. The chapter proceeds to describe briefly the MASW tests (and the theory that underlies them) carried out on site necessary, lacking samples at the site, or results of dynamic tests already carried out and without the ability to perform invasive tests, to know the equivalent parameter of the soil dynamic behaviour under cyclic load: the shear modulus and the damping ratio. Finally, reports the dispersion curve and the shear velocity profile obtained from the in situ test.

In the sixth chapter is implemented a procedure for selecting the correct seismic input for the park on the sea of Villa Favorita: at first, with the help of seismic Italian code (D.M. 14.01.2008), are identified the return periods  $T_R$  and the PHA for the site for different ratio of exceedence PVR. Then with the same percentage of exceedence was obtained from maps of disaggregation events that contributed most to the hazard of the site, identifying the magnitude  $M$  and distance  $R$ . The value pairs  $(M, R)$  which corresponded to the major contributions were used to search for in the Italian seismic catalogue

(ITACA) events compatible with this hazard. For each of the records the NS and EW components were composed, so as to obtain the resultant that had the highest energy content in terms of Houssner intensity, according to an ad hoc procedure developed. Of all the accelerograms obtained were then selected those ones of significant duration, which presented the minor individual deviation from the reference spectra and the FSC closer to unity, as well as those whose average was closer to the reference spectra. Spectrum-compatibility was estimated with three different coefficients.

The seventh chapter discusses the modeling and analysis of local seismic response of the site. The first paragraph is devoted to the problems of choice of modeling methods to follow and the different analytical procedures for the solution of the dynamic equilibrium equations, taking into account the nonlinear behavior of soil. The second paragraph indicates the one-dimensional analytical solution of the problem of seismic site response for a layered soil. It then provides a brief description of the calculation software used, of the model characteristic as deduced from the geo-lithological and seismic survey executed on the site, with regard the dynamic curve assigned to each layer. Finally, are described the analyzed cases and the results.

The eighth chapter presents the historical and monumental building under study: the Palazzina of the mosaics. At the first is devoted to the historical and territorial and architectural context of which the villa is a part. After is carried out the detailed architectural, dimensional and structural description of Palazzina under consideration: for this purpose, is shown the results of geometric and photographic survey on it. Subsequently, in order to achieve an adequate level of knowledge, prerequisite necessary to the construction and the analysis of a numerical model, a thorough investigation of the works carried out over the decades on the structure, was conducted. Finally, with the information previously obtained, an inspection conducted on the building showed, in an expeditious way, what might be its criticality.

The ninth chapter shows the numerical modelling and evaluation of seismic vulnerability of the House of mosaics carried out: the numerical model was implemented in three-dimensional domain with use Tremuri software

(Galasco et al. 2001). The characteristics of the model are derived from the knowledge process conducted in chapter eight. On the model was performed a non-linear static analysis (pushover) to obtain the capacity curve of the building. The analysis results are integrated with the seismic site effect analysis results: the capacity curve was so compared, both in terms of acceleration, with the spectra obtained for the site, in relation to each of the treatments identified.

## *Chapter 1*

# Issues of intervention on monumental buildings

## **1.1 INTRODUCTION**

Since ancient times man has tended to give value to the existing built. Value at many levels: historical, cultural, social. Hence the requirement to preserve built heritage. The conservation of a building, unchanged over the centuries, now appears, undertaking difficult as questionable implementation. The contemporary concept architectural restoration, in fact, includes a series of very different, ranging from simple protection, consolidation, rehabilitation to achieve the renewal of the building. Of great interest is, now, also the reduction of seismic vulnerability of monuments and eventually their protection, but it must be inserted in the right context and treated with due respect: the conservation of cultural heritage, in fact, a lot depends also on the nature of projects that are carried out. An intervention of poor quality is worse than no intervention. In order to clarify the delicate context in which the present work is intended to fit, in this chapter presents a brief historical evolution of the concept of restoration, then moved to define its fundamental principles. In the following is then presented a more detailed overview on the techniques of passive protection by the earthquake (dissipation and seismic isolation) and their application on historical-monumental buildings in Italy and worldwide, highlighting the propriety or not of each technique.

## 1.2 HISTORICAL EXCURSUS

The historical consciousness related to architecture, and its values of art and civilization, are developed only in the XIX century. In this period we come to define also the first theoretical ideas related to the restoration, in particular due to Eugene Viollet-le-Duc and John Ruskin.

Viollet-le-Duc (1814-1879), theorized the so-called "stylistic restoration," which is to restore a building in its stylistic unity, giving it an appearance that may not have ever had in the past ("restaurare un edificio significa ristabilirlo in uno stato di integrità che può non essere mai esistito"). In this restoration, it tends to erase the following history of a building, demolishing the parts that are not consistent with its original style, and redoing the missing parts or demolished in the original style of the building.

John Ruskin (1819-1900) was radically opposed to this conception of stylistic restoration calling it "lies". According to him, always involves restoring a falsification, for which the only operation allowed is "romantic restoration" that is to cure the buildings as possible, but to do nothing if they are falling into ruin.

Luca Beltrami (1854-1933), in the late XIX century, theorized a new idea called "historical restoration". This restoration is not differed much from that style of Viollet-le-Duc, but admitted that any additions must be made not by an abstract criterion of stylistic consistency, but based on documented historical and archival sources.

Camillo Boito (1836-1914), during the Congress of Italian architects and engineers held in Rome in 1883, defined the first criteria of restoration in the modern sense. This position was defined "philological restoration", halfway between the one intended by Le Duc and that intended by Ruskin.

According to Camillo Boito:

- Monuments must be "rather consolidated than repaired, rather repaired, than restored".



- Must comply with all parts of a building, including those added in the course of its history.
- If is necessary add a new part in the building, it should be differentiated between materials and characters, but without altering the overall appearance of the monument.

During the '800s, increasingly, felt the need to share unique principles about the restoration, so that this activity became more and more scientific and less empirical, thus giving rise to the "Athens Card".

It is composed of more than 10 points that rather determine the true principles, than give some recommendations to the Governments of the States:

take care of its architectural heritage,

standardize the laws so as not to give precedence to the private interest of the public,

expand the study in order to inculcate in the populations the love and respect for its architectural heritage.

From a technical point of view the "Athens Card":

calls for a philological restoration, refusing the stylistic one,

admits the use of modern materials for the consolidation, such as reinforced concrete,

admits in the case of archaeological restoration only anastylosis.

The 1932 the Supreme Council for Antiquities and Fine Arts at the Ministry of Education, issued a "Card of restoration" that can be considered the first official directive of the Italian State in the field of restoration. It is stated principles similar to those of the "Athens Card", but with the addition of the position expressed by Gustavo Giovannoni in those years (1873-1947), defined as "scientific restoration". Giovannoni was the first who suggested that any intervention should take advantage of all the latest technology in order to reach scientific work of restoration.

The Second World War, with all the physical destruction also brought to the Architectural Heritage of Europe, reported that the topical problem of architectural restoration. In this situation particularly for the psychological effects of deleting the destruction of war, almost always extended a practice of

restoring, reconstructing the existing even at the risk of making false true historians. Out of the phase of post-war reconstruction, the international architectural culture is questioned again about the correct practice of restoration and, in the Second International Congress of Architects and Technicians of Historic Monuments, which met in Venice 25 to 31 May 1964, was defined a new card restoration called "the Venice Charter." Card consists of 16 articles and summarized in an admirable way the principles of the methodology can be considered immutable architectural restoration. This paper especially emphasizes the importance of the historical value of the building, and introduces for the first time the concept of conservation of the urban environment that surrounds even the monumental buildings.

In 1972, the Italian State, issued the text of the Italian Card of restoration, with an explanatory memorandum and four annexes relating to the execution of restoration archaeological, architectural, painting and sculpture as well as the protection of historical places. In 12 articles the Card defines the objects affected by preservation and restoration actions: these actions extend from the individual works of art to the monumental complex of buildings of interest, historic or environmental, historic centers, the art collections, furniture, gardens, parks and ancient remains discovered in research on land and underwater. In this case, it theorizes more precisely the correspondence between "restoration" and "cultural heritage".

In the international architecture, the European Community issued a new card restoration entitled "Principles for the conservation and restoration of built heritage", known as the "Charter of Krakow", named after the Polish town where the conference took place. This paper states explicitly refer to principles already contained in the Charter of Venice. The great news is that this document speaks of "heritage" and no more than "monument" architecture, implying thus that the principles of the restoration should not be applied only to buildings but to the entire city centers. In fact, in its articles the Card of Krakow aims to raise awareness of conservation and maintenance of the entire area, including landscaped areas are not built, as it is to keep the whole very important elements of history and culture human.

### 1.3 FUNDAMENTAL CONCEPTS

Due to the sensitivity of any intervention on an historical-monumental building is good to clarify fundamental concepts underlying these actions:

- Conservation is to maintain an artifact in its state to avoid any alteration;
- Integration means, however, add parts or elements to the existing structure;

The replacement implies, finally, the elimination of a preexisting part to make way for a new element to be inserted into the building.

The same concepts can be used in more specific structural terms: the preservation of a building shows a series of intervention, usually temporary, and to ensure the persistence and the safety of the building, to avoid partial or total collapse of the same.

- The consolidation and rehabilitation can be seen as a higher level of intervention, where the operations performed on the building, must restore its structure and function, bringing it back to baseline, before the sustained deterioration over time.
- The renewal of the construction, finally, strengthens and improves the original structural performance to satisfy new functional requirements. The difference between the different types of interventions is not so much in the entity of the same, but more in the relationship between the building before and after restoration.

It should be underlined that any intervention, however small, carries a change to the object restored: think of a painting, even dusting or application of transparent film on it is itself a modification of the status quo. The awareness of the statement leads to reiterate how much care is needed in the definition of a recovery, either partial or global. Based on this concept, all modern standards and, in general, all the "cards" on international restoration, fix, the same as a necessary condition, the safety assessment. To obtain a careful analysis and evaluation of the most appropriate intervention to each situation, it is necessary to identify the existing structural system, its state of stress, the changes incurred during the time of the construction process and the events which been subject.

Will, therefore, investigated the building history, execute a complete geometric relief and of material constituents, their quality, and the crack pattern. These investigations, carried out directly on the artifact, are associated with those relating to the construction site, relative to the geotechnical characterization of the foundation soils, past and present state of the water table and so on. In this sense, the technology in the last decades comes to the rescue, allowing us to obtain the required data without invasive interventions, often made difficult by the degradation of the structure. It 'clear that the built heritage embodies very different types of construction and that each will adopt a different solution: a building vaulted will, of course, needs of different restoration respect to floors; so a masonry building can not be recovered using the same techniques and the same materials used for a steel, wood or concrete. Despite the wide variety of techniques and materials for restoration is possible to outline the main lines of intervention, common to each type.

Basic concepts are:

reversibility;

- compatibility;
- durability;
- minimum intervention;
- authenticity;
- maintenance.

The reversibility is a very complex concept. Sought by every restorer is, however, the reality is often unclear. The need of this requirement, for any restoration work, is related to the certainty that in future the building will be subject to other interventions. The purpose of a restoration is, in fact, not only to ensure the existence of the building, but also to forward it to the future, it is therefore necessary to facilitate future operations and not exclude them.

The concept of compatibility should be one of the components that characterize any action on the ancient manufacture and should cover all phases of project execution. As for the reversibility concept also this is open to a different set of meanings: physical and chemical compatibility of new materials with existing ones; mechanical compatibility, historical or functional compatibility with the image of the monument, and so on. This leads to say

that every restoration is not merely overlapping of different but independent fields: is a time when historical knowledge and technical-scientific blend. Compatibility is not, therefore, a problem solved by the mere substitution of materials equal to those damaged, also taking into account the fact that these materials are often unavailable or no longer exist in the workforce able to work with traditional techniques.

Based on what said on reversibility and compatibility, the concept of durability may seem contradictory, but only because it is calibrated on parameters other than what has gone before. The materials of the past were designed and manufactured to last for hundreds of years and today, more and more aware of the continuous and rapid innovation, the average length of material is of the order of tens of years.

Another fundamental concept, traceable even in the current regulations, is of minimal intervention, i.e. the possibility to intervene only where strictly necessary, in order not to compromise the monumental historical integrity of the construction.

This intervention philosophy also includes the concept of authenticity: to operate even in the event of additions or replacements, the authenticity of the original elements must be safeguarded and this becomes possible only if new interventions are recognizable and distinguishable from the original. Finally, the great debate focuses on the concept of maintenance of heritage buildings that, contrary to what is happening today, should be perpetual and constant, to be implemented before pathological degradation of the building and not latter, in which case it is more correct to speak of "repair".

On the basis of the above, is of great importance to develop new research on methodologies for the use of innovative techniques and materials for restoration. Advocating an increasing development of innovation in the field of intervention on historic monuments, is, however, underlined that "every intervention must be such as not to prevent future actions" [Carta Italiana del restauro 1972]. An important indication that emphasizes the "transitional" of every restoration, is experienced as a time when imagination, creativity, fantasy, historical and technical-scientific knowledge interact, not to steal the scene, but to get the results shared conservatively. [G. Carbonara 1996]

## **1.4 MONUMENTAL BUILDINGS IN SEISMIC AREAS: ADAPTATION OR IMPROVEMENT**

Within the specifically seismic field, the first “Recommendations for interventions on the monuments to the specialized type in seismic areas” date back to 1986, following a number of erroneous interventions on monumental buildings in seismic areas, carried out in the years, particularly following the destructive earthquakes of Friuli and Campania, Basilicata, and other less violent events.

Even in those recommendations are several factors did find difficulties in implementing such interventions:

The intrinsic sensitivity related to the nature and age of the building concerned;

The need of an interdisciplinary approach;

- The lack of legal clarity about the technical aspects of the interventions, worsened by the tendency to improperly apply technical standards, written for ordinary buildings on monumental buildings such as churches and palaces including generally vaults, frescoed walls and horizontal elements or precious materials;
- The conflict between the needs of conservation and restoration on the one hand and protection from the seismic risk of the building and lives on the other hand,
- The lack of clarity, technical, technological and even cultural or conceptual, that is around the use of modern materials in old buildings;

So, over the decades, the interventions on the monuments were often conceived as static restructuring implemented a series of massive interventions by criteria that reflect the culture of widely extensive new materials, especially steel and concrete, thus developing a structural restoration strategy that seeks to reshape the old factories according to their resistance patterns of modern materials. Results of this often lead to:

- interventions unnecessarily “heavy” except sometimes counterproductive), which often distort the monument from the point of view of its identity and value;
- interventions too costly;

- security guarantees often wholly illusory, since they are based on model calculations unreliable;
- widespread inability, substantially and formally, to monitor the effectiveness of the interventions.

As examples of the phenomena mentioned are listed some project positions as widespread as dangerous:

- Projects carried out without any objective knowledge about the structure and foundation soils;
- inclusion of new structures which are entrusted entirely static function, reserving, so, to the ancient structure only formal function;
- inclusion of structural elements that perform static functions considered by the designer is not compatible with the existent building, in which case, as well as to give rise to a hybrid mechanical behavior, particular uncertainties may be introduced due to the interaction of structural patterns and materials;
- trying to achieve through intervention, a behavior modeled with its new construction scheme;
- unwarranted use, compared to the present cracks pattern to the original structural design of the monument, the “seams” and “injections”;
- unmeditated use of new materials especially with reference to the durability and the interaction with the original materials.

To counter the situation reported above, already the D.M. 24/1/86 of the Ministry of Public Works (G.U. n.108 of 12/5/86), to the point C9, introduced in the technical regulations for construction in seismic areas a new approach to the problem of the interventions on existing buildings, allowing to operate in based prevention, instead of repair. The main innovation was represented by the introduction of two levels of objectives pursued by means of structural measures aimed at increasing the seismic resistance of buildings; it identified, in fact:

“Adaptation interventions, defined as a set of works necessary to make the building capable of resisting design actions equivalent to those required for new construction”

“Improvement works defined as the set of works designed to achieve a

greater degree of safety against seismic actions without substantially altering the global behavior of the building”.

Emphasizing, in the execution phase of operations, how important were:

- a particular attention to original material, and the subsequent transformations;
- a careful reconstruction of the seismic history of the building, with a focus on repairs to follow past earthquakes;
- a rigorous and systematic interdisciplinary approach in all project phases, with particular reference to the contributions architectural, historical, geotechnical, structural, plant;
- the use of techniques and materials as close as possible to the originals.

On the basis of the above, arise today, after a decades-long process elaborative, the “Linee Guida per la valutazione e riduzione del rischio sismico del patrimonio culturale” (2010). The same, aligning them to the “Norme tecniche per le costruzioni” D.M. 14.01.2008, recalling the principles contained in the “Codice dei Beni Culturali e del paesaggio” D.lgs. 22 gennaio 2004, n. 42, that, in fact, according to art.29, for building of cultural interest into seismic areas is, in any case be limited, making its safety assessment, to the only interventions for improvement.

Once again are reminded that action in terms of improvement design must mean only on the basis of knowledge of the factory, only realizing a project that, while giving appropriate security guarantees, is respectful of the building cultural value. The term improvement, it was, once again, an issue of compatibility, which means realized only what is respectful of the building architectural nature, excluding else.

The above guidelines state expressly the strategies for the choice of an intervention rather than another, pointing out that the main purpose is the preservation not only of "matter" of the factory, but also established the structural functioning of the same. Interventions should be selected to avoid the inclusion of elements that alter significantly the distribution of the original stiffness, giving priority, among other, less invasive techniques possible



executive.

The ministerial circular n.617 of 02.02.2009 states expressly that such building should be avoided interventions that alter them so evidently and require the execution of invasive works, focusing, among others, measures that mitigate the seismic effects. The conceptual approach of the seismic risk mitigation applied to the field of structural restoration has the undeniable advantage of reducing the seismic action on building under intervention, up to an order of size comparable with available capacity, rather than trying to improve, with invasive interventions, these capabilities. This philosophy appears, therefore, best suited for operations on historical monuments. It 'also, undeniably, economically advantageous, mainly because of minor damage on the factory in question, and consequently the reduction of remedial and maintenance, taking into account that every action of monumental buildings is complicated and expensive.

### **1.5 PASSIVE SEISMIC PROTECTION OF CULTURAL HERITAGE**

Great efforts are being devoted in several countries to the development and application of passive vibrations control systems and devices for the seismic protection of all kinds of structures and valuable objects, including cultural heritage (Dolce et al. 2005, Dolce et al. 2006, Martelli 2007, Martelli & Rizzo 2007, Martelli et al. 2008, Santini & Moraci 2008, Sannino et al. 2008;). In keeping with the fact that Italy owns a large part of the cultural heritage existing in the world, this country is very engaged in the field of its seismic protection; however, important activities have been undertaken in other countries, as well in Japan, the USA, the People's Republic of China, the Russian Federation, New Zealand, Greece, Armenia, etc. (Martelli 2009).

All seismic protection techniques can include into two main categories: passive protection and active protection. The so-called active seismic protection techniques are based on the idea of "intelligent" building that responds in an active way to the actions induced by the earthquake: depending on the size and type of stress perceived and recorded, at the time of the earthquake, are activated, devices that counteract the external action, in real

time by changing the characteristics of the structure. The passive protection using concepts such as dissipation and isolation, that is inserted into the structure elements that increase its period and its damping capacity, but that once defined their characteristics, during the earthquake remain constant. However, even the use of such systems should be "calibrated" on the different needs that protection of monumental building, compared to a new building construction.

### 1.5.1 Energy dissipation

The dissipation systems can be divided into three categories:

- Devices activated by the displacement (Displacement-Activated Dampers - DAP);
- Devices activated by the velocity (Visco-elastic Dampers - VEDs; Viscous Damper VDS);
- Motion-activated devices.

The following Table 1.1 summarizes the different types of heat sinks in accordance with the criterion of activation.

*Table 1.1 – Definition of partial factors of confidence*

Displacement	Velocity	Motion
Metallic dampers Friction dampers Re-centering dampers	Viscous Dampers (V.D.s.)	Tuned masses dampers (T.M.D.s.)
Visco-elastic dampers (V.E.D.s.)		

The devices activated by the displacement dissipate energy according to the relative displacement between two points connected. The dissipative capacity of these devices is independent of the frequency of motion. This category can include dampers metal, friction Dampers (FDS) or recentering. The dissipative capacity of these devices is due to the hysteretic behaviour of metals and friction generated between two elements in relative sliding between them. The mechanical behavior can be considered as elastic perfectly plastic.(Figure 1.1)

The devices activated by the velocity (Figure 1.2) dissipate the energy of the earthquake through the relative velocity between two points of the device. In contrast to the earlier response of these devices depends on the frequency of

the action. This category can include visco-elastic and purely viscous dampers. The dissipation of energy in these devices is achieved, generally through the passage of a high viscosity fluid inside a steel piston with holes.



*Figure 1.1 – Steel hysteretic dampers*



*Figure 1.2 – Viscous damper*

The devices activated by the motion carry dissipation by channeling the energy transmitted by the earthquake to the secondary vibration systems. Known system, belonging to this category, is the Tuned-mass Damper, which is designed to resonate at the same frequency of the structure on which it is installed, but in phase opposition. The energy transmitted by the earthquake is, thus, dissipated by the inertia forces of the system damping applied to the main structure. The most recent application of this system is in Taipei 101 tower. (Figure 1.3)

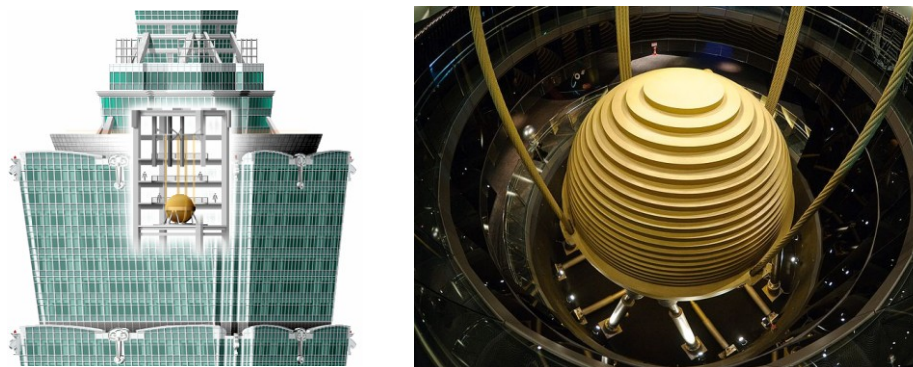


Figure 1.3 – Taipei 101: tuned mass Damper (<http://en.wikipedia.org>)

Energy dissipation systems have found a widespread area of the recovery of existing buildings being less invasive than other techniques. Their effectiveness, however, is more limited than the concept of isolation at the base, to be able to work, they require that the dissipative structure undergoes deformation, without improving in any way what are the intrinsic dynamic characteristics of the same. Do not reduce interstorey drifts, not increasing the fundamental vibration period of the structure, reducing of the action on the structure, acting, prior, on the stresses transmitted by the earthquake, but simply to reduce the consequences of such transmission. Finally, often the installation of devices dissipation is incompatible with the requirements of the recovery, because they can be unaesthetic, as in the case of those included inside the Upper Basilica of St. Francis at Assisi during its retrofit in 1999. (Figure 1.4)

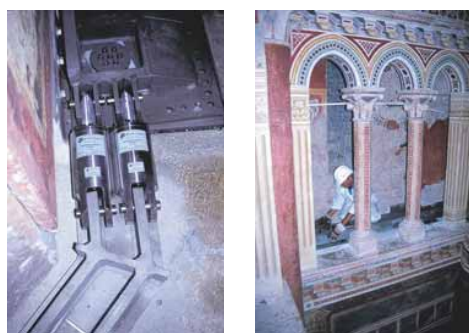


Figure 1.4 – Two STUs inserted inside the Upper Basilica of St. Francis at Assisi

### 1.5.2 Base isolation

The concept of seismic isolation has ancient origins: rudimentary isolation systems have been used by peoples such as Greeks and Incas. Plinius, in his “Naturalis Hystoria”, describes the use of a sliding isolation system, consisting of “a layer of ferment of carbon and another of a fleece of wool” during the construction of the Temple of Diana at Ephesus in middle VI century b.C. [Dolce, Cardone, Ponzo, di Cesare, 2009]. Even in Italy similar seismic protection techniques are attributed to the ancients, such as Paestum, where some temples built on layers of sand. The first document that certifies the idea of decoupling the motion of the structure from the ground was in 1870, thanks to Jules Touaillon. His system involved the use of bearing spheres located between the base of the structure and the foundation. (Figure 1.5) In 1906, Jacob Bechtold (Munich, Germany) made an application for a U.S. patent for an earthquake-proof building involving a mass of spherical bodies of hard material to carry the base plate.

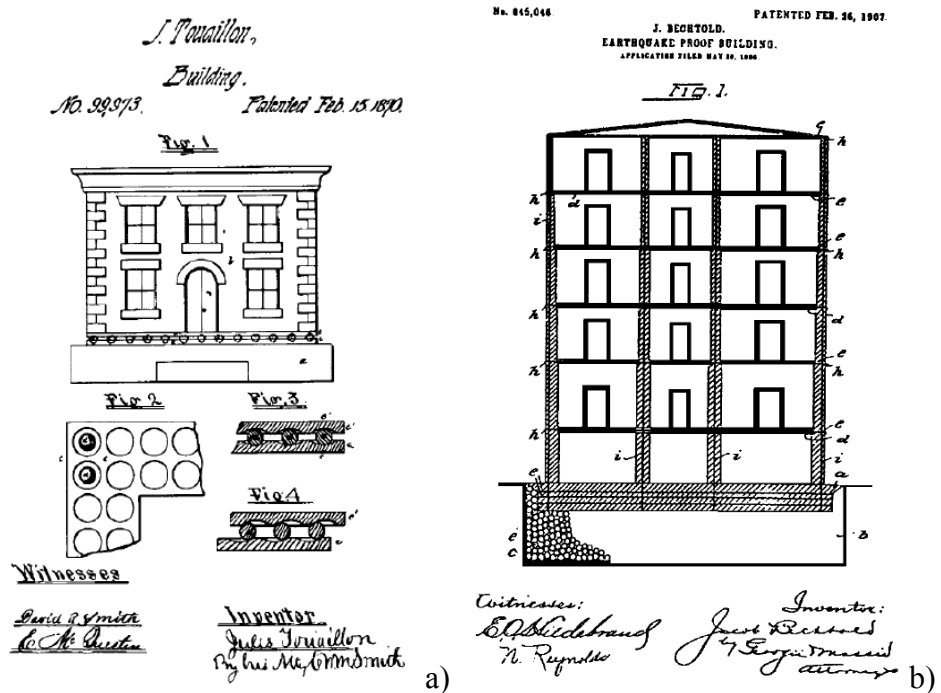


Figure 1.5 – First idea of isolation system: a) Jules Touaillon b) Jacob Bechtold

But they were only concepts: it is in 1909 An English medical doctor J. A. Calantarients realized a real project, complete with construction details, apparently inspired by a Japanese approach. The isolation was achieved by a layer of fine sand and talc. (Figure 1.6) He understood that the isolation systems reduce the acceleration at the cost of large relative displacement between buildings and foundations [Naeim and Kelly, 1999].

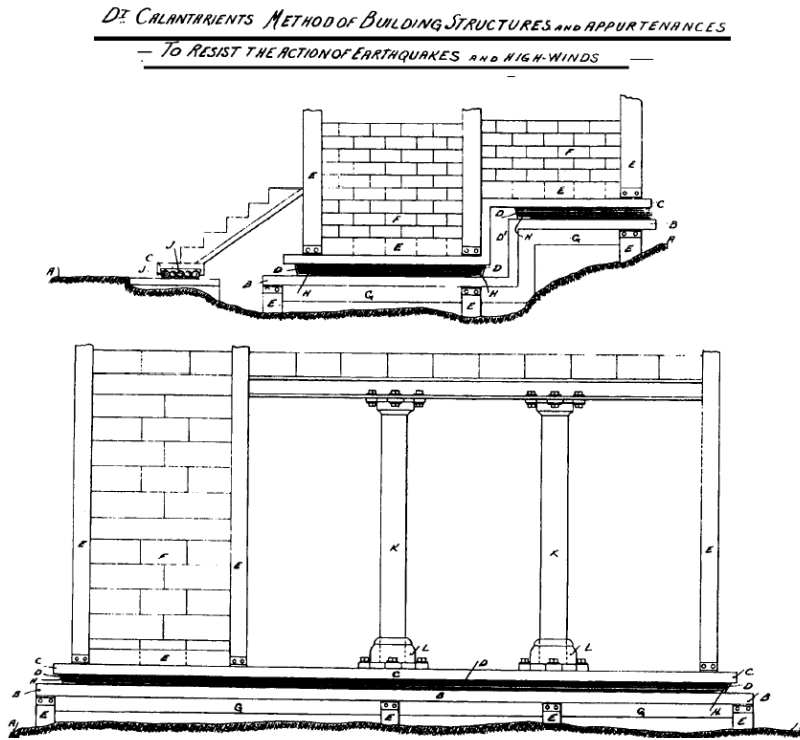


Figure 1.6 - J.A. Calantarients - Improvements in and Connected with Buildings and other Works and Appurtenances to Resist the Action on Earthquake and the Like - Paper 325371, Engineering Library Stanford, California - years 1909

The system Calantarients incorporated all the elements that are now still necessary for a system of this type and for all base isolation systems, namely:

- Separation of the building from the ground;
- Appropriate joint allowing the large displacements of the building horizontally;
- Restraint device for small horizontal actions like the wind.

The isolation was considered as a strategy for seismic protection in Italy for the first time in 1908, after the earthquake of Messina. After this disaster the government issued regulations for the safe and economic reconstruction and appointed a special commission for this purpose. The commission, in the report published by the Accademia dei Lincei in 1909 [Naeim and Kelly, 1999], considers two design approaches for buildings to be rebuilt: a first approach was to isolate the building from the ground by a layer of sand in the foundation using rollers under the columns to allow the building to move horizontally, the second approach was to design the structure on forces resistant criteria. This latter approach was recommended and the first was not taken into account by the operators.

The seismic isolation creates a horizontal “disconnection” between the masses of structure in elevation and its foundation, in order to decouple the motion of the latter, in agreement with the ground one, from the structure. The presence of isolation guarantees an increase of deformation, thus increasing the fundamental period of the whole system isolation-structure so to have low spectral acceleration. Thus the accelerations transmitted to the building from the ground and are severely limited compared to a fixed-base configuration. This will enable building to remain in the elastic range in the presence of particularly violent earthquakes without damage.

Consequently to the elongation of fundamental period is an increase of displacements, but are concentrated exclusively in the isolation system, allowing, thus, the elevation structure behave as a rigid body, limiting the relative interstoreys displacements.

The advantages are many:

- The reduction of the forces of inertia, then stress, avoiding damage to the structure for violent earthquakes;
- Reduction of the interstory drift;
- Reducing costs of intervention in the post-seismic building.

The only drawback is the need to create a joint around the building, allowing it to move. Hence the use of this type of intervention is possible only for buildings that are not bound laterally by the presence of other buildings.

The design of an insulation system is carried out taking into pursuing, then, three fundamental objectives:

- minimize the base shear of the structure,
- minimize the base displacement of the structure;
- minimize floor accelerations at high frequencies ( $> 2$  Hz)

Conceptually, it totally reverse the design practice of any adaption traditional intervention, because first determines the resistant capacity of the structure with respect to horizontal loads and then the isolation characteristics are calibrated so that the demand is minor of capacity. The applicability of such systems to existing buildings has a considerable value, especially in a country with a large built heritage and contemporary in which the seismic hazard is high, such as Italy. The base isolation system, infact, can limit the intervention only in foundation, avoiding the traditional interventions that probably would require reinforcement of structural elements or the introduction of new elements which the what, is expressly prohibited by the Code. It should be, also, considered that the design and calculation of an isolated structure are easier than those of conventional earthquake-resistant structure. [Dolce, Cardone, Ponzo, di Cesare, 2009]. Finally, it should be emphasized that an isolated building at the base has a simple dynamic behaviour, making the overall system building-isolation system very close to a system with two degrees of freedom.

Characteristics required to an isolation system, therefore, are:

capacity to support dead loads both in static and dynamic conditions;

- highly deformable in the horizontal direction;
- good dissipative capability;
- adequate resistance to horizontal not seismic loads (such as wind or traffic).
- re-centering capacity, as to have residual displacement after the earthquake negligible;
- durability;
- easy to realization;
- low cost.



An isolation system is generally composed of a series of devices. The types of devices developed in recent decades are quite numerous, but they can basically be divided into two main categories: elastomeric and steel device and friction -sliding isolators.

Typically, these devices perform only the first three features mentioned above, leaving the task of tying the side structure is not subject to seismic horizontal loads, to refocus and to dispel much of the earthquake-induced energy devices, so-called auxiliary.

Elastomeric isolators and steel are divided into:

- Low-damping rubber bearing (LDRB), made of reinforced rubber obtained by alternating a layer of elastomer with sheet steel ( $D=2-4\%$ )
- High damping rubber bearing (HDRB) (Figure 1.7a) compounds obtained by using “loaded” rubber. The equivalent viscous damping up to 20% for shear strain as much as 100% [Kelly, 1991].
- Lead rubber bearing (LRB) is very similar to the elastomeric isolators, with the insertion of one or more cylinders of lead attached to the steel end plates (Fig. 6), reaching the equivalent viscous damping values also 35% (Figure 1.7b)

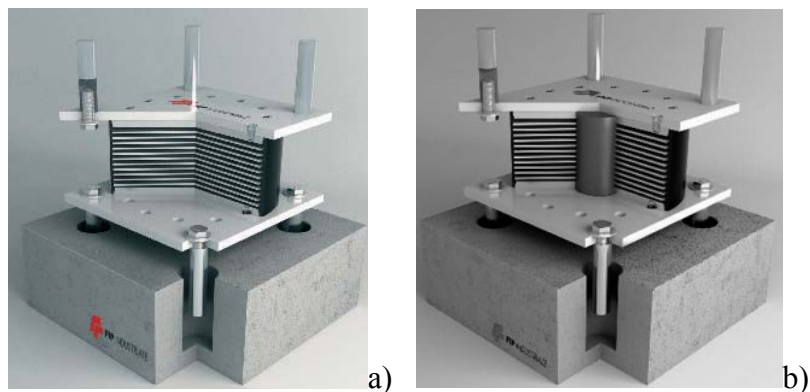


Figure 1.7 – Elastomeric bearing: a) Low damping rubber bearing, b) Lead rubber bearing

The friction isolators can be divided into unidirectional and multidirectional. Generally, for the buildings the second type used, so as to obtain a horizontally homogeneous behaviour. These devices consist of two discs of different diameters that slide over one another [Dolce, Cardone, Ponzo, di Cesare, 2009]. The contact surfaces of the disks are made of special

materials, such as to result a frictional resistance very low. In many cases, the Teflon is used, taking into account that the friction characteristics of this material depend on temperature, sliding velocity and contact pressure, and the distance from the surface during the relative sliding of one over other. In current practice, these devices are, always, coupled to other devices to solve the questions of re-centering and dissipation. This choice is due to the impossibility of sliding isolators to ensure energy dissipation, as a consequence of the excessive variability of the friction coefficient is influenced by environmental factors such as humidity, temperature, surface cleaning. The best known sliding isolation system for buildings is, certainly, the Friction Pendulum System (FPS), which also incorporates the functions of re-centering and dissipation due to the curvature of the surfaces in contact. (Fig. 7) (De Luca & Serino, 1989; Zayas et al., 1987). FPS principle advantage is the independence of the fundamental period of the structure. Disadvantage, however, is their large dimensions, the vertical movements accompanying horizontal ones, and the high cost.

### ***1.5.3 Passive protection application to cultural heritage in the World***

SI is a technique that is easily enforceable in the case of buildings or other structures of new construction, but it can also be used for the retrofit of already existing structures: in this case, SI is usually obtained for buildings through cuts of the foundations or load-bearing structures (columns and walls) positioned at the lower floor, or by excavating a new underground floor and inserting the isolators there. Retrofit with SI has already been often successfully used, at first in New Zealand and the USA and now also in Italy, Japan, Armenia, the People's Republic of China, the Russian Federation, Turkey, etc. (Martelli, 2009)

The first case of seismic adjustment of a historic building using base isolation dates back to 1987/89, when this system was used for the recovery of the Salt Lake City and County Building. (Figure 1.8) The building, constructed between 1891 and 1894, with a masonry structure and wooden floors, foundations plinths with different heights and sizes and a massive square base in concrete, was widely damaged by the earthquakes of 1934 Hansel Valley and Idaho in 1983. The restoration was done by introducing 447 elastomeric devices, 208 of which with lead core.

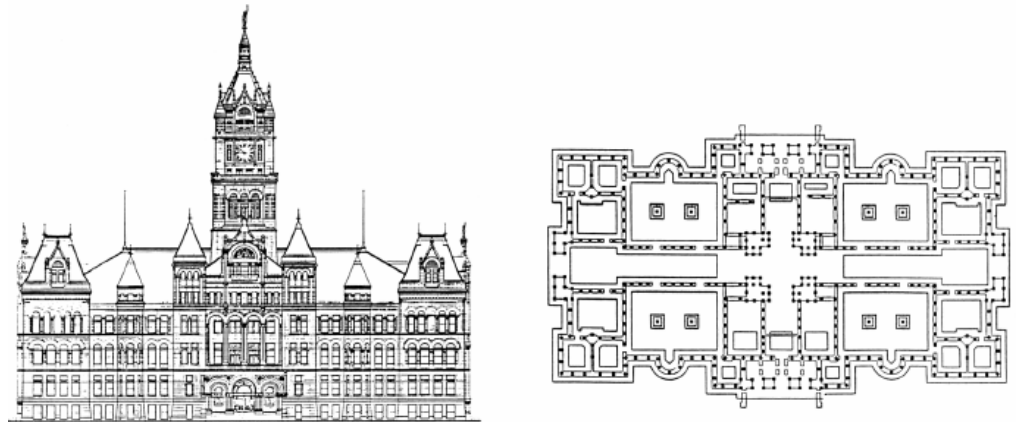


Figure 1.8 - Salt Lake City & County Building facade e plan

The installation of the devices (Figure 1.9) included the following:

- transfer of load from masonry wall to pairs of reinforced concrete beams, built on both sides of the wall;
- creation of niches within the walls for the siting of isolators;
- construction, above the isolators, of pre-stressed transversal reinforced concrete beams and a concrete rigid diaphragm;
- creating a grid below the isolators consist of steel beams welded together to spread the loads transmitted to foundations, and transfer them to isolators

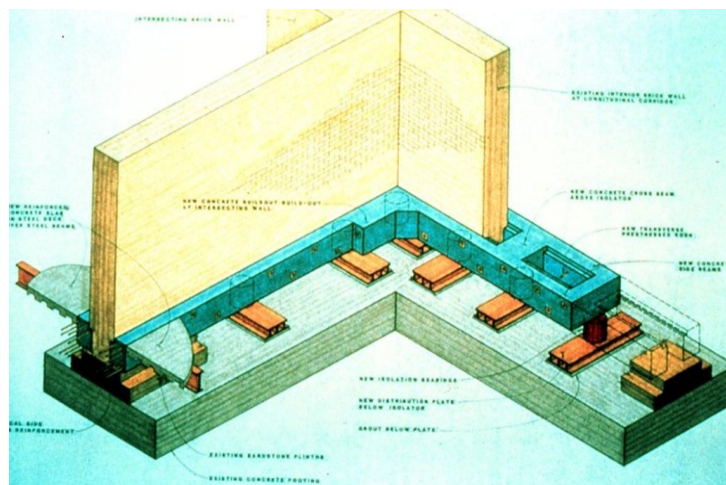
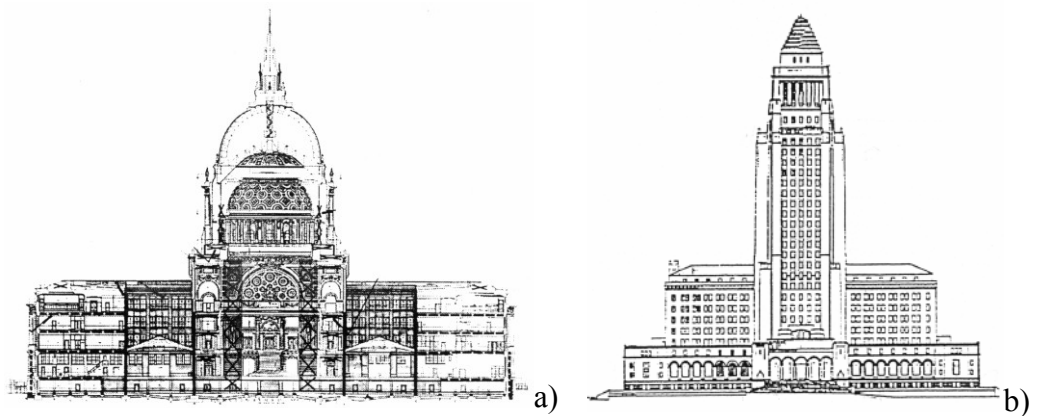


Figure 1.9 - Salt Lake City & County Building elastomeric devices installation



Two other examples of U.S. use of base isolation systems in historical and monumental buildings are the San Francisco city hall (Fig. 12a) and the Los Angeles City Hall (Fig. 12 b). Both structure framed with steel and concrete floors, the first, built in 1913 and damaged by the Loma Prieta earthquake of 1989, the second most recent 15 years (1928), damaged by the Northridge earthquake of 1994; were adjusted by the introduction of the base isolators with the coupling of dissipation of other devices.



*Figure 1.11 – a) San Francisco City hall b) Los Angeles City hall*

Historical-monumental building, recently base isolated by the use of the LRB is the Asian Art Museum of San Francisco. (Figure 1.12)

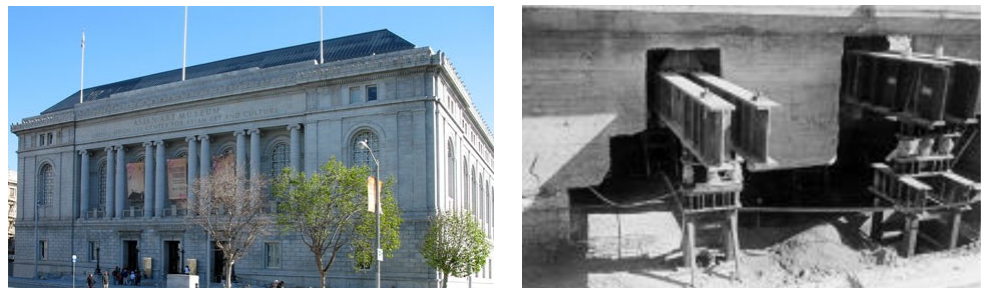


*Figure 1.12 – Asian art Museum of San Francisco City: façade and devices installation*

At the same time, the seismic isolation technique, using LRB, was used for the recovery of other historic buildings in New Zealand, such as the Maritime



Museum in Auckland and Wellington Parliament, dating back to 1921, both rehabilitated in 1993. (Figure 1.13)



*Figure 1.13 – Asian art Museum of San Francisco City: façade and devices installation*

Examples of applications are several projects in the East, especially in Japan, where to report isolation of "Daigokuden" in Nara, Japan (Figure 1.14) and in Armenia, where, in Yerevan, was made to move the small chapel of San Cathoghikkeh (Figure 1.15). The sketch of the project consisting in cutting its foundations, inserting a reinforced concrete support slab, displacing the chapel on wheels applied to the slab as shown on the right (so as to make it visible) and, finally, positioning such a slab on NBs manufactured in Armenia. (Martelli 2009)

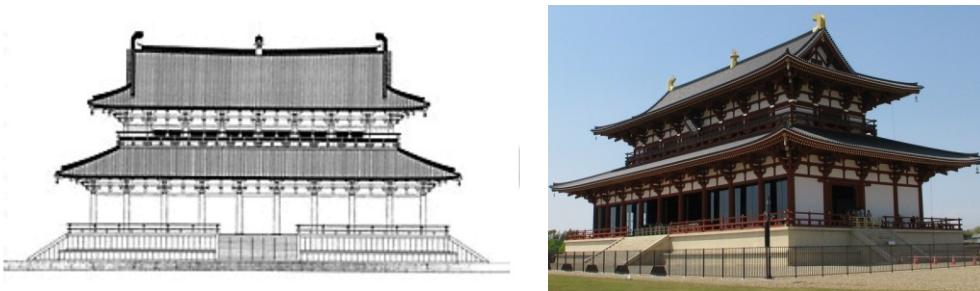


*Figure 1.14 – "Daigokuden" a Nara, in Giappone (Martelli 2009)*

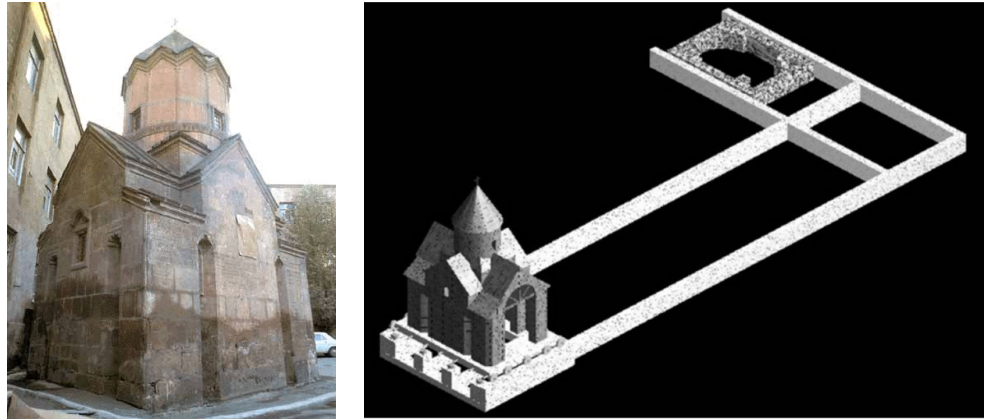


Figure 1.15 –San Cathoghikheh Chapel, Yeveran – Armenia (Martelli 2009)

#### 1.5.4 *Passive protection application to cultural heritage in Italy*

In Italy, the first two modern applications of antiseismic devices to monumental buildings date back to 1990 and 1996 and are due to Prof. F. Mazzolani: they concerned the rehabilitation of the Church of San Giovanni Battista in Carife, near Avellino, and, respectively, that of the new Library of the University of Naples “Federico II”, where STUs were installed in the new roof structures.

In 1999, shape memory alloy devices were used for the rehabilitation of the Upper Basilica of St. Francis of Assisi. Shortly after same devices were used for the rehabilitation of the bell tower of San Giorgio in Trignano in Reggio Emilia, and for other churches such as San Feliciano in Foligno, the Church of St. Seraphim Montegranaro and St. Peter's in Feletto, in Treviso.

With regard to the application, however, energy dissipation devices, there are several recent examples, such as the Cathedral of Santa Maria of Collemaggio in L'Aquila (Figure 1.16) and the facade of Siena Cathedral (Figure 1.17). In the first case was used dampers activated by displacement in the second have been used viscous dampers. (Martelli 2009)



*Figure 1.16 - Santa Maria of Collemaggio Basilica in L'Aquila*

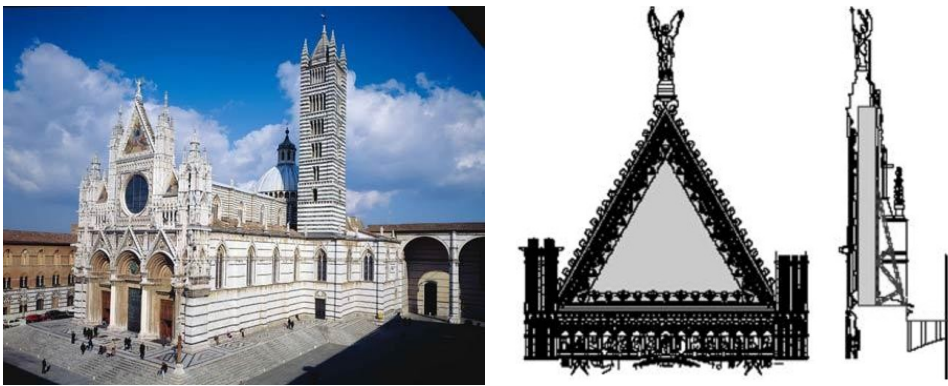


*Figure 1.17 –Siena Chatedral*

Finally, as far as the application of SI to the monumental buildings is concerned, none exists yet in Italy, contrary to countries like the USA and New Zealand: in fact, as mentioned, this kind of rehabilitation is quite costly and delicate in Italy, because the conservation requirements do not allow for any cut of foundations in this country and, thus, SI requires the creation of a sub-foundation, where to install the isolators. However, a pilot project has already been developed, for the Umbrian Churches of San Giovanni Battista at Apagni, near Sellano, which had been severely damaged by the 1997–98 earthquake. The project involved the construction of a sub-foundation below which will be arranged with high damping elastomeric isolators 8 (HDRB)



and 6 sliders (Figure 1.18). The project is, unfortunately, until now, unrealized due to lack of funds.

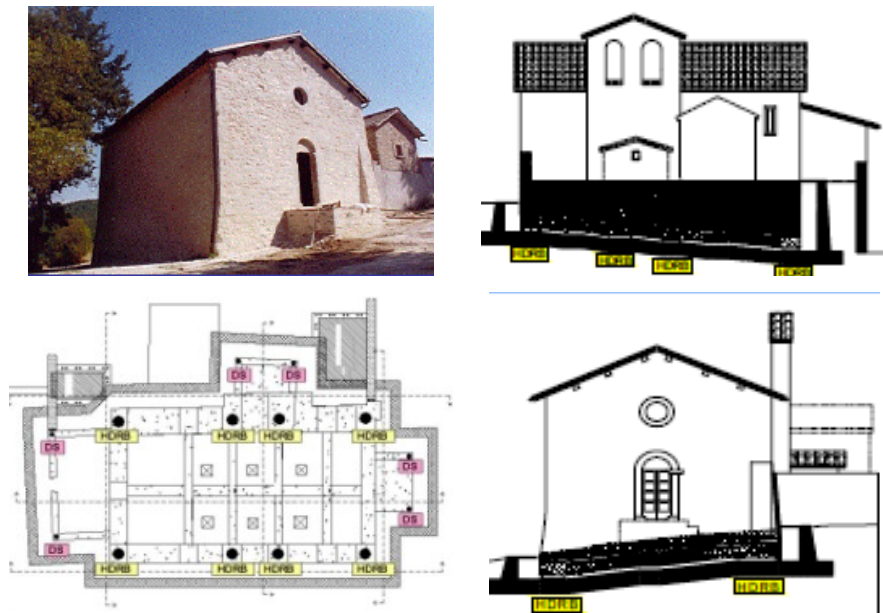


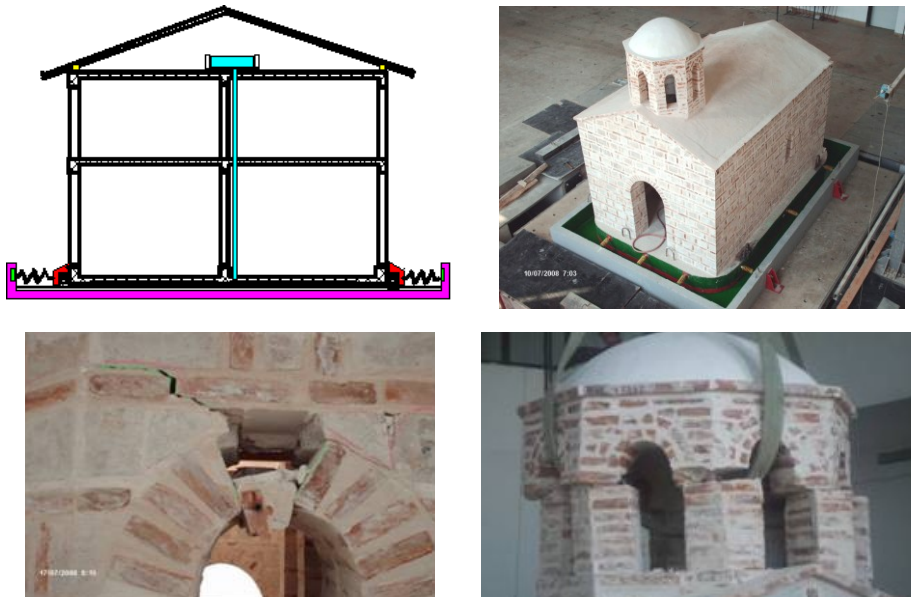
Figure 1.18 –San Giovanni Battista Church at Apagni: seismic isolation project

SI is not applicable or is hardly applicable when:

- the building is too flexible
- the building walls are not structurally connected to one another (as for many historic buildings, in particular churches);
- soil on which the building rests is too soft;
- building is not sufficiently distant from the adjacent ones.

Based on the above it is interesting to cite some studies: Tashkov, Antimovski and Kokalevski (2001) developed a specific sliding system called ALSC. The sliding coefficient between 0.05-0.10 was achieved by using low liquid pressure at the contact instead of that classical teflon pads or sliding bearings, that result expensive solutions, because of high cost of the low friction materials and sliding devices. The upper structure slides over a smooth surface under low pressure. Under horizontal load effect, the structure slides along the foundation base. By controlling the pressure of the liquid, which is located in the empty space under the sliding base, the friction force and the

sliding of the structure are controlled as well. The contact surface must be smooth to reduce the friction between the plates and prevent leakage of the liquid, which is under pressure. Sufficient smoothness can be achieved by coating both contact surfaces with epoxy resin. The sliding and fixed foundation plates are designed to sustain the pressure of the liquid. The zone of the empty space between the two plates is filled with liquid on which pressure is exerted. The horizontal displacement of the structure as well the designed frequency is controlled by horizontal springs.



Very recently, during the international research project PROHITECH, the same concept has been applied on a model of the Byzantine church “St. Nicholas”-Psacha to the scale of 1/3 (Tashkov, Krstevska and Gramatikov-2008). (Fig. 22) In a first phase has been tested the base-isolated model with the ALSC floating-sliding system and in a second phase has been tested the original fixed-base model; in this way has been possible to compare the seismic response for the two different models. From the results is possible to see that the isolation system drastically reduce the transmitted energy to the elevated structure, safeguarding it. Unlike this model, the fixed base model is

very vulnerable. The consequence of the seismic input is an early damage to the dome and and severe damage to the walls.[Tashkov et al. 2009].

This system respect the principal criteria of a good retrofit:

- to apply ALSC system it is necessary to make intervention not in the structure itself, but only in the foundation;
- aesthetic appearance is not disturbed, because all interventions are made under the foundation, which is not visible from outside;
- is totally reversible, infact for restore the original condition of the building is only necessary to exclude the liquid pressure at the contact by simply emptying the compensation reservoir.

Other interesting studies concerning the possibility of obtaining an attenuation of the seismic signal by means of the surface soil treatment interventions, coupled or not with structural elements: (Costanzo et al., 2007), (David Muir Wood, 2006)

Wood, in the NEMISREF (New Mwthods of Mitigation of Seismic Risk on Existing Foundations) project's ambit, carried out experimental studies on the earthquake shaking table at Bristol University. The main motivation of the NEMISREF project was to investigate how an engineered modification of the characteristic of foundation soil could produce an artificial site effetet which would significantly improve the effect of earthquake motion on the structure itself. The mitigation scheme studied involved the construction of a "soft cassion" around and beneath an existing foundation (Figure 1.19), by inserting an horizontal slip layer at some moderate depth (for example aronud 10m), and also inserting soft trenches around the foundation. In this way the foundation can be in somewhat isolated from up ward propagating shear waves. In addition, the soft cassion adds the mass of the soil within the cassion to the mass of the structureand this modifies the dynamic performance by reducing the resonant frequencies. The advantage of a this system is to avoid the classical mitigation techniques that sometimes could be quite costly, intrusive and damaging for monumental building.

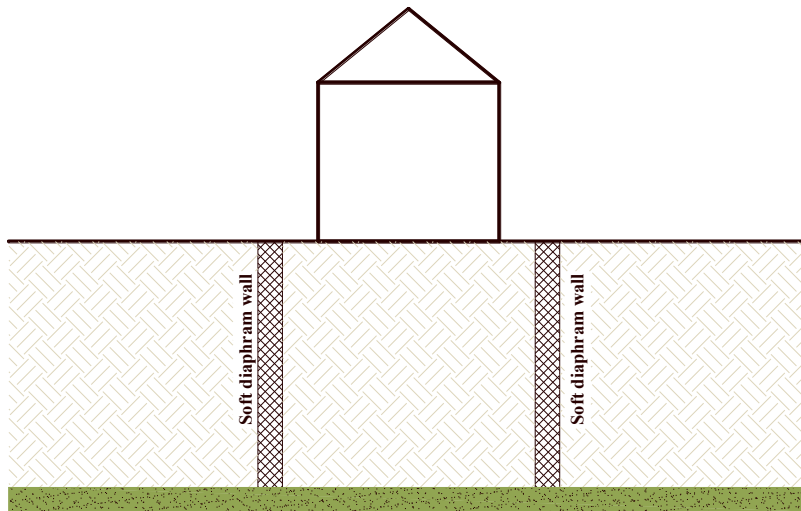


*Figure 1.19 – Scheme for improvement of seismic performance of existing foundation by introducing of a soft caisson*

## BIBLIOGRAPHY

Carbonara G. Il Restauro architettonico (1996) - Utet

Circolare n. 617 del 2.II.2009. Istruzioni per l'applicazione delle nuove norme tecniche per le costruzioni. Ministero delle infrastrutture e dei trasporti

Costanzo et al 2007

DM 14/1/2008. Norme Tecniche per le Costruzioni. S.O. n. 30 - Gazzetta Ufficiale della Repubblica Italiana, No. 20 - 4/2/2008

D.M. 24/1/86 of the Ministry of Public Works (G.U. n.108 of 12/5/86)

De Luca A., Serino G. [1989] "Nuovi sistemi strutturali per la difesa dal rischi sismico" – *Ingegneria sismica 1: 3-18*.

Dolce, M., Cardone, D., Ponzo, F.C., Di Cesare, A. – Progetto di Edifici con isolamento sismico 2007 – *IUSS Press Pavia* - Italia

Dolce, M., Martelli, A., Panza, G. 2005. Proteggersi dal Terremoto– Le Moderne Tecnologie e Metodologie e la Nuova Normativa Sismica (Let's Protect Ourselves from Earthquakes– The Modern Technologies and Methodologies and the New Seismic Code), Seconda edizione. Milano: 21mo Secolo.

Dolce, M., Martelli, A., Panza, G. 2006. Moderni Metodi di Protezione dagli Effetti dei Terremoti (Modern Methods for the Protection from Earthquake Effects), *Special edition for the National Civil Defence Department* (A. Martelli editor), Milano: 21mo Secolo.

Kelly J.M. [1991] "Dynamic and failure characteristics of Bridgestone isolation bearings" *EERC Report no. 1991-04, College of Engineering, University of California, Berkeley*.

Kelly T. [2001] “Base Isolation of Structures – Design Guidelines” *Holmes Consulting Group Ltd, Wellington, New Zealand*.

Linee Guida per la valutazione ed riduzione del rischio sismico del patrimonio culturale - *Ministero per i Beni e le Attività Culturali* – Circolare n. 26 del 2.12.2010

Martelli, A. 2007. Moderni sistemi antisismici per la protezione del patrimonio storico, artistico, architettonico ed archeologico (Modern anti-seismic systems for the protection of cultural heritage). *Invited lecture in Proceedings of the Congress “Conservazione: una Storia Futura” (“Conservation: a Future history”)*, Salone dell’Arte del Restauro e della Conservazione, Ferrara, 2007. Rome: Ministero dei Beni e delle Attività Culturali.

Martelli, A. & Rizzo, S. 2007. Development and application of innovative anti-seismic systems for the protection of cultural heritage. *AIDA IV – Annuario Italiano di Archeometria* 4: 28–30.

Martelli, A., Sannino, U., Parducci, A., Braga, F. 2008. Moderni Sistemi e Tecnologie Antisismici – Una Guida per il Progettista (Modern Anti-Seismic Systems and Technologies – A Guide for the Designer). Milan: 21mo Secolo.

Martelli, A., 2009. *Proceedings of International Conference Prohitech09*. Rome June 2009 Italy.

Naeim F. Kelly J. M.- Design of seismic isolated structures- *From Theory Practice*- J. Wiley & Sons, New York, 1999.

Sannino, U., Sandi, H., Martelli, A., Vlad, I. 2008. Modern Systems for Mitigation of Seismic Action – *Proceedings of the Symposium Held at Bucharest*, Rumania, on October 31, 2008, Bucharest: AGIR Publishing House.

Santini, A. & Moraci, N. (eds.) 2008. *Proceedings of the 2008 Seismic Engineering International Conference Commemorating the 1908 MEssina and Reggio Calabria EArthquake (MERCEA'08)*, Volume 1020. Danvers, MA: American Institute of Physics.

Tashkov, Lj., Krstevska, L. & Gramatkov, K. 2008. Shaking table test of model of St. Nicholas church to scale 1/3.5., *PROHITECH*, Final Report. Skopje:IZIIS

Tashkov L., Krstevska L., Gramatkov K., Mazzolani F. - Shake- Table Test of the Model of St. Nicholas Church in Reduced Scale 1/3.5 [2009] - *Proceedings of the International Conference Prohitech' 09 Protection of historical building, Volume I. F.M. Mazzolani editor*

Wood David Muir – *4th International Conference on Earthquake Geotechnical Engineering – Invited Lectures* June 2006 Thessaloniki, Greece, Kryazis D. Pitilakis editor

Zayas V. A., Low S. S. Mahin S. A. [1987] “The FPS earthquake resisting system: experimental report”, *UCB/EERC-87/01, Berkeley, California, USA*.

This page is, intentionally, left blank



## Chapter 2

# The question of the seismic site response

### 2.1 INTRODUCTION

During an earthquake, when seismic compression (P waves) and shear waves (S waves) approach a site, they undergo modifications while propagating through surface deposits (Figure 2.1). The variations of ground shaking in space, amplitude, frequency content and duration are called “site effects”.

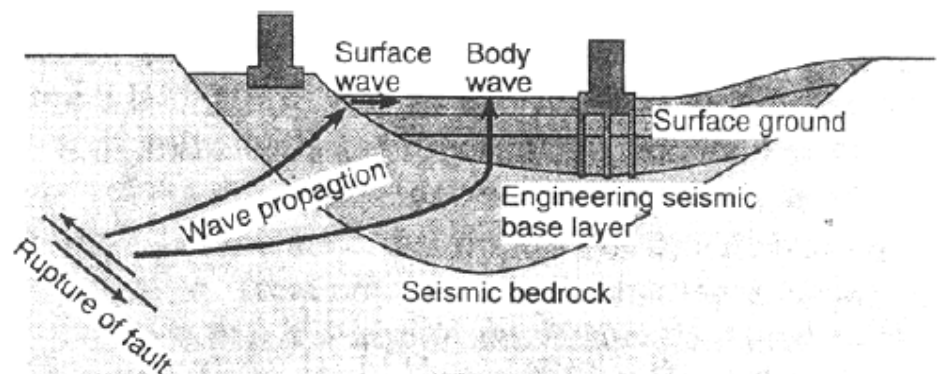


*Figure 2.1 – Schematic illustration of the wave propagation from fault to ground surface  
(Pitilakis, 2004)*

It is now widely recognized that local seismic effects can have a significant influence on the level and distribution of seismic motion and damage during

earthquakes. (Pagliaroli 2006)

The variability of properties of soil, which is seen passing from one vertical to another of the same area of investigation, infact, induces an also very great differentiation of the seismic response within very limited areas (seismic response). The phenomenon has emerged from the observation of numerous cases in which there was, during a seismic event, damage highly differentiated in the same area due to local conditions. In 1906 San Francisco earthquake of local amplifications, corresponding to unconsolidated sediments, caused variations in intensity up to 2 degrees (MM scale), while Mexico City is built on the lacustrine soft clay deposits, which have caused large amplification of seismic motion, responsible for large losses of human lives and economic damage during the earthquake of 1985. (Figure 2.2)



San Francisco, California 1906



New Mexico City, New Mexico 1985

*Figure 2.2 –Site effects in the San Francisco and new Mexico City earthquakes*

Earthquakes in Niagata in Japan and Anchorage in Alaska, both in 1964, many serious damage was attributable the liquefaction of sandy soils. (Figure 2.3)



Niigata, Japan 1964



Anchorage, Alaska 1964

*Figure 2.3 – Site effects in the Niigata and Anchorage earthquakes*

Almost all recent destructive earthquakes (Spitak, Armenia 1988, Loma Prieta, 1989, Iran 1990, Philippines 1990, Northridge 1994, Kobe 1995, Armenia, 1999 Columbia, El Salvador 2001, Chile 2010, Japan 2011) have provided further evidence of importance of site effects (Figure 2.4). (Savoldelli, 2008)



Izmit, Turkey 1999



Japan 2011



Chile 2010

*Figure 2.4 – Site effects in some recent destructive earthquakes*

Possible seismic hazard scenarios related to local effects are:

- a) Amplification
- b) Liquefaction
- c) slope instability
- d) densification of loose granular soils
- e) collapse of underground cavities

The site effects are the result of many physical phenomena (multiple reflections, diffraction, focus, resonance, etc.) that the waves undergo because of the heterogeneity and discontinuity of the surface layers and of topographic irregularities.

They include the effects of impedance contrast of surface soil deposits to the underlying bedrock, or firm soil considered as rock; deep basin effects, and basin edge effects, produced from strong lateral geological discontinuities (e.g. faults). Finally, site effects also include spatial variation of ground shaking characteristics due to surface topography (Lanzo and Silvestri, 1999). (Figure 2.5)

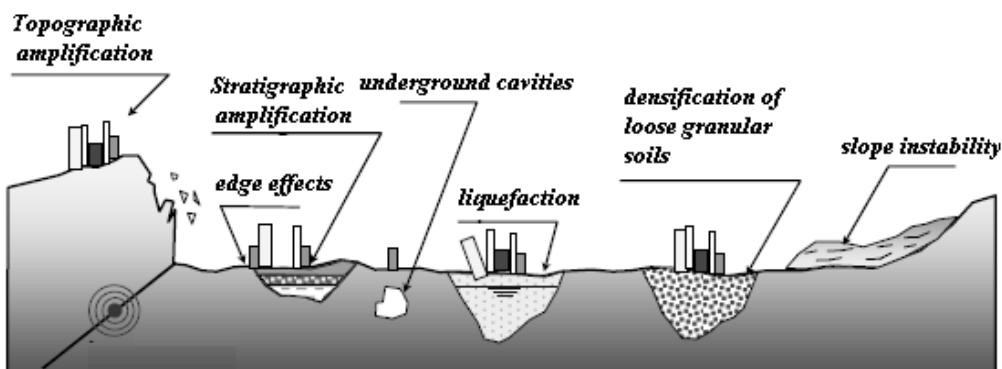


Figure 2.5 – Seismic hazard scenarios related to site effects (modified from Lanzo 2010)

Depending, therefore, the main physical phenomena responsible for the site effect can be distinguished (Figure 2.5):

- stratigraphic effects (or 1D)
- topographic effects
- edge effects (or downstream)

This division is particularly significant also from a operational point of view as to the different categories are also different methods and tools for quantitative evaluation of local seismic response. (Pagliaroli 2006)

The site effects evaluation requires a study of local seismic response, which can be conducted on different levels of detail. The output can then be in terms of analytical functions that define the filter effect on the seismic signal (transfer function) or by synthetic parameters that express the amplification on the surface through the ratio of kinematic quantities associated with the seismic motion (amplification factor). In the chapter, are therefore recalled some theoretical and experimental evidences respect to each category of site effects, focusing on the stratigraphic effects.

## **2.2 STRATIGRAPHIC EFFECTS (1D)**

The stratigraphic effects are all the modification that a seismic motion undergoes propagating itself, almost vertical direction, within a deposit to the free surface plane, characterized by substantially horizontal stratification and negligible lateral variation. This situation is usually analyzed through a one-dimensional modeling, in which the various layers define a sequence of homogeneous elements, with constant thickness, undefined in the plant, different in terms of physical characteristics and mechanical properties of materials that constitute them. Even with the simplification of considering each layer of soil homogeneous and isotropic, it is impossible to ignore the heterogeneity due to alternating layers that implies the presence of separations surface that represent discontinuities for propagating waves generated by the earthquake.

When, in fact, an elastic wave impacts on a discontinuity between two materials with different mechanical properties is in part reflected in coming medium in part refracted i.e. it goes beyond the interface.

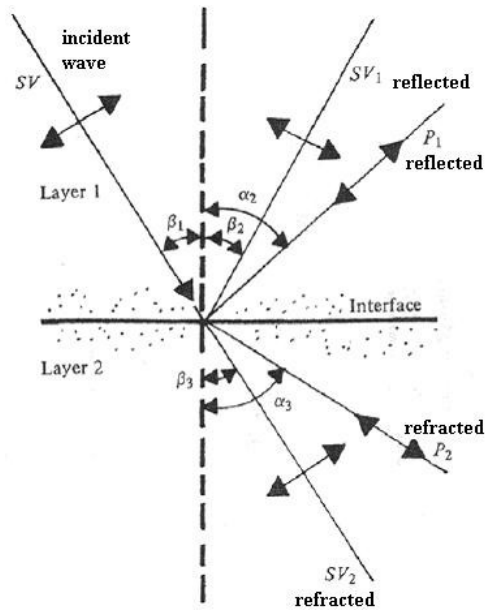


Figure 2.6 - Reflection and refraction of incident waves of SV type at an interface between two materials with different mechanical properties (modified from Das, 1993).

The waves reflected and refracted from the original take on different directions according to Snell's law:

$$\frac{\sin i}{V} = \frac{\sin t}{V} \quad (2.1)$$

In which  $i$  is the angle between the radius of the seismic wave and the normal to the interface and  $V$  is the propagation velocity of the wave of interest (P or S).

From (2.1) can be deduced that:

- angle of reflection equals the angle of incidence for both S waves and for those P;
- angle of refraction and angle of incidence is related to the ratio of the velocities of propagation of the waves on the two materials separated by the interface.

In particular, therefore, if the waves are traveling from a material characterized by a velocity to a another characterized by lower velocity the refracted ray come close the normal to the interface, in other words, waves that propagate upward in layers with decreasing stiffness, as is usual at the surface of the earth, tend to be refracted in a direction that tends to approach the vertical. However, if the waves traveling to medium at greater stiffness, the wave refracted tends to move away from the normal to the interface. This is the case for example of the waves, reflected at the topographic surface, travel to the bottom layers characterized by increasing stiffness.

At the interface as well as a change of direction of wave propagation and generation of different phases of the incident one, even a change of the amplitudes of the waves. The amplitudes of the waves reflected and refracted can be expressed as a function of the incident wave amplitude by imposing conditions of continuity of displacements and forces at the interface. The discussion is particularly complex for general angle of incidence while greatly simplifies for the case of vertical incidence.

In this case, indicating the amplitude of phase with  $A_I$  incident  $A_R$  and  $A_T$ , respectively, the amplitudes of the phases of reflected and refracted, we have:

$$\begin{aligned} A_R &= \frac{1 - \mu}{1 + \mu} A_I \\ A_T &= \frac{2}{1 + \mu} A_I \end{aligned} \tag{2.2}$$

where  $\mu = \frac{\rho_2 V_2}{\rho_1 V_1}$  is the ratio impedance between the layer 2 (destination and layer 1 (origin)

From (2.2) is easy to see that when the provenance medium is more rigid than destination one ( $I < 1$ ) the amplitude of the transmitted wave increases compared to that of the incident waves ( $A_T > A_I$ ). To a decrease in stiffness of the medium is accompanied thus increased the amplitude of the waves. Conversely, when the wave encounters a medium that can be considered infinitely rigid than that of origin ( $I \rightarrow \infty$ ) the amplitude of the reflected wave tends to be equal and opposite to that of the incident wave while that of the transmitted wave tends to zero—that is, the wave is completely reflected in the middle of origin.

From the above, then you wrote that the incident waves at the base of the deposit and fully reflected at the free surface are, in turn, in part reflected in part refracted at the interface-deposit base. The reflected energy “trapped” in the deposit increases with increasing seismic impedance contrast between the soil layers and the bedrock of the deposit while the refracted energy go away from the deposit resulting in a loss of energy indicated, generally, as radiation damping. The waves “trapped” in the deposit interfere with each other and the incident waves in relation to the geometric characteristics of the deposit, the physical and mechanical properties of soils and the frequency content of the signal.

Analytically solving the problem of wave propagation in a layered medium, although very complex, is solved in closed form in the frequency domain. For more detailed discussion of this issue, please refer to Chapter 7, for the time to understand the essential features of the stratigraphic site effects is possible refer to a simple scheme consisting of a one-dimensional homogeneous soil deposit of thickness  $H$ , resting on a base subject to vertically propagating shear waves. (Figure 2.7)



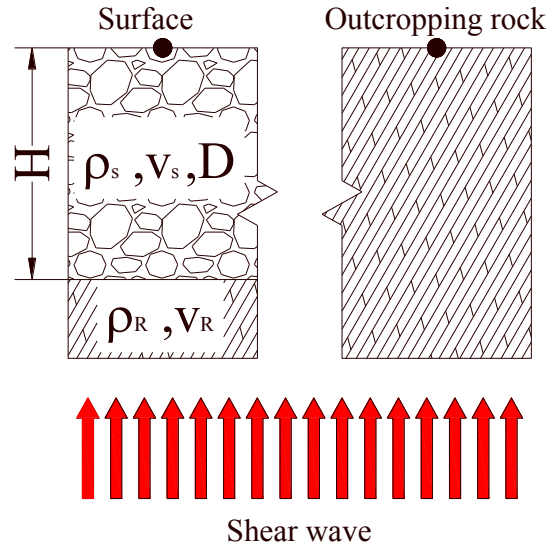


Figure 2.7 - Scheme 1D to study the problem of wave propagation in a layered soil: visco-elastic linear homogeneous soil deposit on elastic bedrock with vertical incident shear wave

The soil is assumed to linear visco-elastic behaviour with  $\rho_s$  density, shear wave velocity  $v_s$  and damping ratio  $D$ , while the parameters for the bedrock are  $\rho_R$ ,  $v_R$  and  $D_R = 0$ . The variation of the seismic motion is evaluated by comparing the parameters of motion at the surface of the deposit to the corresponding parameters of the bedrock (reference site).

The theoretical analysis of the problem (Kramer, 1996; Lanzo and Silvestri, 1999) shows that, if the incident shear waves are sinusoidal with frequency  $f$ , the acceleration of the outcropping rock and of the surface of the deposit are also sinusoidal with frequency  $f$  and amplitude  $a_{max,r}$  and  $a_{max,s}$ , respectively. The relationship between the two above-mentioned amplitude  $a_{max,s}/a_{max,r}$  is defined amplification factor and it depends on the frequency and harmonic excitation, the damping ratio  $D$  of the soil and the seismic impedance contrast between soil deposit and bedrock. The variation of the amplification factor with the frequency defines the amplification function  $A(f)$  of the deposit where the typical trend for a given value of the impedance ratio and the damping ratio  $D$  is shown in.

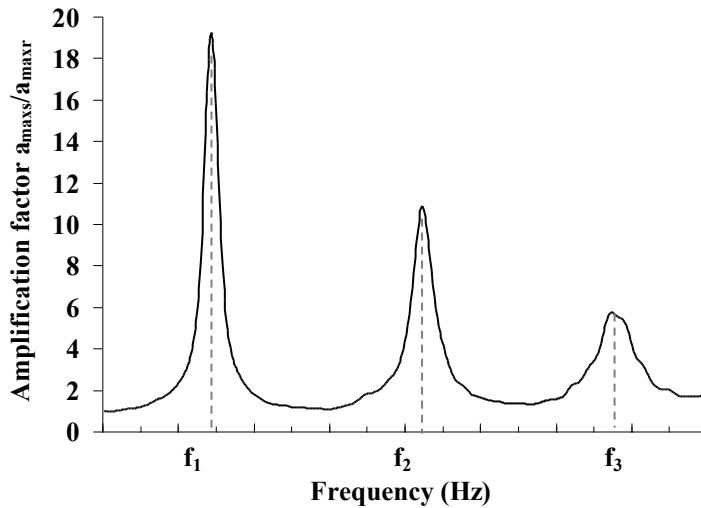


Figure 2.8 – Typical trend of amplification function

It is known that the ground motion is amplified at certain frequencies  $f_n$  defined natural frequencies of vibration of the deposit:

$$f_n = \frac{V_S(2n-1)}{4H} \quad n = 1, 2, \dots, \infty \quad (2.3)$$

In which we have the fundamental and higher amplification peak for  $n=1$  corresponding to the fundamental frequency of the deposit:

$$A_{\max}(f_1) = \frac{1}{\frac{1}{I} + \frac{\pi D}{2}} \quad \text{with } f_1 = \frac{V_S}{4H} \quad (2.4)$$

For loads with significant energy content near to the natural frequencies, important phenomena of amplification seismic motion occur.

Despite the simplicity of the model assumed, previous relationships clearly show the main geotechnical parameters that govern the amplification effects related to stratigraphy. The shear wave velocity  $V_S$  is a fundamental parameter

because it, not only the geometric characteristics, determines the fundamental frequency of the deposit. The  $f_1$  can vary typically between 0.2 Hz (very thick deposits much like the subsoil of the city of Los Angeles and Tokyo or deposit extremely soft as those of Mexico City) and 10 Hz (for very thin deposits and/or land more rigid).

In addition,  $A_{\max}(f)$ , as evident in (2.4) depends on the impedance contrast between the soils of the deposit and the basement (I) and on dissipative characteristics of the soil (D): increases at I increasing and decreases with D increasing.

Experimental and analytical studies have shown that the amplitude of the peaks of the amplification function very often reaches values between 6 and 10 and, in extreme cases such as Mexico City (high impedance contrast and low damping), exceed 20.

In practice, a rapid and simple quantitative estimate of the local seismic response of a site is provided by the amplification factor is calculated by comparing the maximum values of the accelerograms (PHA) recorded (or calculated) to the surface of the deposit and the reference site. The amplification function, however, allows quantify the variations in the frequency content of the seismic signal and is estimated by the ratio of the corresponding Fourier spectra.

The vibration frequencies and with it the function of amplification of the deposit, as evident by (2.3) in linear field, are independent from the input seismic and therefore an intrinsic feature of the site in question.

This last statement becomes invalid when the soil enters the field is not linear. By increasing the intensity of the input seismic shear deformations in fact exceed the threshold of linearity (Figure 2.9) and the local seismic response is also influenced by non-linear behavior of soil.

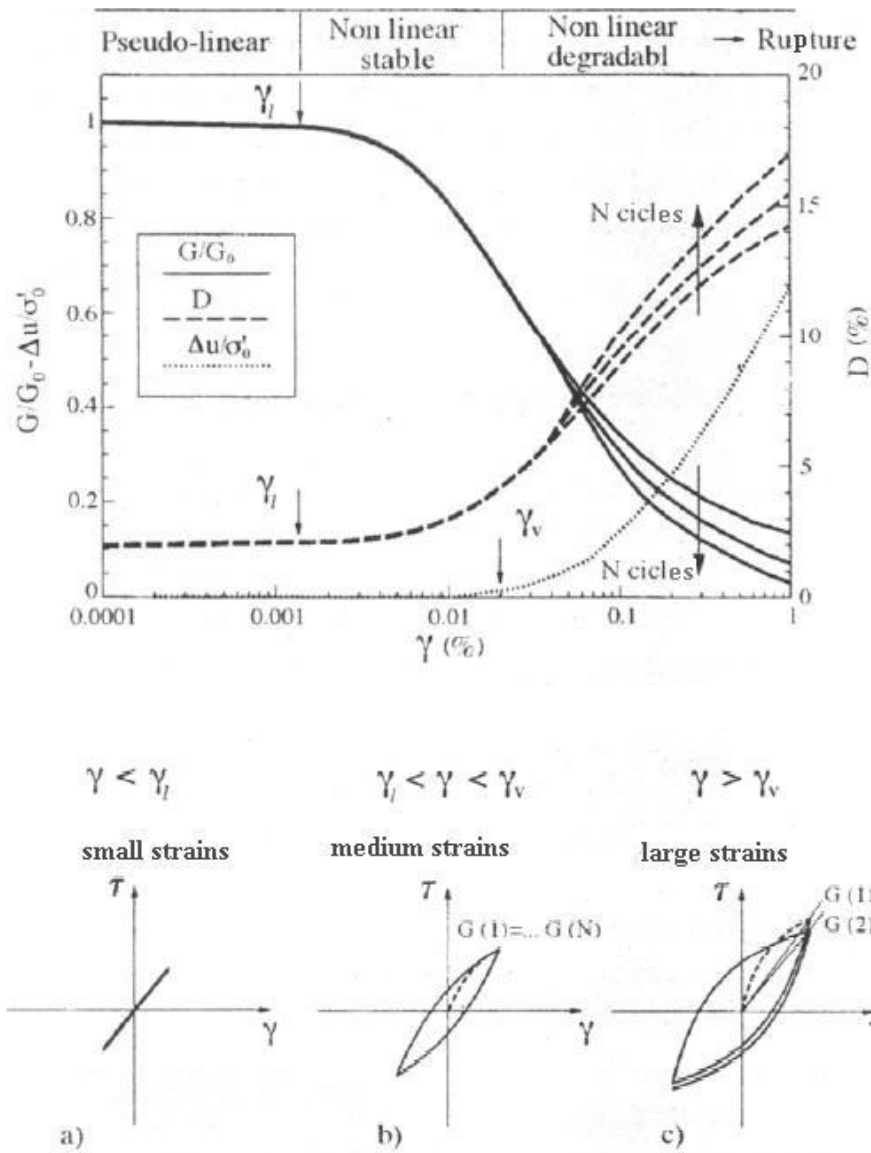


Figure 2.9 - Typical range of behaviour for a soil under cyclic shear load (modified from Lanzo Silvestri 1999)

In a stratified soil real then, a proper assessment of site effects can not but take into account variations the characteristics of stiffness and damping with the level of deformation induced by the earthquake. In general, the increasing

incidence of non-linear behaviour, the fundamental frequency decreases (or increases the fundamental period) due to the decrease in shear stiffness (i.e.  $V_s$ ) with increasing shear strain  $\gamma$ , the maximum amplification given by (2.4) is reduced instead to the effect of damping ratio with  $\gamma$ . (Figure 2.10)

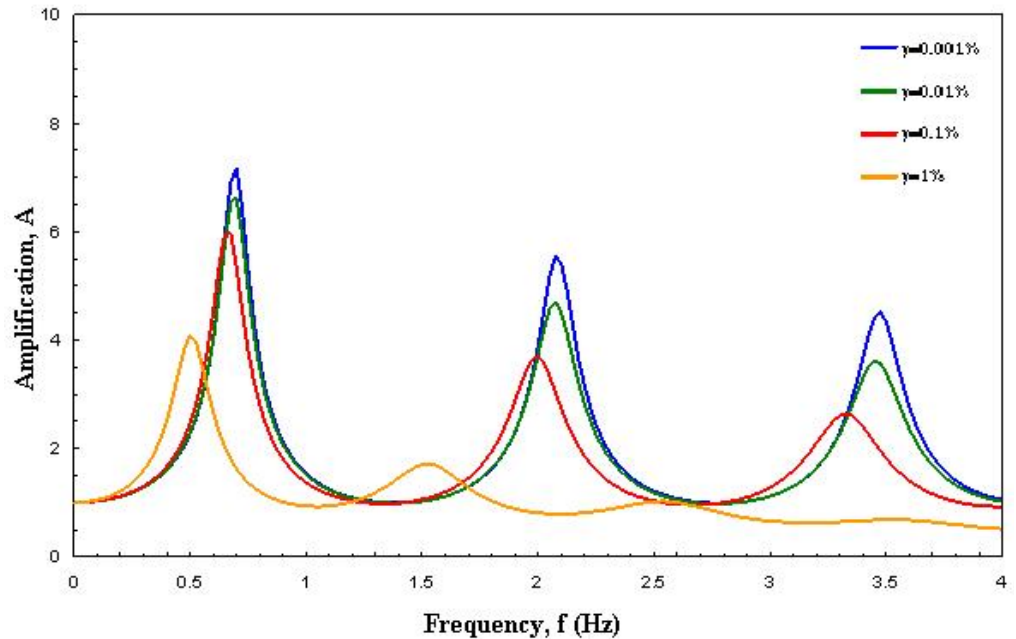


Figure 2.10 – Non linearity effect on the amplification function

From previous observations it follows, therefore, that the amplification function for a real ground is not a property of the site as well as characteristics of the subsurface stratigraphic also depends on the amplitude and the frequency content of the seismic motion at the base and the incidence of non-linear behavior.

Numerical and experimental evidence show that for low energy levels of the reference earthquake, the peak ground acceleration at the surface of the deposit is generally amplified compared to the outcrop of the basement. For high energy levels, however, the peak acceleration can back down.

For sandy soils data collected (Silva 1991) seem to indicate the dependence of the amplification factor also on the thickness of the deposit. For deposits of small thickness (generally less than 30 m) the factor is of high value until the measured values of acceleration on rock reaches the order of 1.0g, while the

same sandy deposits with high thickness (greater than 100-150 m), giving rise to a deamplification for acceleration input values above  $a_{max,r} \approx 0.4g$ .

There are many experimental, analytical and numerical studies on site effects due to the presence of soft soil layers overlying bedrock. The most famous example is certainly the Kobe earthquake of 1995 during which the surface layer (about 15 m thick) liquefied: because of the non-linearity effect the horizontal component of motion on the surface, consequently, attenuated compared to motion in depth and showed the appearance of significant low-frequency components, while the vertical component not resulted influenced showing a substantial amplification along the profile. (Pagliaroli, 2006)

### 2.3 EDGE EFFECTS (OR DOWNSTREAM)

The amplification phenomena observed at the edges of alluvial valleys can be significant and accompanied by significant increases in the duration of seismic motion than predicted by theory on the one-dimensional propagation of shear waves with vertical incidence.

In the case of alluvial valleys or basins to the phenomena described for the one-dimensional case, they add up others due to two-dimensional (or three) configuration and mainly:

- seismic waves focusing in areas close to the valley edge due to constructive interference between the incident and diffracted wave field;
- generation, at the base-soil interface at the edge of the valley, of surface wave propagation with horizontal direction;
- 2D resonance of the entire valley.

The first phenomenon has been indicated at several seismic events, such as damage due to localized areas placed along the edge of the alluvial valleys (see eg. Pitarka et al., 1996).

The second phenomenon is well documented by experimental observations (see eg. Phillips et al. 1996; Raptakis et al., 2000). The surface waves generated at mechanical discontinuities, remain, in the presence of significant impedance contrasts, trapped in the valley and are subject to multiple reflections at the edges of the valley as their movement limited only by the

damping of the soils. They can then give rise to important phenomena of interference between them and the waves of volume incidents. One consequence of these phenomena is a seismic response markedly different from point to point along the surface of the valley, over distances comparable with the wavelengths involved, which may also be of the order of few tens of meters. This has important differential movements of the ground with significant applicative implications for seismic design of structures at a considerable linear development.

The seismic response of a sedimentary valley is fundamentally conditioned by its geometry. A very significant parameter is the aspect ratio defined as the ratio between the maximum depth  $h$  of the valley and its half-width  $l$ . When the ratio  $h / l$  is low (approximately  $<0.2$ ) is called shallow valleys and the phenomenon of amplification has, in the frequency domain, the same characteristics of a 1D phenomenon. In other words, the fundamental frequency, at which the maximum amplification of the motion, it is next to the one-dimensional.

Under these conditions, for points away from the edges, the fundamental characteristics of the motion can sometimes be predicted with simple 1D models (Bard and Gariel, 1986). For higher values of  $h / l$  (deep valleys) the dynamic response of the valley is significantly different because of two-dimensional resonance.

The main features of the phenomenon of resonance of a 2D sedimentary valley, is highlighted by numerical studies (Bard and Bouchon, 1985) and experimental (Tucker and King, 1984), are as follows:

- the frequency corresponding to the maximum spectral amplification (fundamental frequency of resonance) is the same anywhere in the valley, regardless of the local thickness of the sediments,
- the corresponding amplification is maximum at the center of the valley and decreases moving towards the edges at which you cancel,
- the resonant frequency of the ground motion is in phase at all points of the valley.

As in the 1D case, there are different modes of vibration each with a resonance frequency, usually in the presence of typical values of the damping of soils that tends to lower the higher modes, the dynamic response of the

valley is controlled by the first three modes vibration. The fundamental frequency of resonance 2D assumes values significantly higher than the fundamental frequency and it is responsible 1D amplifications very high (up to 4 times the one-dimensional case), it is also insensitive to the angle of the waves. If the semi-length of the soil structure is comparable to its thickness (deep basins), and the rebervarating back and forth surface waves are in phase, the waves interfere with each other leading to 2D resonance patterns. The same resonance effects are involved in the seismic wave modulation due to 3D soil structures. The consideration of the second and third lateral dimension in the wave propagation phenomena, in case of 2D and 3D resonance, leads to an increase in ground motion amplification and a shift towards higher values of the peak frequencies (Figure 2.11). (Bard e Riepl-Thomas, 1999)

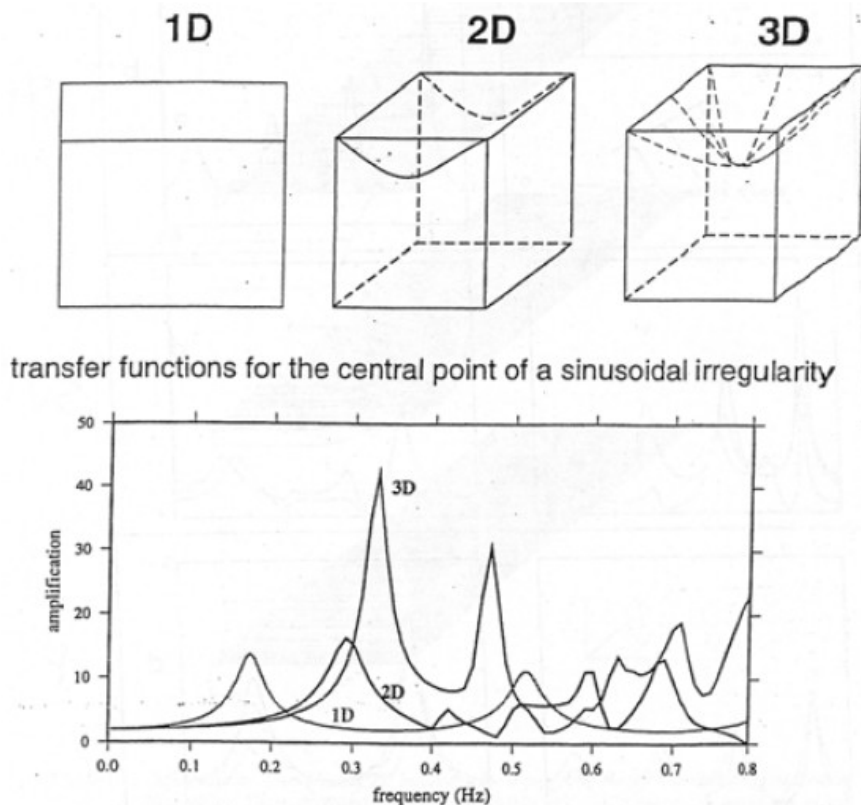


Figure 2.11 –Amplification function in the center of a valley for 1D, 2D or 3D geometric configuration (Bard e Riepl-Thomas, 1999)



## 2.4 TOPOGRAPHIC EFFECTS (2D OR 3D)

The term “topography effects” refers to the variations in ground motion due to the geometry of the ground surface. The damage pattern during earthquakes often shows that most damage tends to concentrate around hilltops and slope crests. Moreover, there is clear instrumental evidence that surface topography affects both the amplitude and frequency content of ground motion. (Bard and Riepl-Thomas, 1999)

The phenomenon's importance is widely documented: Alaska 1964 (Idriss e Seed, 1967), Friuli 1976 (Brambati et al., 1980), Irpinia 1980 (Siro, 1982), Cile 1985 (Celebi, 1987), Northridge 1994 (Celebi, 1995; Bouchon and Barker, 1996), Egion 1995 (Athanasopoulos et al., 1999), Umbria-Marche 1997 (Rovelli et al., 1998; Marsan et al., 2000), Eje Cafetero-Colombia 1999 (Rastrepo e Cowan, 2000), Atene 1999 (Athanasopoulos et al., 2001; Kallou et al., 2001).

From the engineering point of view topographic amplification of seismic motion affects the assessment of seismic risk of numerous historical centres built on relief, of important works such as bridges and dams as well as natural and artificial slopes.

The size of topographic amplification and physical phenomena that cause it vary with the type of morphological configuration considered. According to Stewart et al. (2001) we can distinguish three main categories: isolated relief, slope and canyons (Figure 2.12).

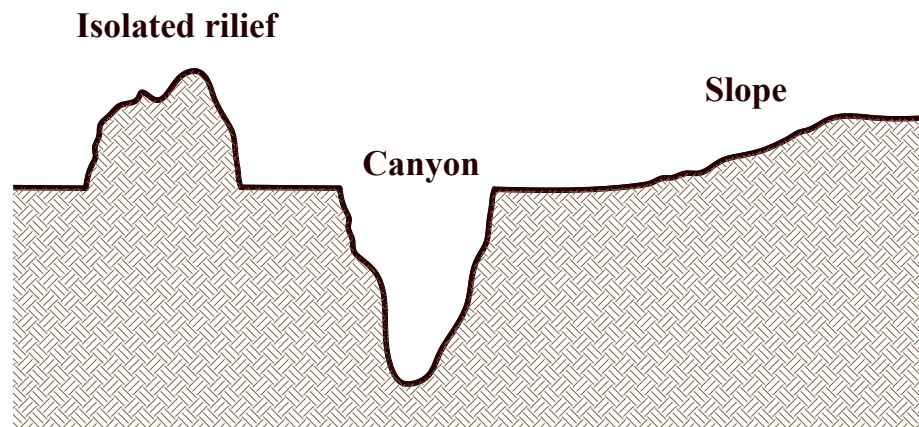


Figure 2.12 – Main topographic configurations

The typical situation of the cliff for small width in crest can be reduced to the case of isolated relief and for widths greater it tends to the limit case of a slope. A summary of the main conclusions of literature studies on topographic amplification regarding to the first two mentioned categories has reported, while for the canyons to see a thorough study by Pagliaroli (2006).

#### **2.4.1 *Isolated relief***

It must be said that the first difficulty in the study of the effects of natural topographic irregularities is related to the fact that they are characterized by a heterogeneous subsurface in general, thus the effects of topography coexist with those associated with variations in impedance of the materials involved, i.e. with stratigraphic effects.

The main conclusions can be derived from an examination of the major numerical studies and experimental literature and are summarized below (see also the states of the art of Geli et al., 1988 and Bard and Riepl-Thomas, 1999):

- on top of a topographical survey the ground motion is amplified compared to the base,
- in the frequency domain topographic amplification is maximum in a frequency band corresponding to wavelengths comparable to the width of the relief,
- topographic amplification tends to increase with increasing the gradient of the relief, ie the aspect ratio  $H/L$ ,  $H$  being the height of the relief and the half length  $L$  measured at the base,
- if the incident wavelengths are lower than the extension of relief along the slopes of these may occur with rapid alternations of phenomena of amplification and attenuation, and consequently important differential movements,
- topographic amplification is lower for incident P waves than in the case of S waves,
- topographic amplification depends in a complex way on the angle of incidence of the waves and it is not possible to draw general conclusions, in first approximation does not impact the area of maximum vertical

amplification tends to move from the ridge to the side opposite to the relief the propagation direction,

- experimental reports of amplification (especially in the frequency domain) are generally greater than those expected theoretically due to multiple factors: amplification and stratigraphic effects of morphology generally included often buried in the site so far, wrong choice of the reference station, the effects markedly three-dimensional topographic influence of adjacent effects of directivity of the source mechanism.

Regarding the main physical phenomena responsible of topographic effects, the following factors can be identified: the sensitivity of the surface motion to the incidence angle; the focusing or defocusing of seismic waves reflected along the topographic surface; the diffraction of body and surface waves, leading to interference patterns between the direct and diffracted waves (Bard and Riepl-Thomas, 1999). (Figure 2.13)

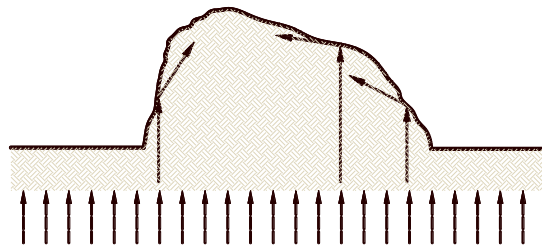


*Figure 2.13 – Waves focusing mechanism to the crest of a relief*

More recently Faccioli et al. (2002) have attributed topographic amplification to two different phenomena. The first is still the waves focusing due to the incidence of morphologies locally convex and can be interpreted as densification of seismic rays on the basis of simple methods geometrical optics (see Sanchez-Sesma 1990). The second phenomenon is the relief resonance that occurs if the wavelength of the seismic action is comparable with the horizontal dimension of topographic irregularity. The two phenomena have different effects: if the focus tends to produce very specific amplifications located in determinated areas of relief alternating with deamplifications areas (destructive interaction between the waves), the resonance involves in an amplification that affects the entire relief, increasing from the base to the crest. (Pagliaroli, 2006)

### 2.4.2 Slopes

The technical literature relating to studies on morphology like a slope (or step) is much weaker than the case of isolated relief. Possible explanations for this lack are the absence of experimental measurements and analytic complication related to the topographical asymmetry. Since the early numerical studies on the topic (Idriss and Seed, 1967; Idriss, 1968), most researchers have dealt with particular aspects of the phenomenon (Boore, 1972; Ohtsuka and Harumi, 1983; Sitar and Clough, 1983 ; Tagliani, 1985) or, more recently, specific case studies (Athanasopoulos et al. 1999; Kallou et al. 2001; Sholtis Stewart, 2004). The only parametric studies that have systematically investigated the topographic amplification factors influential for this particular morphological configuration, are constitutive of the work of Ashford et al. (1997), Ashford and Sitar (1997) and Bouckovalas and Papadimitriou (2004).

In particular, we report some evidence resulting from this last study (Bouckovalas and Papadimitriou, 2004) on the variation of seismic motion of a homogeneous slope with linear viscoelastic behaviour, subject to harmonic SV wave incident vertically to vary several factors (inclination of the slope, damping material, number of stress cycles and  $H/\lambda$ ,  $H$  being the height of the relief and the incident wavelength  $\lambda$ ):

- ground motion is, generally, amplified at the crest and deamplified at the foot, then the topographic amplification factor is significantly overestimated at the crest when the motion at the crest is related at the base of the slope;
- presence also of a purely horizontal action, a significant vertical motion is induced at the surface: at the crest vertical accelerations can achieve the same order of magnitude of the horizontal acceleration of free-field conditions;

on the shelf behind the crest of the slope are alternated, even within small distances, areas of deamplification and zones of amplification of seismic motion, whose experimental verification would require extremely dense array and the amendment of the seismic motion due to the topography is not located at the crest but goes sensitive to distances, typically varying between 2 and 8 times the height of the slope  $H$ .

The authors attribute the last two results to the incidence on the shelf behind the crest of the reflected waves SV and P on the surface of the slope, to the

propagation, on it, of Rayleigh waves generated at the crest and to the possible interaction between these waves (reflected and diffracted ) with the incident wave field. Moreover, the same study it was found that the sensitivity of topographic amplification is greater towards the slope inclination and the ratio  $H/\lambda$ , not in relation to the damping and the number of cycles, which have a limited influence. Finally, both the amplification at the crest that deamplification at the foot of the slope increases with increasing slope. (Figure 2.14)

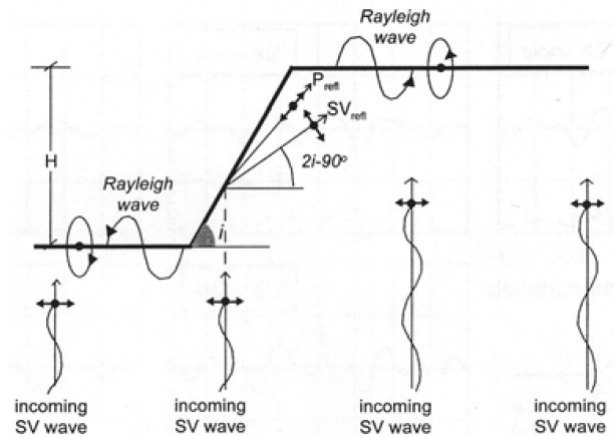


*Figure 2.14 - Schematic representation of the main physical phenomena occurring in a slope subjected to vertically propagating SV waves*

It seems obvious that the analysis of a problem related to topographic irregularities and edge effects (or downstream), according to the specific morphology of the case, it should be made through the implementation of 2D or 3D model.

## BIBLIOGRAPHY

- Ashford S. A., Sitar N., Lysmer J., Deng N. (1997). Topographic Effects on the Seismic Response of Steep Slopes. *Bulletin of the Seismological Society of America*, 87: 701-709
- Ashford S. A., Sitar N. (1997). Analysis of Topographic Amplification of Inclined Shear Waves in a Steep Coastal Bluff. *Bulletin of the Seismological Society of America*, 87: 692-700
- Athanasopoulos G. A., Pelikis P. C., Leonidou E. A. (1999). Effects of surface topography on seismic ground response in the Egion (Greece) 15.VI.1995 earthquake. *Soil Dynamics and Earthquake Engineering*, 18: 135-149.
- Athanasopoulos G. A., Pelikis P. C., Xenaki V.C. (2001). Topography effects in the Athens 1999 earthquake: the case of Hotel Dekelia. *Proc. of 4th Int. Conf. on Recent Advances in Geotechnical Earthquake Engineering and Soil Dynamics*, San Diego, California
- Bard P.-Y. (1982). Diffracted waves and displacement field over two-dimensional elevated topographies. *Geoph. Journ. Royal Astr. Soc.*, 71: 731-760.
- Bard P.-Y., Bouchon M. (1985). The two-dimensional resonance of sediment-filled valleys. *Bulletin of the Seismological Society of America*, 75: 519-541.
- Bard P.-Y., Gariel J.C (1986). The seismic response of two-dimensional sedimentary deposits with large vertical velocity gradients. *Bulletin of the Seismological Society of America*, 76: 343-346.
- Bard P.-Y., Riepl-Thomas J. (1999). Wave propagation in complex geological structures and their effects on strong ground motion. In *Wave motion in Earthquake Engineering*, Kausel and Manolis eds., WIT Press, chapter 2: 37-95.

Boore D. M. (1972). A note on the effect of simple topography on seismic SH waves. *Bulletin of the Seismological Society of America*, 62: 275-284.

Bouchon M., Barker J. S. (1996). Seismic response of a hill: the example of Tarzana, California. *Bulletin of the Seismological Society of America*, 86: 66-72

Bouckovalas G. D., Papadimitriou A. G. (2004). Numerical evaluation of slope topography effects on seismic ground motion. *Proc. of 11th Int. Conf. on Soil Dynamics and Earthquake Engineering and 3th Int. Conf. on Earthquake Geotechnical Engineering*, Berkeley, California, 7-9 Gennaio 2004, vol. 2: 329-335

Brambati A., Faccioli E., Carulli G. B., Cucchi F., Onofri R. Stefanini S, Ulcigrai F. (1980). Studio di microzonazione sismica dell'area di Tarcento (Friuli). *CLUET*, Trieste.

Celebi M. (1995). Northridge (California) earthquake: unique ground motions and resulting spectral and site effects. *Proc. V Int. Conf. On Seismic Zonation*, Nizza, Francia, vol. 2.

Das B. M. (1983). Fundamentals of Soil Dynamics. *Elsevier*.

Faccioli E., Vanini M., Frassiné L. (2002). "Complex" site effects in earthquake ground motion, including topography. *12th European Conference on Earthquake Engineering*, Barbican Centre, London, UK.

Geli L., Bard P.-Y., Jullien B. (1988). The effect of topography on earthquake ground motion: a review and new results. *Bulletin of the Seismological Society of America*, 78: 42-63.

Idriss I. M. E Seed H. B. (1967). Response of earth banks during earthquakes. *Journal of the Soil Mechanics and Foundations Division, ASCE*, 93 (SM 3): 61-82

Idriss I. M. (1968). Finite element analysis for the seismic response of earth banks. *Journal of the Soil Mechanics and Foundations Division, ASCE*, 94 (SM 3): 617-636.

Kallou P.V., Gazetas G., Psarropoulos P.N. (2001). A case history on soil and topographic effects in the 7.IX.1999 Athens earthquake. *Proc. of 4th Int. Conf. on Recent Advances in Geotechnical Earthquake Engineering and Soil Dynamics*, San Diego, California.

Kramer S.L. (1996). Geotechnical Earthquake Engineering. *Prentice-Hall*, New Jersey, 653 pp

Lanzo G., Silvestri F. (1999). Risposta sismica locale – Teoria ed esperienze. *Hevelius edizioni*.

Ohtsuki A., Harumi K. (1983). Effect of topography and subsurface inhomogeneities on seismic SV waves. *Earthquake Engineering and Structural Dynamics*, 11: 441-462.

Pagliaroli A. 2006 Studio numerico e sperimentale dei fenomeni di amplificazione sismica locale di rilievi isolati, PhD tesi, Università Degli Studi Di Roma “La Sapienza”

Phillips S. W., Kinoshita S., Fujiwara H. (1996). Basin-induced Love waves using the strong motion array at Fuchu, Japan. *Bulletin of Seismical Society of America*, 83: 64-84.

Pitarka A., Irikura K., Iwata T. (1996). Was the basin edge geometry responsible for the ground motion amplification in the disaster belt-like zone during January 17, 1995, Kobe (Hyogo-ken Nambu), Japan earthquake *Proc. Int. Work. On Site Response subjected to Strong Earthquake Motions* , January 16-17, Yokosuka, Japan Idriss and Seed 1967



Pitilakis K. (2004). Chapter 5: Site Effects. *In: Recent advances in Earthquake Geotechnical Engineering and Microzonation*, Atilla Ansal ed., Kluwer Academic Publishers, pp. 139-198.

Raptakis D., Chavez-Garcia F.J., Makra K., Pitilakis K. (2000). Site effects at Euroseistest – I. Determination of the valley structure and confrontation of observations with 1D analysis. *Soil Dynamics and Earthquake Engineering*, 19: 1-22. Tucker and King 1984

Rastrepo J. I., Cowan H. (2000). The “Eje Cafetero” earthquake, Colombia of January 25 1999. *Bulletin of New Zealand Society of Earthquake Engineering*, 33: 1-29.

Rovelli A. Et Al. (1998). Amplification of ground motion due to topography and sedimentary filling in the Nocera Umbra area (Central Italy). *Proc. International Conference on the Effects of Surface Geology on Seismic Motion*, Yokohama, Japan, vol. 2: 531-536 Marsan et al 2002

Sanchez-Sesma F. J. (1990). Elementary solutions for response of a wedge-shaped medium to incident SH and SV waves. *Bulletin of the Seismological Society of America*, 80: 737-742.

Savoldelli V., 2008, Caratterizzazione di alcuni siti della rete accelerometrica nazionale al fine di individuare la risposta sismica locale, Tesi di Laurea in Scienze e Tecnologie Geologiche, Università degli Studi di Milano-Bicocca, Facoltà Di Scienze Matematiche, Fisiche e Naturali

Silva W. (1991). Site geometry and global characteristics. *Proc. NSF/EPRI Workshop on dynamic soil properties and site characterization*, EPRI NP-7337, 1: 6.1-6.80

Siro L. (1982). Emergency microzonations by Italian Geodynamics Project after November 23, 1980 earthquake. *Proc. Int. Conf. Microzonation*, Seattle, USA, vol. 3.

Sitar N., Clough G. W. (1983). Seismic response of steep slopes in cemented soils. *Journal of Geotechnical Engineering*, 109: 210-227.

Stewart J. P., Chiou S.-J., Bray J. D., Graves R. W., Somerville P. G., Abrahamson N. A. (2001). Ground motion evaluation procedures for performance-based design, *Pacific Earthquake Engineering Research Center (PEER)*, Report 2001/9.

Stewart J. P., Sholtis S. E. (2004). Case study of strong ground motion variations across cut slope, *Proc. of 11th Int. Conf. on Soil Dynamics and Earthquake Engineering and 3th Int. Conf. on Earthquake Geotechnical Engineering*, Berkeley, California, 7-9 Gennaio 2004, vol. 1: 917-922.

Tagliani A. (1985). Una nota sull'amplificazione di onde sismiche SH causata da irregolarità topografiche a forma di gradino, *Ingegneria Sismica*, Anno II, n. 2: 12-18.

---

## *Chapter 3*

# Hazard analysis and criteria of seismic input selection

### 3.1 INTRODUCTION

The choice of an appropriate seismic input is a critical step in the modeling of local seismic response of a site problem. The engineer has, therefore, the necessity to adequately represent the seismic excitation. (Bommer & Acevedo, 2004) In this sense, the most accurate representation of a seismic event is achieved by an acceleration time history, as it is full of information about the earthquake properties, about the nature of earthquake waves that propagate from the epicenter to recording station.

The accuracy of the results obtained by dynamic analysis performed using accelerograms strictly depends on the correct selection of the same.

The seismic input is chosen, then, correctly, albeit with the necessary approximations and simplifications, if it reflects the real design seismic event. It should be finally emphasized that the nature of the application itself influences the selection criteria input. (Esposito M. 2009)

From the above comes the need to select a suitable set of accelerograms.

### 3.2 ACCELEROGRAMS

To obtain time histories of acceleration can operate in three different ways, all provided by the most modern technical Codes, corresponding to three different types of accelerograms:

- Natural, resulting from records of real seismic events, by recognized database;
- Artificial, obtained by the alteration of real seismic events records, modified in order to achieve compatibility with a target-spectrum, through the manipulation in the frequency domain;
- Synthetic, generated through modeling, both deterministic and stochastic methods, able to simulate the characteristics of the seismic source of motion, energy-related issue, the surface wave propagation and the response to the site.

With regards to artificial spectrum-compatible accelerograms is possible generate them using programs such as SIMQKE (Gasparini, Vanmarcke, 1979) or BELFAGOR (Mucciarelli et al. 2004).

This approach may appear very attractive, because it allows generate acceleration time histories, fully compatible with any target spectrum, which could be, sometimes, the only information available to the structural engineer.

It should, however, say that generally this type of accelerograms not represent correctly the physics of an earthquake: it is established that they have an excessive number cycles of strong motion, as well as unrealistically high energy content. In addition to the above mentioned problems, then there is the issue of the matching to a uniform hazard elastic spectrum (UHS), obtained from a probabilistic seismic hazard analysis (PSHA) and thus takes account of different seismic sources, ie the near source and low intensity events characterize the high frequency spectrum, while the distant and high-magnitude seismic events affect the low frequencies spectrum. (Reiter, 1990; Bommer et al 2000) This will mean that the spectrum-compatible artificial accelerograms will not be realistic.

The creation of synthetic accelerograms, using different methods and programs, has had some development (i.e. Zeng et al 1994; Atkinson, Boore 1997; Beresnev, Atkinson 1998; Boore 2003), but the application of this approach is complex: it is necessary to have specific knowledge of seismology and requires modeling parameters often affected by considerable uncertainty. (Bommer & Acevedo, 2004)

The natural accelerograms are those who most faithfully reproduce the characteristics, in terms of energy, duration, amplitude and frequency content, of real events. (Iervolino, Maddaloni, Cosenza 2006) Finally, the availability of many existing database strong-motion records allows find simply real acceleration time histories.

### **3.3 SEISMIC HAZARD ANALYSIS**

Despite considerable progress, there isn't still a commonly accepted procedure for the selection of accelerograms, in particular for what concerns the compatibility criteria related to a target frequency content and to determinate a possible scale factors. (Costanzo, 2006)

The variety of selection procedures, is mainly linked to the information available about the case as seismic hazard or the design ground motions of the site under study.

The codes, on the other hand, specify, in a very general, only that the choice must be made so that the recordings are representative of the local seismicity. It is therefore not easy to identify the most suitable for the scenario earthquake site. (Bommer & Acevedo, 2004)

The different selection procedure can be summarized in three categories:

- a) Deterministic Seismic Hazard Analysis (DSHA)
- b) Probabilistic Seismic Hazard Analysis (PSHA)
- c) Other imposed by Codes (Figure 3.1)

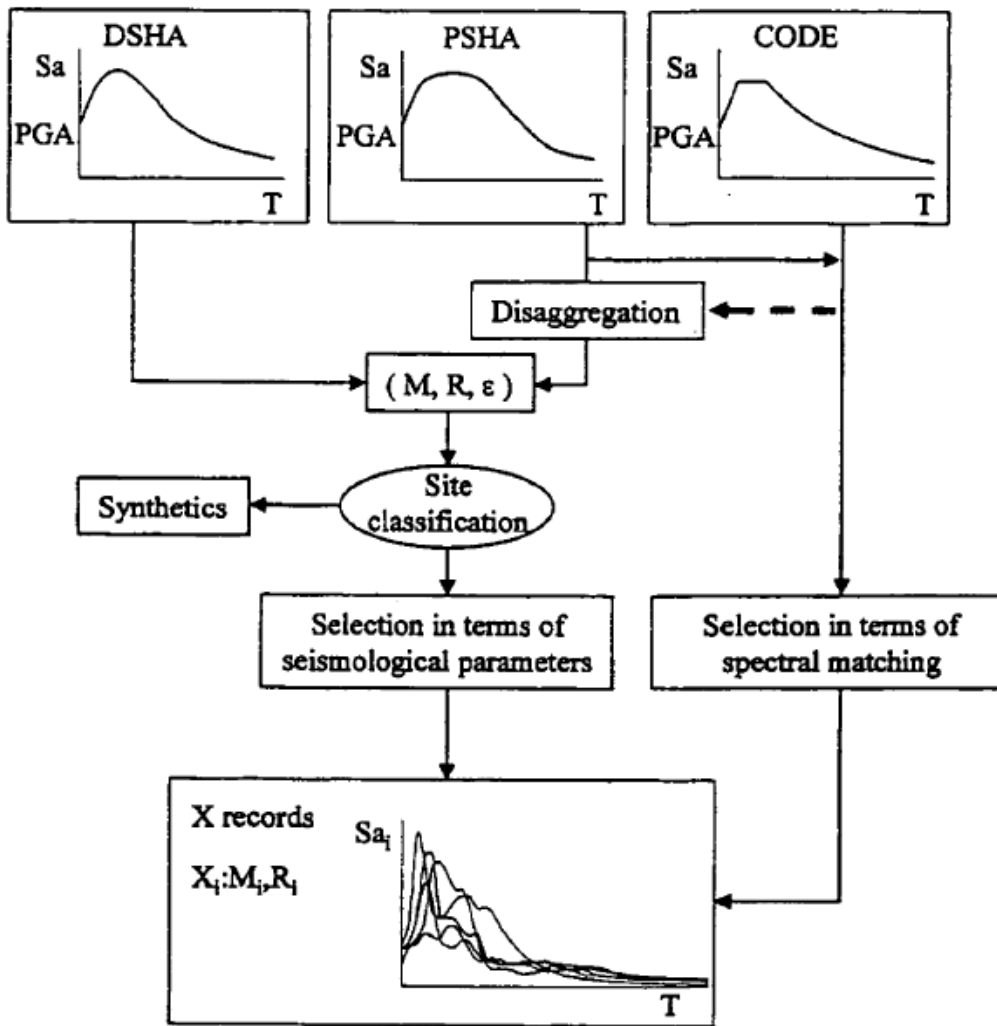


Figure 3.1 - Overview of the available options for selecting accelerograms to be used in engineering analysis and design (By Bommer & Acevedo, 2004)

### 3.3.1 *Deterministic Seismic Hazard Analysis*

This is the procedure traditionally used in engineering studies for seismic risk assessment of large areas. This system identifies the occurrence of an earthquake of a given intensity at a specific site. The approach involves the development of one or more "Earthquake Scenarios", from which the maximum amplitude of motion at an outcropping bed-rock is determined.

The method is summarized in the following phases (Figure 3.2):

- PHASE 1 The identification and characterization of the earthquake sources able to produce a significant excitation at the investigated site. In this procedure, the source's geometry and the potential maximum magnitude of each earthquake have to be defined. It should be emphasized that the choice of such event, called "maximum probable earthquake" (MPE), defined as the maximum historical earthquake occurred in the site, is very cautionary.
- PHASE 2 For each source zone surrounding the site, the shortest site-source distance have to be identified. Is possible to express the distance as epicentral distance, or hypocentral one or the fault plan distance, in relation to available knowledge and the attenuation law that will be used.
- PHASE 3 For each seismogenetic source is selected the earthquake that is expected to produce the strongest level of shaking (controlling earthquake), expressed in terms of peak ground acceleration  $a_{\max,r}$ , or about a generic spectrum of acceleration ordinate  $S_{a,r}(T)$ ; or pseudo-velocity  $S_v(T)$ . The chosen seismic parameter is expressed as a function of the assumed maximum magnitude and distance from the source. The selection is made comparing the levels of shaking produced by potential earthquake (Phase 1) at the distance defined in phase 2.
- PHASE 4 The hazard at the site is then defined in terms of the ground motion produced at the site by the selected earthquake, that can be generated by seismogenetic source and scaled to the distance through the attenuation law.

DHSA is a simple procedure to evaluate worst ground motion conditions. Yet, it is not interrelated to the likelihood occurrence of an event, its location, the level of shaking expected during a period of occurrence related to the life span of the structure and the uncertainty effects of the resulting ground motion characteristics. Many of the decisions taken, particularly in phase 1, are subjective. Such decisions should be backed by structural, seismological, geological, economical and political experience of the engineer. This can lead to different selections in the third step. (Kramer, 1996)

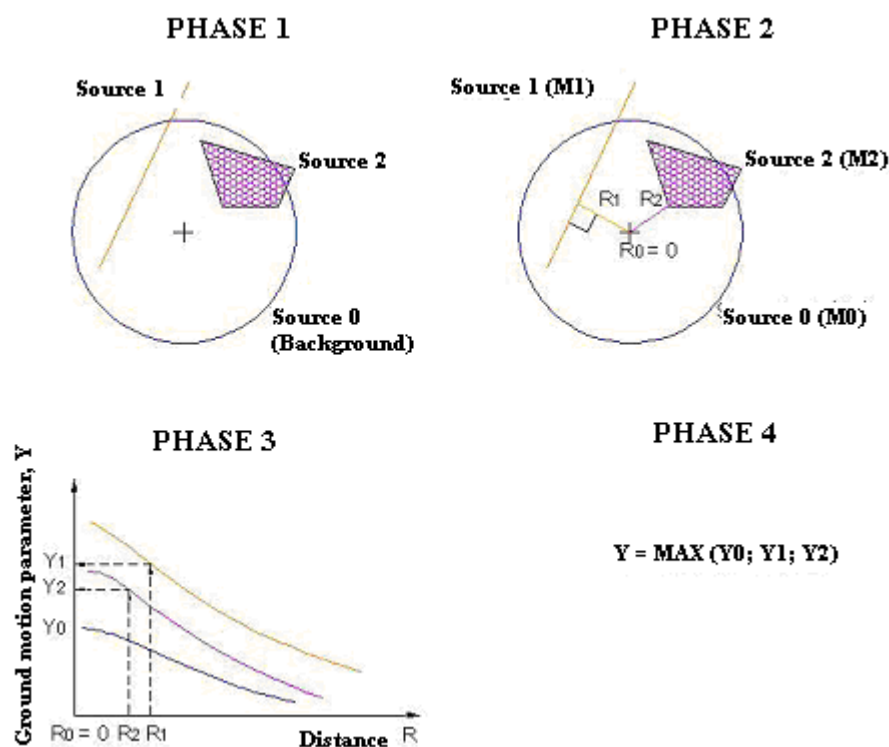


Figure 3.2 – Outline of Deterministic Seismic Hazard Analysis (adapted from PIANC 2001)



### 3.3.2 Probabilistic Seismic Hazard Analysis

This methodology has been developed during the last 40 years since it allows for uncertainties in the parameters such as size, distance, location, and the recurrence rate of earthquakes. The PSHA method identifies, quantifies and combines these uncertainties in a rational way to provide a complete picture of the seismic risk. Its classic conception has been formulated for the first time by Cornell in 1968 and currently investigated and improved by many experts (Algermissen et al. 1982, Iervolino & Cornell 2005).

Currently, in most cases, the seismic hazard analysis is based on Poisson statistical models, characterized by 4 key hypotheses:

1. The rate, that the expected number of "events" that occur in unitary time, is constant.
2. Each event is completely independent of any other event before and after. The process, ie, has no memory.
3. The probability of having more events per unit time is negligible.
4. The probability of occurrence of an event increases with the temporal interval of observation.

The assumptions at the base of the Poisson processes are all checked for events such as earthquakes and therefore it appears correct to study the hazard with similar models. From these assumptions follows that, for each seismogenic zone, the return period increases with the magnitude of the earthquake, while the location of the source is still completely random.

The main advantage of this method is the possibility to evaluate the seismic hazard without having to report to the place or the time when the last significant event has occurred, but it is necessary a simple catalogue of events in terms of magnitude (or/and other strong motion or geophysical parameters) of a fixed observation period, regardless of the date and location.

The Poisson method defines, so, a probability of occurrence of events with a given intensity in a given return period  $T$ , probability that, we must remark, is constant over time. If, that is, set a certain probability of passing a measure of earthquake, magnitude  $M$  for example, a time interval  $T$ , although

the time  $T$  expires without a significant seismic events, in the next period  $T$  the probability would remain the same. (Costanzo 2006)

Is possible describe PSHA method in four phases (Figure 3.3):

PHASE 1 Identification and characterization of earthquake sources, as in DSHA, but in PSHA must be evaluate also the probability of geometric distribution of potential rupture. In DSHA is, implicitly, assumed a probability of occurrence equal to 1 for the source point closest the site of interest, 0 for the most distant. In PSHA, however, the probability distribution within the source must be characterized, although generally use uniform probability distributions within the source.

PHASE 2 Characterization of seismicity or temporal distribution of recurrence seismic. For each seismic source, is determined, based on historical data, the recurrence relation, which specifies the average frequency over time of earthquakes as a function of energy (expressed in terms of magnitude). This, in turn, gives the probability of exceeding a given intensity parameter (for example magnitude) of a fixed reference time.

PHASE 3 Using predictive relationships, the ground motion produced by earthquakes of any size at the site occurring at any point in each source zone is determined. The predictive attenuation law relationship already considers its statistical uncertainty

PHASE 4 Finally, the uncertainties on the location of the source, energy and on the parameter of seismic ground motion are combined, obtaining the probability function of seismic intensity parameter is exceeded during a fixed period.

In the probabilistic seismic hazard assessment, the basic elements include: earthquake catalogues, earthquake source models, strong seismic ground motion, and the seismic hazard probability itself.

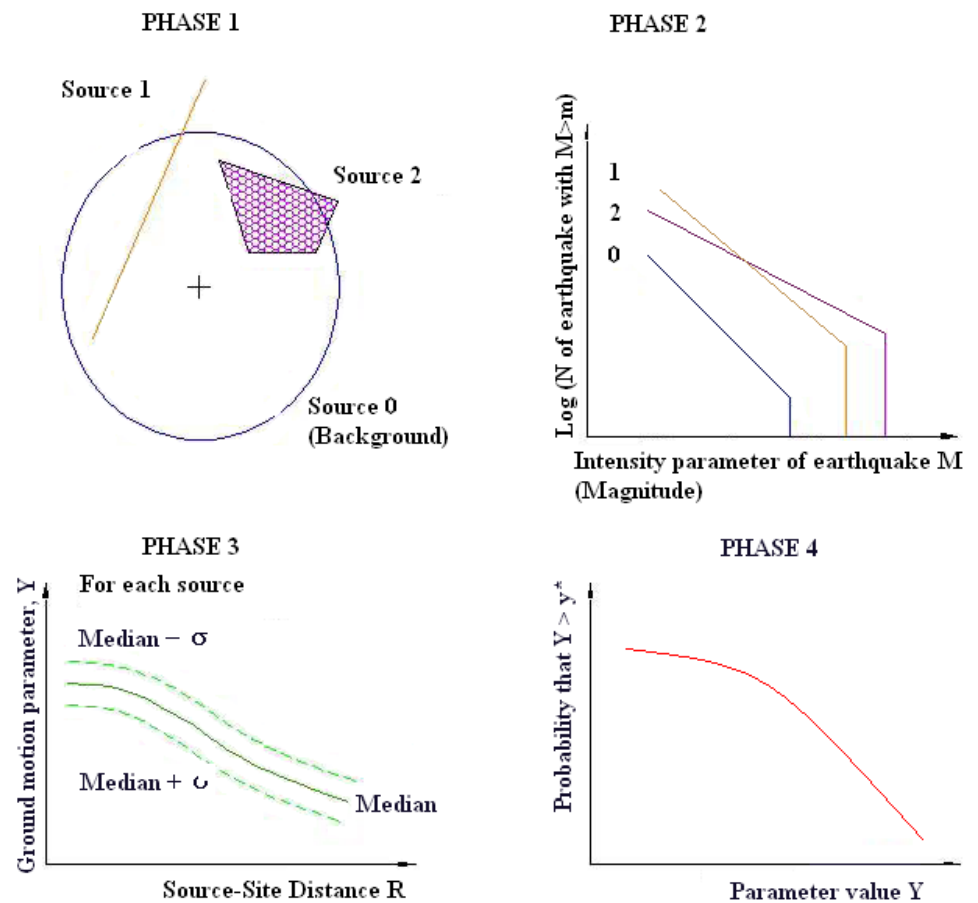


Figure 3.3 – Outline of Probabilistic Seismic Hazard Analysis (adapted from PIANC 2001)

The earthquake source is one of the uncertainties. Its special geometry can be a point source, areal source or a volumetric source. Another uncertainty characterizing the hazard is the earthquake size. A recurrence law describes and relates the recurrence of an earthquake with its time interval of occurrence. PSHA assumes that the recurrence law obtained from past seismicity is appropriate to predict future seismicity. A recurrence law, classically used, is the Gutenberg-Richter law, created for southern California earthquakes.

There were many variations of such law, due to dependent events such as aftershocks and foreshocks proposed by Merz and Cornell. It is difficult to establish which is the most precise or whether they are correct or not since they are all based only on a data base 50-60 years old which is relatively short.

For PSHA probabilistic computations to combine the uncertainties, are used different ways. One of these common approaches is the development of seismic hazard curves where they give the annual probability of exceedence of different values of ground motion parameter. These are obtained for each individual zone and are eventually combined in order to obtain the aggregate hazard at the investigated site. Combining hazard curves with temporal uncertainty models, as Poisson model, is possible to obtain the probabilities of exceedence in finite time interval:

In conclusion the PSHA procedure computes the mean rate of exceedence in a finite time interval at a particular site. The computation of this rate of exceedence is based on the aggregated risk from potential earthquakes of many different magnitudes occurring at many different source-site distances. The rate of exceedence, therefore, is not associated with any particular earthquake magnitude or source-site distance, but with all the couple M-R considered.

In some cases, however, it is useful to evaluate rate of exceedence at a particular site associated with every specific earthquake magnitude and source-site distance, in order to select the most likely earthquake magnitude and/or the most likely source-site distance. It is possible, in fact, using these parameters to select existing ground motion records for response analysis. This procedure is named Deaggregation and it provides maps in which the rate of exceedence in a finite time interval is expressed as function of a couple magnitude-source-site distance. (Kramer, 1996)

### 3.4 PARAMETERS USEFUL FOR STRONG-MOTION RECORDS SELECTION

The selection of real accelerograms from a database can be performed based on different categories of parameters:

1. ground motion parameters
2. seismological parameters related to the source
3. propagation parameters

#### 3.4.1 *Ground motion parameters*

In engineering the characteristics of an earthquake are primarily important amplitude, frequency and duration. Each parameter ground motion gives information on one or more of these three characteristics, it is, therefore, generally use more than one parameter for the correct characterization of a seismic event.

The most widely used ground motion parameters are derived from a representation of the same in the time domain. The motion parameters can be in terms of acceleration, velocity or displacement. Typically, only one of these quantities is measured directly to get the other by integration and/or differentiation.

The parameter most commonly used as a measure of the amplitude of particular ground motion is the PHA, or peak horizontal acceleration, ie the maximum absolute acceleration value measured horizontally.

It emphasises that for each event are, usually, recorded two orthogonal horizontal components. Common practice for selection of input earthquake, although controversial, is considered them independent and choose between the two that shows the peak acceleration higher. It should, however, said that the horizontal acceleration of a real event is a vector whose direction, usually, does not coincide with any of the two components.

The PHA, furthermore, is not always proportional to the destructive power of an earthquake, which also depends on its duration and seismic energy released, as was evident in the case of numerous seismic events, which, although characterized by a relatively PHA low, have resulted in serious problems. The scientific community agrees, now, in considering this parameter less meaningful as an indicator of ground motion and structural damage, as is typically associated with a high pulse frequency. Moreover, just because it is related to the high frequency components of the recording, it is very sensitive to the accelerometer data correction technique. (Paciello 2004)

Finally must be taken in account that with increasing epicentral distance, there is a reduction in acceleration, while the harmonic content changes, ie the higher frequency harmonics are more attenuated than those with lower frequency.

The peak horizontal velocity (PHV) is another parameter used to characterize the amplitude of ground motion, but unlike the acceleration is not very sensitive to high frequency components, therefore, appears more suitable than the PHA, to accurately represent the intermediate frequencies. (Kramer 1996)

Peak displacement, however, is associated with low frequencies of an earthquake and not very used as a parameter from the previous ones, because of the difficulty of an its accurate determination due, often, the processes of signal filtering or numerical errors in the integration. (Kramer 1996)

A single parameter, such as peak acceleration and velocity, given the complexity of the dynamic response of an object like a building or a soil deposit, is not sufficient to describe the seismic motion. Greater influence on the seismic behavior assumes, however, the frequency content of the event, which is why it is often more effective representation of motion in the frequency domain. This category includes parameters such as amplitude Fourier.

Significant is, also, the response spectrum, which describes the maximum (absolute value) of a single degree of freedom system response SDOF as a function of frequency or the fundamental period and damping rate. The spectrum can be expressed in terms of acceleration, velocity or displacement. The response spectrum shows some information on the frequency content of earthquake that are not directly deductible from the accelerometer record; furthermore, it allows to quantify the transferred actions to structures similar to systems in more degrees of freedom that are known features essential physical and mechanical properties. It is noted that the peak spectral acceleration, the velocity and the displacement corresponding to different frequencies (or periods).

In particular, for the absolute acceleration response spectrum can make the following considerations:

- the value of intercept of the plot with the y-axis ( $T = 0$ ) is the maximum acceleration of the ground, PHA, because the oscillator being infinitely rigid, there is no relative movement between the mass and the base and thus the maximum acceleration it undergoes mass coincides precisely with the maximum value of the accelerometer recording;
- by increasing the period  $T$  of the oscillator is generally observed amplification of the order followed by a decrease until, theoretically, to zero values for endless periods.

An important parameter of ground motion is the duration. It strongly influences the structural damage of buildings: processes such as the degradation of stiffness and strength, in fact, are related to the number of loading and unloading cycles. A motion with a high amplitude but short duration may not produce significant structural damage, because of few hysteresis cycles; while a long-term earthquake, even with moderate amplitude could be very destructive. The duration, furthermore, is related to the release time of accumulated strain energy along the fault, thus a larger rupture fault corresponds to a longer release time, then a longer duration. This consideration implies that greater magnitude earthquakes have longer durations.

In addition to the above-defined parameters, is possible to refer to other parameters representative of the energy content of the earthquake, and consequently of its destructive potential. Among them are important Housner spectral intensity (Housner, 1952) Arias intensity (Arias, 1970).

Housner intensity is a particularly effective measure of the destructive power of a seismic event in respect of buildings. It is, in fact, defined as the area under the pseudo-velocity response spectrum to the site within a certain range of frequencies. Its mathematical expression is:

$$I_H = \int_{0.1 \text{ sec}}^{2.5 \text{ sec}} PSV(\xi, T) dT \quad (3.1)$$

where PSV is the pseudo-velocity response spectrum; T and  $\xi$  are the structural natural period and damping, respectively.

Housner Intensity is dimensionally a displacement (cm).

The (5.1) shows clearly how the Housner intensity is function of the relative damping and natural period of simple-deegree-of-freedom oscillator T, sec in the range  $0.1 < T < 2.5$  sec. The range of periods in which it's estimated is very significant for structures. This parameter can, thus, to capture important aspects of motion simultaneously in terms of amplitude or frequency content.

The Arias intensity is a measure of seismic intensity, depending on the energy dissipated by the buildings due to the earthquake. Denoted with W the energy dissipation per unit mass of a simple oscillator with natural frequency  $\omega$  and relative damping  $\xi$  Arias intensity can be defined as:

$$I_a = \int_0^{\infty} W d\omega = \frac{\pi}{2g} \cdot \int_0^{\infty} [a(t)]^2 dt \quad (3.2)$$

where a(t) is the acceleration at time t and g the gravity acceleration.

Arias Intensity is dimensionally a velocity (cm/s).



Table 3.1 summarized the above-defined ground motion parameters and the them related earthquake characteristics

*Table 3.1 – Ground motion parameters and related earthquake characteristic*

Parameters	Earthquake characteristic		
	Amplitude	Frequency content	Duration
Peak acceleration PHA	•		
Peak velocity PHV	•		
Peak displacement PHD			
Duration ( $T_d$ )			•
Housner intensity $SI(\xi)$		•	•
Arias intensity $I_a$	•	•	•

### 3.4.2 Seismological parameters related to the source

The second category of parameters useful for the selection of input seismic will focus on the earthquake source. The parameters of this class, useful in engineering practice, are related to geometric characteristics of the fault, and of rupture mechanism that occurs along it.

An earthquake, infact, occurs when a volume of rock, subject to deformation mechanisms of tectonic origin, ruptures along a weak surface, which is denoted as fault, resulting in a relative displacement between the two blocks of rock separated by the fault. To locate the fault plane position and the slip direction, the following definitions are usually considered:

- Strike: clockwise angle formed by the intersection of the fault plane with the ground surface and the North direction.
- Dip: angle formed by the fault plane and the horizontal direction.
- Rake: angle formed, with respect to the intersection of the fault plane with the surface, by the vector defining the relative displacement (slip) between the block above the fault plane (hanging wall) and the one below (foot wall). The rake angle determines the fault type, corresponding to different focal mechanism, i.e. different geometry of fault rupture during an earthquake.

The possible focal mechanism are divide in Dip-slip and strike-slip movement (Figure 3.4):

- strike-slip (rake =  $0^\circ$  or  $180^\circ$ , often associated to dip angles close to  $90^\circ$ ), which is associated a vertical fault plane and relative horizontal displacement of the two blocks divided by the fault. Two movement are possible: Right lateral strike-slip if an observer standing near such a fault would observe the ground on the opposite side of the fault moving to the right; and Left lateral strike slip if observer standing near such a fault would observe the ground on the opposite side of fault moving to the left. The angle between the rupture plane and the surface on the hanging wall side is always acute and it is always obtuse on the foot wall side.
- Dip-slip movement can be: normal (rake =  $-90^\circ$ ), in which the Earth's crust is in compression along a dipping fault plane, with the hanging wall moving upwards relative to the footwall; or reverse (rake =  $+90^\circ$ ), that is the Earth's crust is in extension along a dipping fault plane, with the hanging wall moving downwards relative to the footwall. A special type of reverse fault is a thrust fault, which occurs when the fault plane has a small dip angle. (ITACA Glossary; Kramer 1996)

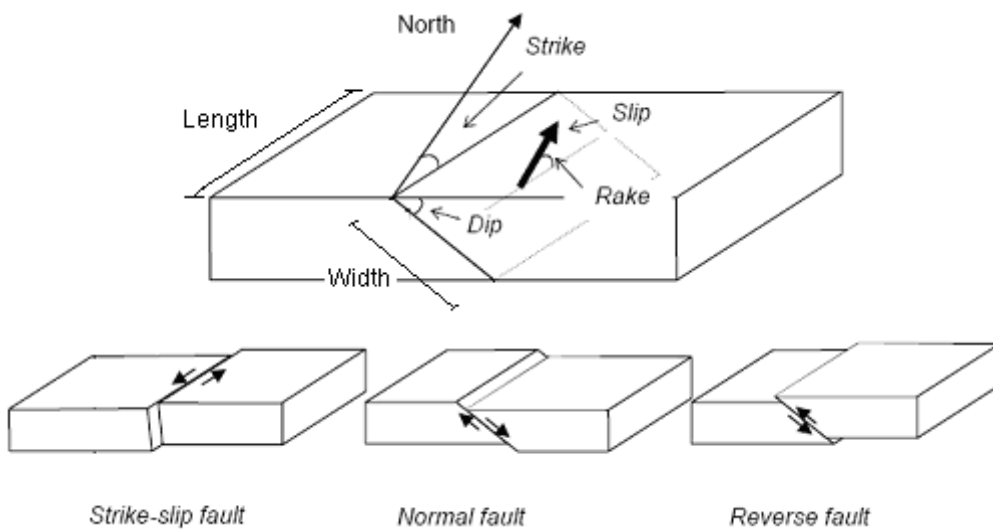


Figure 3.4 – Definition of the fault types (modified from ITACA Glossary)

All other types of rupture mechanisms can be represented as a combination of those defined above. (Figure 3.5)

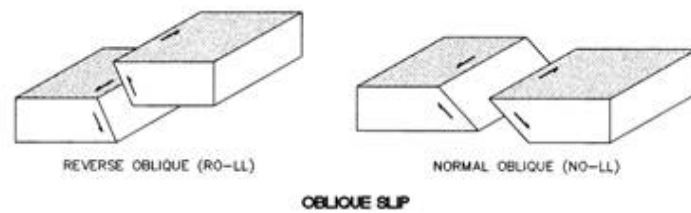


Figure 3.5 – Oblique focal mechanism

The study of focal mechanism is based on the polarity of the first arrivals of P and S waves recorded by a network of far field seismic stations. Finally, as geometric characteristics, important is the width and the length of fault.

Other important characteristic of the seismic source is the focal (or hypocentral) depth which is the depth at which the rupture begins. The focal depth is only important for small magnitude earthquakes, when the rupture dimensions are small compared to the thickness of the seismogenic layer of the crust; in this case the focal depth is the parameter that controls how deep below the surface the source of energy is located. Conversely, larger earthquakes, which do rupture the entire seismogenic layer, usually nucleate at the base of the seismogenic layer so focal depth is less important. (Scasserra, 2008)

Finally a very significant parameter, used in engineering application, is the Magnitude. It measures the intensity of a seismic event by an appropriate processing of the seismic signal. It is not directly a measure of physical quantity but it is calculated from some characteristics of earthquake seismograms, usually from the wave amplitudes. As result of this, different magnitude measurements exist.

The first and most well-known definition of magnitude, called local magnitude, is due to Richter, hence the name of the corresponding magnitude scale. He gave, in 1935, the definition in relation to the earthquakes in Southern California, using a Wood-Anderson seismometer. The local

magnitude is the logarithm to base ten of the maximum displacement of the track (with respect to zero, expressed in micrometers) in the seismograph for an event to an epicentral distance of 100 km. The (3.3) shows this relationship:

$$M_L = \log A + \log A_0 \quad (3.3)$$

where:  $A$  = peak amplitude, in micrometers, of the track recorded by a Wood-Anderson seismograph at a given distance;  
 $A_0$  = amplitude corresponding to the reference earthquake (“zero”) at the same distance.

The Richter magnitude scale is logarithmic, so an increase of a unit of  $M_L$  implies an increase of 10 times in the motion amplitude. Therefore, in moving from  $M_L = 4$  (low intensity earthquake) to  $M_L = 7$  (strong intensity earthquake), there is an increase in amplitude of 1000 times.

One limitation of the magnitude scale  $M_L$  is the tendency to saturation for magnitude around 7.0-7.5; this depends on the bandwidth limitations of the WA seismograph, which do not make it suitable for recording the long period oscillations generated by large earthquakes. (ITACA Glossary)

Because earthquakes excite both body waves, which travel into and through the Earth, and surface waves, which are constrained to follow the natural wave guide of the Earth's uppermost layers, two magnitude scales evolved - the  $m_b$  and  $M_S$  scales. (<http://earthquake.usgs.gov>)

The  $M_S$  (Surface wave magnitude), was defined in 1936 by Richter and Gutenberg, on the base of the Rayleigh waves amplitudes with a period of about 20 sec. It is expressed as (3.4):

$$M_S = \log A + 1.66 \log \Delta + 2.0 \quad (3.4)$$

where  $A$  = maximum ground displacement in  $\mu\text{m}$   
 $\Delta$  = the epicentral distance in degrees.

The surface wave magnitude is most commonly used to describe the size of shallow (less than about 70 km focal depth), distant (further than about 1000

km) moderate to large earthquakes (Kramer, 1996).

In 1945 Gutenberg defined body wave magnitude  $m_b$  as:

$$m_b = \log\left(\frac{A}{T}\right) + 0.01\Delta + 5.9 \quad (3.5)$$

where  $A$  is the p-wave amplitude in micrometers and  $T$  is the period of the p-wave.

This type of magnitude is suited to represent deep-focus earthquake, as for these event the surface waves are small respect to body waves. (Kramer 1996)

It's important to note that the scales of magnitude, defined so far, are related to different measures of the ground-shaking characteristics. This means that they are not a direct measure of the energy of the earthquake. All, in fact, are subject to the phenomenon of saturation, ie if the energy released during the earthquake increases, beyond a certain level, magnitude is not growing, because of the low sensitivity of the measures of the characteristics of ground shaking at the surface.

In this regard, the only magnitude scale not subject to saturation is the moment magnitude scale  $M_w$  (Hanks and Kanamori 1979 and Kanamori 1977), linked to the seismic moment  $M_0$ , whose definition takes into account the most important physical parameters associated with the energy release during an earthquake.  $M_0$  definition depends, infact, from the mathematical modelling of an earthquake fault as a shear displacement discontinuity (dislocation) across a surface in an elastic medium.  $M_0$  is the total moment, on this surface, of double couples equivalent to the dislocation. (Kanamori and Anderson, 1975):

$$M_0 = G \cdot \overline{\Delta u} \cdot A \quad (3.6)$$

Where  $G$  is the shear modulus of the crustal material where the seismic rupture occurs,  $A$  the area of the rupture surface in the seismogenic fault,  $\Delta u$

the average coseismic slip on the rupture surface.

The moment magnitude is calculated based on the seismic moment as follows:

$$M_W = \frac{\log M_0}{1.5} - C \quad (3.7)$$

where  $C=10.7$  if  $M_0$  is measured in  $\text{dyne}\cdot\text{cm}$  and  $C=6.0$  if  $M_0$  is in  $\text{Nm}$ .

$M_0$  is a quantity that can increase indefinitely as the source and dislocation dimensions increase, so  $M_W$  does not saturate.

The saturation phenomenon for different magnitude is illustrated in Figure 3.6 by the relationship between  $M_W$  and the other commonly used magnitude scales. This shows that, in practice,  $M_W = M_L$  for  $M_W \leq 6.2$  can be assumed.

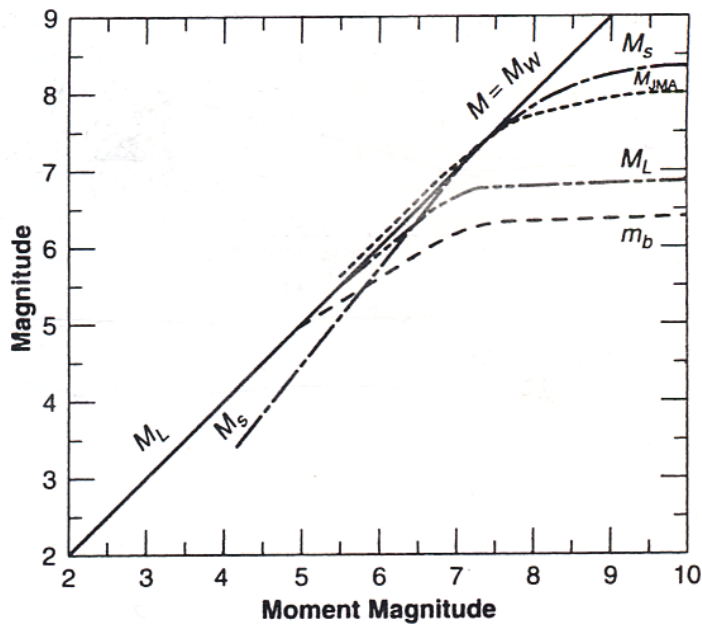


Figure 3.6 – Relationship between  $M_W$  and other definitions of magnitude

Finally, the magnitude is related to the release energy during the seismic event, through Gutenberg and Richter (1956) formula (3.8):

$$\log E = 11.8 + 1.5M_s \quad (3.8)$$

Where E is in ergs.

In 1983 Kanamori showed that the (3.8) was applicable to magnitude moment.

### 3.4.3 *Seismological parameters related to propagation-path*

Each seismic event, from the source, travel through the soil and is subject to attenuation of wave amplitude, reflection and refraction at the interface of different rock types and wave scattering from small-scale heterogeneities in the crust. Only after this modification the signal is recorded at a given distance.

As a result of this is evident that the characteristics of seismic waves recorded are influenced, by the source as the distance from it.

Different ways to measure the distance between the source of an earthquake and a specific site are actually used in engineering application. (Figure 3.7)

The most commonly used are:

- Epicentral distance, ( $R_{ep}$ ) defined as the distance on the surface between the site and the earthquake epicentre.
- Hypocentral distance ( $R_{hyp}$ ) defined as the distance between the site and the earthquake hypocenter (or focus)
- Joyner & Boore distance ( $R_{JB}$ ) defined as the minimum distance between the site and the projection of the fault on the ground surface.
- Rupture distance ( $R_{rup}$ ) is the minimum distance between the fault plane and the site.

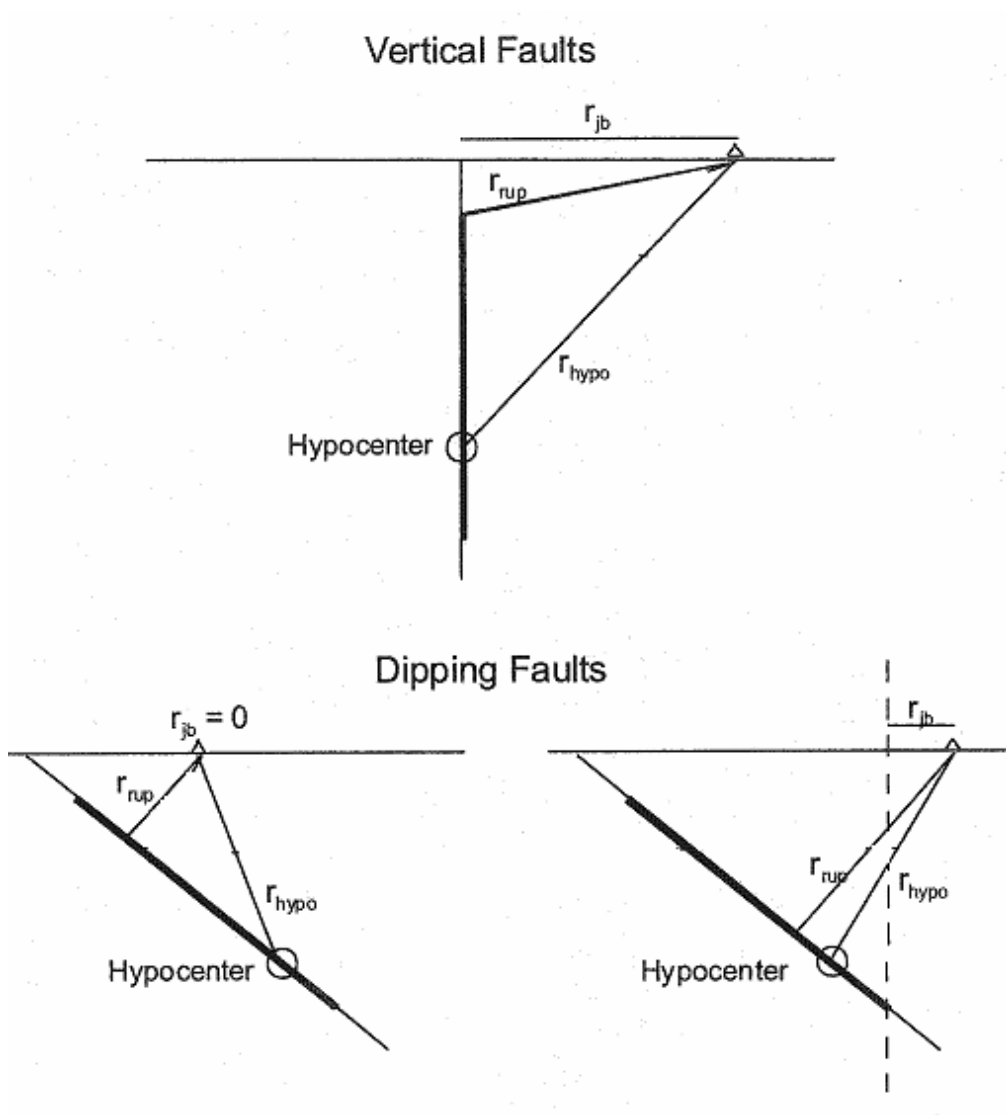


Figure 3.7 – Source-site distance: various definitions (Abrahamson and Shedlock 1997)



### 3.5 CRITERIA FOR SELECTING STRONG-MOTION RECORDS

The criteria used for the selection of accelerograms are many and are often linked to the information available to the engineer to characterize the seismic hazard of the site studied. In this section we want to give a nod to the different criteria to make some reflections on them.

The criterion, certainly more widespread, is the compatibility with a target response spectrum shape. The compatibility between two spectral shapes can be estimated using various indices, among other, we can mention:

- the average root-mean-square deviation  $D_{rms}$  (Bommer & Acevedo, 2004):

$$D_{rms} = \frac{1}{N} \sqrt{\sum_{i=1}^N \left( \frac{Sa_0(T_i)}{PHA_0} - \frac{Sa_s(T_i)}{PHA_s} \right)^2} \quad (3.9)$$

Where

$N$  is the number of periods at which the spectral shape is specified,  
 $Sa_0(T_i)$  is the spectral acceleration from the record at period  $T_i$ ,  
 $Sa_s(T_i)$  is the target spectral acceleration at the same period;  
 $PHA_0$ , and  $PHA_s$ , are the peak ground acceleration of the record and the zero-period anchor point of the target spectrum, respectively.

Smaller is the value of  $D_{rms}$  closer is the match between the shape of the record and target spectrum. Bommer & Acevedo (2004) suggest a different maximum value of  $D_{rms}$  depending on the range of periods where you need to have compatibility. In any case the maximum value of 0.15 is proposed.

- Pearson correlation coefficient  $R^2$

$$R^2 = \left\{ \frac{N \cdot \sum_{i=1}^N \left( \frac{Sa_0(T_i)}{PHA_0} \cdot \frac{Sa_s(T_i)}{PHA_s} \right) - \left( \sum_{i=1}^N \frac{Sa_0(T_i)}{PHA_0} \right) \cdot \left( \sum_{i=1}^N \frac{Sa_s(T_i)}{PHA_s} \right)}{\sqrt{\left[ \sum_{i=1}^N \left( \frac{Sa_0(T_i)}{PHA_0} \right)^2 - \left( \sum_{i=1}^N \frac{Sa_0(T_i)}{PHA_0} \right)^2 \right] \cdot \left[ \sum_{i=1}^N \left( \frac{Sa_s(T_i)}{PHA_s} \right)^2 - \left( \sum_{i=1}^N \frac{Sa_s(T_i)}{PHA_s} \right)^2 \right]}} \right\}^2$$

Where the symbols assume the same meaning as in the (3.9)

On the contrary of coefficient  $D_{rms}$  for  $R^2$  the best correlation is represented by a value near unity.

- the square average root-mean deviation  $\delta_i$  (Iervolino et al, 2009):

$$\delta_i = \sqrt{\frac{1}{N} \sum_{i=1}^N \left( \frac{Sa_0(T_i) - Sa_s(T_i)}{Sa_s(T_i)} \right)^2} \quad (3.11)$$

It is emphasized that the spectrum-compatibility through the use of these indices, regardless of the specific ratio chosen, evaluated and expressed through an average value of the same over the entire range of periods of the spectra in question. This implies that the value of the difference between the two forms can vary significantly in different spectral intervals of time, so to avoid rough estimates we always recommend a graphic comparison of the spectra.

In addition, a significant problem is the choice of reference spectral shape. The form proposed by the Italian legislation for the horizontal components is defined by the same expressions given dall'EN1998, in which, however, has not taken a single value for the maximum amplification but the grandeur,  $F_0$ , according to the hazard of site together with the quantities  $a_g$ ,  $T_C$  and, consequently,  $T_B$ ,  $T_D$ , for each limit state. (Circolare n. 617)

The spectrum obtained using the above parameters, since they are the

maximum values, inevitably leads to an overestimation of the shares. In addition, the spectral shape proposed by the Italian legislation is the same for each event regardless of seismological characteristics, such as magnitude and distance, otherwise dall'EN1998 suggesting two different spectral shapes depending on whether if the earthquakes that contribute most to the seismic hazard defined for the site for the purpose of probabilistic hazard assessment have a surface-wave magnitude,  $M_s$ , greater or not than 5.5.

For low and moderate magnitude earthquakes ( $M < 5.5$ ) the spectral shape in terms of horizontal acceleration of the Italian legislation in most cases overestimate the following descending order of the horizontal section corresponding to the maximum value, which is rather underestimated. In addition, for these earthquakes the horizontal stroke is shorter and shifted to low periods. Reverse situation occurs for high-magnitude earthquakes ( $M > 5.5$ ) for which the maximum accelerations occur along a range of periods  $T$  broader, shifted towards higher values of the same, of how things should be taken into account in choosing an appropriate spectral shape is certainly different from that used for events with  $M < 5.5$ .

In this regards most studies do specify that magnitude should be a search parameter, indeed even Shome et al. (1998) recommend in their conclusions that the user should use "records from roughly the same magnitude". Others, such as Stewart et al. (2001), state that it is important to select records from events of appropriate magnitude because this parameter strongly influences frequency content and duration of the motion, going on to recommend selecting records of events within 0.25 units of the target magnitude. Since there is little doubt that earthquake magnitude exerts a very pronounced influence on duration (or number of cycles) and on the shape of the response spectrum, we are of the opinion that it is an indispensable selection parameter (Bommer & Acevedo 2004)

Finally, the most serious limitation with any selection procedure based solely on the ordinates of the elastic spectrum is that the records obtained can have very different durations and scale factors could be very high ( $>4$ ), which would lead to unrealistic energy content (Kramer 1996). Already Krinitzsky

and Chang (1977) proposed that if scaling factors of 4 (that is the normally accepted upper limit) or more needed to be applied to accelerograms, then the records should be rejected, although no justification was given for this assertion.

If the engineer has at his or her disposal a site-specific seismic hazard assessment, then the possibilities for selecting suitable records are quite different. If a deterministic seismic hazard assessment (DSHA) has been employed, the design earthquake scenario will be fully defined, at least in terms of the earthquake magnitude, the distance from the site to the fault rupture, and the nature of the surface geology at the site (Figure 3.1). The search could then be performed directly in terms of these three parameters, as well as others such as style-of-faulting. If PSHA has been used, then the controlling earthquake scenarios need to be obtained by disaggregation. (Bommer & Acevedo, 2004)

That said, using maps of disaggregation available to the site of interest, a second parameter, with the magnitude, must be included in defining that the search window is distance. It 'good to point out, however, that the spectral shape appears to be much less sensitive to distance than to magnitude, consequently, we proposed, that in the making, selections of real records, the search window as narrow as possible should be in terms of magnitude, and if it needs to be widened to capture the required number of records, that the distance range be extended. (Bommer & Acevedo, 2004)

If, under the above criteria, the number of records selected is wide, to reduce it, you can use additional criteria, such that the records do not come from the same station, unless it is very close to the site and therefore it is particularly significant. Another criterion is to consider a single registration for each seismic event (Esposito M. 2009). Finally, about the size of the sample to be selected accelerograms Italian seismic code (D.M. 14/01/2008) requires to use, for analysis a number of groups of at least 3, where each group is made up of two horizontal and vertical recordings of an earthquake, significant only for particular structures. If the selected set is the minimum number of accelerograms allowed, the downstream analysis of the structures

will be considered the maximum effect.

From a seismological perspective to approach preferable to use at least may be seven records and then use the average response obtained from the structural analysis (Bommer & Acevedo, 2004). In addition, the use of only three accelerograms would fail to adequately assess the variability of the structural response (Iervolino et al. 2009). The dispersion of the results of dynamic analyses has been shown to be inversely proportional to the square root of the number of records used. Shorne et al. (1998) demonstrated that seven is a suitable number to produce acceptably low dispersion in the results. (Bommer & Acevedo, 2004)

### **3.6 CRITERIA FOR MATCHING PROCEDURE OF SELECTED RECORDS**

Once you select the records is required in many seismic codes, including the Italian, that the average spectral ordinate of the selection, does not present a large gap compared to the corresponding component of the elastic spectrum.

The adaptation to the reference spectrum (spectrum matching) can be run in two different ways:

- a) scaling the individual records in the time domain using a scale factor, uniformly without changing the frequency content of the accelerogram selected. It does so simply by amplification or reduction, depending on whether the factor is greater or less than unity, in terms of amplitude, trying to minimize the differences between the response spectrum and the spectrum scaled targets.
- b) adding to the single record originally selected a series of waves (wavelets) with a specified time period and limited duration of the input time history.

Except for specific cases is, however, generally preferable to alter as little as possible to the real records. With regard, however, the first method, please note that generally the scaling factor is calculated to draw each record, so that the PHA of the same anchor value coincides with the target spectrum.

In this regards Figure 3.8 provides an overview of the available options for adjusting the selected records.

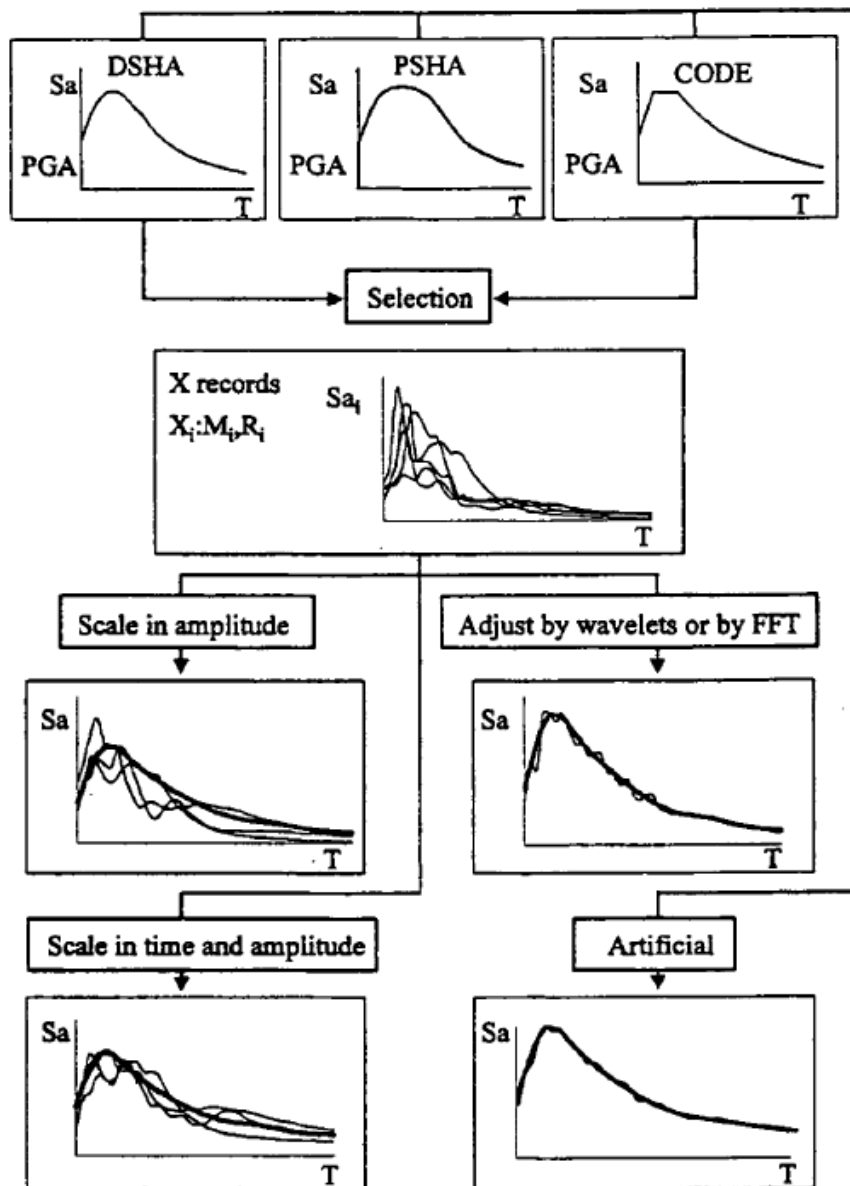


Figure 3.8 - Overview of the options available for scaling selected accelerograms match the ordinates of the elastic response spectrum specified for design.

## BIBLIOGRAPHY

Abrahamson, N.A., and Shedlock, K.M. (1997). Overview of modern attenuation relationships *Seism.Res. Letters*, 68(1), 9-23

Algermissen, S. T., D. M. Perkins, P. C. Thenhans, S. L. Hanson, and B. L. Bender (1982). Probabilistic estimates of maximum acceleration and velocity in rock in the contiguous United States, *U.S. Geol. Surv. Open-File Rept. 82-1033*, 99 pp.

Arias, A. (1970). A measure of earthquake intensity, in *Seismic Design of Nuclear Power Plants*, R. Hansen (Editor), M.I.T. Press, Cambridge.

Atkinson, G. M., and Boore, D. M., (1997). Stochastic point-source modelling of ground motion in the Cascadia region. *Seismological Research Letters*, 68, 74-85.

Beresnev, I. A., and Atkinson, G. M., (1998). FINSIM – A Fortran program for simulating stochastic acceleration time histories from finite faults. *Seismological Research Letters*, Vol. 69, No. 1, 27-32.

Bommer J. J., Acevedo A. B. (2004). The use of real earthquake accelerograms as input to dynamic analysis. *Journal of Earthquake Engineering*, 8, special issue 1: 43-91

Bommer, J. J. and Martinez-Pereira, A. (2000). Strong-motion parameters: Definition, usefulness and predictability, *Proceedings of the XX World Conference on Earthquake Engineering, Auckland*, Paper No. 206.

Boore D.M.,(2003). Simulation of Ground Motion Using the Stochastic Method. *Birkhäuser Verlag*, Basel, 2003.Iervolino,

Circolare n. 617 del 2.II.2009. Istruzioni per l'applicazione delle nuove norme tecniche per le costruzioni. Ministero delle infrastrutture e dei trasporti

Cornell C.A.(1968) Engineering seismic risk analysis. *Bulletin of the Seismological Society of America*, 58, No. 5, 1583-1606.

Costanzo, A. (2006). Analisi di fenomeni deformativi di pendii e rilievi in condizioni sismiche: il caso di Gerace. PhD dissertation, Università della Calabria

De Luca F., Iervolino I., Cosenza E. (2010). Compared seismic response of degrading systems to artificial and real records. XIV ECEE

Esposito M. (2009), Accelerogrammi spettrocompatibili per la progettazione delle strutture: valutazione comparativa della risposta sismica, Tesi di Laurea in Ingegneria Civile, Università di Napoli Federico II

Gasparini, D. A. and Vanmarcke, E. H. (1979). Simulated earthquake motions compatible with prescribed response spectra. *Evaluation of Seismic Safety of Buildings Report No. 2*, Department of Civil Engineering, MIT, Cambridge, Massachusetts, 99 pp

Hanks, T. C. and H. Kanamori (1979). A moment magnitude scale, *J. Geophys.Res.* 84, 2348-2350.

Housner G.W. (1952) Spectrum intensities of strong-motion earthquakes. Duke C.M., Feigen M.,(Eds). Proc. Symp. On Earthquake and Blast Effects Structures. Univ. of California, Los Angeles.

Iervolino I., e Cornell C.A., 2005. Record selection for nonlinear seismic analysis of structures. *Earthquake Spectra*, Vol.21,No.3, pp 685-713

Iervolino, I., Maddaloni, G., Cosenza E. (2008). Accelerogrammi naturali compatibili con le specifiche dell'OPCM 3431 per l'analisi sismica delle strutture, Atti del convegno ANIDIS 2008

Iervolino I, Galasso C., Cosenza E. (2009). Rexel 2.3.1(beta) e la selezione normativa dell'input sismico per analisi dinamica non lineare delle strutture,



## ANIDIS 2009

Kanamori, H. and Anderson, D.L. (1975). Theoretical basis of some empirical relations in seismology. *Bull. Seism. Soc. Am.* 65 (5), 1073–1095.

Kanamori, H. (1977). The energy release in great earthquakes. *Journal of Geophysical Research*, 82, 2981-1987.

Kramer S.L. (1996). Geotechnical Earthquake Engineering. *Prentice-Hall*, New Jersey, 653 pp

Krinitzsky, E. L. and Chang, F. K. (1977). Specifying peak motions for design earthquakes. State-of-the-Art for Assessing Earthquake Hazards in the United States, Report 7, Miscellaneous Paper S-73-1. US Army Corps of Engineers, Vicksburg, Mississippi

Mucciarelli M., Spinelli A., Pacor F. (2004), Un programma per la generazione di accelerogrammi sintetici, “fisici” adeguati alla nuova normativa, atti del XI congresso “L’ingegneria Sismica in Italia”, Genova 25-29.I.2004

Paciello A., Clemente P. (2004) Sistema software che consente l’integrazione automatica di carte tematiche sui beni culturali ed ambientali con scala, riferimento e grafia diversi, Programma Nazionale di Ricerca Beni Culturali e Ambientali PARNASO. ENEA

Reiter, L. (1990) Earthquake Hazard Analysis: Issues **and** Insights. Columbia University Press.

Scasserra G. (2006). Site characterization of Italian recording Stations for new ground motion predictions. PhD dissertation, Università di Roma La Sapienza

Shome, N., Cornell, C. A., Bazzurro, P. and Carballo, J. E. (1998). Earthquakes records and nonlinear responses. *Earthquake Spectra* 14 (3) , 469-500

Stewart, J.P., Chiou, S.J., Bray J.D., Sommerville, P.G., Graves, R.W. and Abrahamson, N.A. (2001). Ground Motion Evaluation Procedures for Performance-Based Design. Pacific Earthquake Engineering Research Center-Report. September 2001

Zeng, Y., Anderson, J. G. and Yu, G. (1994) "A composite source model for computing realistic synthetic strong ground motions," *Geophysical Research Letters* 21(8), 725-728.

## *Chapter 4*

# Soil treatments

### 4.1 INTRODUCTION

The chapter provides a quick view of the soil treatment techniques: a first paragraph that makes a general classification of all possible treatments techniques, followed by a more detailed description only relatively techniques considered most appropriate in the case of interventions on existing buildings and in particular monuments and for which it was pointed out the possibility of obtaining an attenuation of the seismic signal at the surface.

It is noted that these interventions, extensive use in geotechnical practice, are born and are still used to solve static problems such as settlement or subsidence due to the presence of layers of soft soils. The purpose of the chapter is, therefore, explain the technologies and indicating how and on what parameters they act, how to evaluate the possible use of soil behavior improvement in dynamic range.

Finally, it is emphasises, despite the widespread use of these techniques in practical applications, a paucity of experimental studies on their effects and a complete lack of specific test methods and in the normative field. The methods of execution, often, vary from case to case and the effects are empirically verified.

## 4.2 SOIL TREATMENTS CLASSIFICATION

The soil treatment techniques are classified in the technical literature in different ways:

- 1) based on technological processes,
- 2) according to treatment duration (temporary or permanent),
- 3) based on the presence or absence of filler material.

According Burghignoli (1995) can be classified according to the actions that have on the characteristics of these soils and the resulting change.

At first instance, we can identify two main categories of intervention techniques: one that alters widely the mechanical properties of the soil treated, or acting on the constitution or on the state, with or without filler material, which is eventually distributed uniformly in the subsoil at different levels (micro or macro-element). The second, usually called "reinforcement", change geometrically the ground by inserting structural elements, usually "megaelements", which are distinct from the medium that contains them.

Within the first category we can act on the conditions of the soil modifying factors such as total stresses, interstitial pressures or the index of voids; acting on the constitution, instead, by modifying the interstitial fluid and soil particles. In the case of reinforcement treatment, clearly, only thing modifiable is the megastructure that is taking place in the soil.

First category of interventions include techniques such as drainage (which modifies the total pressure and the interstitial), compaction (which reduces the rate of voids), injections of hydrofracturing and permeation (that fill discontinuities or replace the interstitial fluid cementing mixtures), compaction grouting (reducing the voids ratio and modify the stresses and pore pressure), freezing (which consolidates the interstitial fluid), the stabilization of particle size, chemical, electrochemical and thermal (that modify the soil particles) Figure 4.1, briefly, show the interventions of the first abovementioned category. In this regard it should be noted that some treatments, for example those of injective type, have effects on both the constitution of the state and conditions that may or may not configure elements distinct from the soil. Consequently, their position is not unique.

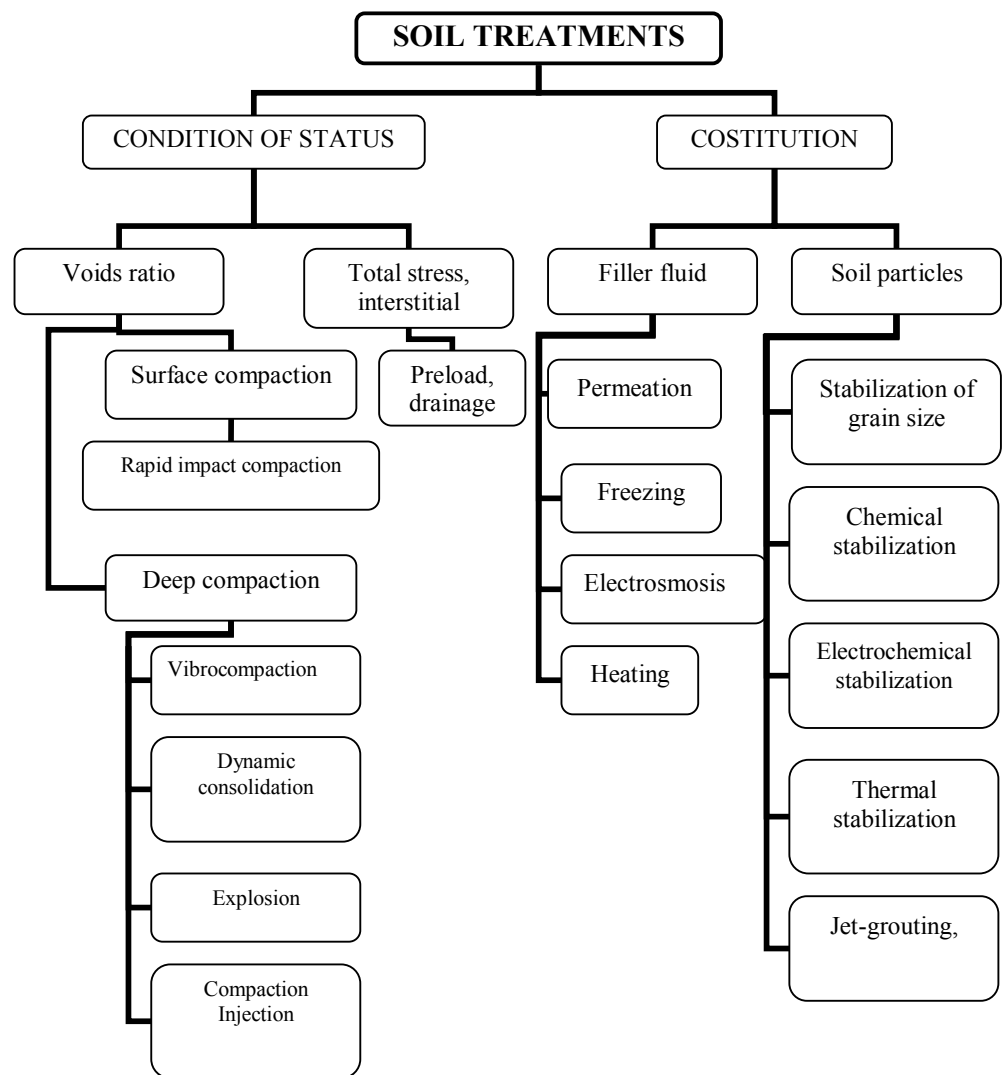


Figure 4.1 – Soils treatment classification

### 4.3 SOIL TREATMENTS DESCRIPTION

This paragraph gives a description of injective interventions that work on the constitution: the strengthening interventions, in fact, beyond the scope of the present work, while those operating conditions was not considered suitable for operations on existing buildings, more so on those of historical monuments.

The interventions of compaction, for example, get the densification of the soil through the vertical application of mechanical vibrations or dynamic type: a heavy mass is dropped from several meters in height on the surface of the deposit, causing compaction and sometimes long-term consolidation of the soil. The equipment used (rollers and plates), moreover, often large (Figure 4.2), evil and just lend themselves to be, possibly introduced into the building. Similar objections could be made for interventions for preload or vibro-compaction (with a drill or a pile) or through the use of explosives, detonated on the surface, or more frequently in a series of holes and causing the collapse of the structure of a loose soil and a more compact structure of the resulting particles. Obviously these types of intervention can not be operated in the presence of a building.

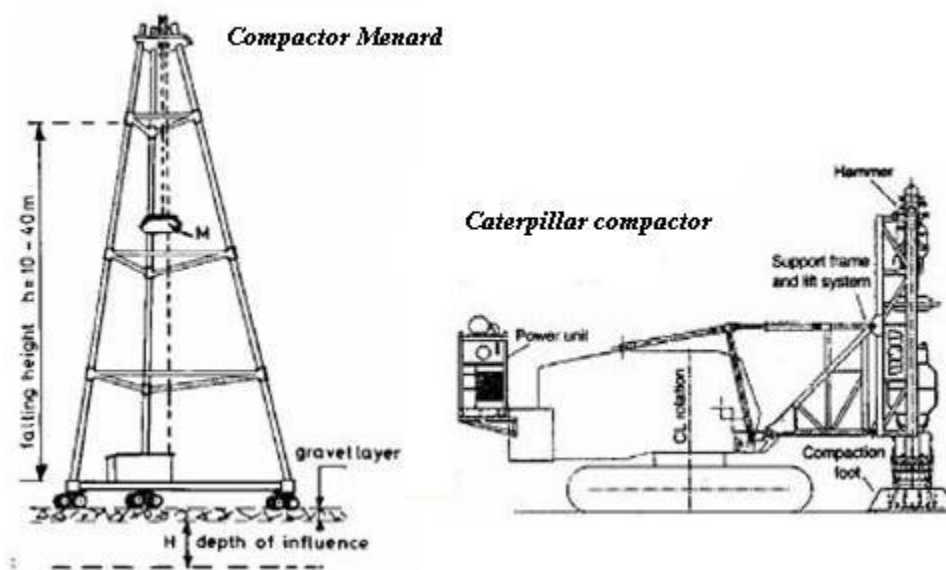


Figure 4.2 – Soil compactor

### 4.3.1 *Injective treatments*

Injection means the inclusion of fluid mixtures in the voids of the soil or in the spaces between it and adjacent structures. Many of them are designed to gelling or harden after the release, or instantly or after some 'time. The improvement occurs to replace (in whole or in part) of liquid and gaseous phases with other substances with properties suitable for achieving the objectives of the intervention. The main objective of the injection is to make the soil more resistant, dense and/or less permeable, ie modify its mechanical and hydraulic characteristics.

However, they may also be used only to fill the gaps that are otherwise inaccessible with other techniques, and encourage the development and transfer efforts by soil or by the same structure. The injectable soils are constituted of alluvial materials or detrital up to a certain lower limit of permeability (from gravel to sandy silt), rocks (from small cracks in karst) and defective masonry.

To project an intervention with injections includes the choice of the substance to be injected, the measurement of the pressure of work, the executive details. Are injected into the soil in the holes of the polls, mixtures whose composition is highly variable in relation to the permeability of the material. More precisely, in soils with high permeability are commonly used cement mixtures, while in soils with low permeability are preferred chemical mixtures (organic or inorganic) capable harden rapidly in the presence of water. All chemical solutions (organic, inorganic and synthetic) can produce an intense and pollution of groundwater that is why their use is limited. The additives have important functions (plasticizer, plasticizer, accelerator); suitably proportioned mixture can give the most suitable characteristics for the purpose of the intervention. (Guidelines GNDT)

The different injections are classified here according to the method of insertion into the ground (Figure 4.3), but it would be possible to consider other criteria of differentiation, such as the type of material injected, the applications:

- 1) injections by penetration (impregnation or obstruction);
- 2) injections for lifting (or hydrofracturing compaction);
- 3) jet grouting.

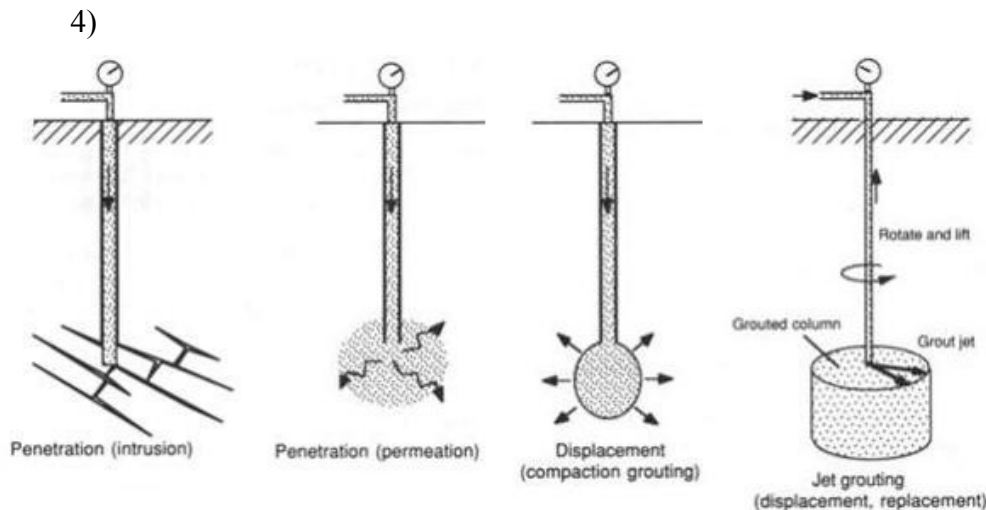


Figure 4.3 – Different typologies of injection

Methods for impregnating or clogging consist of filling mixtures in the soil voids, and/or in stratification joints and/or fractures in rocks, in which case the entries are made at low pressure and no change in the size of the voids or pores filled.

The methods for lifting and moving the affected soil is divided into injections for compaction and hydrofracturing. In the first case (compaction grouting) a dense mixture is melted and injected into a soil shaped bulbs that move and densify the surrounding soil, without penetrating into the voids. In the process of hydrofracturing mixtures are placed under high pressure and cause cracks, the displacement of the ground here is not limited, as in the previous case, but it is considerable.

The jet grouting involves the injection of cement grout, mixing soil is harnessing the erosive power of a jet of air or water or grout is injected at high speed rotating horizontal rod (monitor).



### **Compaction grouting**

In the compaction grouting procedure of injections, as already mentioned, the objective is to inject controlled masses of viscous fluid in the subsoil, without fracturing, or permeate it, for this purpose the fluid must have adequate rheological properties to be pumped: generally a silty sand to which are sometimes added bentonite or cement, chemicals rarely. The injections are made along a line or a grid with a mesh varying in the range 1-4.5m.

The executive procedures can be divided into down-stage grouting in which the injector moves from top to bottom and Up-stage grouting in which it proceeds from the bottom up. (Figure 4.4)

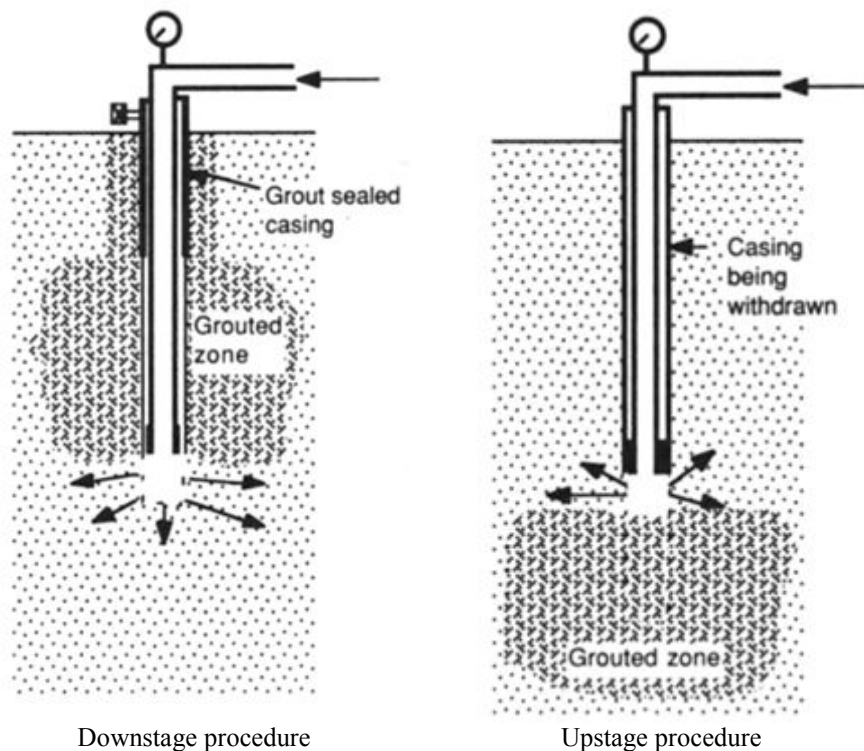


*Figure 4.4 – Different typologies of injection*

The first of the two methods and is used profitably when you should inject loose soils with highly variable granulometry. Is performed a section of the hole, withdrew a few meters of the drilling tool and injected through auctions;

therefore expects the hardening of the mixture, it repeats the drilling and continue in subsequent sections with the same sequence. With this system the injection operations are very long because of having to wait for the deepening of the hole, the hardening of the mixture injected. Upstage mode, however, the forum is performed until the end, putting in place a temporary lining which is then connected to the injector and retired gradually with the progress of the injection. The risk working with coating pipes is that the mixture, coating the outside of the back, the lime to the ground or from spreading uncontrollably in the horizons not yet treated. Is not possible, moreover, continue the injection on the injected sections for the first time.

The downstage procedure allows get better results, since moving from top to bottom, and not having the mixture injected as no escape upwards, increases the confining pressure; in contrast Upstage procedure is much more advantageous economically since it allows separate the phases of drilling and injection, minimizing downtime. But there is a problem of keeping the shutter, which must be ensured throughout the hole: the mixture could climb above the disc and cemented it.

Increasing the pressure of injections you can get the effect of permeation, or pushing it further, the billing of the soil and the formation of mix arms or lenses which develop in least resistance directions. Repeating pressure cycles after the first fracturing you will get an increase of the arms, with an appreciable displacement of the soil. Generally fracturing grouting are executed with valved tubes. (Figure 4.5)

The order of injection holes is determined by the needs of individual cases, but in general it is a good idea to start with the outer to create a containment the whole procedure is very effective, because you can work with it multiple shots on the same injection valve already injected. As often has to do with alternating layers with different characteristics of particle size, density and permeability, valved tubes also allow to vary the characteristics of injection for the various layers: it allows the controlled injection of different mixtures in any order at every level and at any time.

Needless to say, in relation to the granulometry of the soil, the injection pressure and viscosity of the mixture, the results vary considerably, not only from soil to soil, but also within the same soil.

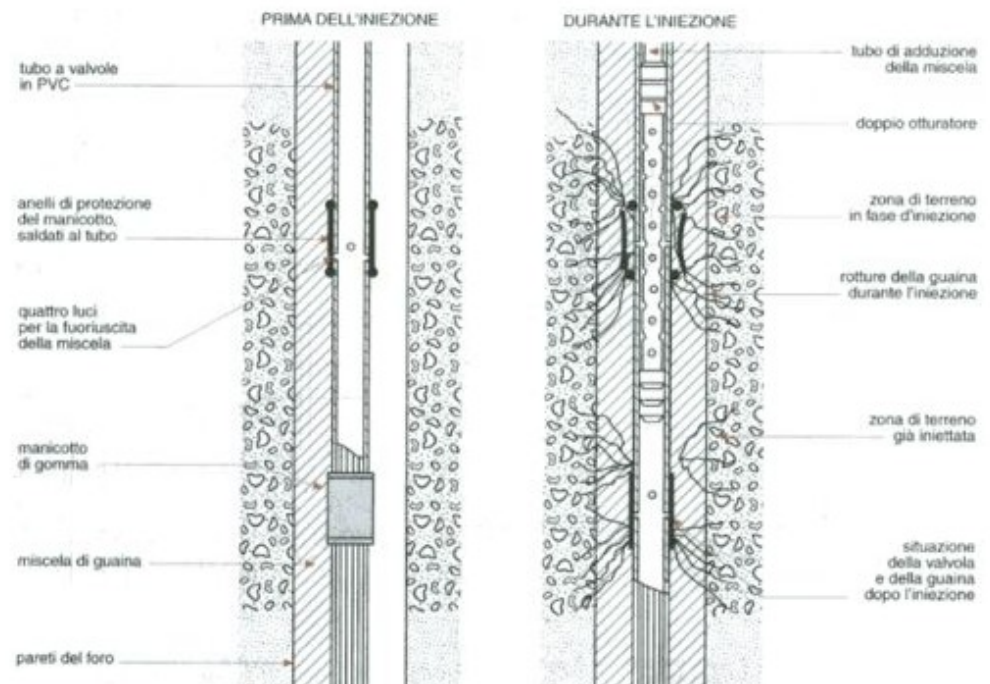


Figure 4.5 – Valved tubes

One of the advantages of compaction grouting is the lack of vibration, which lets to use this technique in all types of soil: often used in the sands and silts, but also in clays. Injections can be made from any angle, including horizontal, and at any depth, although often not why the reservation is canceled after 30m. (Figure 4.6-Figure 4.7)

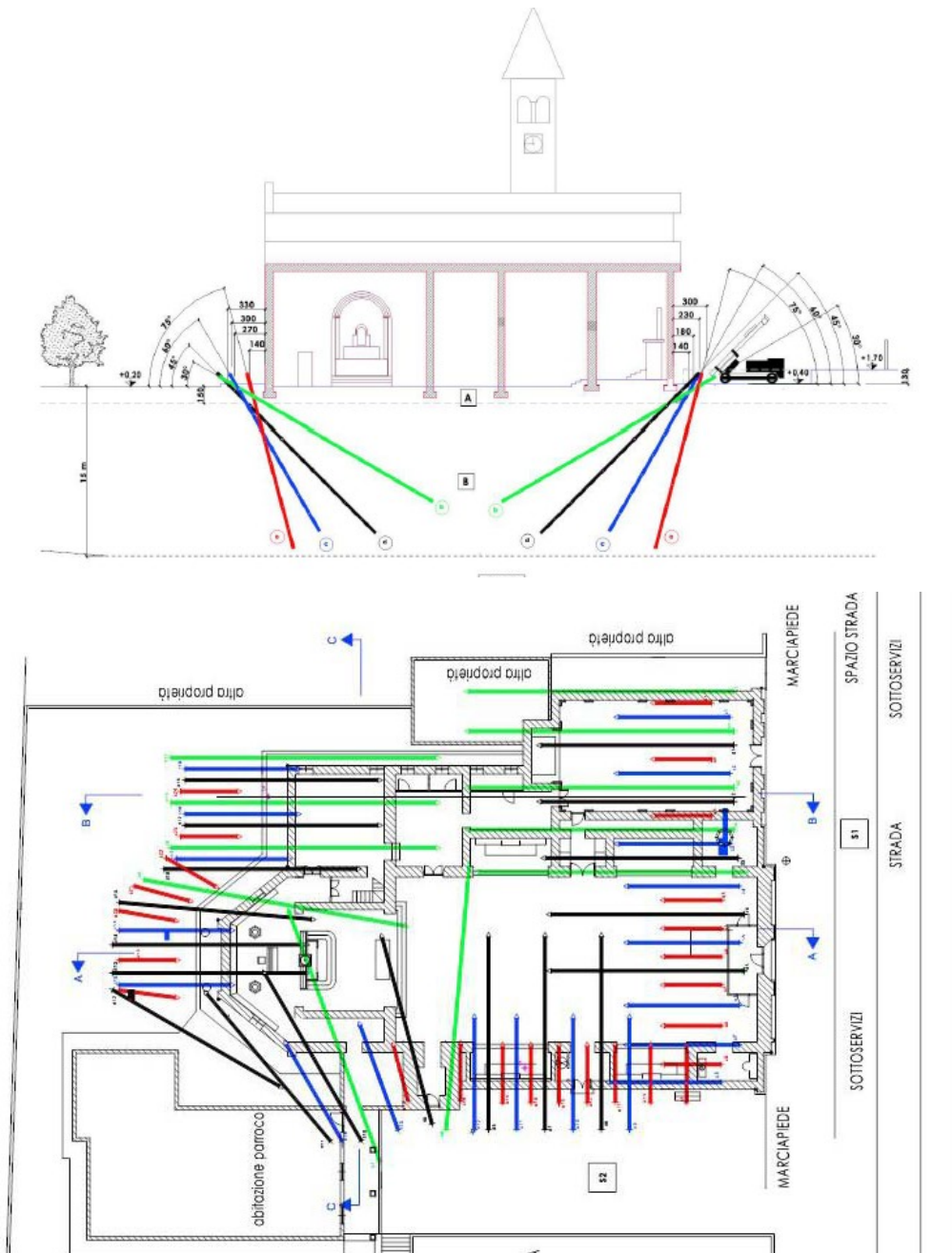


Figure 4.6 – Example of intervention with soil fracturing injection on S. Giorgio martire Church – Verona Technical paper (Nanni et al 2006)

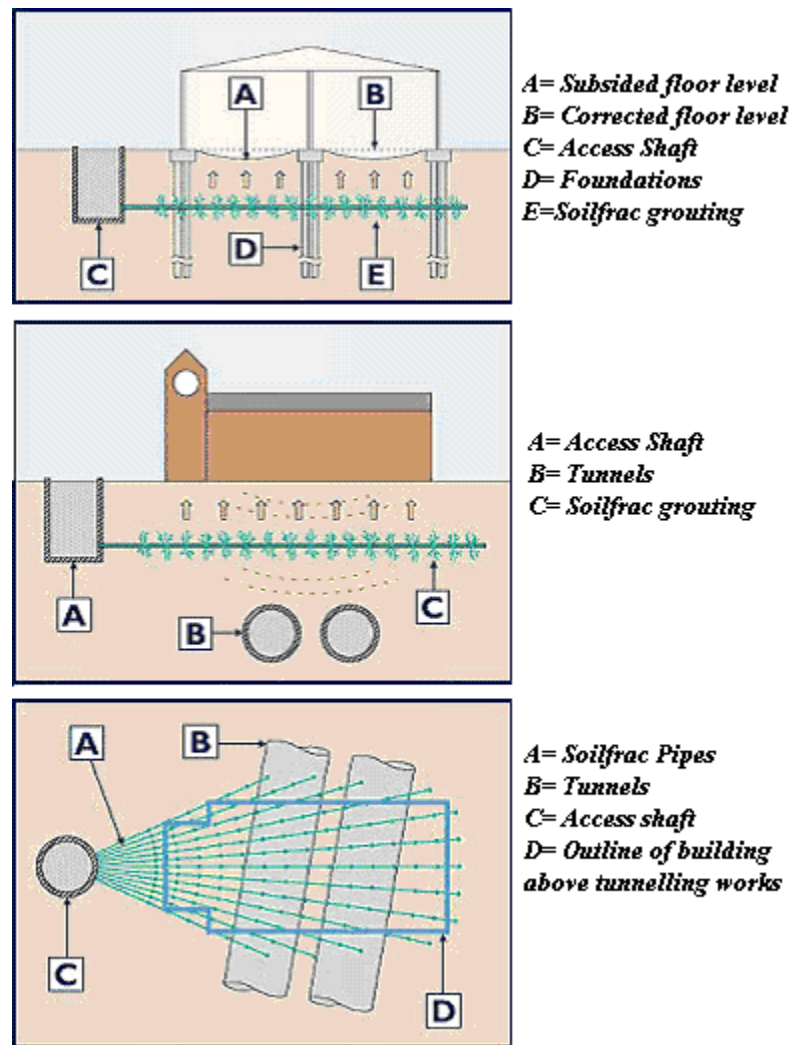


Figure 4.7 – Example of intervention with soil fracturing injection on S. Giorgio martire Church – Verona Technical paper (Nanni et al 2006)

The seismic efficiency of these interventions is evaluated in terms of average increase along the depth of the shear velocity  $V_s$ , from Massa (1998), through the parameters  $E_v$  (for its definition see §7.5): compaction grouting were used along a section of Los Angeles (Reed et al 1998) to restore integrity and stability to a stretch of about 5.1Km by reducing liquefaction. Cone Penetration Testing (CPT) established the condition of soils around the storm

drains prior to compaction grouting. A true low-mobility grout mixture was then injected to fill voids and improve soil properties from a depth of 1.5 m below the freeway, to a depth of 1.5 m below the bottom of the storm drain. Post-grouting CPT data established that the design performance criteria for the compaction grouting program had been achieved, including a marked decrease in the liquefaction potential of sandy soils in areas of groundwater table as shallow as 1.5 m. The average values of efficiency in relation to depth are shown in Table 4.1

*Table 4.1 – Shear velocity before and after compact grouting intervention*

Depth (m)	$V_{s0}$ Before intervention	$V_s$ After Compaction grouting	$V_s/V_{s0}$	$V_s/V_{s0}$	$E_v$
3	120	250	2.05	-	-
4.5	120	220	1.83	1.64	3
6	220	290	1.32	1.83	2.45
7.5	-	275	-	2.18	-
8.5	160	260	1.62	1.92	3.15
		Mean	1.8	1.7	3

In conclusion, the average efficiency can be assumed to  $E_v=1,8 \cdot 1,7=3$ .

### **Jet grouting**

This technique allows realize underground consolidated elements of different shape and size of low permeability and good mechanical properties: the procedure requires the injection of fluid mixtures, projected at high velocity into the ground through one or more small diameter jets at the extremities of a metal rods battery.

Because of the high pressure, in contrast to the compact grouting techniques, we have not a compaction effect but a disaggregation action on the soil. The disaggregated soil is, then, mixed with additives and partially replaced. The jet grouting manufactures, as well, elements of cemented soil (soilcrete), roughly cylindrical in shape, which is called the consolidated column. By decreasing the spacing of injections is possible connect multiple columns in order to obtain the elements considered as a two-dimensional.

Great advantage of the jet grouting is the ability to work under all conditions, even in small spaces and to treat a very wide range of soils, although it was more cost effective in a gravel-sandy soils.

The treatment is divided into two stages: a first perforation and a second input for rotation orotopercussione thanks to a special drill head.

The mixtures used are mainly concrete. The execution systems can be divided into:

- one-fluid, which uses a unique cementing agent,
- two-fluid, cementing agent in which air is added,
- tri-fluid system in which a bi-fluid water is added.

The diameter of the columns depends on the sub-soil conditions (particle size range, density, size of particle), the erosive jet (speed, specific gravity and air pressure of the fluid that surrounds the jet itself) and slope parameters (rate of ascent and rotation).

The depth of execution is tied to the size of the drilled hole. (Croce et al 2004) For evaluation of efficacy was made based on data provided by Croce et al. (1994) from which we can deduce that for coarse-grained soils you have an average effectiveness  $E_V = 1.5-2.0$ , while the clay is the value of  $E_V = 1.2-1.4$ . (Massa 1998)

Table 4.2 shows a summary of the approached typologies intervention: in it we report the soil type in which they are executed, the geometry of the cemented element, the maximum depth of intervention, the diameter of the column and the efficacy ratio  $E_V$ .

*Table 4.2 – Summary of the approached treatments characteristic*

Treatments	Soil type	Geometry	$H_{max}$ (m)	D (cm)	$E_V$
Compaction grouting	Course-grained	Columns	15	70-80	1.7
	Fine-grained			30-50	
Chemical compact grouting	Course-grained	Columns	10	70-80	3
	Fine-grained			30-50	
Jet grouting	Course-grained	Columns	40	50- 350	-
	Fine-grained				
Chemical stabilization	Course-grained	Columns	20	80- 100	1.4-
	Fine-grained				1.7





## BIBLIOGRAPHY

Burghignoli A, (1995) – Miglioramenti delle caratteristiche meccaniche dei terreni argillosi mediante trattamenti colonnari a secco con cemento ed inerte, *XIX Convegno Nazionale di Geotecnica, Pavia 19-21 Sett. 1995*

Croce P, Flora A., Modoni G (2004) – Jet grouting – *Hevelius edizioni*, Benevento

Croce P, Gajo A., Mongiovì L., Zaninetti A. (1994) – An experimental assessment of the effects jet grouting, *Rivista Italiana di Geotecnica*, 2, p. 91-101 (In italian)

Linee guida per interventi di riduzione del rischio di instabilità dei pendii: tipologie e metodi di dimensionamento GNDT (2006)

Massa U (1998) – Trattamenti di miglioramento del sottosuolo per la riduzione del rischio sismico: aspetti tecnologici e progettuali – *Tesi di laurea, Università degli studi di Napoli “Federico II”*

Nanni E., Macaccaro R., (2006) - Stabilizzazione della Chiesa di San Giorgio Martire di Cazzano di Tramigna (VR) a mezzo sistema SOILFRAC– *technical paper - Keller fondazioni*

Reed John W., Hourihan, Daniel T. Thornton, Gregory J. (1998) - Compaction grouting to reduce seismic risk and collapse potential for freeway storm drain system – *Geotechnical Earthquake Engineering and Soil Dynamics III*, pp. 666-667

This page is, intentionally, left blank

## *Chapter 5*

# Study case: the site of Villa Favorita sea park

## 5.1 DESCRIPTION

The area studied is located in the coastal part of the most famous Villa Favorita's park in Herculaneum. (Figure 5.15)

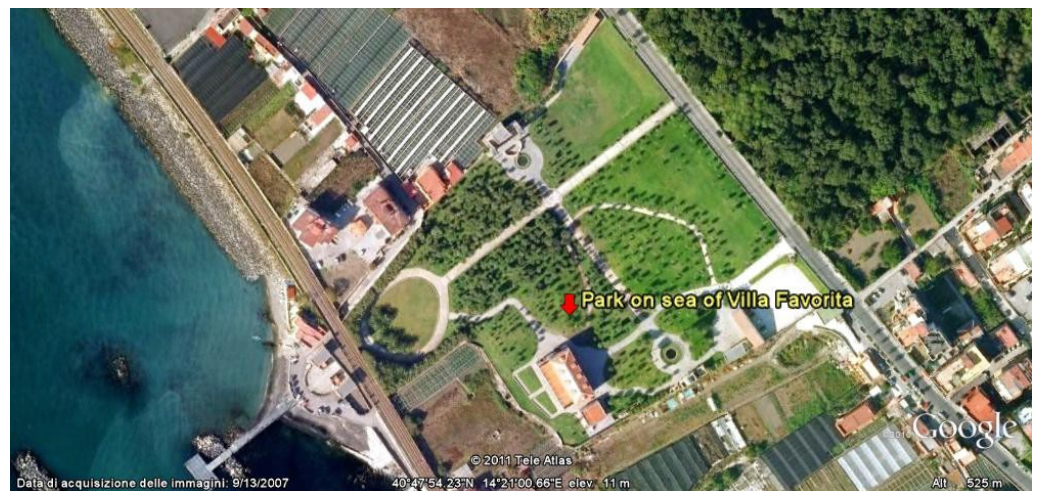


*Figure 5.15 – Studied site location*

The large area of the Villa Favorita's park, rich in mediterranean and exotic essences quite rare, interrupted in its continuity from the railway line and a roadway, ending into the sea with the port Bourbon.

In this park is located, with other buildings of remarkable value, the house of the mosaics of the most sumptuous Villa annex, and its two coffee house near the coast.

In order to mend the fabric of Herculaneum and wider area around the Golden Mile the "Ente Ville Vesuviane", after years of neglect, (Figure 5.2) in 1990, has recovered the area.



*Figure 5.2 – status of area before 1990 (<http://www.dentronapoli.it>)*

## 5.2 GEOLOGICAL FRAMEWORK

The area of city of Herculaneum (until 1969 Resina) is situated at the foot of the volcanic complex of Somma-Vesuvius and, therefore, the geology of the place is closely linked to the eruptions that occurred over the centuries.

Over the past 17,000 years Vesuvius has been characterized by widely varying types of activities, related to ease of description, three main types:

- a. Moderate eruptions, mainly effusive;
- b. Strong eruptions, mainly explosive ("sub-Plinian");
- c. Catastrophic eruptions, explosive only ("plinian").

The first type is characterized by small volumes of magma emitted (in the order of  $0.01 \text{ km}^3$ ), brief periods of quiescence preceding the eruption (in the order of years) and kind of just evolved magmas.

The second volume includes about  $0.1 \text{ km}^3$ , substantially longer (several decades to several centuries) and moderately evolved magma composition.

The third type are associated with eruptions of large volumes of magma ( $0.1 \text{ K}$  or more:  $\text{m}^3$ ), very long residence times (several hundred to over a thousand years) and highly advanced products. (Lodigiani S.P.A. Ente Ville Vesuviane Archive)

For this reason, the subsoil presents substantial and irregular variations among areas not very far apart.

In order to well understand the nature the subsoil object of study is necessary a description, even though concise, of major eruptions which, from 79 A.D. affected area.

79 A.D. is the most famous eruption in the volcanology history. It has been described in two letters of Plinio il Giovane (61-114 A.D) to Tacito. In the eruption Herculaneum and Pompeii were completely destroyed. The city was

buried by pyroclastic flows and surges, resulting from the second eruptive phase, creating layers of the order of 10-20m.

After the 79 AD eruption of the most significant was that of 472 AD. Thereafter, up to 1631, the events are historically reported at long intervals from 30 to 350 years.

From 1631, Vesuvius begins a phase of persistent activity that lasts, except for short periods, until 1944. The rest intervals, found in these three centuries, have a maximum duration of 7 years.

Because, therefore, of the constant activity of the volcano, due to the habit of it active, it is probable that smaller events are not reported in the chronicles that dwell only on particularly violent eruptions.

Many eruptions of this period are similar: the initial activity is effusive, with lava flowing from cracks or overflow from the edge of the cone. This phase may be accompanied by small strombolian explosions.

After a few days, the eruption becomes explosive with the formation of 2-4 km high lava fountains. In the final stage, a sustained eruption column, 5-15 km high is created, then the central part of the crater collapses and has a resting phase for a few years until the activity takes up with a new effusive phase.

This period ends with the eruption of 1944 that blocked the pipe and arrested the eruptions. Have, since, been found only the emission of vapors (fumaroles) and a modest seismic activity.

During these three centuries, the volcano, symbol of the city, has been described, studied and shown in many documents, so it was possible to reconstruct the story.

Table 5.1 (G. Scarpato et al. 2005;) shows the main events of the volcano over the centuries.

*Table 5.1 – Chronology of the Vesuvius' main events over the centuries*

Date	Eruption type	Places	Volcanological observations
203	Ex		The roar of explosive phenomena were warned to Capua
472 5-6 Nov	Ex-Sb Pl	Pollena; Ottaviano, Napoli	Product of fall-rich lava stone. Massive pyroclastic flows in NW
512	Ex		Extensive ashes flows
685 Feb-Mar	M		Lava flows to the sea. Large ash clouds.
787	Ex		Strombolian activity. Mudslides.
968	M		Probable lava flows to the sea.
999	Ef		
1007	Ex		
1036 or 1037 Jen-Feb	Ef		Lava flows to the sea.
1139 29 May	Ex		Large ash clouds.
1500	Ph		Reddish ashes emission. Doubt event: there isn't stratigraphic feedback
1631 16-17 Dec	Ex-Sb Pl	Pyroclastic flows in Barra, S. Sebastiano, Leucopetra, Portici, Resina, Torre del Greco. Mudflows in S.Paolo Belsito, Pomigliano, Mariglianella	Fall of Pyroclastic fragments in E and NE. Pyroclastic flows to the sea did advanced the shoreline. (Figure 5.3) Mudflows. Output of juvenile material.
1637	Ex		Emission of "white and bituminous ash"
1649 Nov	Ex		Ash clouds
1660 July	M	Damages in Resina, Torre Annunziata, Torre del Greco.	Emission of black ash.
1682 Aug	M	Torre del Greco, Ottaviano, Nocera, Pagani, Cava and S. Sebastiano	Strombolian activity. Lava fountains. Ash fall.
1685 Oct.	M		Strombolian activity. Lava fountains.
1689 Dec	M		Strombolian activity. Lava fountains.
1694 6 Apr- 2 May	M	S. Giorgio a Cremano, Torre del Greco, Boscorecase.	Lava flows at NE and S. Ash on Naples

Legend TYPE: Ex = Explosive; Sb Pl= sub-plinian; M = mixed; Ef= Effusive; Ph=Phreatic

Date	Eruption type	Places	Volcanological observations
1696 25 Jul – 13 Aug	M	S. Giorgio a Cremano	Ash clouds. Lava flows to NW
1697 Feb; Sept; Dec.	M	Resina, Torre del Greco	Strombolian activity. Lava flows to WSW.
1698 19 May – 19 Jun	M	Torre del Greco, Ottaviano	Strong strombolian activity. Lava flows to W, SW and NE
1701 1-7 July	Ef	Boscotrecase, Campitiello di Ottaviano (S. Giuseppe Vesuviano)	Lava flows to E and S
1707 20 July-18 Aug.	Ex	Ottaviano, Boscotrecase e Naples	Ash clouds with pyroclastic products fall. Mudslides
1714 21-30 June	M	Lava to Boscotrecase, Torre Annunziata and Ottaviano.	Lava Flows to E and S. Ashe cloud to NE
1717 6-8 June	M	Torre del Greco, Trecase	Fluid lava flows to SE and W. Lava fountains.
1723 25 June – 4 July	M	Lava on Ottaviano; pyroclastics on Ottaviano, Nola, Palama, Sarno, Gragnano, Nocera, Pagani, Cava, Sanseverino and Salerno	Strombolian activity and pyroclastics falls to E. Lava flow to NE
1724 12-22 September	M	Torre del Greco	Lava flows to S
1730 19-30 March	Ef	Ottaviano	Lava flow to E
1737 19May – 6 June	M	Lavas in Torre del Greco and Boscotrecase. Pyroclastics product falls on Somma Vesuviana, Ottaviano and Nola.	Strong explosive activity with dispersal of pyroclastic products. Lava flows to W.
1751-1752 25 Oct-25 March	Ef	Lavas in Ottaviano, Boscotrecase and torre Annunziata	Lava flows.
1754-1755 2 Dec-17 March	M	Lavas in Ottaviano, Boscotrecase and Boscotrecase Pyroclastics falls in Torre del Greco and Portici.	Strombolian activity. Lava flows. Lava fountains.
1760-1761 23 Dec – 5 Jan	M	Lavas in Torre del Greco and Boscotrecase. Ashes fall in Sorrento peninsula and in Cilento	Lava to S near the sea. Explosive activity. Ash clouds.

Legend: Ex = Explosive; Sb Pl= sub-plinian; M = mixed; Ef= Effusive; Ph=Phreatic



Date	Eruption type	Places	Volcanological observations
1767 19-27 October	M	Lavas in Ercolano, S. Giorgio a Cremano and Boscotrecase	Lava flow to NW and to S. Explosive cloud with ash fall. Mudslides. Lowering of groundwater
1770 March	M	Eastern side of Vesuvius	Strombolian activity. Lava flow to E.
1771 1-11 May	M	Western side of Vesuvius	Lava flow.
1779 3/8-15 Aug.	M	Lave to Resina. Pyroclastic fall on Ottaviano, Somma, Massa, Nola, S. Paolo Belsito, Palma ed Avella. Crack in Torre Annunziata	Lava from northern fracture. Strong strombolian activity with lava fountains. Mudslides on the north side. Pyroclastics fall. Ash clouds.
1794 15-24 June	M	Lava on Torre del Greco to the sea and near Ottaviano	Lava flow to NE. Intense explosive activity in the cone with lava fountains and ash clouds.
1804 15 Aug. – 15 Oct.	M	Lava between Torre del Greco and Torre Annunziata	Lava flows to SO. Explosive strombolian activity in the central crater.
1805 13 Feb. – 12 Aug.	M	Ercolano, Torre del Greco and between Torre del Greco and Torre Annunziata.	Fluid lava flows to SW and S to the sea. Lava fountains. Strombolian activity
1806 31 May – 5 June	M	Lava in Torre del Greco. Ashes fall up Nola, Sorrento, Massalubrense to Benevento	Lava fountains and flow to S-SW.
1810 11 September	M	Ercolano, Boscotrecase and Ottaviano.	Lava flows to W-NW and to SE. Ash clouds
1812 1-4 Jan	M	Torre del Greco	Lava fountains and flow to SW
1813 25-27 Dec.	M	Lava in Boscotrecase and Torre del Greco. Ash falls up Acerra, Napoli and Ischia	Strombolian activity. Lava flow to S.
1817 22-26 Dec.	Ef	Torre del Greco	Lava flows to E and another to SW

Legend: Ex = Explosive; Sb Pl= sub-plinian; M = mixed; Ef= Effusive; Ph=Phreatic

Date	Eruption type	Places	Volcanological observations
1822 21 Oct. – 10 Nov.	M	Lavas to Ottaviano, Boscotrecase and Ercolano. Pyroclastics fall to Boscotrecase and Torre Annunziata. Red ashes in Ottaviano, Pomigliano, Casoria, Napoli, Barra and Resina.	Lava flows. Pyroclastics fragments to SE. Ashes fall. Lava fountains. Red Ashes cloud to N. Mudslides to N and E side of volcano.
1834 23 Aug. – 10 Sep.	Ef	Lava between Boscoreale and Ottaviano	Lava on the eastern side.
1839 1-5 Jan	M	Lava in S. Giorgio a Cremano and Boscotrecase. Ash fall in Boscotrecase and Ottaviano to Sorrento	Lava flows to W and SE. Explosive activity. Ash fall to S. Lapilli fall.
1850 5 Feb. – 2 March	M	Lavas to Terzigno. Ash and lapilli falls in Ottaviano and Torre Annunziata	Lavaflows to SE. Lapilli fall. Ash cloud. Lowering of the groundwater
1855 1-28 May	Ef	Massa di Somma, S. Sebastiano and S. Giorgio a Cremano	Lava flow to NW
1861 8-10 Dec.	Ef	Torre del Greco	Lava from western crack to SO. Fumaroles in the sea.
1868 15-25 Nov.	Ef	Cercola, S. Sebastiano, Novelle di S. Vito	Lava form northern side to NW
1872 24 Apr. – 2 May	M	Massa di Somma and S. Sebastiano	Lava from northwestern crack to S and W. Explosive activity in the central crater. Strombolian activity.
1891-1894 7 June 1891– 5 Feb. 1894	Ef		Lava flows.
1895-1899 3 July 1895- 1899	M		Lava flows. Explosive activity with the launch of juvenile material and seismic activity.
1900 4-9 May	Ex		Strong strombolian activity in the central crater with lava fountains. Seismic activity in Portici, Ercolano and Torre del Greco.

Legend: Ex = Explosive; Sb Pl= sub-plinian; M = mixed; Ef= Effusive; Ph=Phreatic

Date	Eruption type	Places	Volcanological observations
1903-1904 27 Aug 1903 - Sept 1904	Ef		Fluid lava flows
1906 4-22 April	M	Lava in Boscotrecase and Torre Annunziata. Pyroclastics fall to Ottaviano, Somma Vesuviana and S. Giuseppe Vesuviano	Lava flow. Strombolian explosive activity in the crater. Ash clouds. Pyroclastics fall. Pyroclastic flows. Red ash falls. Mudslides
1929 4-10 June	M	Terzigno and surrounding areas (Avini, Pagani, Campitelli)	Lava flows from the central crater to E. Explosive activity with lava fountains and intense seismic activity.
1944 18 Mar. – 7 Apr.		Lavas in S. Sebastiano and Massa di Somma. Pyroclastics fall up Terzigno, Pompei, Scafati, Angri, Nocera, Poggiomarino and Cava.	Lava from north side of crater to E, S and N. Lava fountains. Black clouds. Little pyroclastic flows. Eruptive clouds. Lapilli and ash fall to SE.

Legend: Ex = Explosive; Sb Pl= sub-plinian; M = mixed; Ef= Effusive; Ph=Phreatic

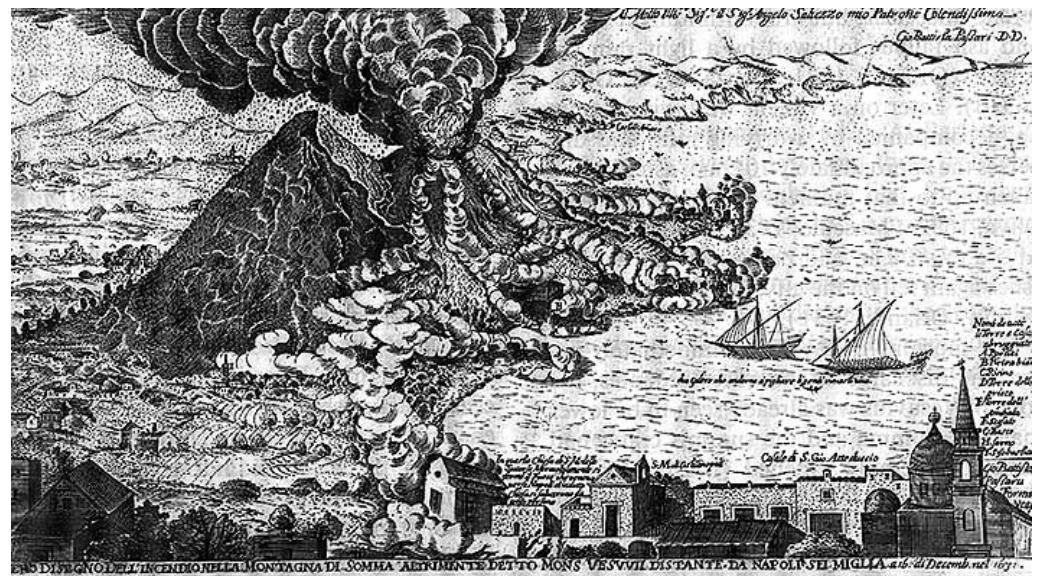


Figure 5.3 –Vesuvius eruption in 1631–Print by G.B. Passari (Museum of S. Martino-Napoli)

### 5.3 LITHOLOGY

The substrate of Herculaneum territory is very chaotic and discontinuous in the longitudinal succession of the various lithotypes, so in this direction the heteropies give it not homogeneous features. Figure 5.4 shows an historical map of Vesuvius with the principal eruption until 1832; in red highlights the area in question, where the name “la Favorita” is clearly legible.

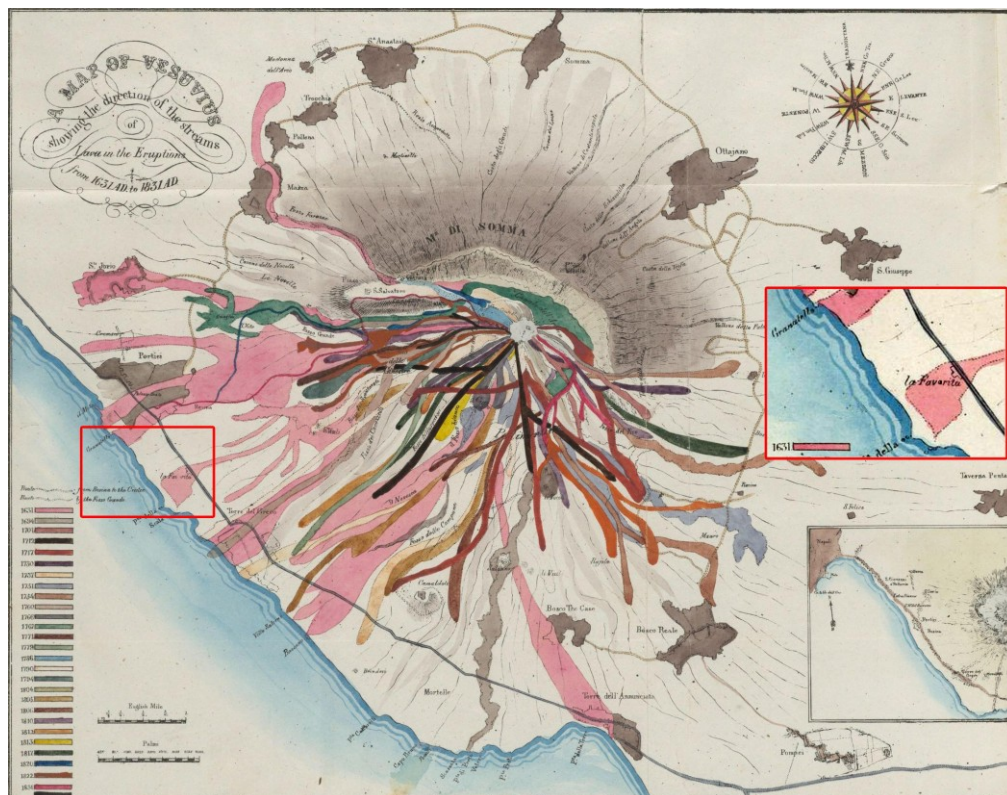


Figure 5.4 - Sketches of Vesuvius : with short accounts of its principal eruptions, from the commencement of the Christian era to the present time / by John Auldjo. Naples : G. Glass, 1832. Houghton Library, Harvard University, Cambridge, Mass.

In 1983, as part of preparing the master plan of the city of Herculaneum, a geological and technical survey of the whole municipal area was carried out by Prof. Geo. Aldo Velotti. We report, below, briefly his conclusions.

«The municipal area in order to the geo-lithological characterization was divided into sectors, namely A, B and AB:

- a) the sector A consists of lava, ciner and pyroclastic products with a thickness of over 20 meters;
- b) the field B is composed of gray trachy lava outcropping or partially covered with topsoil;
- c) the sector AB is constituted by lava partially covered with a pyroclastic thick varies widely from area to area, average about 10m.»

The subsoil of the investigated area, bounded on the north by the Via Gabriele d'Annunzio and downstream from the coastline, is characterized by the Vesuvius eruptions products that in various stages have reached the coastline, changing its profile. (Figure 5.5)

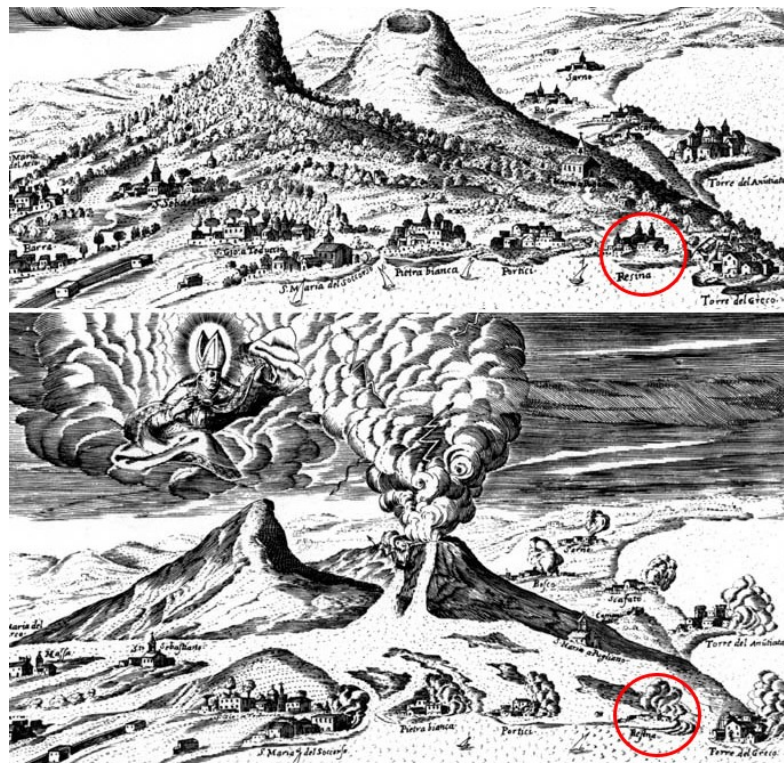
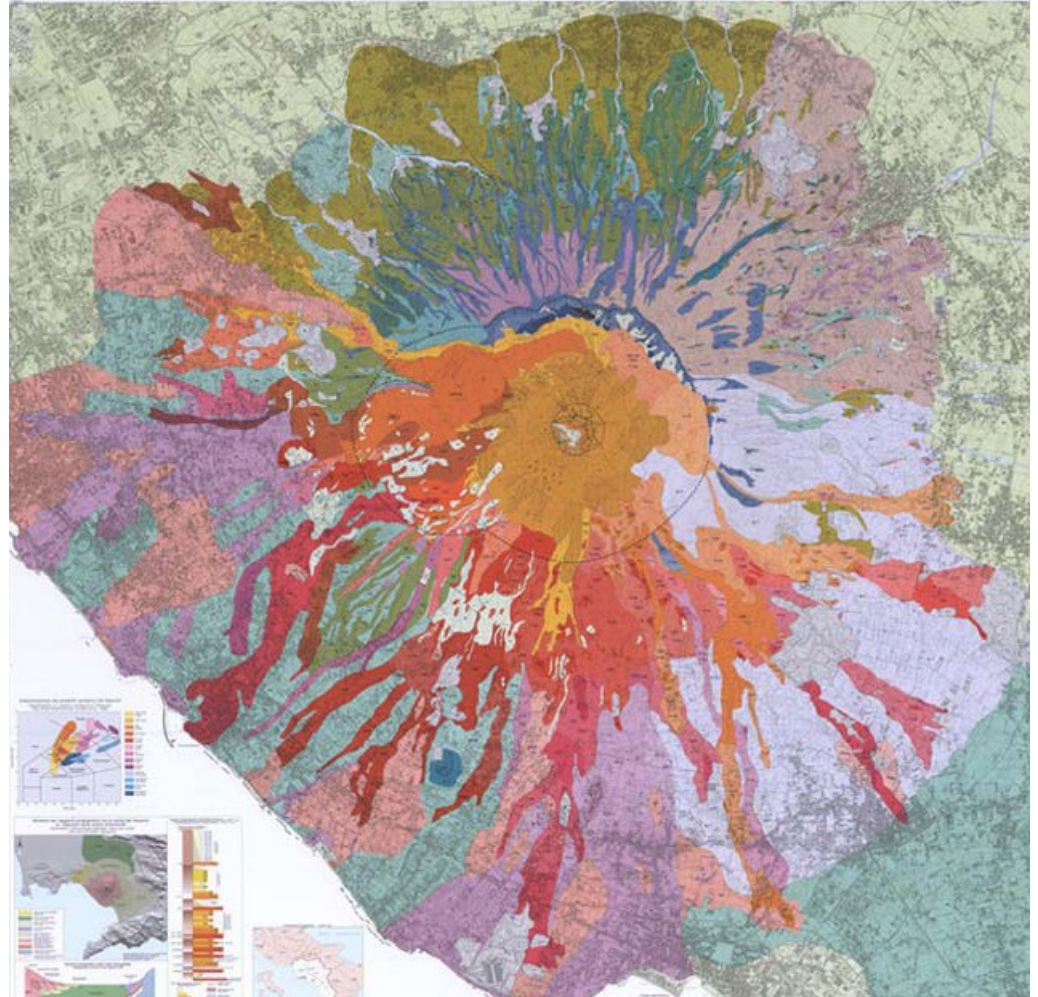


Figure 5.5– The coastline before and after the Vesuvius eruption in 1631 – Table by N. Perrey (1632) taken from “Trattato del Monte Vesuvio” di G.B Giuliani, Longo, Napoli, 1637.





The lithologies in outcrop in the area consist of lava flows subsequent to 79 AD and prior to 1631, and by thick pyroclastic flow (ash clouds, lahars) of the 1631 eruption, which frequently cover these lavas, as shown in detail in the geological map of Vesuvius. (Figure 5.7)



*Figure 5.7—Geological Map of Vesuvius (Sbrana et al 2003)*

In particular are found:

- a) Volcaniclastic product (loose material): are constituted by blackish sand with variable grain size with the inclusion of lava, slag and fragments of lava and ash gray levels stored so uneven and discontinuous. These products are deposited by sub-aerial leaching or transport of meteor and cover layers of lava, therefore, they may have both small thickness to some tens of meters (in the areas sub-level alternated by lava). The loose material have mainly sandy particle size, and can incorporate natural stone fragments of lava or slag, typically, their density is quite high.
- b) Lava (lithoid material): tephritic and basaltic formation produced by the cooling of the material poured out by volcano is, where exist, the bedrock upon which rests the aforementioned pyroclastics. The stratigraphic relationship between the two formations are very irregular where the outcrops are very limited. The trend of the lava substrate thickness that varies both extensions, in some areas it may even be absent. The overlap of material in various effusive stages have influenced the thickness of the pyroclastic that have mainly a lenticular shape evident in lateral facies heteropy with lava layers. Where the lavas are missing, these products constitute the bed-rock.
- c) Sands: under the lava formations are found coastal blackish sand with pebbles of the shore, algal debris, shell fragments and layers with intercalations pozzolanic and cinder layers.

## 5.4 THE GROUNDWATER

The static level of water is very deep from the ground level, greater than 10m, it is not, therefore, be taken in account either the change in water level due to exceptional contributions to meteorological events, either as a result of an earthquake. It should be noted, moreover, a good permeability of the subsurface soil components, which together with the natural slope of the slope provide rapid drainage of surface infiltration. (Velotti A.1983)



### 5.5 AVAILABLE IN SITU SOIL TEST (Velotti A. 1983)

In the geognostic survey carried out, in 1983, by prof. Geo. A. Velotti, 48 perforations were executed throughout the municipal territory, starting from an altitude of 300 m down the valley to the level of the sea. The geognostic study made use also 23 surveys, carried out before, provided by the Technical Office of the City.

During the drilling samples were taken 37 of which are determined by disturbed about the general physical characteristics of soils and undisturbed samples No. 4 on which the shear tests performed. Were also carried .16 n static penetration tests mainly distributed in the first 15.00 m depth.

The geognostic were performed using either a probe C MV K800 automatic rotation by fluid circulation, with a core bit  $\Phi$  100, rotary probe to feed dry core bit  $\Phi$  400 diameter.

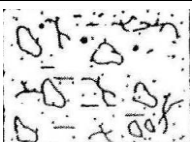
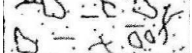
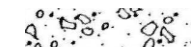
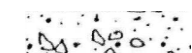
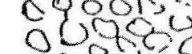
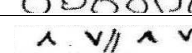
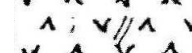
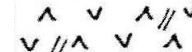
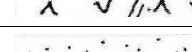
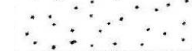
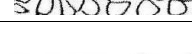
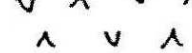
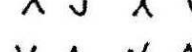

The penetration tests were static-mechanical penetrometer execute with Dutch Gouda from 10 tons conical tip with cm 3.6 in diameter and then with an area of 10 cm, equipped with "Friction Jacket –cone" side-sleeve area of 150 cm<sup>2</sup>.

The survey allowed to identify, on average, within each sector, the mechanical properties of soils in static terms shortly listed below. (Table 5.2) The location of the perforations is, partially shown in Figure 5.6, which shows that the only one executed in the investigated site is N°11 of which is shown the stratigraphy (Table 5.3).

*Table 5.2 – Mechanical properties of soils (Modified from Velotti A., 1983)*

Sector		A	AB	B
Property				
$\gamma$	[KN/ m <sup>3</sup> ]	16.285	15.696	24.525
R <sub>p</sub>	[N/cm <sup>2</sup> ]	785	687	Q <sub>r</sub> = 1600
$\phi$	[°]	35	35	
D <sub>r</sub>	[%]	50-60	50-60	
R <sub>p</sub> /R <sub>L</sub>	[-]	≥60	≥60	

Table 5.3– Stratigraphic column n°11 (Modified from VelottiA., 1983)

Location: Ercolano city “Scogli della Favorita”		Stratigraphic column n. 11			
		Date: 11-12/02/1982 altitude 10.50 s.l.			
Representantation of soils	Depth [m]	Thickness [m]	Samples	Solis description	
1 	-1.8	1.8	-	Topsoil with volcanic rocks and “proietti”	
2 					
3 	-3.4	1.6	-	Pozzolanic sand with lava breccias and “druse”	
4 	-4.6	1.2	-	Sands with great lava breccias	
5 	-5.8	1.2	-	Big breccias and slags	
6 					
7 	-8.6	2.8	-	Trachy blackish-gray fractured lava	
8 					
9 					
10 	-9.80	1.2	-	Slightly silty blackish-gray sand	
11 	-10.20	0.4	-	Reddish lava slags	
12 	-13.80	3.60	-	Trachy blackish-gray compact lava	
13 					
14 					

## 5.6 AD HOC IN SITU MASW TEST (Evangelista L. et al., 2007; Evangelista L., 2010)

In order to perform the analysis of local seismic response is necessary to know the behaviour of soil under cyclic and dynamic loading. In these conditions, the response of soil is essentially determined by so called equivalent parameter, the shear modulus and the damping ratio.

Lacking samples at the site, or results of dynamic tests already carried out and without the ability to perform invasive tests, have been performed a MASW (Multi-channel Analysis of Surface Waves) test

The test was conducted in July 2011, at the same point of the geological survey N°11, which is reported stratigraphy in Table 5.3 and the position in Figure 5.6.

### 5.6.1 *Introduction*

The MASW method is a non-invasive in situ test, based on the measurement of surface wave at several places on the soil surface, aimed to the definition of the shear wave velocity,  $V_s$ , profile ,.

The basic principle of the experimental technique is founded on the dispersion behaviour of Rayleigh waves: waves with different wavelength (or frequencies) sample different parts of the medium, allowing them to be used in determining the variation of material properties with depth (Figure 5.8)

So that, the dispersive nature of Rayleigh waves is due to the direct relationship between their wavelength and their zone of influence, known as the following dispersion relation:

$$V_R = \lambda \cdot f \quad (5.1)$$

where  $V_R$  is the phase velocity of Rayleigh wave,  $\lambda$  is its wavelength, and  $f$  its frequency.

In particular Rayleigh waves in homogeneous isotropic linear elastic halfspaces are not dispersive; the velocity of propagation is a function of the

mechanical properties of the medium, but it is not a function of frequency. In a real soil deposit, however, soil stiffness usually increases with depth, due to the increase of stress state under the soil selfweight; Rayleigh waves of longer wavelengths (high frequency) tend to propagate faster than Rayleigh waves of shorter wavelengths (low frequency). So that Rayleigh waves enable their use in detecting changes in soil stiffness with depth by measuring the wavelength and the velocity of propagating waves.

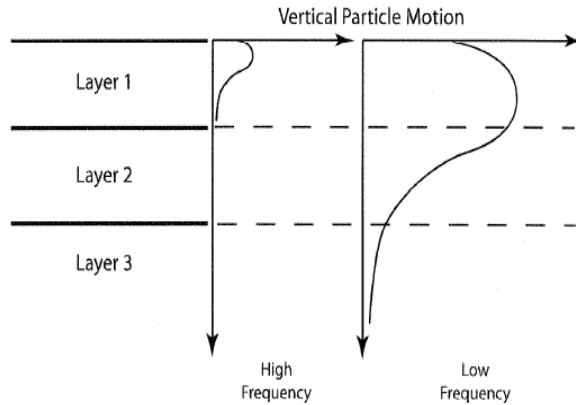


Figure 5.8 - Vertical particle motions of Rayleigh waves with different frequency (Rix, 2005)

Figure 5.9 shows an example of dispersion relation and underlines how for a given frequency, there may be multiple modes of Rayleigh: wave travelling at different phase velocity. Multiple modes of Rayleigh wave propagation at a certain frequency can be explained by the constructive interference occurring among waves undergoing multiple reflections at the layer interfaces (Lai, 1998)

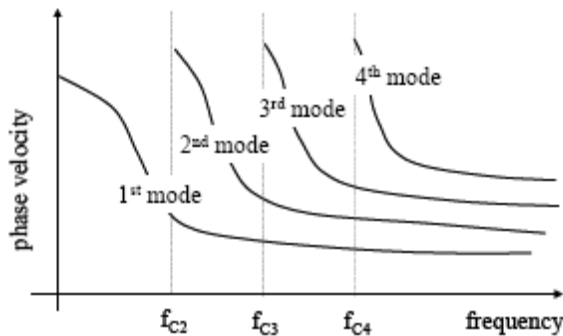


Figure 5.9 - Example of Rayleigh Wave Dispersion Curve (Phase Velocity – Frequency) (Lai, 1998)

The possibility to detect correctly the multiple modes of Rayleigh wave, as we will be seen in the following, is linked to a correct experimental procedure that requires essentially the following three steps:

- 1) Generation of the perturbation on the surface of the deposit using a dynamic point source;
- 2) Detection of the subsequent wave through some sensors placed on the ground surface and determination of the dispersion curve ( $V_r$ - $f$ ) by the signal processing procedure.
- 3) Assessment of the stiffness profile with an inversion process.

### 5.6.2 Field Equipment

The basic testing equipment is composed of a source of broad-band surface waves and some receivers - deployed in linear array at several distance from source - connected to an acquisition system to record the artificial vibration. In Figure 5.10 is reported all the equipment, in its experimental setup.

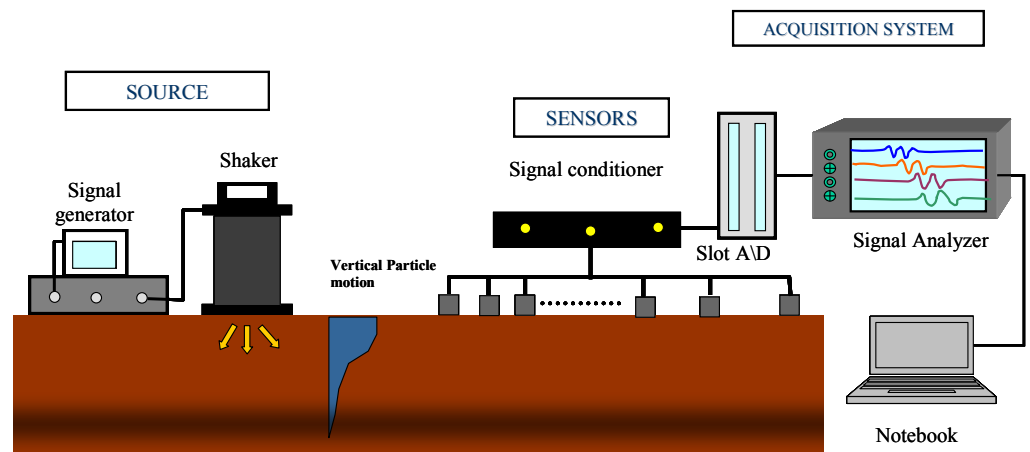


Figure 5.10 - Experimental Setup

The choice of the equipment and testing configuration is linked to the goal of the test and to the technique to be used in the interpretation.

For Surface Wave Test the common source is active and might be produced either transient or continuous surface energy. Active continuous sources usually generate harmonic waveforms and include electro-mechanical shakers or larger field vibrators. One major advantage of active surface wave measurements is the ability to completely control the source. They allow each frequency to be tested individually, permitting the analysis to be concentrated around a narrow frequency range which dramatically decreases the effects of external noise. Active transient sources are hammers and large dropped weights. These sources allow an entire range of frequencies to be measure simultaneously; however, they are often not repeatable and limit the removal of external noise.

Many active sources are limited to higher frequencies due to their relatively small mass and might not produce sufficiently long wavelengths to develop shear waves profile to the desire depth. In these cases, passive sources such as microtremors and antropic noise produce energy at lower frequencies than most active sources and thus allow deeper Vs profiling. However their propagation characteristics are not known a priori, increasing the complexity of the post-measurement analyses.

Relating to receivers, they could be geophones to measure the velocity or accelerometers, though geophones are more common.

It is important that the sensors have a frequency response that corresponds to the range of frequencies that will be used in the test and that all the receivers are properly calibrated; more simply, have identical frequency response characteristics.

The number of sensors used in the array is governed by their availability and by the capabilities of the data acquisition equipment.

Care should be taken in coupling the receivers to the ground surface to ensure that the particle motion is accurately measured, the location of each receiver should be recorded.

### *Sources*

The source system is composed by three elements:

- 1) Signal Generator
- 2) Electro-dynamic Force Generator
- 3) Power Amplifier

The continuous source is an electro-mechanical vibratory shaker (Model 400 Electro-Seis Shaker manufactured by APS Dynamics, Inc.), supported by a Dual-Mode Power Amplifiers, designed to provide drive power. The shaker is a force generator specifically designed to be used for studying dynamic response characteristics of various structures. The shaker mass is 73 kg but with additional moving mass reaches 100 kg. Thanks to the long stroke (maximum 16 cm) of its armature, thus shaker is capable of impart its maximum dynamic force at low frequencies. Auxiliary reaction mass are added to the armature to decrease the low frequency limit for rated force operation.

The input voltage from a function generator is converted by the shaker in a dynamical force that has the same frequency characteristic and magnitude controlled by the magnitude of the input voltage.

The force envelope is depicted in the amplifier that has been used for the test is a model 144.

It gives on the frequency range adopted for the test (3-120 Hz) using the maximum input voltage amplitude (2 V) force amplitudes ranging from 445 N to 60 N. (indeed the acceleration spectrum range from about 1.5g @ 5 Hz to 0.2g @ 100 Hz). (Figure 5.11)



*Figure 5.11 - Model 400 Electro-Seis Shaker manufactured by APS Dynamics and DUAL-MODE Power Amplifiers*

### *Signal generator*

A waveform generator or function generator waveform or trainer is an electronic instrument capable of generating signals with different shape and with characteristics chosen a priori by the operator. The generator allows to act on parameters such as frequency and amplitude of the wave. It is used to give stable and precise commands to shaker.

In our test has been used the Agilent Technologies 33210A Function/Arbitrary Waveform Generator. It uses direct digital-synthesis techniques to create a stable, accurate output on all waveforms, and with low distortion, as well as square waves with fast rising edges and falling up to 10 MHz and linear ramp up to 100 kHz.



*Figure 5.12 – Waveform generator Agilent technology 33210A*



### *Receivers*

The frequencies of interest for near-surface soil characterization range from about 2 Hz to 120 Hz for soils from 0 to about 200 m in depth, so receivers must be selected with this range of frequencies in mind. Other characteristics include high sensitivity and adequate resolution. Based on such criteria, Wilcoxon Research 731A Ultra-Quiet, Ultra- Low-Frequency seismic accelerometers providing a flat response between 0.5 Hz and 300 Hz with a resonant frequency near 950 Hz and sensitivity of 10 V/g were used during all surface wave field tests in this study.

Each sensor is connected to a signal conditioner, Model PR710, specifically designed to furnish the constant DC current necessary to operate the internal amplifiers of piezoelectric transducers (accelerometers and velocity sensors) requiring a constant current power supply.

Each channel has an amplifier gain switch. The amplifier gain (amplification) can be set to amplify by a factor of 1 (0 db), 10 (20 db), or 100 (40 db). Each channel has a filter available that can be applied to the sensor signal or the accelerometer signal can be integrated to provide a velocity signal output from an accelerometer signal input.

Wilcoxon Research low-noise coaxial cables were used with the receivers. For the typical frequencies of seismic interest, the loss of signal quality caused by driving long cables can be ignored (Zywicki, 1999). (Figure 5.13)



*Figure 5.13 - Wilcoxon 731A Ultra-Quiet, Ultra- Low-Frequency seismic accelerometers and Signal Conditioner*

### *Recorder devices*

The acquisition device consists of a modular VXI multi-channel system, a breakup box and a laptop.

A HP VXI digital signal analyzer with 16 channels is used as the data recording device. Its mainframe contains an analog-to-digital converter, dynamic signal analysis module and 16 bit IEEE 1394A interface module allows sampling of each channel up to 51.2 kSamples/sec.

The connection to the sensors is done by a breakup box, that can work in ground or differential, while the graphical user interface, that makes setting up a multi-channel analog measurement easy, is provided by an adaptive software DAC Express. (Figure 5.14)

It facilitates one to input spatial array and digital signal processing parameters as well as sampling frequency, number of blocks of data to be averaged, block length, and receiver locations. During measurements, time history and Fourier Transform data of each receiver are displayed to check and monitor the raw data.



*Figure 5.14 - HP VXI digital signal and breakup box*

### 5.6.3 Testing configuration

Before executing any testing, the choice of sampling parameters both in time and space has significant effects on the quality of measurements, this is because a signal is sampled at a finite number of times and locations. Sampling parameters in time are set on the acquisition device, while sampling parameters in space are determined by the layout geometry and are typically subjected to a number of restrictions due to available receivers and testing space.

Two factors dominate the selection of test frequencies: the nature of Rayleigh wave propagation and the number of points to be used in the frequency domain calculations.

First, the dispersive propagation of Rayleigh waves makes it necessary to obtain samples at smaller frequency intervals as frequency decreases (Figure 5.15).

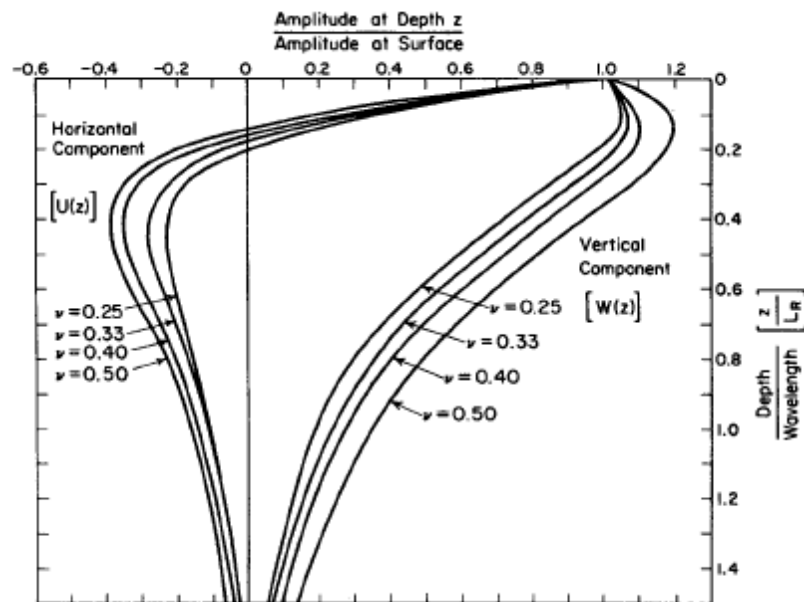


Figure 5.15 - Amplitude Ratio vs. Dimensionless Depth for Rayleigh Waves in a Homogeneous Half-Space (Richart et al., 1970).

Such as, the spacing of the discrete test frequencies narrows towards the lower end of the frequency spectrum. Secondly, since all of the dispersion analysis calculations are completed using a limited amount of discrete temporal data, there is an inherent limit to the frequency resolution of the calculations. Consequently, if the active source consists of waveforms generated at given discrete frequencies, it is necessary to test at frequencies that correspond to the exact values calculated in the Fourier dispersion analysis. The frequency resolution,  $\Delta f$ , can be calculated using Equation:

$$\Delta f = \frac{f_s}{N} \quad (5.2)$$

where  $f_s$  is the sampling frequency and  $N$  is the number of time domain data points collected at  $f_s$  for each sensor. The chosen test frequencies must all be multiples of  $\Delta f$  resulting in a minimum temporal spacing of  $\Delta f$ .

Additionally, the upper limit of frequency resolution, known as the Nyquist frequency, is theoretically defined the half of the sampling frequency (Shannon, 1949).

However, because anti-aliasing filters are not ideal filters, the maximum frequency is less than one-half the sampling frequency in practice. The number of frequency measurements and the distribution of those frequencies is controlled by the amount of data that can be practically collected and analyzed, and the dispersive nature of Rayleigh wave propagation. The exact choice of the frequencies to be measured depends on site specific conditions and objectives, and needs to be adjusted slightly throughout the testing. Consequently the engineer in charge of a particular test must use proper discretion and judgement to choose the appropriate frequencies spacing for a particular test site.

Source frequencies spaced at  $\Delta f = f_s/N = 320/1024 = 0.3125$  over ranges of 4.375-15 Hz, and 0.125 over ranges of 16.25-35 Hz, and 2.5 over ranges of 37.5-100 Hz

The experimental parameters used during the active testing included the standard array configuration 15 receivers non-uniform spacing and three

frequency resolution configurations.

Note that in order to receive the signal from the accelerometers were not affected by an error has been removed the turf, so that the receivers be placed in direct contact with the ground.

Distance array 14 receivers: (2.4, 3, 3.7, 4.6, 5.5, 6.7, 8.5, 10.4, 12.8, 15.2, 18.3, 21.3, 24.4, 29 m) (Figure 5.16)



*Figure 5.16 – Accelerometers position in situ test.*

The dispersion calculations are performed in the frequency domain to let both the magnitude and the phase to be elegantly and efficiently represented using complex notation. Current dispersion calculations are conducted using a frequency wavenumber ( $f-k$ ) procedure (Zywicki, et al., 1999), obtained as the amplitude peaks in the  $f-k$  (frequency-wavenumber) domain, where different curve branches identify the multi-modal response of the layered subsoil.

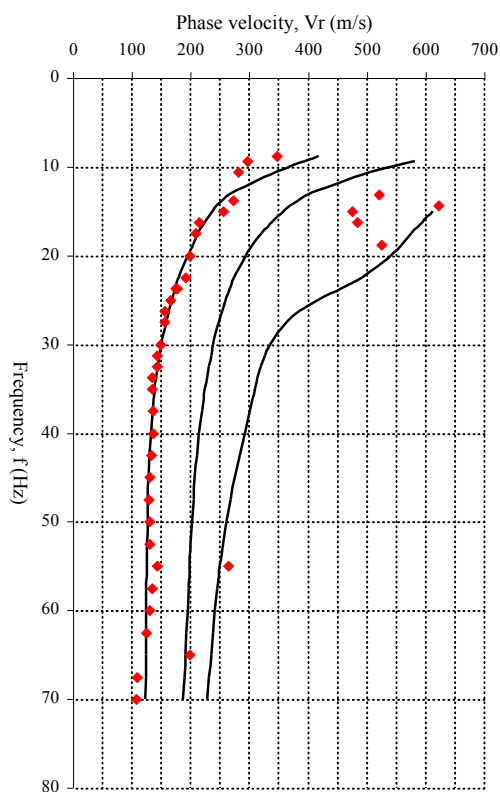
The evaluation of the shear wave velocity profile is obtained with the resolution of the inversion problem with global algorithms, such as Monte Carlo (Evangelista, 2009).

The inversion methods are based on simple idea: a large number of soil profiles are randomly generated. For each profile, the correspondence with the experimental data is assessed. Only the profiles fitting the experimental data are accepted.

In this approach, the inversion of surface wave dispersion is done with horizontally homogeneous model.

### 5.6.4 Experimental results

In the following figures we report the dispersion curve and the shear velocity profile obtained from the in situ test.



F	Vr			
	1°	2°	3°	Exp.
[Hz]	[m/s]	[m/s]	[m/s]	[m/s]
8.75	415.96			346.50
9.375	393.35	580.29		297.00
10.625	342.97	505.38		280.50
13.125	263.29	397.49		519.75
13.75	252.09	381.65		272.25
14.375	242.90	368.08		621.00
15	235.13	356.15	610.29	475.20
15	235.13	356.15	610.29	254.57
16.25	222.26	335.74	592.47	482.63
16.25	222.26	335.74	592.47	214.50
17.5	211.50	318.69	575.19	207.90
18.75	201.96	304.19	557.92	524.12
20	193.35	291.82	539.49	198.00
22.5	178.57	272.24	490.40	190.93
23.75	172.27	264.47	454.21	173.63
23.75	172.27	264.47	454.21	176.34
25	166.57	257.73	415.16	165.00
26.25	161.40	251.77	383.72	155.93
27.5	156.71	246.45	361.51	155.57
30	148.67	237.25	334.21	148.50
31.25	145.29	233.23	325.36	142.79
32.5	142.30	229.53	318.31	143.00
33.75	139.69	226.13	312.48	133.65
35	137.41	223.01	307.46	134.13
37.5	133.71	217.53	298.81	135.00
40	130.93	212.96	290.77	135.77
42.5	128.81	209.14	282.54	132.87
45	127.20	205.94	274.19	130.39
47.5	125.95	203.22	266.32	128.25
50	124.98	200.85	259.40	129.13
52.5	124.22	198.76	253.48	129.94
55	123.62	196.84	248.41	264.00
55	123.62	196.84	248.41	142.04
57.5	123.13	195.03	244.01	133.94
60	122.75	193.27	240.12	129.60
62.5	122.43	191.51	236.58	123.75
65	122.18	189.71	233.30	198.00
67.5	121.98	187.80	230.18	108.36
70	121.81	185.75	227.17	106.62

Figure 5.17 - Experimental result of the test in the site: dispersion curve

The dispersion curve, as can be noted from the Figure 5.17, does not contain all frequencies sampled, have been eliminated since the data at frequencies that correspond to wavelengths that are not compatible with the length of the stringing (array).

Furthermore, based on what is said in the previous paragraph, the velocity profile (Figure 5.18) was obtained by merging the layers of similar materials and tying the solution thus obtained to the depths. For each layer, set the thickness, the solution is obtained by freeing up the velocity to vary within a reasonable range of values appropriate to the materials constituting each layer, the inversion-iterating until convergence.

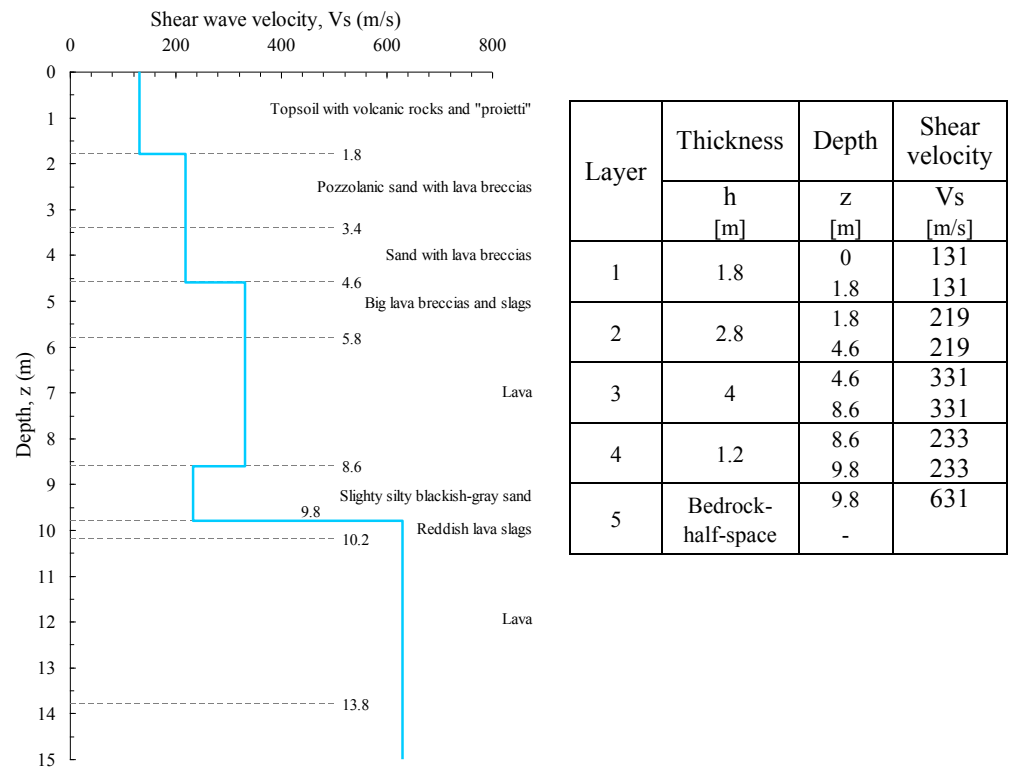


Figure 5.18 - Experimental result of the test in the site: shear wave velocity profile

## BIBLIOGRAPHY

Scarpato G., Ricciardi G. P., Giudicepietro F., De Lucia M.. (2005); L'evoluzione morfologica del Vesuvio in relazione alla sua storia eruttiva attraverso un'applicazione web: slideves - *Open file report n°6* - INGV-Osservatorio Vesuviano

Velotti A. (1983). Personal communication – *Archivio Ente per le ville Vesuviane*,

Evangelista L., Santucci de Magistris F., Vinale F., (2008); Evaluation of soil stiffness by in situ innovative techniques, Mitigation of the Earthquake Effects in the Towns and in Industrial regional districts-*MEETING Project-Final Conference- Università degli Studi del Molise*, Termoli 14 Luglio 2008.

Evangelista L., (2010) A Critical Review of the MASW Technique for Site Investigation in Geotechnical Engineering, *PhD. Thesis, Università degli Studi di Napoli Federico II*

Lai, C.G. (1998) Simultaneous Inversion of Rayleigh Phase Velocity and Attenuation for Near-Surface Site Characterization. Ph.D. Dissertation, Georgia Institute of Technology.

Zywicki, D.J. (1999) Advanced signal processing methods applied to engineering analysis of seismic surface waves. PhD dissertation, Georgia Institute of Technology.

Zywicki, D.J. and Rix, G.J. (1999). Frequency-wavenumber analysis of passive surface waves, Proc. Symposium on the Application of Geophysics to Engineering and Environmental Problems, Oakland, CA, 75-84.

Shannon C.E. e Weaver W. (1949). The Mathematical Theory of Communication, The University of Illinois Press, Illinois





This page is, intentionally, left blank

---

## *Chapter 6*

# Research and selection of real accelerograms for the site under study

### 6.1 INTRODUCTION

In this chapter we propose a procedure for selecting the correct seismic input for the park on the sea of Villa Favorita.

First step is, with the help of seismic italian code (D.M. 14.01.2008), identify the return periods  $T_R$  and the PHA for the site for different ratio of exceedence  $P_{VR}$ . With the same percentage of exceedence was obtained from maps of disaggregation events that contributed most to the hazard of the site, identifying the magnitude  $M$  and distance  $R$ .

The value pairs  $(M, R)$  which corresponded to the major contributions were used to search for in the Italian seismic catalogue (ITACA) events compatible with this hazard.

For each of the records the NS and EW components were composed, so as to obtain the resultant that had the highest energy content in terms of Houssner intensity, according to an ad hoc procedure developed.

Of all the accelerograms obtained were then selected those ones of significant duration, which presented the minor individual deviation from the reference spectra and the  $F_{SC}$  closer to unity, as well as those whose average was closer to the reference spectra. Spectrum-compatibility was estimated with three different coefficients.

## 6.2 SEISMIC HAZARD AND RESPONSE SPECTRA OF STUDY CASE

To determine the seismic actions to be taken for analysis, based on what is required by DM 14.01.2008 and D.P.C.M. 09.02.2011, it is necessary to identify the return period  $T_R$ , depending on the reference life work of reference  $V_R$  and on the probability of exceedence over the reference period  $P_{VR}$ .  $T_R$  is calculated using the expression (6.1)

$$T_R = -\frac{V_R}{\ln(1 - P_{VR})} \quad (6.1)$$

In D.M are identified four different limit state corresponding to different  $P_{VR}$ . The life work of reference  $V_R$  is calculated according to the expression provided by the code:

$$V_R = V_N \cdot C_U \quad (6.2)$$

in which the value of the coefficient of use  $C_U$  is defined as a function of class use of the building and  $V_N$  depends on the building type. In the case the analisys is performed on a monumental Vesuvian Villa, corresponding a class of use III.

In Table 6.1 we report the values of the parameters of the case, in relation to each limit state.

*Table 6.1 – Life of reference and return period of seismic design for each limit state.*

	$C_U$	$V_N$	$V_R$	$P_{VR}$	$T_R$
SLC	1.5	50	75	5%	45
SLV				10%	75
SLD				63%	712
SLO				81%	1462

The characteristics of ground motion expected at the reference site, for a fixed  $P_{VR}$ , are identified by the maximum acceleration and the corresponding elastic response spectra in acceleration.

The selected accelerograms to describe the form of earthquake must be compatible with these characteristics of seismic motion. In particular, the

characteristics of seismic motion of rigid horizontal reference site are described by the spatial distribution national of the following sizes, which are based on fully defined forms spectrum for the generic  $P_{VR}$ .

$a_g$  = maximum acceleration at the site;

$F_0$  = maximum value of amplification factor of the spectrum in the horizontal acceleration;

$T_C^*$  = Time of beginning of the tract at a constant speed in a horizontal acceleration spectrum.

The value of  $a_g$  is taken directly from Italian Seismic Hazard Map (MPS Working Group, 2004) while  $F_0$  and  $T_C^*$  are calculated so that the elastic acceleration response spectra, velocity and displacement provided by the NTC to best fitting the corresponding response spectra elastic acceleration, velocity and displacement arising from the hazards of reference.

From Italian Seismic Hazard Map (MPS Working Group, 2004), we extracted the data hazard inherent in the site of interest, which falls in the town of Herculaneum, identified by geographical coordinates (latitude 40.797; and longitude 14.351).

The numerical values of the parameters  $a_g$ ,  $F_0$  and  $T_C^*$  are reported, for each limit state, in Table 6.2.

*Table 6.2 – Values of parameters for each limit state.*

Limit state	$T_R$	$a_g$	$F_0$	$T_C^*$
SLC	45	0.055	2.340	0.308
SLV	75	0.072	2.341	0.325
SLD	712	0.186	2.418	0.343
SLO	1462	0.233	2.494	0.344

Figure 6.1-Figure 6.3 show the average performance (50° percentile) of parameters  $a_g$ ,  $F_0$  and  $T_C^*$  as a function of return period  $T_R$ . Marked in red are the points corresponding to return periods calculated for the four defined limit states.

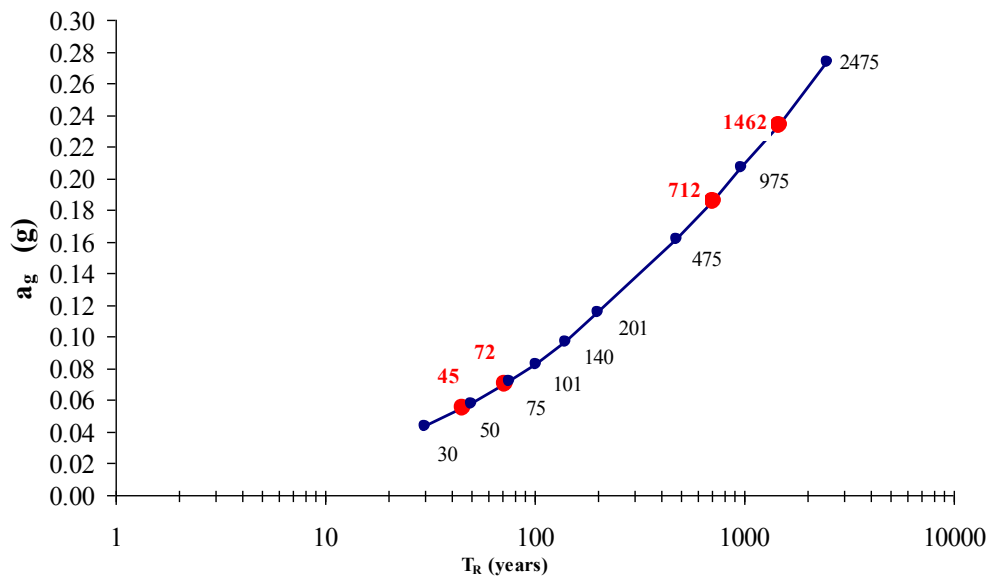


Figure 6.1 – Average (50° percentile) performance in term of expected  $a_g$  as function of  $T_R$

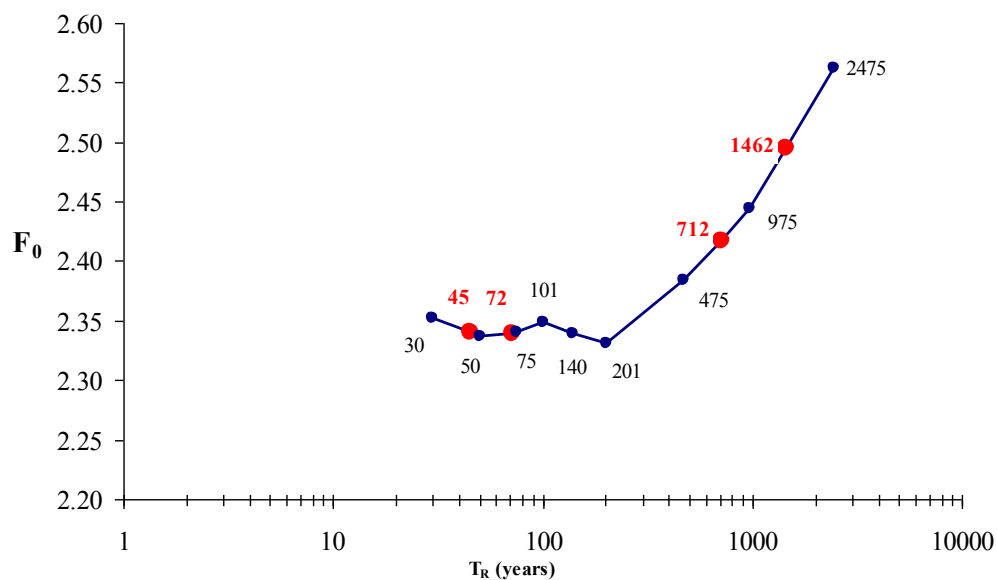


Figure 6.2 – Average (50° percentile) performance in term of  $F_0$  as function of  $T_R$

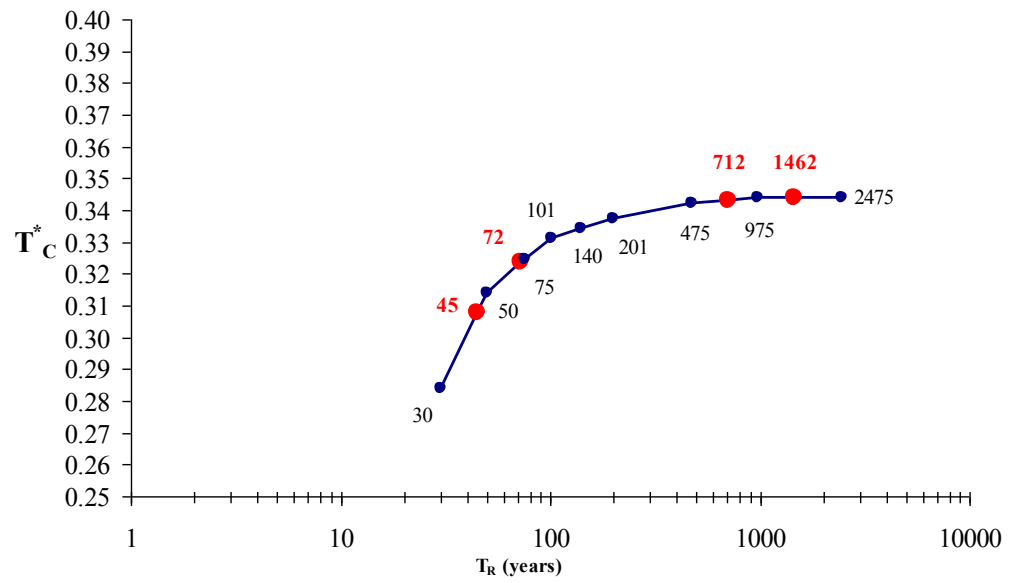


Figure 6.3 - Average (50° percentile) performance in term of  $T_C^*$  as function of  $T_R$

### 6.3 DISAGGREGATION MAGNITUDO-DISTANCE

The rates of exceedance calculated in a PSHA procedure reflect the combined contribution of all the magnitudes,  $M$ , source-to-site distances,  $R$ , and number,  $\varepsilon$ , of (logarithmic) standard deviations by which the (logarithmic) ground motion deviates from the median value predicted by an attenuation equation for a given  $M = m$  and  $R = r$  pair. Seismic hazard disaggregation (or deaggregazione) is a procedure to evaluate the relative contributions of different sources to the seismic hazard of a site. Generally, it is represented in a two-dimensional space ( $M$ - $R$ ), whose axes show the magnitude of the earthquake  $M$  and the source-site distance  $R$ . Specifically, defined the rates of exceedance in a given period of time at a given site, for each couple of  $M$ - $R$  values is calculated what percentage each seismogenic source, at distance  $R$  and capable of generating earthquakes of magnitude  $M$ , contributes. Using the deaggregation can be identified, in terms of  $M$ - $R$ , the type of earthquake that dominates the seismic hazard scenario (earthquake scenario), i.e the event with magnitude  $M$  at distance  $R$  from the site under study, which contributes most to the hazard the site itself. (Spallarossa & Barani, 2007)

In the present work, in order to select adequately the seismic input for the analysis of local seismic response of the study site, we have used the analysis of disaggregation associated with Italian seismic hazard map (MPS Working Group, 2004). The graphs of disaggregation used were found on the web site developed under the project INGV-DPC S1 (<http://esse1-gis.mi.ingv.it>).

In them, the magnitude  $M$  is defined by intervals of constant amplitude of 0.5, while the distance  $R$  has the range of 10km. It should be noted that the definition of the magnitude to which the graphs refer is the  $M$  (Section 5.4.2), while the distance  $R$  has defined as the minimum distance from the surface projection of the fault plane (Joyner and Boore, 1981).

The disaggregation graphics are drawn for the gray reference node closest (about 500m) at the study site (lat. 40.797; lon. 14.351). For each limit state defined in D.M. 14/01/2008, with the associated probability of exceedance in 50 years, to the reference 50th percentile, was drawn relative disaggregation maps on the PHA. (Figure 6.4- Figure 6.7)



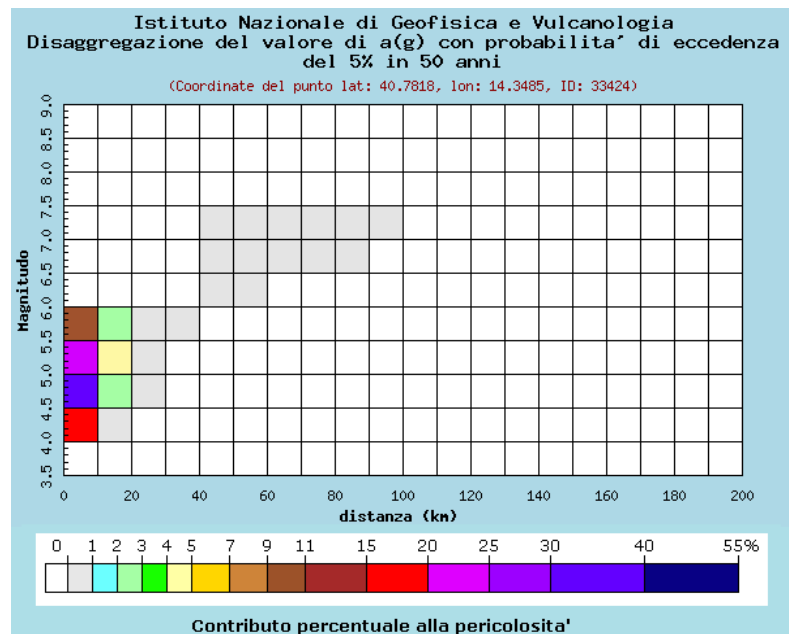


Figure 6.4 – Disaggregation map of PHA for  $P_{VR}=5\%$  in 50 years at site under study

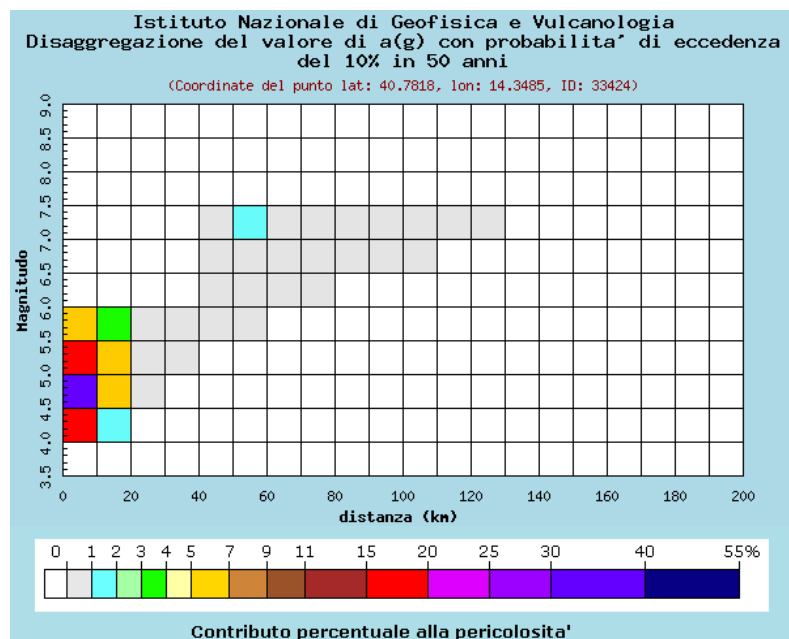


Figure 6.5 – Disaggregation map of PHA for  $P_{VR}=10\%$  in 50 years at site under study

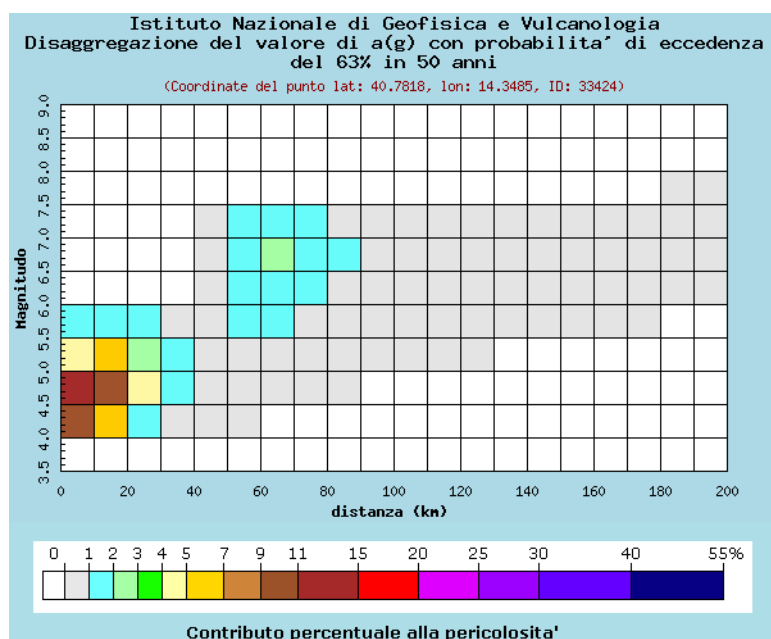


Figure 6.6 - Disaggregation map of PHA for  $P_{VR}=63\%$  in 50 years at site under study

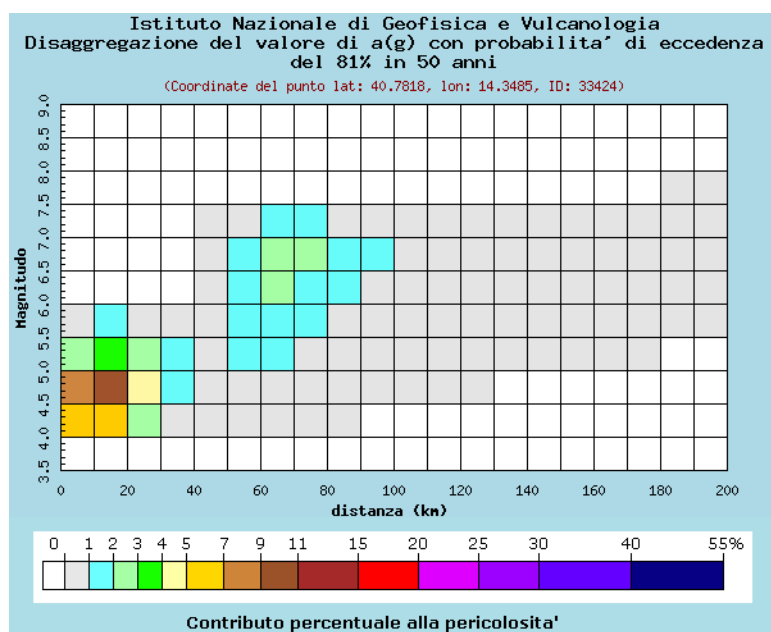


Figure 6.7 - Disaggregation map of PHA for  $P_{VR}=81\%$  in 50 years at site under study

The numerical values for the graphs shown in previous figures are explained in the following tables (Table 6.3-Table 6.10)

Table 6.3 – PHA disaggregation with probability of exceedence  $P_{VR}=5\%$  in 50 years

R <sub>JB</sub> [Km]	(Coord. of point lat: 40.7818, lon: 14.3485, ID: 33424)										
	Magnitude										
	3.5-4.0	4.0-4.5	4.5-5.0	5.0-5.5	5.5-6.0	6.0-6.5	6.5-7.0	7.0-7.5	7.5-8.0	8.0-8.5	8.5-9.0
0-10	0	17.6	36	23	9.65	0	0	0	0	0	0
10-20	0	0.484	2.66	4.06	2.9	0	0	0	0	0	0
20-30	0	0	0.001	0.211	0.409	0	0	0	0	0	0
30-40	0	0	0	0	0.015	0	0	0	0	0	0
40-50	0	0	0	0	0	0.031	0.216	0.31	0	0	0
50-60	0	0	0	0	0	0.015	0.41	0.749	0	0	0
60-70	0	0	0	0	0	0	0.161	0.539	0	0	0
70-80	0	0	0	0	0	0	0.026	0.277	0	0	0
80-90	0	0	0	0	0	0	0	0.063	0	0	0
90-100	0	0	0	0	0	0	0	0.008	0	0	0
100-110	0	0	0	0	0	0	0	0	0	0	0
110-120	0	0	0	0	0	0	0	0	0	0	0
120-130	0	0	0	0	0	0	0	0	0	0	0
130-140	0	0	0	0	0	0	0	0	0	0	0
140-150	0	0	0	0	0	0	0	0	0	0	0
150-160	0	0	0	0	0	0	0	0	0	0	0
160-170	0	0	0	0	0	0	0	0	0	0	0
170-180	0	0	0	0	0	0	0	0	0	0	0
180-190	0	0	0	0	0	0	0	0	0	0	0
190-200	0	0	0	0	0	0	0	0	0	0	0

Table 6.4 – Mean values of Table 9.3

Magnitude M	Distance R <sub>JB</sub> [Km]	Deviation $\varepsilon$
-	-	-
5	6.94	1.09

Table 6.5 – PHA disaggregation with probability of exceedence  $P_{VR}=10\%$  in 50 years

R <sub>JB</sub> [Km]	(Coord. of point lat: 40.7818, lon: 14.3485, ID: 33424)										
	Magnitude										
	3.5-4.0	4.0-4.5	4.5-5.0	5.0-5.5	5.5-6.0	6.0-6.5	6.5-7.0	7.0-7.5	7.5-8.0	8.0-8.5	8.5-9.0
0-10	0	18.1	33.4	18.6	6.88	0	0	0	0	0	0
10-20	0	1.51	5.1	5.4	3.18	0	0	0	0	0	0
20-30	0	0	0.179	0.736	0.701	0	0	0	0	0	0
30-40	0	0	0	0.029	0.106	0	0	0	0	0	0
40-50	0	0	0	0	0.018	0.141	0.354	0.393	0	0	0
50-60	0	0	0	0	0.002	0.238	0.852	1.06	0	0	0
60-70	0	0	0	0	0	0.07	0.609	0.915	0	0	0
70-80	0	0	0	0	0	0.004	0.317	0.609	0	0	0
80-90	0	0	0	0	0	0	0.095	0.242	0	0	0
90-100	0	0	0	0	0	0	0.023	0.105	0	0	0
100-110	0	0	0	0	0	0	0.003	0.04	0	0	0
110-120	0	0	0	0	0	0	0	0.012	0	0	0
120-130	0	0	0	0	0	0	0	0.003	0	0	0
130-140	0	0	0	0	0	0	0	0	0	0	0
140-150	0	0	0	0	0	0	0	0	0	0	0
150-160	0	0	0	0	0	0	0	0	0	0	0
160-170	0	0	0	0	0	0	0	0	0	0	0
170-180	0	0	0	0	0	0	0	0	0	0	0
180-190	0	0	0	0	0	0	0	0	0	0	0
190-200	0	0	0	0	0	0	0	0	0	0	0

Table 6.6 – Mean values of Table 9.5

Magnitude M	Distance R <sub>JB</sub> [Km]	Deviation $\varepsilon$
-	-	-
5.03	9.93	0.914

Table 6.7 – PHA disaggregation with probability of exceedence  $P_{VR}=63\%$  in 50 years

R <sub>JB</sub> [Km]	(Coord. of point lat: 40.7818, lon: 14.3485, ID: 33424)										
	Magnitude										
	3.5-4.0	4.0-4.5	4.5-5.0	5.0-5.5	5.5-6.0	6.0-6.5	6.5-7.0	7.0-7.5	7.5-8.0	8.0-8.5	8.5-9.0
0-10	0	9.27	12.2	4.27	1.12	0	0	0	0	0	0
10-20	0	6.29	10.7	5.25	1.73	0	0	0	0	0	0
20-30	0	1.93	4.12	2.74	1.14	0	0	0	0	0	0
30-40	0	0.446	1.19	1.03	0.523	0	0	0	0	0	0
40-50	0	0.102	0.418	0.596	0.636	0.553	0.529	0.308	0	0	0
50-60	0	0.023	0.311	0.795	1.34	1.75	1.83	1.14	0	0	0
60-70	0	0	0.145	0.617	1.24	1.85	2.15	1.45	0	0	0
70-80	0	0	0.037	0.385	0.939	1.55	1.98	1.39	0	0	0
80-90	0	0	0.002	0.171	0.527	0.939	1.27	0.816	0	0	0
90-100	0	0	0	0.077	0.344	0.652	0.917	0.545	0	0	0
100-110	0	0	0	0.026	0.214	0.445	0.65	0.368	0	0	0
110-120	0	0	0	0.005	0.119	0.295	0.462	0.266	0	0	0
120-130	0	0	0	0	0.065	0.208	0.353	0.218	0	0	0
130-140	0	0	0	0	0.032	0.144	0.266	0.174	0	0	0
140-150	0	0	0	0	0.015	0.103	0.206	0.143	0	0	0
150-160	0	0	0	0	0.005	0.069	0.152	0.109	0	0	0
160-170	0	0	0	0	0.001	0.044	0.112	0.083	0	0	0
170-180	0	0	0	0	0	0.027	0.084	0.064	0	0	0
180-190	0	0	0	0	0	0.015	0.059	0.051	0.001	0	0
190-200	0	0	0	0	0	0.007	0.035	0.044	0.003	0	0

Table 6.8 – Mean values of Table 9.7

Magnitude M	Distance R <sub>JB</sub> [Km]	Deviation ε
-	-	-
5.38	36.3	0.468

Table 6.9 – PHA disaggregation with probability of exceedence  $P_{VR}=81\%$  in 50 years

$R_{JB}$ [Km]	(Coord. of point lat: 40.7818, lon: 14.3485, ID: 33424)										
	Magnitude										
	3.5-4.0	4.0-4.5	4.5-5.0	5.0-5.5	5.5-6.0	6.0-6.5	6.5-7.0	7.0-7.5	7.5-8.0	8.0-8.5	8.5-9.0
0-10	0	6.27	7.74	2.52	0.633	0	0	0	0	0	0
10-20	0	6.13	9.3	3.92	1.16	0	0	0	0	0	0
20-30	0	2.57	4.76	2.6	0.928	0	0	0	0	0	0
30-40	0	0.795	1.75	1.2	0.514	0	0	0	0	0	0
40-50	0	0.262	0.774	0.842	0.732	0.525	0.421	0.215	0	0	0
50-60	0	0.161	0.75	1.29	1.71	1.8	1.56	0.845	0	0	0
60-70	0	0.089	0.564	1.17	1.78	2.1	2.01	1.16	0	0	0
70-80	0	0.025	0.348	0.884	1.49	1.93	2	1.2	0	0	0
80-90	0	0.001	0.157	0.517	0.932	1.27	1.38	0.753	0	0	0
90-100	0	0	0.072	0.358	0.681	0.954	1.07	0.536	0	0	0
100-110	0	0	0.023	0.232	0.486	0.703	0.806	0.385	0	0	0
110-120	0	0	0.003	0.13	0.325	0.504	0.609	0.295	0	0	0
120-130	0	0	0	0.069	0.23	0.385	0.495	0.254	0	0	0
130-140	0	0	0	0.033	0.161	0.292	0.394	0.214	0	0	0
140-150	0	0	0	0.014	0.113	0.228	0.323	0.185	0	0	0
150-160	0	0	0	0.005	0.076	0.172	0.253	0.148	0	0	0
160-170	0	0	0	0.001	0.048	0.127	0.197	0.118	0	0	0
170-180	0	0	0	0	0.029	0.095	0.156	0.095	0	0	0
180-190	0	0	0	0	0.016	0.068	0.117	0.079	0.001	0	0
190-200	0	0	0	0	0.008	0.044	0.076	0.071	0.004	0	0

Table 6.10 – Mean values of Table 9.9

Magnitude M	Distance $R_{JB}$ [Km]	Deviation $\varepsilon$
-	-	-
5.45	46.6	0.38

The results are returned in terms of mean (M, R,  $\varepsilon$ ) and modal values ( $M^*$ ,  $R^*$ ,  $\varepsilon^*$ ) of M, R and  $\varepsilon$  for each site. Note that the mode of the distribution corresponds to the M-R- $\varepsilon$  group that gives the greatest contribution to the seismic hazard and therefore corresponds to a source "real".

The main disadvantage in the use of modal values is that these are sensitive to the width of the bin size (e.g. Abrahamson, 2006). In contrast, the mean values do not depend on the binning scheme adopted in the calculation, but not always correspond to a realistic scenario, that is a real fault, since they depend on contributions from both the local and regional seismicity. The mean values of the couple M-R, could therefore be an unlikely scenario (Spallarossa e Barani 2007).

The above it is evident, for example, the disaggregation on the  $P_{VR} = 63\%$  (SLD) and  $P_{VR} = 81\%$  (SLO). In them, in fact, the average falls in the range of magnitude between M (5.0-5.5) at a distance  $R_{JB}$ , respectively, of 36.3 km and 46.6 km where the percentage contribution to the hazard is close to unit.

The collected disaggregation graphs show, also clearly, that in the studied site there are two "modes": the first corresponding to the range of magnitude M (4.5-5.0) at a distance R (0-10km), the second falls in M range (6.0-7.0) at a distance  $R_{JB}$  (60-80 Km). On the basis of seismic history of the site is easy to understand that the first modal value corresponds to modest size earthquakes with an epicenter at short distance, certainly related to the volcanic activity of Somma-Vesuvius; while the second value related to events of high magnitude, but with its epicenter far, certainly takes into account the influence of earthquakes such as the Irpinia.

#### **6.4 RESEARCH OF REAL ACCELEROGRAMS**

The shown hazard and disaggregation maps have been used to estimate the parameters useful for the definition of the seismic motion reference.

Through the Italian seismic catalog ITACA (ITalian ACcelerometric Archive) [Working Group ITACA, 2010] has been selected a series of accelerometric records for couples M-R close to those obtained by the disaggregation and PHA in the range of values indicated in the corresponding hazard maps.

Were specifically used the following search parameters:

- 55 (cm/s<sup>2</sup>) <PHA <250 (cm/s<sup>2</sup>) and  
 c) For events related to the first modal value 4.5<M<5.5 and 0<R<10 km  
 d) For events related to the second modal value 6.5<M<7.0 and 60<R<80km

It is, then, given as an additional search parameter that records were on rock, i.e. they refer to soils classified as cat. A in D.M. on 14/01/2008.

As results of the research were obtained the events: (Figure 6.8-Figure 6.9)

The screenshot displays the 'Waveforms Search' interface of the Itaca Italian Accelerometric Archive. The search criteria are set as follows:

- Magnitude (M<sub>W</sub> or M<sub>L</sub>): from [2]: 4.5 to [<]: 5.1
- Epicentral distance [Km]: from [2]: 0 to [<]: 10
- Fault distance [km]: from [2]: to [<]:
- Corrected PGA [cm/s<sup>2</sup>]: from [2]: 55 to [<]: 250
- Uncorrected PGA [cm/s<sup>2</sup>]: from [2]: to [<]:
- PGV [cm/s]: from [2]: to [<]:
- PGD [cm]: from [2]: to [<]:
- Housner Int. [cm]: from [2]: to [<]:
- Duration [s]: from [2]: to [<]:
- Arias intensity [cm/s]: from [2]: to [<]:
- Late triggered record?: - Any value -
- Instrument type: - Any value -

The search results are displayed in a table with 12 columns: Date, M<sub>W</sub>, M<sub>L</sub>, Stat. Code, ECB, R. epi. [km], Corr. PGA [cm/s<sup>2</sup>], PGV [cm/s], and PGD [cm]. The results are sorted by Date, showing 12 events from 2009-04-07 to 2008-12-23.

Date	M <sub>W</sub>	M <sub>L</sub>	Stat. Code	ECB	R. epi. [km]	Corr. PGA [cm/s <sup>2</sup> ]	PGV [cm/s]	PGD [cm]
2009-04-07 21:34:29	4.6	4.2	AQM	A*	2.207	231.683	7.281	0.3009
1998-04-05 15:52:21	4.8	4.5	NOCE	A*	8.000	194.797	3.281	0.11162
2009-04-07 21:34:29	4.6	4.2	AQP	A	0.734	166.359	5.713	0.45066
2000-04-01 18:08:03	4.5	3.9	PNS	A*	1.638	147.940	5.620	0.30656
2000-04-01 18:08:03	4.5	3.9	PNC	A*	2.254	146.891	4.648	0.31888
1980-02-28 21:04:40	5.0	4.8	CSR	A*	5.852	128.974	4.609	0.63813
2001-11-26 00:56:55	4.7	4.4	SSG	A*	2.546	127.780	3.156	0.19894
1984-05-11 13:14:56	4.8	4.6	VLR	A*	5.860	125.950	7.024	0.42432
1998-04-05 15:52:21	4.8	4.5	NCM	A*	5.118	91.271	2.706	0.17407
1980-12-01 19:04:29	4.6	4.6	OPB	A*	8.675	82.406	6.322	1.0425
1998-03-21 16:45:09	5.0	4.4	CESM	A*	6.303	74.821	1.737	0.128
2008-12-23 21:58:25	4.9	4.7	NEVI	A*	9.164	64.881	3.362	0.32473

Developed by @IMTeam for INGV

Figure 6.8 – Seismic events found for 4.5<M<5; 0<R<10Km and 55cm/s<sup>2</sup><PHA<250 cm/s<sup>2</sup>



Waveform click to show-hide

Magnitude ( $M_w$  or  $M_L$ ) from [2]: 6 to [2]: 7.5

Epicentral distance [Km] from [2]: 60 to [2]: 80

Fault distance [km] from [2]: to [2]:

Corrected PGA [ $\text{cm/s}^2$ ] from [2]: 55 to [2]: 250

Uncorrected PGA [ $\text{cm/s}^2$ ] from [2]: to [2]:

PGV [ $\text{cm/s}$ ] from [2]: to [2]:

PGD [cm] from [2]: to [2]:

Housner Int. [cm] from [2]: to [2]:

Duration [s] from [2]: to [2]:

Arias intensity [ $\text{cm/s}$ ] from [2]: to [2]:

Late triggered record? Any value

Instrument type Any value

Events click to show-hide

Stations click to show-hide

(( ( mag\_value\_whatever >= 6 ) AND ( mag\_value\_whatever < 7.5 ) ) AND ( ( epi\_dist >= 60 ) AND ( epi\_dist < 80 ) ) AND ( ( pga\_max >= 55 ) AND ( pga\_max < 250 ) ) AND ( EXISTS ( SELECT 'x' FROM station WHERE ( ( station.ec8\_code like 'A%' ) AND ( v\_waveform.magnitude.net\_code =

New Search Search Search + Select

Results 1 - 1 of 1

Date	$M_w$	$M_L$	Stat. Code	EC8	R epi. [km]	Corr. PGA [ $\text{cm/s}^2$ ]	PGV [ $\text{cm/s}$ ]	PGD [cm]
1980-11-23 18:34:53	6.9	6.5	TDG	A*	78.273	58.746	8.061	6.1313

Developed by @IM team for INGV

Figure 6.9 - Seismic events found for  $6 < M < 7.5$ ;  $60 < R < 80 \text{ Km}$  and  $55 \text{ cm/s}^2 < PHA < 250 \text{ cm/s}^2$

In Table 6.11 shows the details of the events resulting from research.

Table 6.11 – Selected records from ITACA Database

RIF.	Event Name	Data	$M_w$	Station	Distance [Km]	Duration[s]
AQM	Aquila	2009-04-07	4.6	V. Aterno	2.2	68.995
AQP	Aquila	2009-04-07	4.6	Pettino	0.7	77.995
NOCE	App. Umbro-March.	1998-04-05	4.8	Nocera Umbra	8	42.995
PNS	Monte Amiata	2000-04-01	4.5	Piancastagnaio (Natali)	1.6	42.895
PNC	Monte Amiata	2000-04-01	4.5	Piancastagnaio	2.3	37.880
CSR	Val Nerina	1980-02-28	5	Casci-Petrucci	5.9	9.995
SSG	Casentino	2001-11-26	4.7	SanSepolcro-Gragnano	2.5	30.410
VLB	Massiccio Meta	1984-05-11	4.8	Villetta Barrea	5.9	33.385
NCM	App. Umbro-March.	1998-04-05	4.8	Nocera Umbra Salmata	5.1	31.120
OPB	Irpinia	1980-12-01	-	Oppido-Balzata	8.7	108.465
CESM	App. Umbro-March.	1998-03-21	5	Cesi Monte	6.3	42.995
NEVI	App. Parmense	2008-12-23	4.9	Neviano degli Arduini	9.2	60.000
TDG	Irpinia	1980-11-23	6.9	Torre del Greco	78.3	53.005

As previously mentioned, the only record that match the search parameters, b), registered by the ENEL station in Torre del Greco (TDG), is the 1980's Irpinia earthquake.

ITACA, for each registration, provides informations regarding the seismic events, the recording stations, the installed instruments, the main features of the recordings and the engineering parameters. In particular, for each recorded event provides both horizontal and vertical components. Each record is, therefore, according to the D.M. 14/01/2008, a group set of accelerograms. In this regard makes it clear that, in the present work, the vertical component has been neglected, in consideration of the fact that it significantly affects the seismic motion only in specific cases. Finally, we note that we used "corrected" records.

## 6.5 RESULTANT HORIZONTAL ACCELERATION

Once selected accelerometer records that, in terms of magnitude-distance and PHA are consistent with the hazard maps and deaggregation of the site, as outlined in the previous paragraph, the next step was to compute the resultant of two accelerometric components provided from the Database.

In this regard, reaffirming what was stated in paragraph 3.4.1 of this work, it is recalled that the horizontal acceleration of a seismic event is a vector whose direction and form do not match either of the two components and these are not the physically independent each other. It would be incorrect to use only one of the two. This choice is even more questionable if one takes into account the frequency content of the seismic signal, different for each component: neglect, therefore, a component of the registration would result in a lack of consideration of frequencies that may, however, be significant for the study of seismic response local site, and consequently for the structures analyzed above.

Based on the foregoing, in the present work, we provided, for each registration to compute the resultant according to the formula:

$$a = a_{NS} \cdot \cos \theta + a_{WE} \cdot \sin \theta \quad (6.3)$$

Where:  $a_{NS}$  is the North-South component;  
 $a_{WE}$  is the West-East component;  
 $\theta$  is the azimuth angle (Figure 6.10)

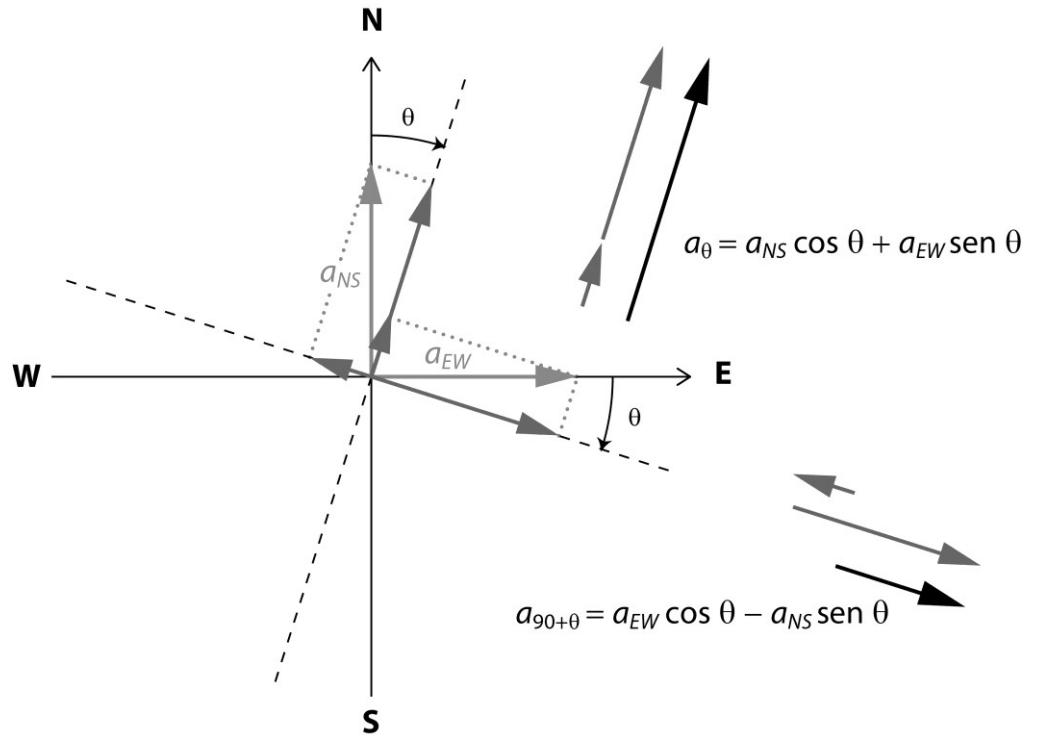


Figure 6.10 - Calculation scheme for the resultant horizontal acceleration

It must be said that the resultant horizontal direction of acceleration, identified by  $\theta$ , changes over time, as shown in (Figure 6.11) that, for example, the plots, in the plane NS-WE, the acceleration vector recorded by Torre del Greco station during the Irpinia earthquake of 1980.

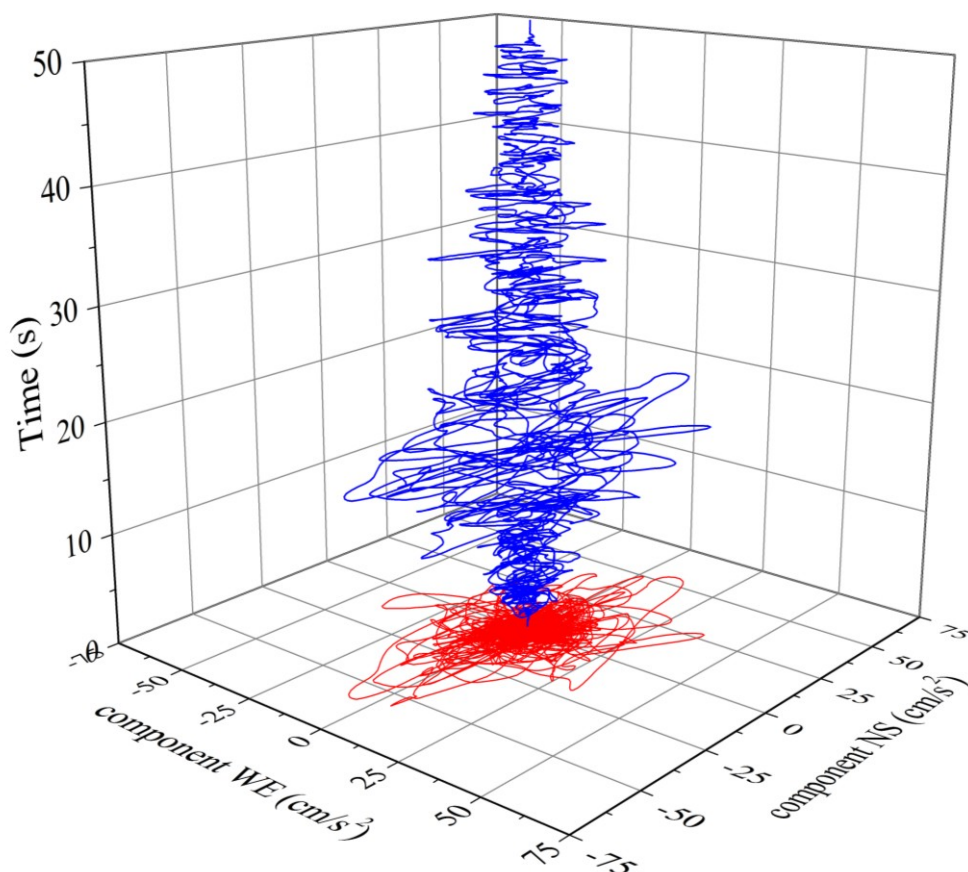


Figure 6.11 – Horizontal acceleration resultant for TDG record

In the present study to calculate the resultant is used the angle  $\theta$  value such that the Houssner intensity of the acceleration response spectrum is maximum. The result thus obtained corresponds to the maximum energy content in the frequency range 0.1s-2.5s. For each records were, then, using an iterative procedure, calculated the response spectra in terms of acceleration, velocity and displacement, relative to the direction  $\theta$  that maximizes the value of Houssner intensity. (Figure 6.12-Figure 6.14)

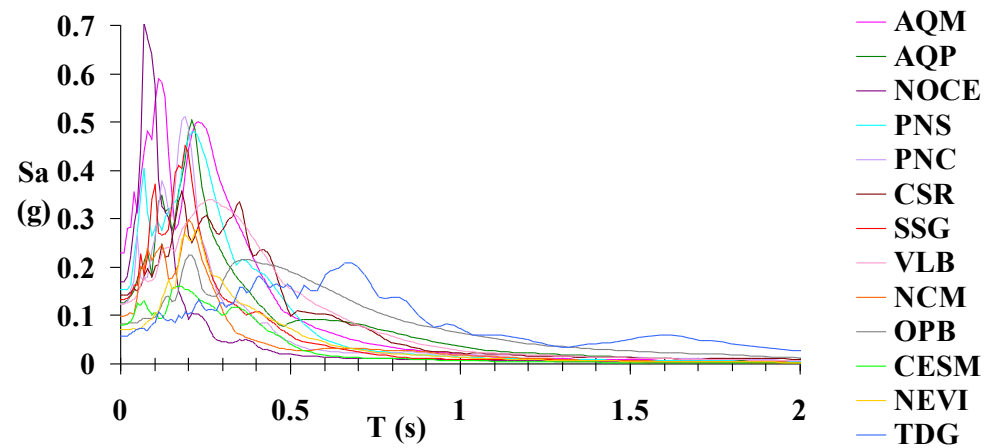


Figure 6.12 – Acceleration response spectra of selected events.

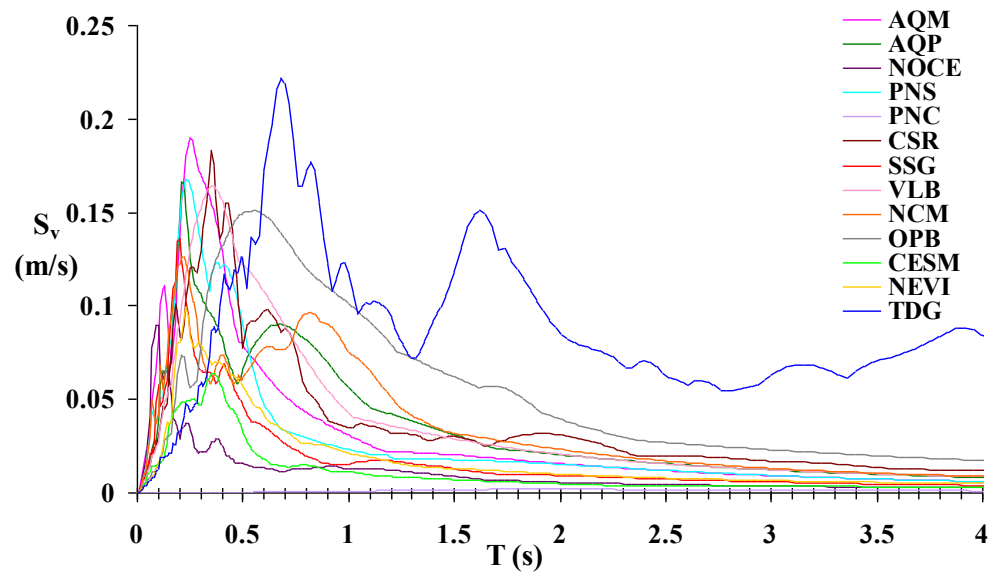


Figure 6.13 – Velocity response spectra of selected events

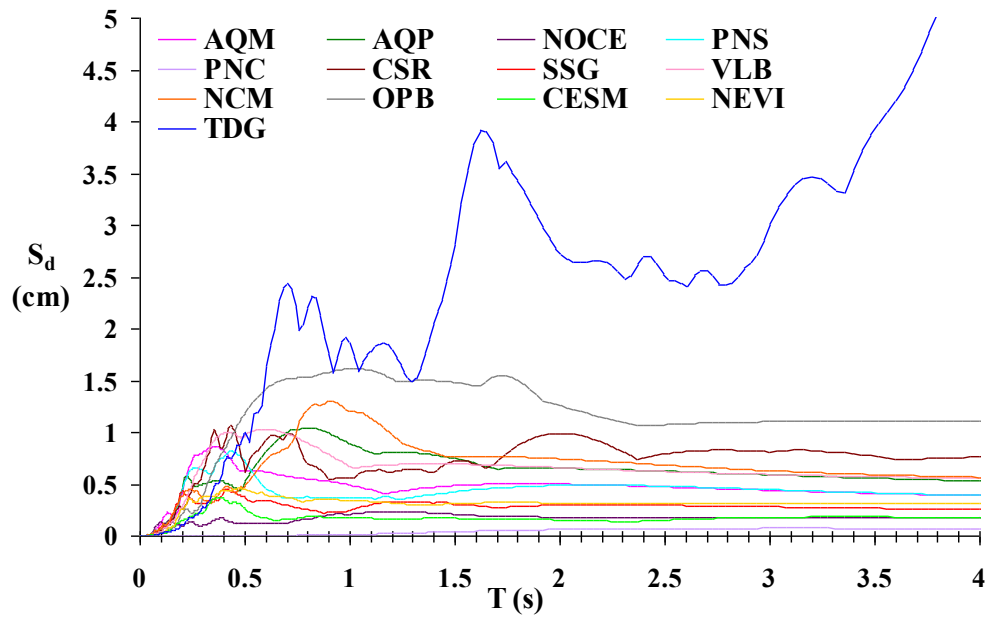


Figure 6.14 – Displacement response spectra of selected events

## 6.6 SELECTING AN ACCELEROMETRIC SET OF SEVEN RECORDS

Of all the records, shown in Table 6.11 and processed as explained in the previous paragraph, it is necessary to make a selection in order to extract, from them, the most appropriate combination of accelerometric histories to local seismic response analysis to be performed for the site under study. The size of the combination, as suggested by the literature on the matter, is seven accelerograms. The selection is done according to the criteria set out below.

### 6.6.1 *Selection criteria adopted*

The criteria used for choosing the combination accelerometer to be used for dynamic analysis, based on those outlined in paragraph 3.5, are:

- a) The best fitting between the spectral shape of each accelerogram and the reference elastic response spectrum for each limit state identified in the D.M. 14/01/2008.
- b) Value of scale factor  $F_{SC} = PHA_0 / PHA_s$ , close to 1 and  $<2$ ;
- c) The minor deviation between the average spectrum of the accelerometric combination and the target one.
- d) As can choose different seismic event in the combination, so that the analysis was not influenced by a few dominant events.
- e) Duration of at least 25s, that means ruling out the event listed in Table 6.11 with the acronym *CSR*.

### 6.6.2 Reference response spectra

Based on the values of the parameters shown in Table 6.2 using the expressions provided by the D.M. 14.01.2008, and below, were calculated by the four elastic acceleration response spectra of horizontal components for the four states limit.

$$0 \leq T \leq T_B \quad S_e(T) = a_g \cdot S \cdot \eta \cdot F_0 \cdot \left[ \frac{T}{T_B} + \frac{1}{\eta \cdot F_0} \left( 1 - \frac{T}{T_B} \right) \right] \quad (6.4)$$

$$T_B \leq T < T_C \quad S_e(T) = a_g \cdot S \cdot \eta \cdot F_0 \quad (6.5)$$

$$T_C \leq T < T_D \quad S_e(T) = a_g \cdot S \cdot \eta \cdot F_0 \cdot \left( \frac{T_C}{T} \right) \quad (6.6)$$

$$T_{DC} \leq T \quad S_e(T) = a_g \cdot S \cdot \eta \cdot F_0 \cdot \left( \frac{T_C \cdot T_D}{T^2} \right) \quad (6.7)$$

Where  $a_g$ ,  $F_0$  are defined in par. 6.2

$$S = S_s \cdot S_T \quad (6.8)$$

being  $S_s$  the amplification coefficient stratigraphy and  $S_T$ , the coefficient of topographic amplification

$\eta$  is the factor that alters the elastic spectrum for high coefficients of viscous damping than conventional  $\xi$  5%, using the relation:

$$\eta = \sqrt{\frac{10}{5 + \xi}} \geq 0.55 \quad (6.9)$$

where  $\xi$  (expressed as a percentage) is estimated on the basis of material,



structural and foundation soil type;

TC is the period that corresponds with the constant speed section of the spectrum, given by

$$T_C = T_C^* \cdot C_C \quad (6.10)$$

where  $T_C^*$  is defined in § 6.2 and  $C_C$  is a coefficient depending on the type of soil;

$T_B$  is the period that corresponds with the section of the spectrum to constant acceleration,

$$T_B = \frac{T_C}{3} \quad (6.11)$$

$T_D$  is the period that corresponds with the sudden shift of the spectrum constant in seconds using the relation:

$$T_D = 4.0 \cdot \frac{a_g}{g} + 1.6 \quad (6.12)$$

The elastic response spectrum equation is calculated considering a soil type A, a topographic category T1 corresponding, according to the Code, to values of  $S_S$ ,  $S_T$ ,  $C_C$  equal to unity.

In Figure 6.15 are shown the spectra for each elastic limit state, used as a reference for the selection of accelerograms.

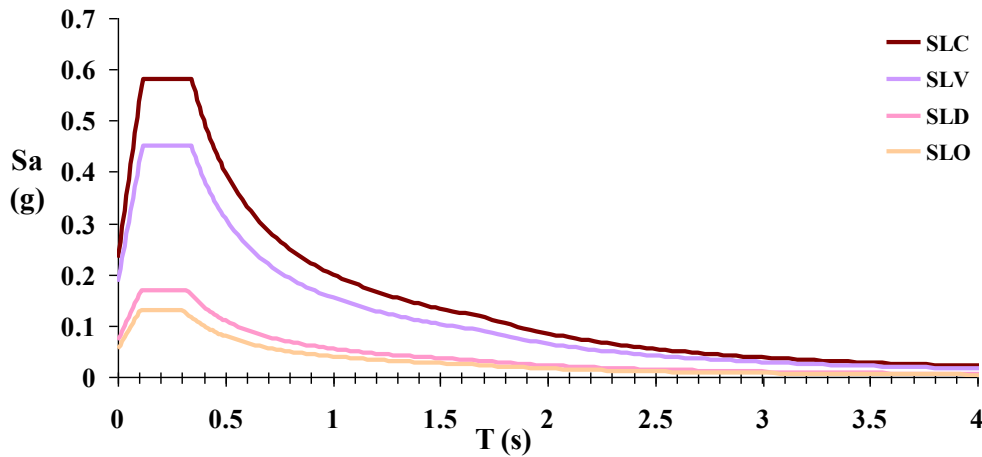


Figure 6.15 – Elastic reference spectra for each limit state

### 6.6.3 Spectrum-compatibility and scale factors

Spectral forms in acceleration, obtained by dividing the ordinates of each spectrum plotted in Figure 6.12 for their own PHA, were compared with those of reference.

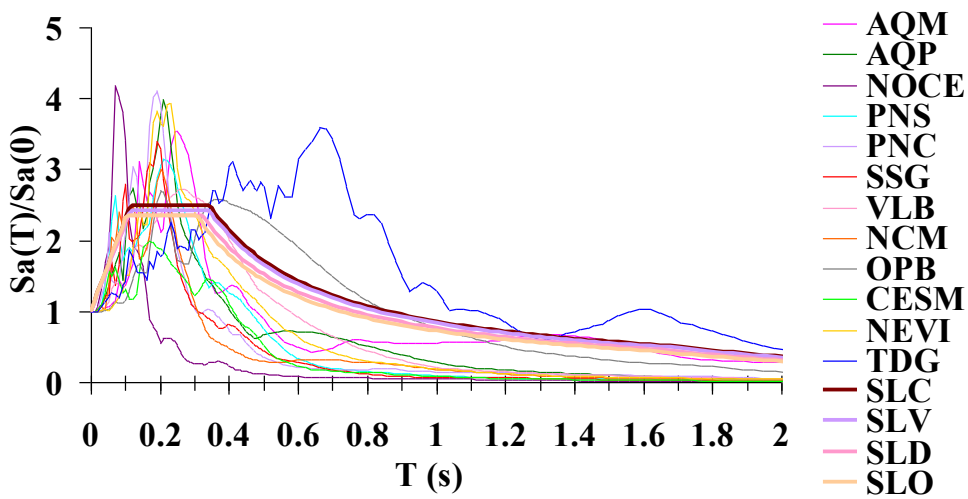


Figure 6.16 - Comparison between the reference spectral shapes and those of selected events

For each event the deviation from reference spectrum, for each limit state, was calculated using the three different coefficients, defined in par. 3.5, in time range of [0-4s]. The same was done for the scale factors. For the final selection of accelerograms have been referred to the examination of pairs  $(D_{RMS}, F_{SC})$ ,  $(\delta_i, F_{SC})$  and  $(R^2, F_{SC})$  for each registration and for each limit state. The following figures Figure 6.17 - Figure 6.22) show, for each accelerogram and relatively to each limit state, the values that assume three different pairs of parameters.

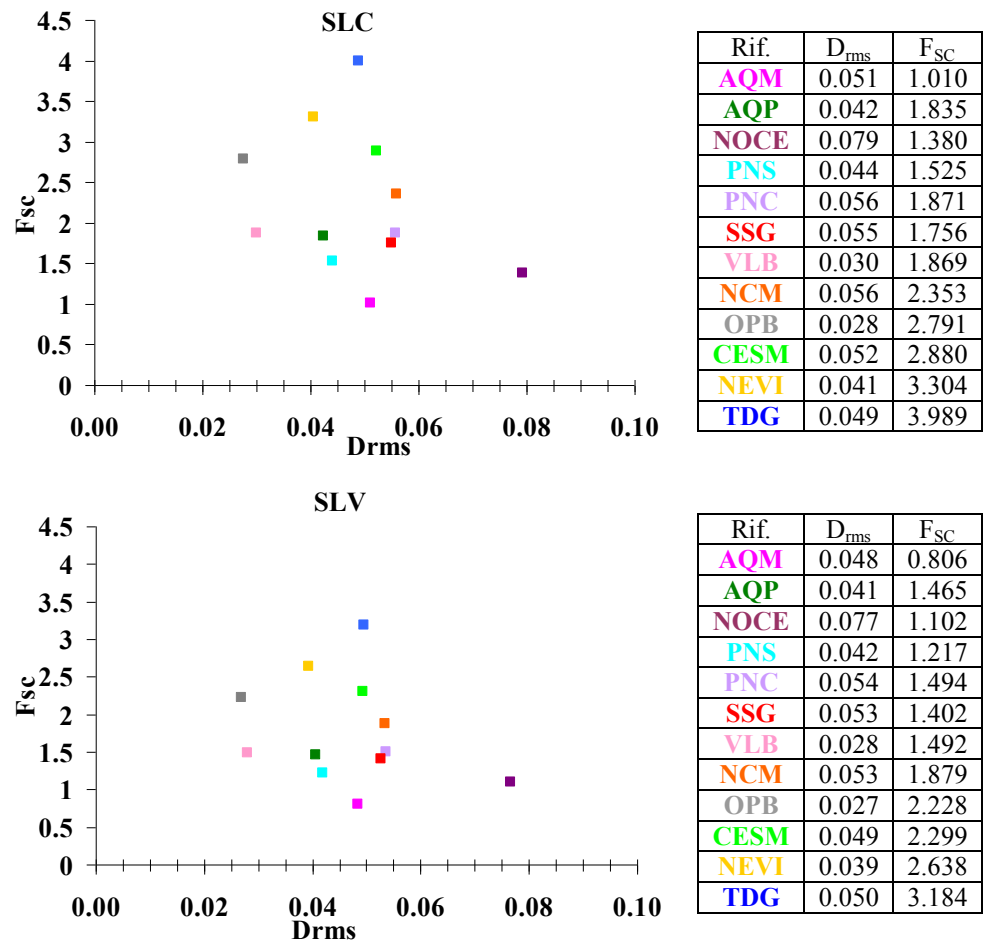


Figure 6.17 - Parameter values  $(D_{rms}, F_{SC})$  for the accelerograms analyzed in relation to the reference spectra of SLU (SLC and SLV)

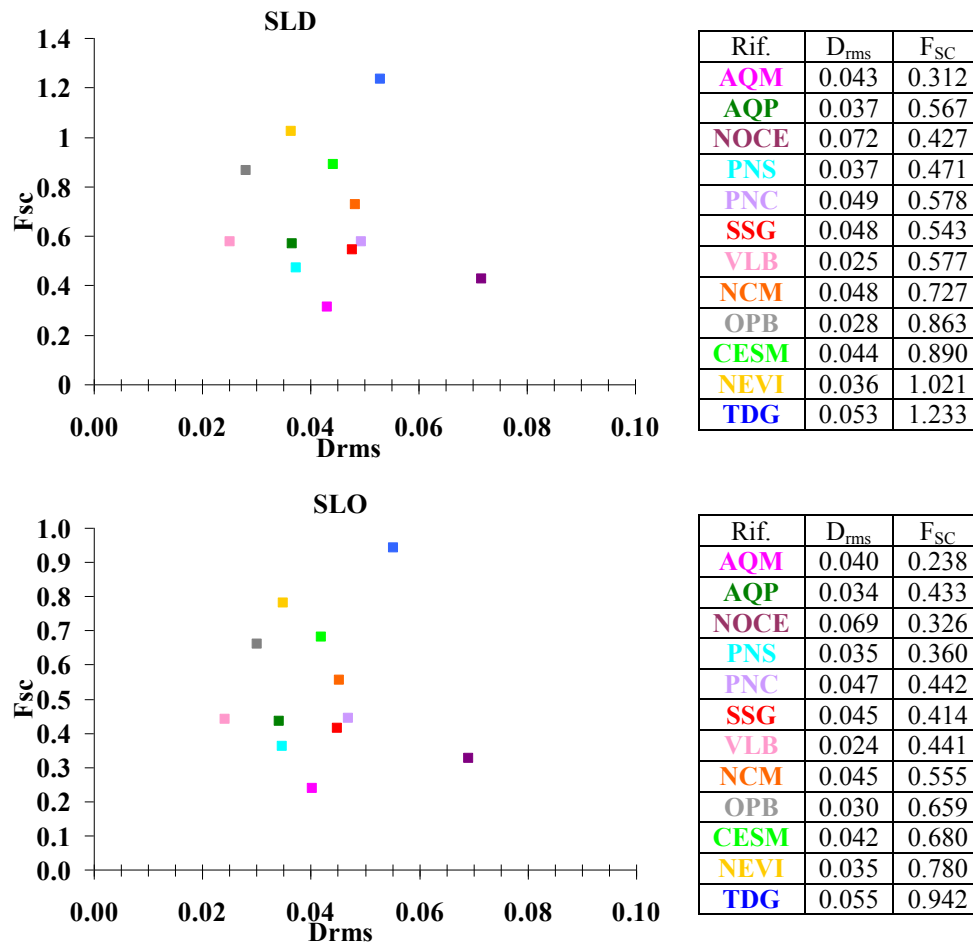


Figure 6.18 - Parameter values ( $D_{rms}$ ,  $F_{sc}$ ) for the accelerograms analyzed in relation to the reference spectra of SLE (SLD and SLO)

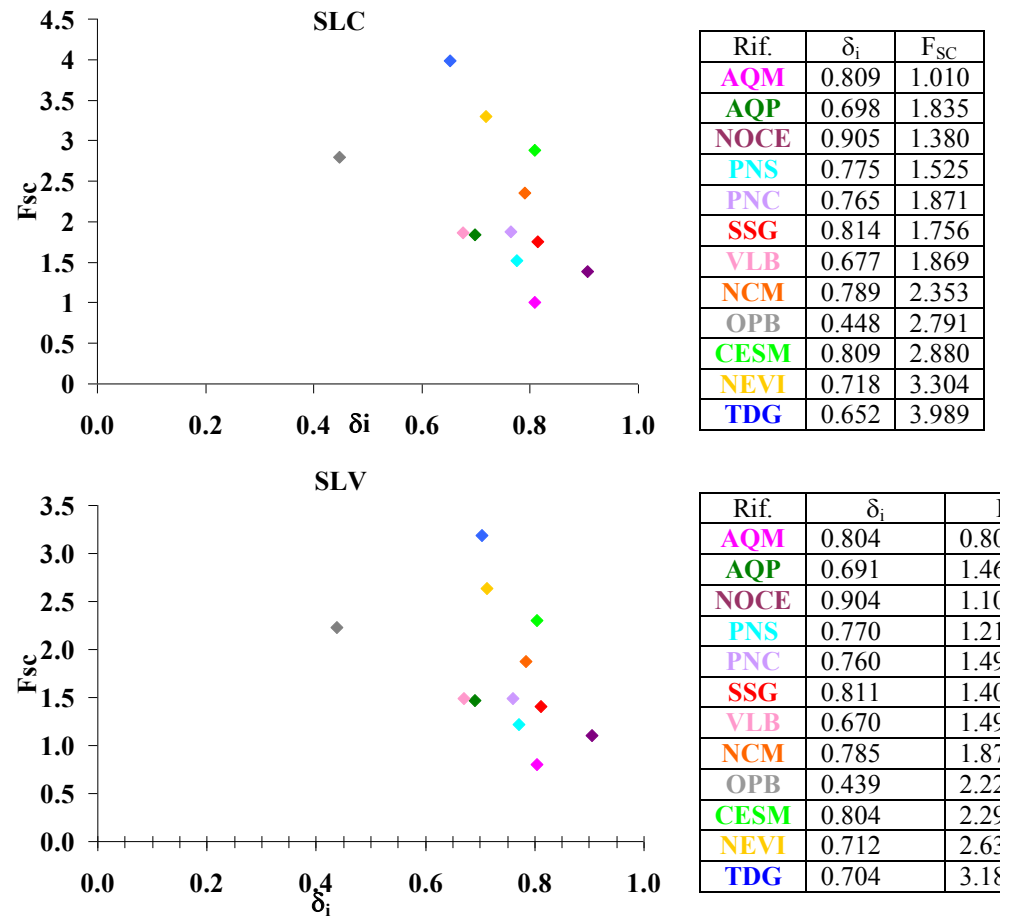


Figure 6.19 - Parameter values ( $\delta_i$ ,  $F_{SC}$ ) for the accelerograms analyzed in relation to the reference spectra of SLU (SLC and SLV)

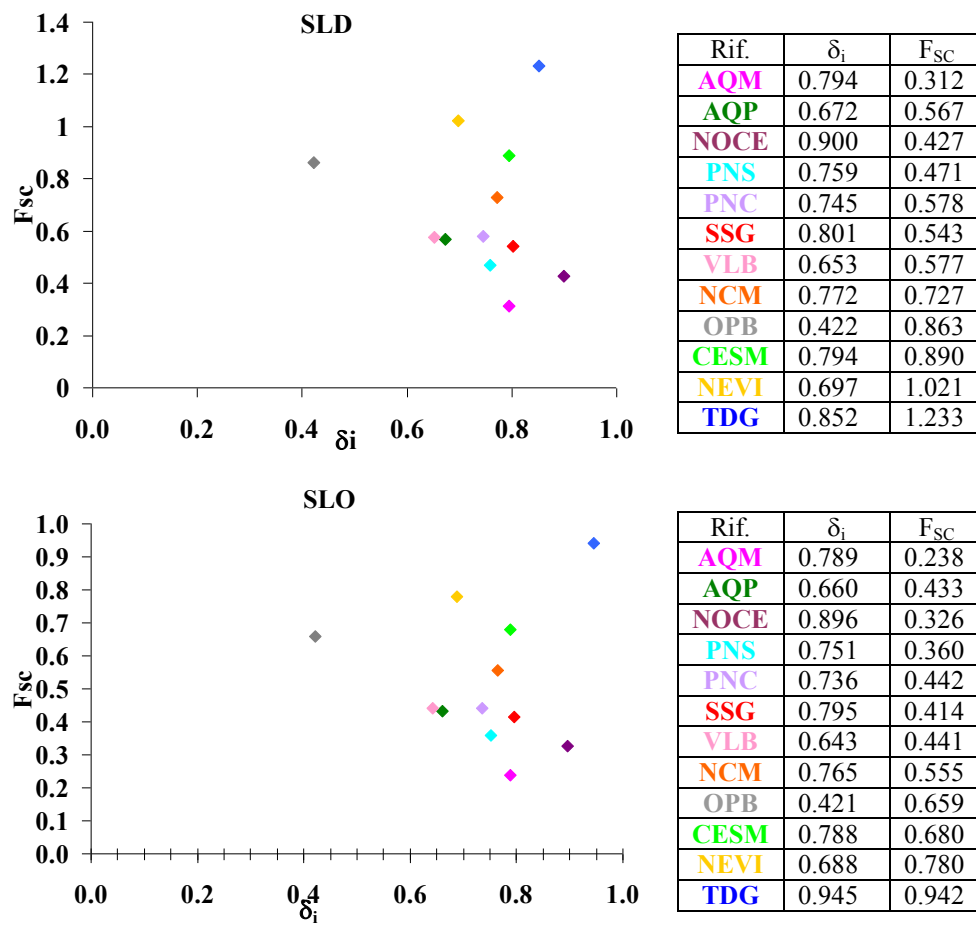


Figure 6.20 - Parameter values ( $\delta_i$ ,  $F_{sc}$ ) for the accelerograms analyzed in relation to the reference spectra of SLE (SLD and SLO)

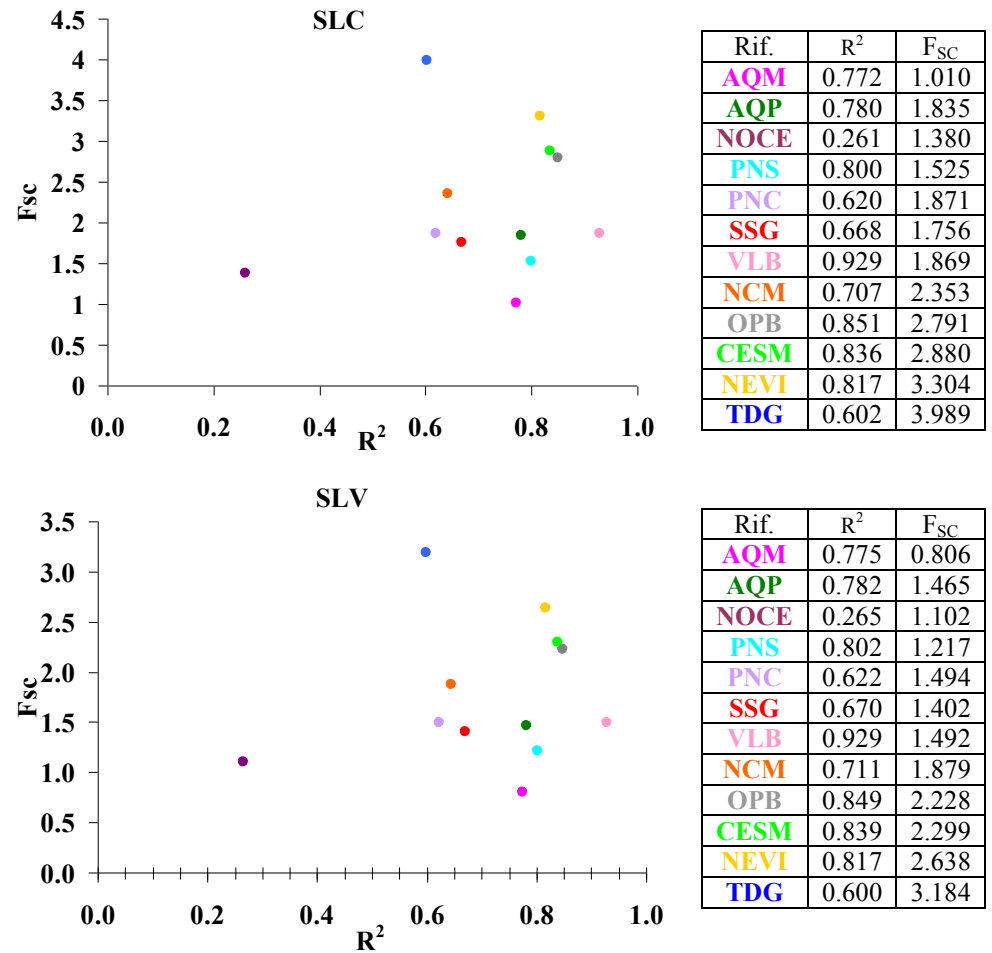


Figure 6.21 - Parameter values ( $R^2 F_{sc}$ ) for the accelerograms analyzed in relation to the reference spectra of SLU (SLC and SLV)

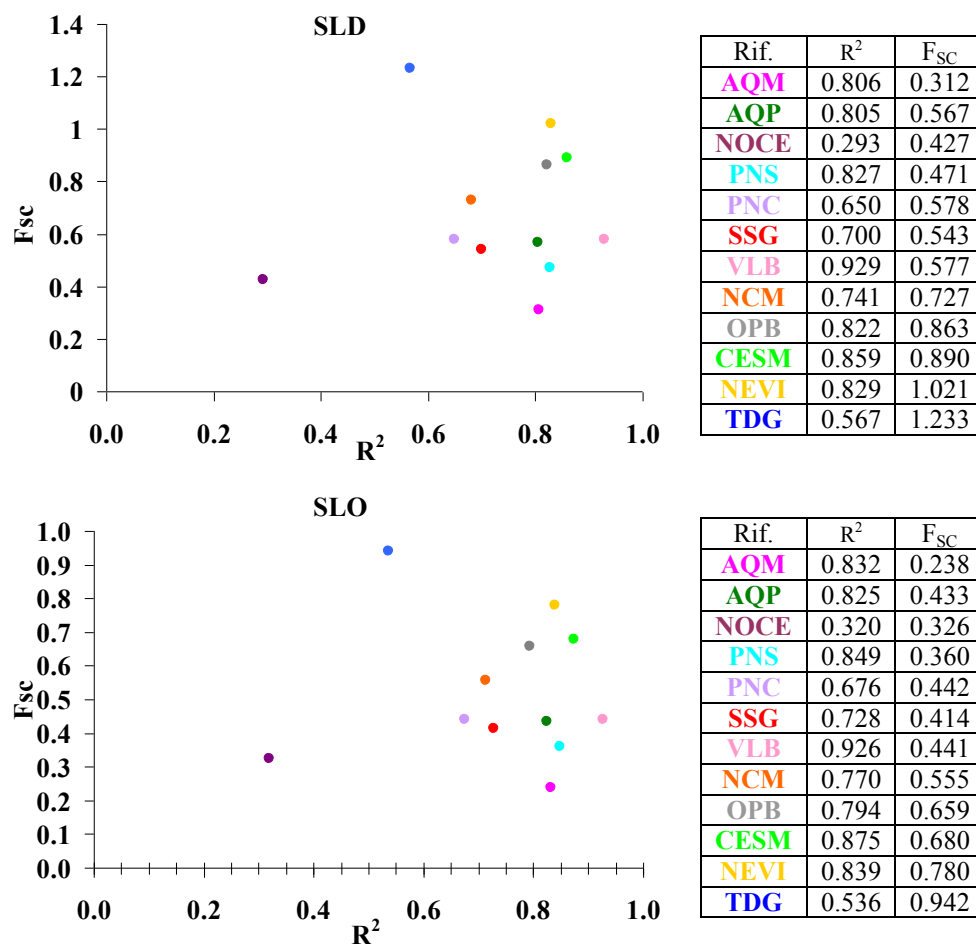


Figure 6.22 - Parameter values ( $R^2$   $F_{sc}$ ) for the accelerograms analyzed in relation to the reference spectra of SLE (SLD and SLO)

As evident from the diagrams above, you can't select a combination of at least seven accelerograms respecting all the criteria set out in paragraph 6.5.1. In view of this, different combinations have been calculated by excluding from time to time one or more criteria. In this regard it is noted that the criterion b) to limit  $F_{sc}$  to the maximum value of 2 is very restrictive: the upper limit usually accepted in literature is 4, limit respected by all selected events.



The calculated combinations are shown in Table 6.12. Please note that the accelerograms were scaled for different limit states, using the corresponding value of  $F_{SC}$ .

Table 6.12 – Calculated combination of seven accelerograms

EVENT	COMBINATION									
	7a	7b	7c	7d	7e	7f	7g	7h	7i	7l
AQM	•	•	•	•			•			•
AQP	•	•	•	•	•	•	•	•	•	•
NOCE			•							
PNS	•	•	•	•	•		•			•
PNC	•	•	•			•	•		•	
SSG	•	•	•	•	•	•	•		•	
VLB	•	•	•		•	•		•		•
NCM		•					•	•	•	
OPB					•	•		•		•
CESM				•	•	•		•	•	•
NEVI				•	•	•		•	•	•
TDG	•			•			•	•	•	

The average spectrum of each combination, for each limit state, was compared with the corresponding reference spectrum. (Figure 6.23)

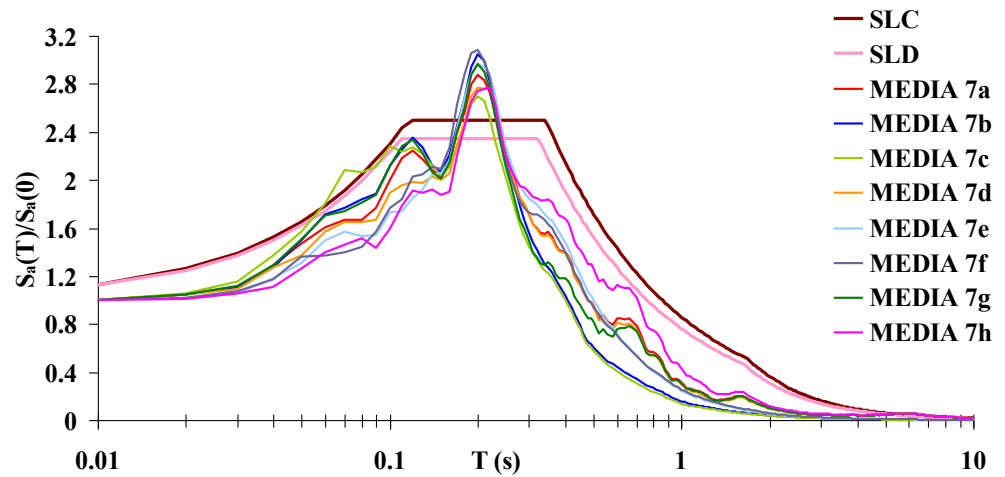


Figure 6.23 - Comparison between the reference spectral shapes and the average of the calculated combinations.

For each limit state, the deviation between the average spectrum of the accelerometric combination and the reference one are calculated through the coefficients  $D_{rms}$ ,  $\delta_i$ ,  $R^2$ . The numerical results are plotted in the following figures. (Figure 6.24 - Figure 6.27)

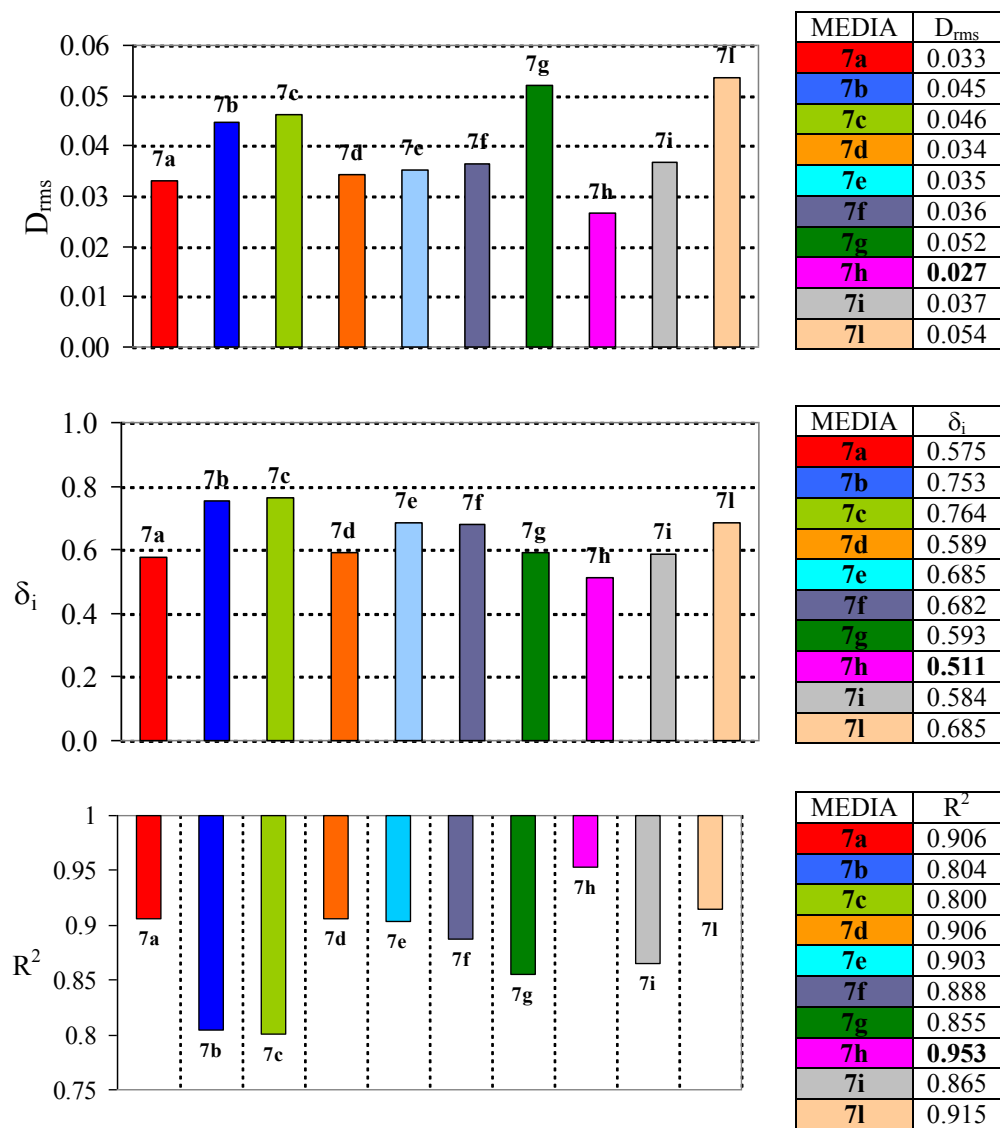


Figure 6.24 - Parameter values ( $D_{rms}$ ,  $\delta_i$ ,  $R^2$ ) for the average spectrum of the accelerometric combination in relation to the reference spectra of SLC

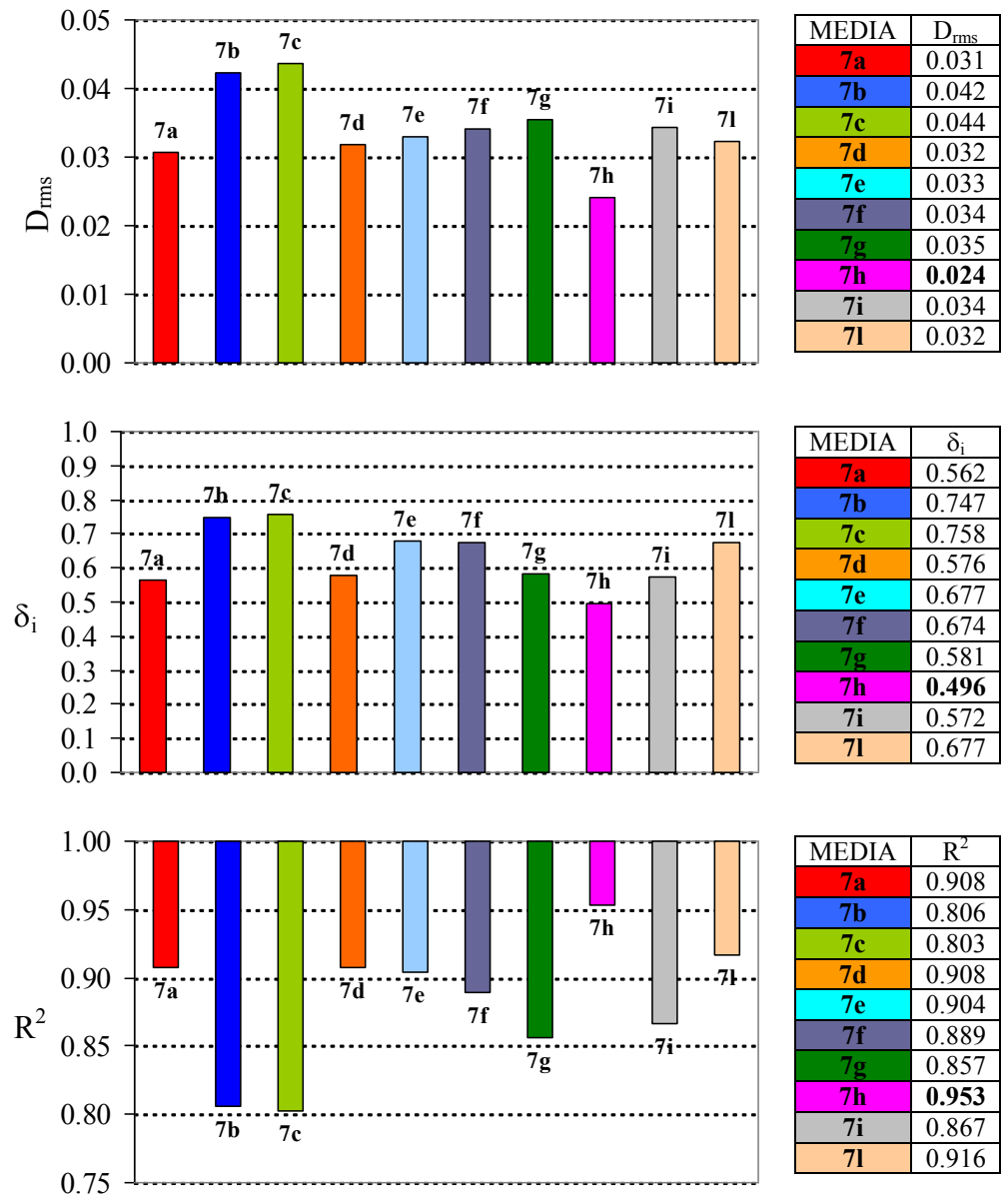


Figure 6.25 - Parameter values ( $D_{rms}$  -  $\delta_i$  -  $R^2$ ) for the average spectrum of the accelerometric combination in relation to the reference spectra of SLV

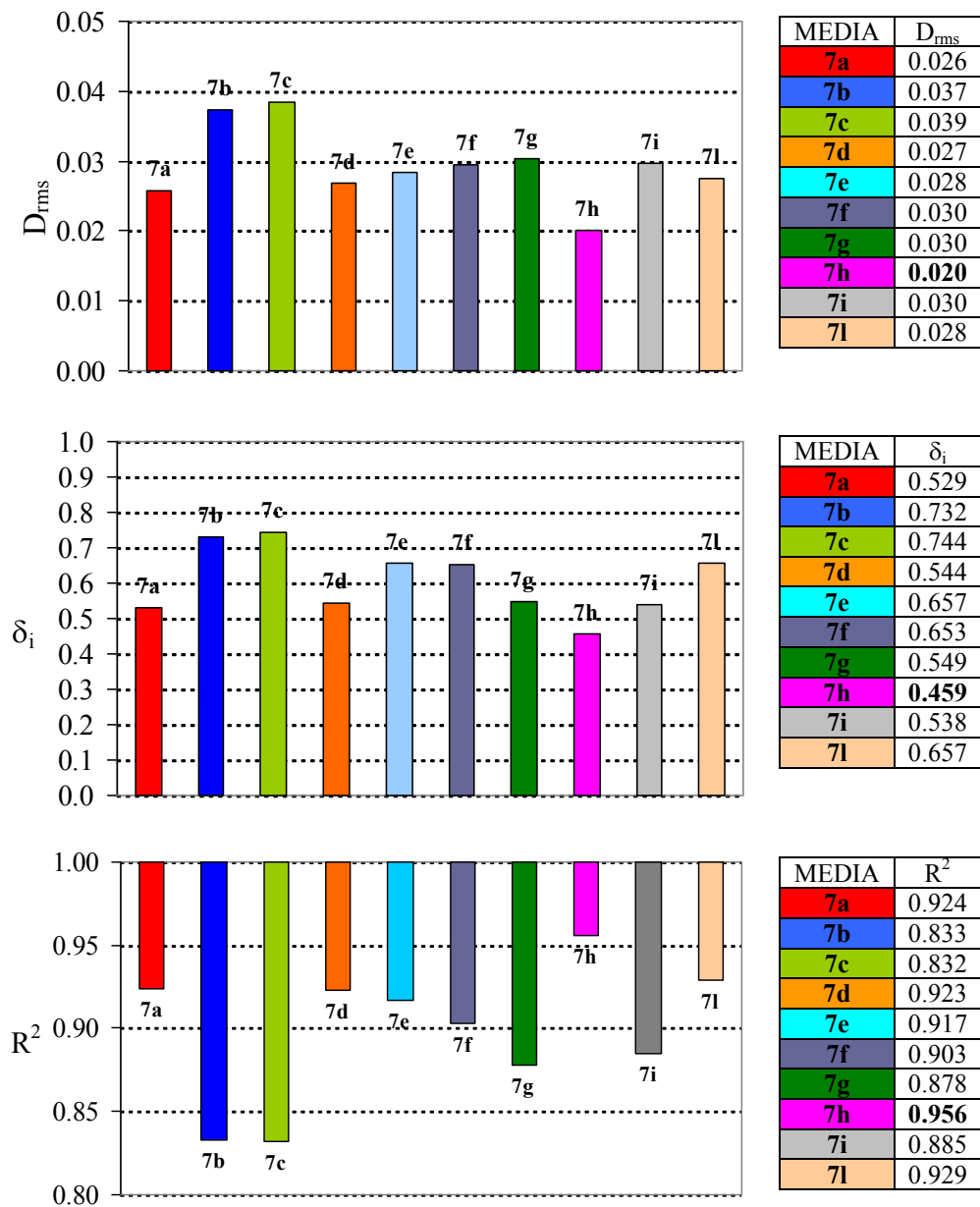


Figure 6.26 - Parameter values ( $D_{rms}$  -  $\delta_i$  -  $R^2$ ) for the average spectrum of the accelerometric combination in relation to the reference spectra of SLD

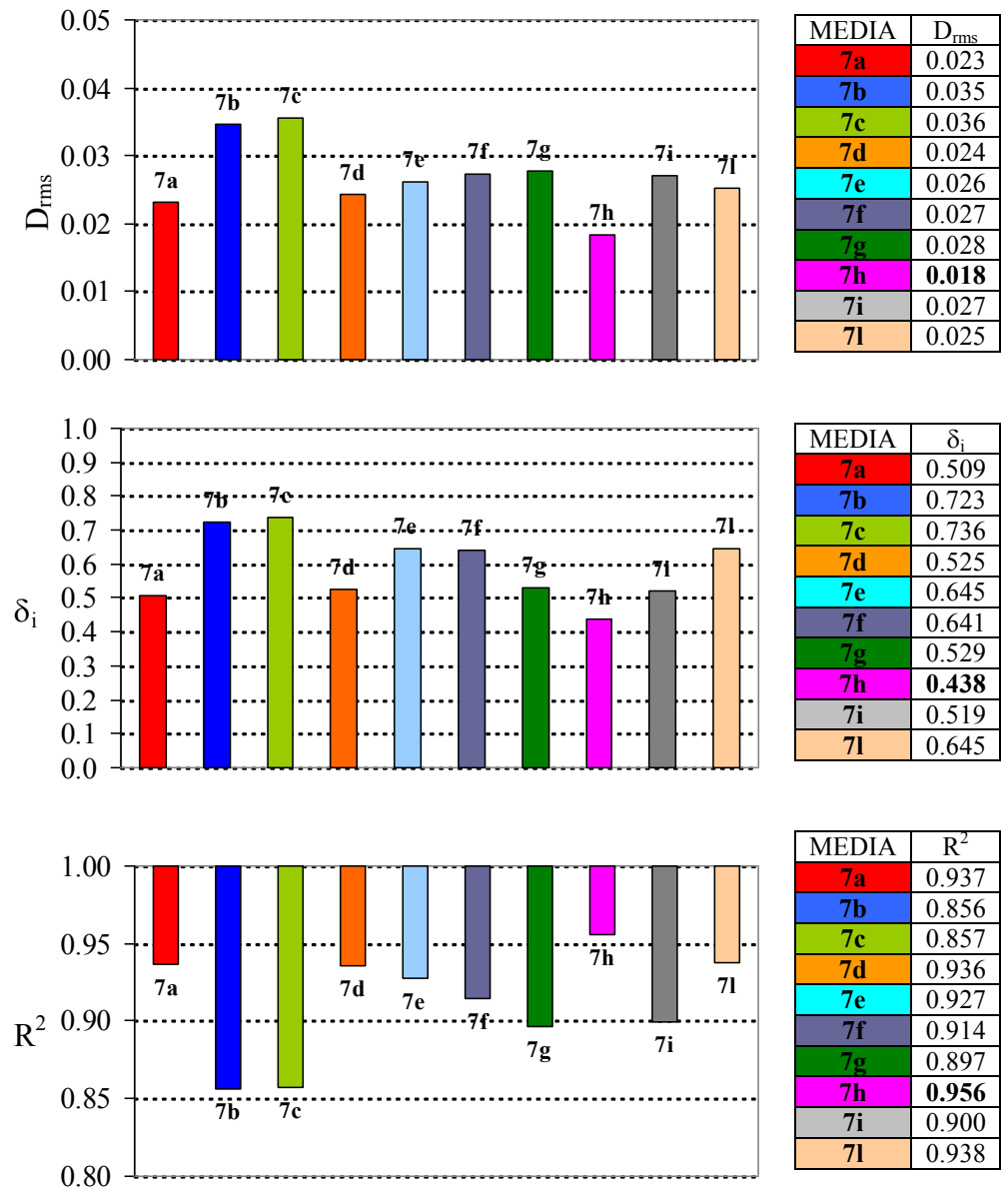


Figure 6.27 - Parameter values ( $D_{rms}$ - $\delta_i$ - $R^2$ ) for the average spectrum of the accelerometric combination in relation to the reference spectra of SLO

In the tables of histograms above is shown in bold the parameter value which corresponds to the best spectrum-compatibility: you can see that all

three coefficients regardless of the limit state considered, indicate the same combination accelerometric (7h).

#### 6.6.4 Real accelerograms selected

Figure 6.28 shows the spectral shapes of the selected accelerograms and their average compared with those of reference.

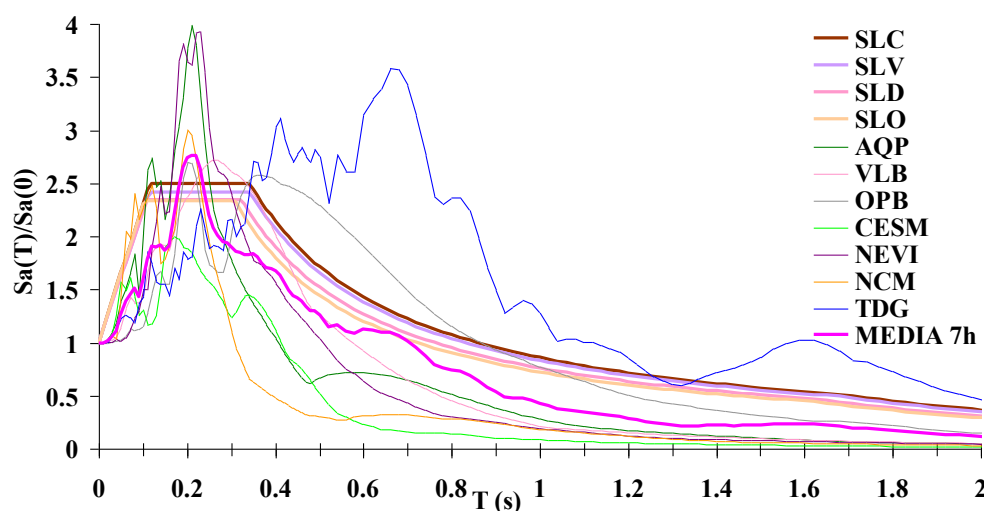


Figure 6.28 – Spectral shapes of the selected accelerograms and their average

Finally we report the seven selected accelerograms to be used for dynamic analysis. (Figure 6.29 - Figure 6.35)

In this regard, in compliance with the D.P.C.M. 09/02/2009 for seismic verification on cultural heritage, will be investigated only the limit state of collapse (SLC) and the limit state of damage (SLD). Each signal will be scaled to limit each State, through the respective factor  $F_{SC}$ .

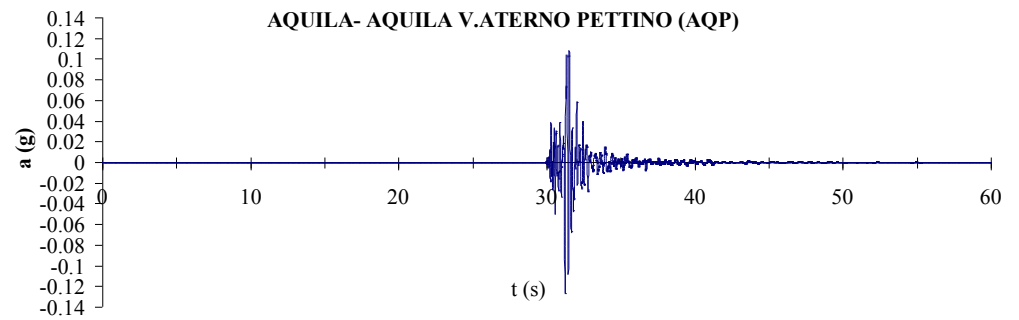


Figure 6.29 – Accelerogram of Aquila Earthquake recorded in Aquila Pettino Station (AQP)

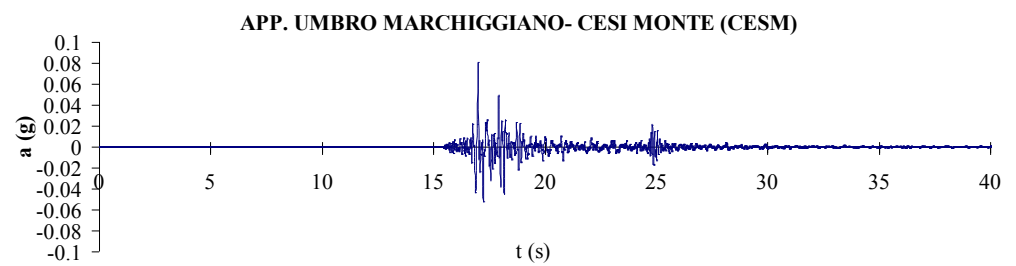


Figure 6.30 - Accelerogram of Umbr-March Earthquake recorded in Cesi Monte Station (CESM)

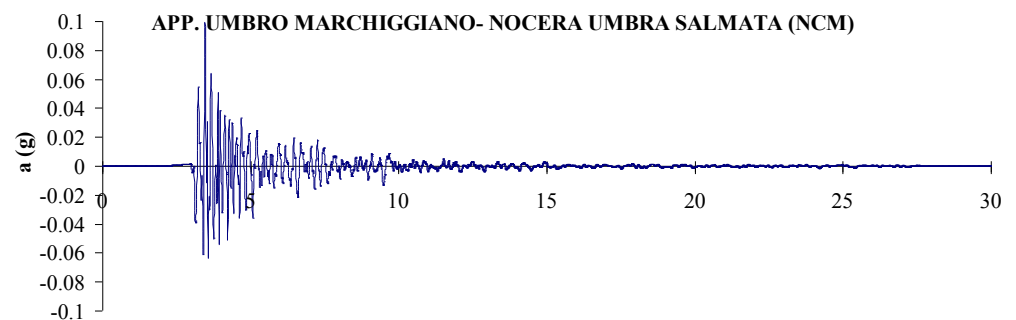


Figure 6.31 - Accelerogram of Umbr-March Earthquake recorded in Nocera Umbra Salmata Station (NCM)

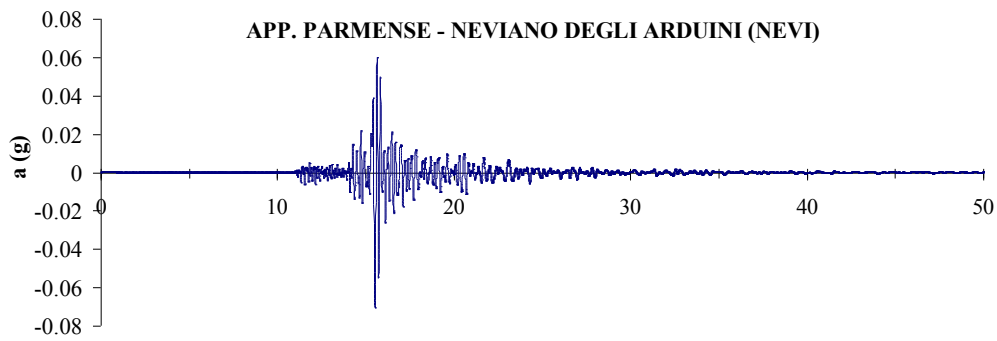


Figure 6.32 - Accelerogram of App. Parm. Earthquake recorded in Neviano degli Arduini Station (NEVI)

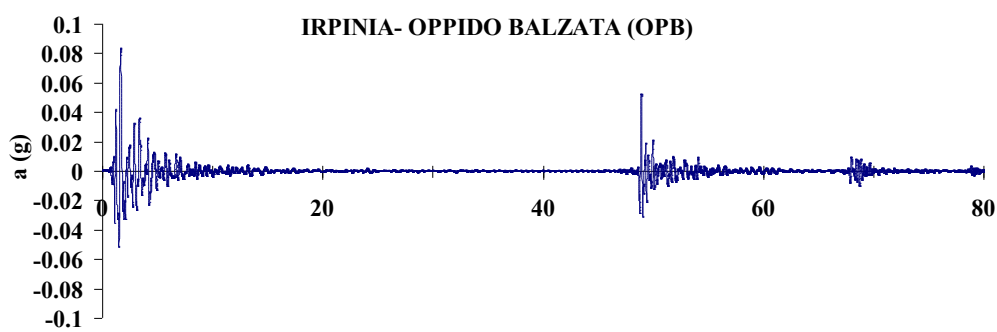


Figure 6.33 - Accelerogram of Irpinia Earthquake recorded in Oppido Balzata Station (OPB)

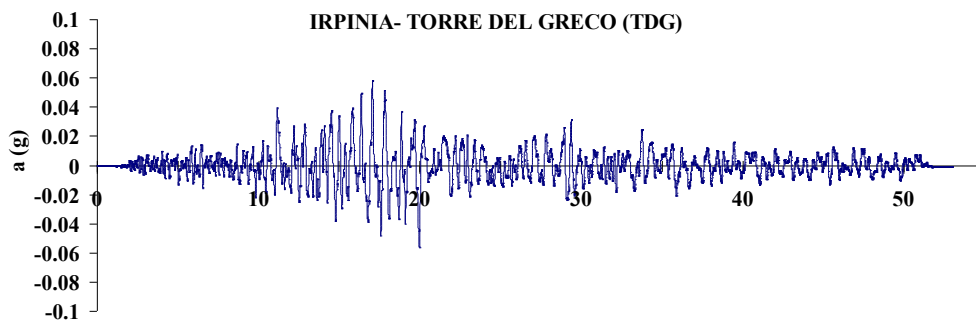


Figure 6.34 - Accelerogram of Irpinia Earthquake recorded in Torre del Greco Station (TDG)



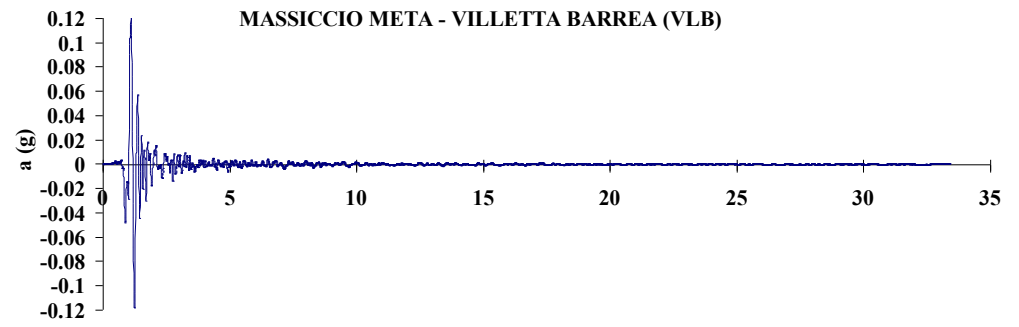


Figure 6.35 - Accelerogram of Massiccio Meta Earthquake recorded in Villetta Barrea Station (VLB)

## BIBLIOGRAPHY

Abrahamson N. A. (2006). Seismic hazard assessment: problem with current practice and future development, First European Conference on Earthquake Engineering and Seismology, Geneva, Switzerland, 3-8 September 2006.

DM 14/1/2008. Norme Tecniche per le Costruzioni. S.O. n. 30 - Gazzetta Ufficiale della Repubblica Italiana, No. 20 - 4/2/2008.

Joyner W. B., Boore D. M. (1981), Peak horizontal acceleration and velocity from strong-motion records including records from the 1979 Imperial Valley (California) earthquake, *Bull. Seis. Soc. Am.* 71, 2011-2038.

MPS Working Group (2004). Redazione della mappa di pericolosità sismica prevista dall'Ordinanza PCM 3274 del 20 marzo 2003. Rapporto conclusivo per il dipartimento di Protezione Civile, INGV, Milano – Roma, Aprile 2004, <http://zonesismiche.mi.ingv.it/elaborazioni/>.

Spallarossa D., Barani S. (2007). Disaggregazione della pericolosità sismica in termini di M-R-ε. Deliverable D14, Progetto S1 (Convenzione INGV-DPC 2004 – 2006). Dipartimento per lo Studio del Territorio e delle sue Risorse, Università di Genova

Working Group ITACA (2010). ITACA (Italian strong motion database) User Manual, Project S4, by Lucia Luzi, Francesca Pacor, Rodolfo Puglia, and Roberto Paolucci

---

*Chapter 7*

# Numerical modelling and analysis of a layered soil deposit

## 7.1 INTRODUCTION

The seismic response of a site is linked to the interaction between seismic waves and the morphological and stratigraphic conditions of the site, as well as by the physical and mechanical properties of the subsurface soil constituents. The numerical models simulate the propagation of waves from the bedrock to the surface through the subsurface. The formulation of adequate physical-mathematical models to represent the complexity of the phenomenon is quite difficult and the resolution of those, almost never, leads to fully analytical solutions.

Seismic site response analysis of a layered soil, in fact, to be reliable, must take into account the nonlinear behavior of soil and therefore can only be accomplished through dynamic analysis resolved by numerical procedures.

For carrying out the analysis, once defined the seismic input, must implement a subsurface model, defining its geometry and constitutive laws describing mechanical behaviour under seismic conditions of the medium: the variations laws of stiffness  $G$  and damping  $D$  with the shear deformation  $\gamma$ . Results of the analysis will be the trend in the time domain (or frequency) of stresses, strains, accelerations, and corresponding spectra, on the surface and at depth. (AGI 2005; Lanzano 2008; Lanzo and Silvestri 1999; Sanò 2008)

For this purpose, there are a lot of softwares, different for resolution algorithm for motion equations, for the basic simplifying assumptions and constitutive models of the soil. Numerical codes operate in total stresses, i.e. the soil is considered a solid single-phase or effective stresses where the solid phase is differentiated from the liquid one. Analytical procedures for solving the dynamic equilibrium equations, taking into account the nonlinear behavior of soil, can be divided into equivalent linear analysis, which is to perform a complete sequence of linear analysis, iteratively updating the values of the parameters of stiffness  $G$  and damping  $D$  to convergence, or non-linear analysis with incremental step of integrating the equations of motion. (Lanzo & Silvestri 1999)

The equivalent linear analysis is carried out in total stresses. It allows a simplified approach to the problem and at the same time, to take into account complex issues such as the heterogeneity of the deposit and the non-linear stress-strain relationship of soil. By contrast the equivalent linear analysis does not allow:

- a) evaluate the induced excess pore pressure,
- b) take into account the decay of the stiffness characteristics of soils resulting from the accumulation process of pore pressure,
- c) calculate of permanent deformation.

The non-linear analysis can be conducted in both total and effective stress. The adoption of a model non-linear in effective stress takes account of important aspects of the cyclic behavior of the soil such as:

- a) the generation of excess pore pressure, particularly important if the analysis of the local response is aimed at estimating the liquefaction potential of a deposit;
- b) the redistribution and eventual dissipation of excess pore pressure during and after the earthquake;
- c) progressive decay of the stiffness characteristics of soils;
- d) permanent deformation.

Compared to an equivalent linear analysis, nonlinear analysis therefore allows more accurate modelling and adherent to the reality of stress-strain behavior of soil. However, the description of the loading stages, unloading

and reloading, requires the definition of additional parameters in each layer, whose determination must be done through specific laboratory investigations.

The choice between equivalent linear analysis and nonlinear simulations must be properly evaluated, depending on the objective analysis and cost required to determine representative values of input parameters required by the analysis. As a first approximation, this choice can be made on the basis of the shear strain level induced in the ground. In particular, the equivalent linear analysis gives satisfactory results for shear deformations  $\gamma$  less than about 1-2% and for peak accelerations on rock  $a_{\max, r}$  less than 0.3 to 0.4 g. (AGI 2005)

Finally, the existing numerical codes are distinguished based on the geometry domain in which they operate: one-dimensional, two dimensional and three-dimensional.

The most used models are one-dimensional geometry. In them the soil is constituted by one or more layers parallel and horizontal, i.e. vertical column laterally homogeneous, above bedrock also horizontal. When the reality, as in case under our study, is similar to such situation, then it is permissible to consider only one dimension of depth, neglecting the other two dimensions.

In a 1-D model, the seismic motion amplification is related to the impedance ratio due to differences between the mechanical properties of the soil between the layers and between them and the bedrock, and the resonance determined by the proximity between frequency of substrate vibration and the natural one of the deposit.

In 1-D model, the individual layers are characterized by the following geotechnical parameters: weight per unit of volume; velocity of shear waves to small deformations  $V_s$  (or, similarly, maximum shear modulus  $G_0$ ); curves  $G(\gamma)/G_0$  and  $D(\gamma)$ , respectively laws of variation of shear stiffness and damping factor with the shear strain  $\gamma$ .

When the free surface or the layers or bedrock are not horizontal the assumption of a 1-D model is unrealistic. In these cases you can use 2-D/3-D models which reproduce the surface topography, stratigraphic contacts and/or

the base of any shape and so to model the effects of board and the topography.

The 3-D models are not widely used in applications and are required when the boundary conditions of the problem or the characteristics of seismic motion in three directions vary significantly. In 2-D/3-D models, in addition to geotechnical parameters assigned in 1-D models, must also be assigned the values of the compression wave velocity ( $V_p$ ) or Poisson's ratio ( $\nu$ ). (AGI 2005)

Below is a small table in the review of existing codes and their differences. (Lanzo 2005)

Table 7.1 - Numerical codes for dynamic analyses (Lanzo 2005)

Table 7-1 Numerical codes for dynamic analyses (Bardet 2002)					
Geom	Boundary conditions	Code	Analysis type		Analysis method
1-D	Elastic	SHAKE (Schnabel <i>et al.</i> , 1972)	T.S.	L.E.	Continuous; Frequences domain
		SHAKE91 (Idriss & Sun, 1992)*			
		PROSHAKE (EduPro Civil System, 1999)			
		SHAKE2000 (www.shake2000.com)			
		EERA (Bardet <i>et al.</i> , 2000)*			
	Rigid	DESPRA 2 (Lee & Finn, 1978)	E.S.	N.L.	Discrete. Time domain
		DESRAMOD (Vucetic, 1986)			
		D-MOD 2 (Matasovic, 1995)			
		NERA (Bardet & Tobita, 2001)*	T.S.		
	DEEPSOIL (Hashash e Park, 2001)				
2-D 3-D	Rigid base and every free surface	QUAD4 (Idriss <i>et al.</i> , 1973)	T.S.	L.E.	F.E.M. Time domain
		QUAD4M (Hudson <i>et al.</i> , 1994)			
		QUAKE/W 5.0 (GeoSlope, 2002)			
	Every base and free surface; absorbent lateral boundary	FLAC 5.0 (Itasca, 2005)	E.S.	N.L.	F.D.M. Time domain
		PLAXIS 9.0 (www.plaxis.nl)			
T.S. = Total stresses; E.S. = Effettive stresses, L. E. = Linear Equivalent; N.L. =Non Linear					*free

The choice of the numerical code is very important and should be carefully assessed in relation to the available data, the type of analysis you want to play, the kind of results you wish to achieve and to their reliability and consistency. An incorrect choice can lead to rough estimates unless incorrect.

## 7.2 ONE-DIMENSIONAL GROUND RESPONSE ANALYSIS OF A LAYERED SOIL DEPOSIT (Lanzo, Silvestri 1999)

The one-dimensional analysis of local seismic response of a layered subsurface is possible by numerical models with continuous layers or lumped parameters. (Figure 7.1)

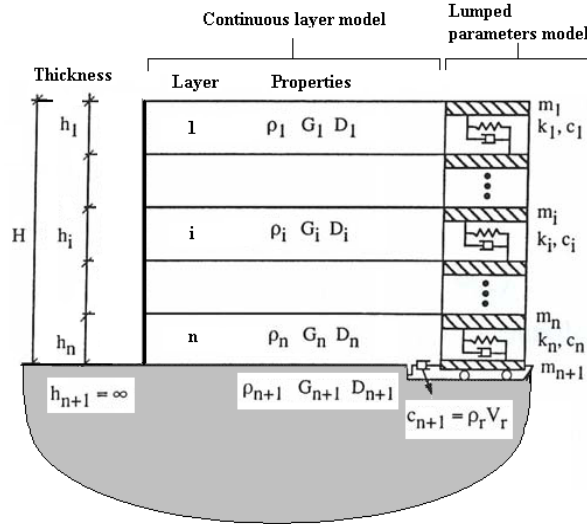


Figure 7.1 - One-dimensional layered soil deposit system (modified by Lanzo, Silvestri 1999)

The one-dimensional equation of motion for vertically propagating shear waves is:

$$\rho_i \frac{\partial^2 u_i}{\partial t^2} - \eta_i \frac{\partial^3 u_i}{\partial t \partial z^2} - G_i \frac{\partial^2 u_i}{\partial z^2} = 0 \quad (7.1)$$

in which  $h_i$ ,  $G_i (= \rho_i V_{Si}^2)$ ,  $\rho_i$ ,  $\eta_i$  and  $D_i$  are respectively the layer thickness, the shear modulus, the unit mass, the viscosity and the damping ratio for each layer. The viscosity and the damping ratio are linearly dependent through the expression:

$$D_i = \frac{\eta_i \varpi}{2G_i} \quad (7.2)$$

The soil deposit is crossed by shear waves, incident vertically to the surface between the layers. All the numerical models are in free-field conditions.

For harmonic waves with frequency  $\omega$ , the displacement  $u_i$  can be written as:

$$u_i(z,t) = p_i(z)e^{j\omega t} \quad (7.3)$$

In which  $p_i(z)$  is a function of form.

Using equation (7.3), (7.1) becomes

$$(G_i + j\omega\eta_i) \frac{\partial^2 p_i}{\partial z^2} + \rho_i \omega^2 p_i = 0 \quad (7.4)$$

Defining the complex wave number  $k_i^*$  as

$$k_i^* = \frac{\omega}{\sqrt{G_i^*/\rho_i}} = \frac{2\pi f}{V_{Si}^*} = \frac{2\pi}{\lambda_i^*} \quad (7.5)$$

and the complex shear modulus  $G^*$  as

$$G_i^* = G_i + j\omega\eta_i = G_i(1 + 2jD_i) \quad (7.6)$$

The solution of (7.4) is

$$p_i(z) = Ae^{jk_i^* z} + Be^{-jk_i^* z} \quad (7.7)$$

So (7.3) becomes:

$$u_i(z,t) = A_i e^{j(k_i^* z + \omega t)} + B_i e^{-j(k_i^* z - \omega t)} \quad (7.8)$$

where  $A_i$  e  $B_i$  are the amplitudes of waves propagating respectively upwards and downwards.



The stress corresponding to (7.8), in a local coordinate system ( $0 \leq z \leq h_i$ ) for each layer, is:

$$\tau(z_i, t) = (G_i + j\omega\eta_i) \frac{\partial u_i}{\partial z_i} = jk_i^* G_i^* \left( A_i e^{jk_i^* z} - B_i e^{-jk_i^* z} \right) e^{j\omega t} \quad (7.9)$$

At the interface between layers  $i$  and  $i+1$ , displacements and shear stress must be continuous, which implies that:

$$\begin{aligned} u_i(h_i) &= u_{i+1}(0) \\ \tau_i(h_i) &= \tau_{i+1}(0) \end{aligned} \quad (7.10)$$

Using eq. (7.8) to (7.10) we obtain:

$$\begin{aligned} A_i e^{jk_i^* h_i} + B_i e^{-jk_i^* h_i} &= A_{i+1} + B_{i+1} \\ k_i^* G_i^* \left( A_i e^{jk_i^* h_i} - B_i e^{-jk_i^* h_i} \right) &= k_{i+1}^* G_{i+1}^* (A_{i+1} - B_{i+1}) \end{aligned} \quad (7.11)$$

Eqs. (7.10) and (7.11) give the following recursion formulas for amplitudes  $A_{i+1}$  and  $B_{i+1}$  in terms of  $A_i$  and  $B_i$ :

$$\begin{aligned} A_{i+1} &= \frac{1}{2} \left[ A_i (1 + \mu_i) e^{jk_i^* h_i} + B_i (1 - \mu_i) e^{-jk_i^* h_i} \right] \\ B_{i+1} &= \frac{1}{2} \left[ A_i (1 - \mu_i) e^{jk_i^* h_i} + B_i (1 + \mu_i) e^{-jk_i^* h_i} \right] \end{aligned} \quad (7.12)$$

Where  $\mu_i$  is the complex impedance ratio at the interface between layers  $i$  and  $i+1$ :

$$\mu_i = \frac{k_i^* G_i^*}{k_{i+1}^* G_{i+1}^*} \equiv \sqrt{\frac{\rho_i G_i^*}{\rho_{i+1} G_{i+1}^*}} \quad (7.13)$$

By imposing the condition of free surface  $\tau_1(0) = 0$ , by (7.9) is  $A_1 = B_1$  (incident and reflected waves of equal amplitude).

Iteratively using the recurrence formulas (7.13) for all layers ( $i = 1 \dots n$ ), we finally get to the transfer functions  $A_i(\omega)$ ,  $B_i(\omega)$  components of ascending and descending from the surface to the layer  $i$ :

$$\begin{aligned} A_i &= a_i(\omega)A_1 \\ B_i &= b_i(\omega)B_1 \equiv b_i(\omega)A_1 \end{aligned} \quad (7.14)$$

Introducing (7.14) in (7.8) we can express the displacement function  $u(z, t)$ . The relationship between the amplitudes of the displacement between any two levels  $i$  and  $k$ , is expressed by the transfer function  $H_{ik}(\omega)$  given by:

$$H_{ik}(\omega) = \frac{|u_k|}{|u_i|} = \frac{A_k + B_k}{A_i + B_i} = \frac{a_k(\omega) + b_k(\omega)}{a_i(\omega) + b_i(\omega)} \quad (7.15)$$

Being harmonic functions, is  $|\ddot{u}| = \omega|\dot{u}| = \omega^2|u|$ , the (7.15) also expresses the transfer function of velocity and acceleration between layer and layer. For  $k=1$ ,  $i = n$ , (7.15) provides, varying  $\omega$ , the amplification function of the motion between the bedrock and the free surface of a soil profile divided into homogeneous strata.

The application of (7.15) in the frequency domain allows operate the convolution of a seismogram from a point to another in profile, using Fast Fourier Transform algorithms that perform (FFT) and inverse (IFFT). For example, given an accelerogram  $a_r(t)$  at the bedrock, to determine numerically the motion corresponding to the surface as  $(t)$ , we can make a series of operations:

$$a_s(t) = \text{IFFT}\{a_s(\omega)\} = \text{IFFT}\{H_{rs}(\omega) \cdot a_r(\omega)\} = \text{IFFT}\{H_{rs}(\omega) \cdot \text{FFT}[a_r(t)]\}$$

where  $H_{rs}$  is the transfer function between the bedrock and the free surface.

### 7.3 EERA (Bardet et.al 2000)

The software EERA (Equivalent-linear Earthquake site Response Analysis) is an implementation of the equivalent-linear earthquake site response analysis, which was previously implemented in the original and subsequent versions of SHAKE (Schnabel et al., 1972; and Idriss and Sun, 1991). EERA evaluates the seismic site response (SSR) of a soil deposit: the medium is modelled as a system of continuous horizontal layer, which are homogeneous, isotropic and visco-elastic, based on a uniform half-space.

EERA implements the SHAKE processor in a Microsoft Excel file, which is composed by the sequent worksheets:

- Earthquake
- Profile
- Mat1, Mat2, Mat3, etc.
- Iteration
- Acceleration, Strain, Ampli, Fourier, Spectra

In the worksheet “Earthquake” the input signal can be loaded in order to perform the ground shaking. Before the earthquake is loaded, in the worksheet was definable five entries (recognizable in blue): the earthquake name; the time step  $\Delta T$ , which is the time interval between the evenly spaced data points of the time history of input ground motion; the desired maximum acceleration, in order to scale the input values; the maximum frequency cut-off in order to eliminate the annoying high frequencies; the NFFT number of the points of the Fast Fourier Transform, which is larger than the earthquake points. The input earthquake data are imported from a text file using the command “Process earthquake data”.

The characteristics of the soil deposit are showed in the section “Profile”, in which the geometry and the properties are defined layer by layer. The user can be chosen the type of the analysis to perform: visco-elastic linear or non linear. When a linear visco-elastic analysis is performed, each layer is defined by the thickness  $h$ , the maximum shear stiffness  $G_0$ , the value of the initial damping  $D_0$ , the volume unit weight  $\gamma_s$ , and the apparent shear wave velocity layered  $V_s$  (linearly dependent from the others parameters). When a non linear analysis is carried out, all the previous parameters was defined, except for the

damping ratio, which was directly defined by the  $D(\gamma)$  law (initial value).

Therefore for each soil layer can be defined a different variation curve (in the worksheets Mat1, Mat2, etc.) for the shear stiffness  $G(\gamma)/G_0$  and the damping  $D(\gamma)$ . The non linear analysis consists in an equivalent visco-elastic analysis: a set of linear analyses are performed sequentially, updating for each step the value of the shear stiffness  $G(\gamma)$  and the damping ratio  $D(\gamma)$ , depending by the convergence on shear strain reached. The location and type of earthquake motion is defined by specifying Outcrop for an outcropping rock motion, or Inside for a non outcropping motion (Figure 7.2). In the case of Inside motion the acceleration time histories is directly applied at the soil layered base; instead a Outcrop motion corresponds to a acceleration time history applied on the soil surface and reported at the base through a deconvolution analysis.

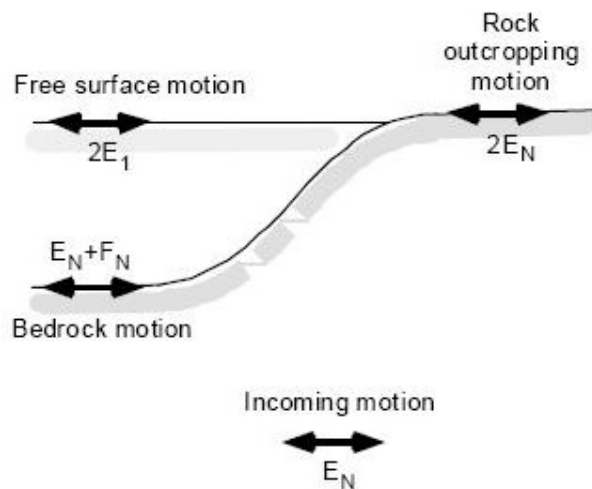


Figure 7.2 - Outcrop or inside input motion (Bardet et al. 2000)

In the Iteration worksheet the motion equations, described in §7.2, are solved in the frequencies domain. Three option for the calculation are included in this section: the number of iterations, which can be increased depending by the convergence of the calculation; the ratio of equivalent uniform strain  $R_\gamma$  for the effects of earthquake duration, which is typically between 0.3 and 0.75 depending on earthquake magnitude; the type of linear equivalent model (SHAKE or SHAKE91).

The calculation starts clicking on the command “Calculate Compatible Strain”. The iteration procedure for equivalent linear approach in each layer is as follows (Figure 7.3):

Initialize the values of  $G_i$  and  $D_i$  at their small strain values.

Compute the ground response, and get the amplitudes of maximum shear strain  $\gamma_{\max}$  from the time histories of shear strain in each layer.

Determine the effective shear strain  $\gamma_{\text{eff}}$  from  $\gamma_{\max}$  as:

$$\gamma_{\text{eff}} = R_\gamma \gamma_{\max} = \frac{M-1}{10} \gamma_{\max} \quad (7.17)$$

where  $R_\gamma$  is the ratio of the effective shear strain to maximum shear strain.  $R_\gamma$  is specified in input and is the same for all layers.

Calculate the new equivalent linear values  $G_{i+1}$  and  $D_{i+1}$  corresponding to the effective shear strain  $\gamma_{\text{eff}}$ .

Repeat the steps until the differences between the computed value of shear strain in two successive iterations  $|\gamma_{k+1} - \gamma_k|$  is the same in less than a predetermined tolerance value  $\varepsilon$ .

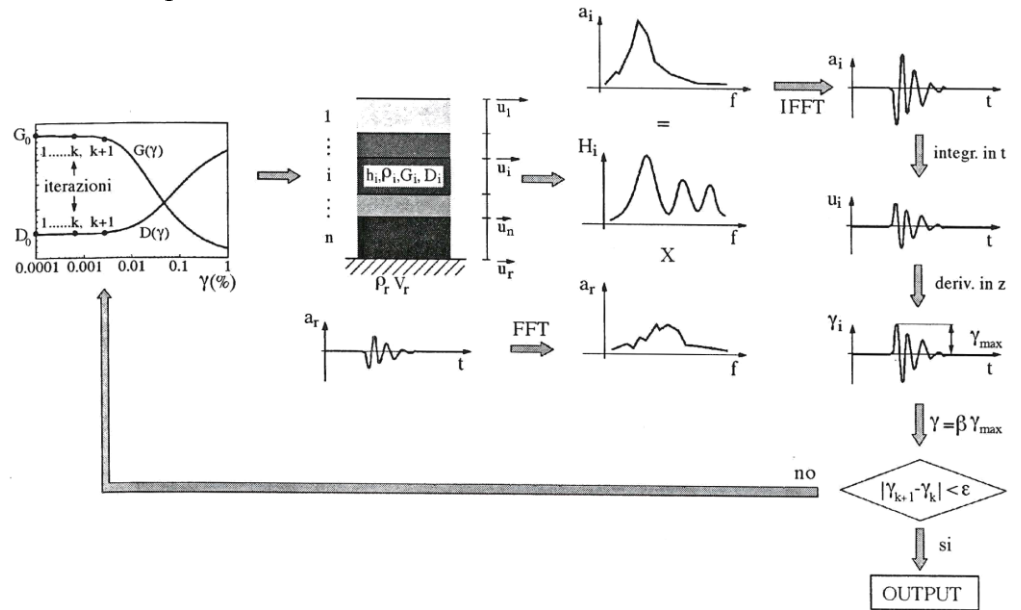


Figure 7.3 - Iteration procedure used in EERA. (Lanzo, Silvestri 1999)

The accuracy of the solution obtained is proportional to the number of elements (degrees of freedom) introduced in the discretization, whose growth conditions, however, the computation time. A good rule to optimize the discretization is to use at least 3 to 4 points to describe the generic half length of the vibration waveform of an element with thickness  $h$  and velocity  $V_s$ . (Kuhlemeyer & Lysmer, 1973)

The condition implies that if  $f_{\max}$  is the significant maximum frequency of input signal, the maximum thickness element  $h_{\max}$  to should be (Figure 7.4):

$$h_{\max} = \frac{\lambda_{\min}}{6 \div 8} = \frac{V_s}{(6 \div 8)f_{\max}} \quad (7.18)$$

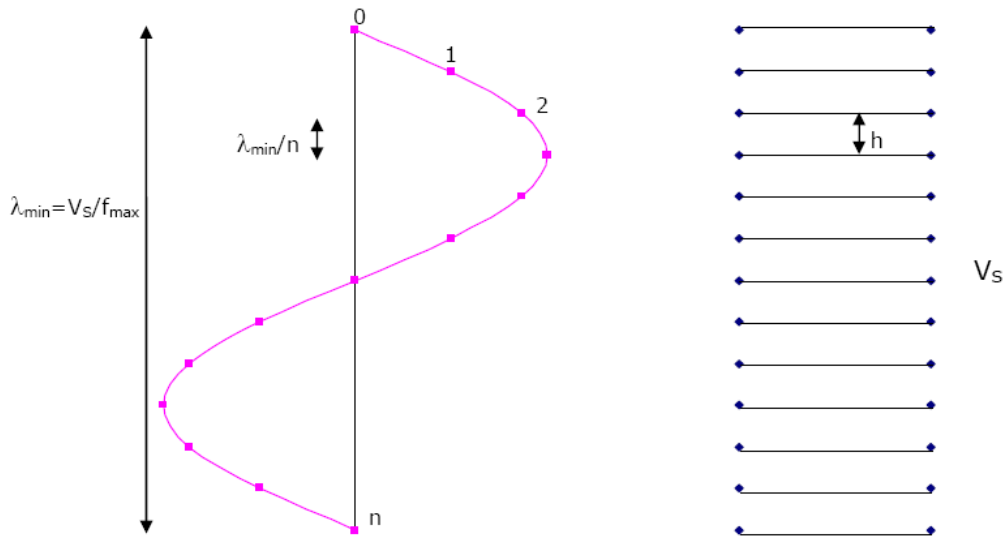


Figure 7.4 – Maximum thickness of mesh element as function of  $V_s$

After the calculation is performed, the results, for each iteration, were showed as table and as graphs for the profiles of maximum shear stress, shear strain and acceleration. Moreover the distribution with depth of the mobilized  $G$  and  $D$  were graphically reported.

In the Output worksheets the results of the calculation were reported as time histories or through signals transform in the frequency domain at specific layers: the Acceleration and Strain worksheets give the time histories of acceleration, velocity and displacement or of shear stress and strain corresponding to a specific layer (outcrop or inside); in the Fourier and Spectra worksheets the spectrum of Fast Fourier Transform and the response spectrum are evaluated; in the Ampli worksheet the amplification function is obtained as a ratio between the Fourier spectra in two different layers. The worksheet can be duplicated in order to obtain the output data in different layers. Once in all the worksheet the soil layer number and the type of layer (inside or outcrop) are specified, the results are given clicking on the command “Calculate Output” and “All of the Above”.

Advantages of using the EERA are:

- conceptual simplicity of the model, which makes the computer code can be easily applied in many situations even complex;
- limited number of input data that it requires;
- large amount of results suggests that output in the time domain and frequency;
- accuracy and stability of the numerical solution;
- capability to consider the characteristics of frequency-dependent;
- high number of searches that have significantly improved the reliability and the well-defined range of validity of this program.

The main limitations are:

- constitutive model behaviour adopted for the soil, not always is reliable, especially when the nonlinearity effect becomes dominant on the soil behavior and the seismic site response as for soft soil or high magnitude earthquakes (0.3-0.5Hz), probably due to effects of resonance;
- overestimation of the maximum stresses than those experimental or estimated using nonlinear codes;
- analysis is conducted in terms of total stresses and does not allow you to control any increments of pore pressure and all the phenomena connected with it (liquefaction).

## 7.4 STUDY CASE MODEL

The model used for the analyses are deduced from the geo-lithological and seismic survey executed on the site under study, showed in cap. 5: the stratigraphy, escluding the topsoil layer, consists of alternating flow deposit (lavas) and fall ones (pyroclastics).

The various layers, as well as for MASW survey, were merged taking into account the similar geo-lithological and mechanical characteristics of soils, resulting in the finale 3 layer on the lava-bedrock: a top layer of pozzolana thickness of 2.8m, a layer of 4m thick fractured lava (corresponding to tehe eruption of 1631), a thin layer of sand (1.2m) resting on compact lava, dating from the eruption of 79 a.C, considered as bed-rock. The top layer was divided into two to taking into account, after, a treated area or not. The model, teherefore, consists of four layer above the bedrock. From MASW test (cap. 5) have been obatined the seismic velocity assigned in the model to each layer and consequently the characteristics related to them, as shear modulus  $G_0$ , calculated through teh relation:

$$G_0 = \rho V_s^2 \quad (7.19)$$

In (Table 7.2) and (Figure 7.5) the values of parameters assigned to each layer are shown.

Table 7.2 – Mechanical characteristic of soil for each layer

Layer	Thickness	Depth	Soil Type	Unit Weight	Density	Shear velocity	Shear Modulus
	h [m]	z [m]	- -	$\gamma$ [KN/m <sup>3</sup> ]	$\rho=\gamma/g$ [KN/ (m <sup>3</sup> ·g)]	Vs [m/s]	G <sub>0</sub> [Mpa]
1	1.0	0 1.0	Pozzolanic sand	15.70	1.6	219	76.74
2	1.8	1.0 2.8		15.70	1.6	219	76.74
3	4	2.8 6.8	Fractured lava	24.53	2.5	331	273.90
4	1.2	6.8 8.0	Pozzolanic sand	15.70	1.6	233	86.86
5	Bedrock- half-space	8.0	Compact lava	24.53	2.5	1200	3600



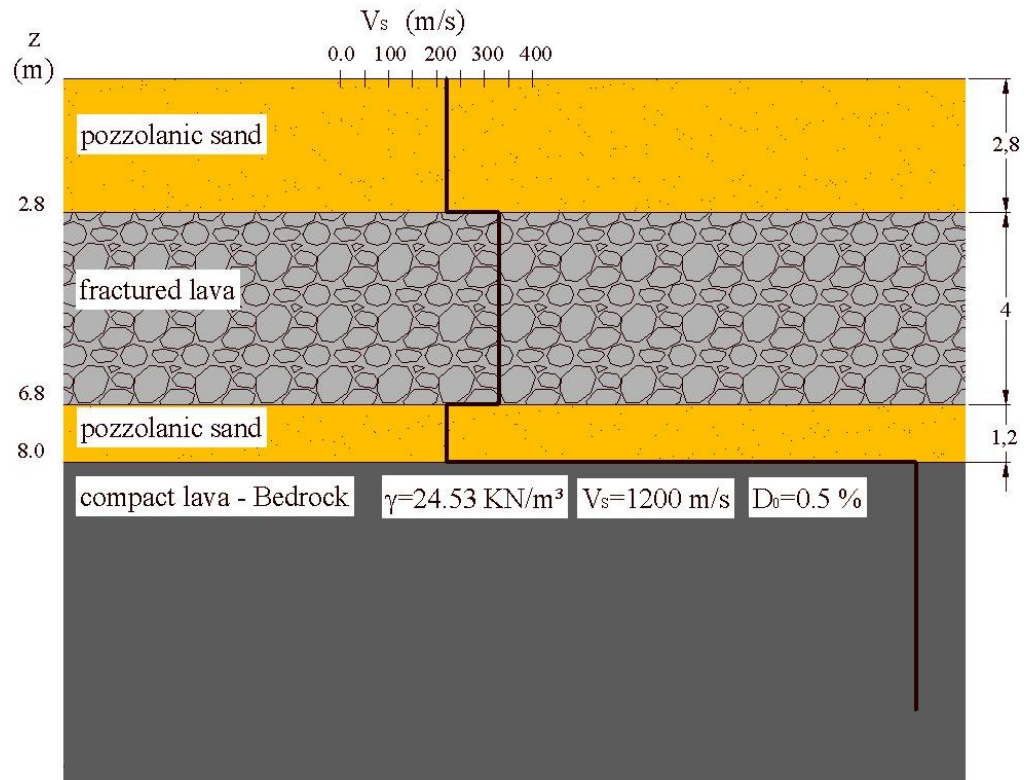


Figure 7.5 – Geometry and  $V_s$  profile of study case

For dynamic analyses, the soil stiffness and damping curves,  $G(\gamma)/G_0$  and  $D(\gamma)$ , depending on the shear strain level,  $\gamma$ , induced by the earthquake. In this case literature empirical relationship was used in order to define  $G(\gamma)/G_0$  and  $D(\gamma)$ .

Figure 7.6 shows the adopted curves and given by:

- for pozzolana from experimental test executed by Papa et al. (1988);
- for fractured lava, the Seed & Idriss (1970) curves for rock, implemented in EERA;

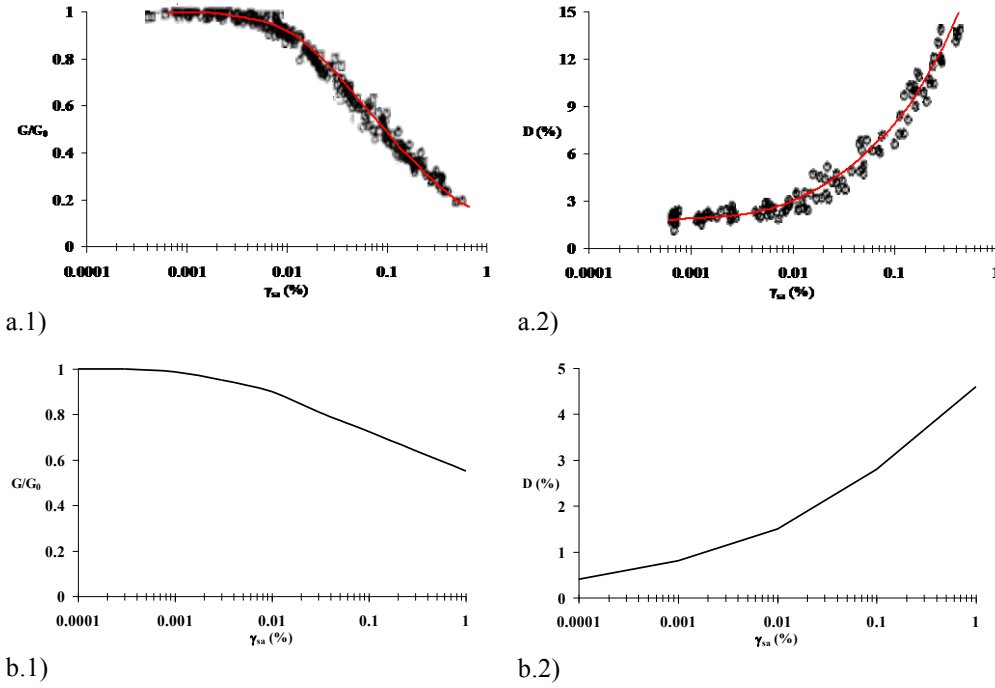


Figure 7.6 – Soil stiffness  $G(\gamma)/G_0$  (1) and damping  $D(\gamma)$  curves (2): a) pozzolana; b) rock

In order to investigate the behaviour of studied soil when the shear deformation is  $1\% < \gamma < 2\%$  the experimental curves of pozzolana, shown in Figure 7.6, have been fitted through Ramber-Osgood model (1943). The Ramber-Osgood model is an inverse formulation of nonlinear model and is defined as follows:

$$\gamma(\bar{G}) = \left( \frac{1 - \bar{G}}{C \cdot \bar{G}^R} \right)^{\frac{1}{R-1}} \quad (7.20)$$

where

$$\bar{G} = \frac{G}{G_0} \quad (7.21)$$

$G$  is the shear modulus.

$G_0$  is the shear stiffness modulus value when strain are zero, typical of the soil behaviour in elastic field.

$C$  and  $R$  are calibration parameters for the model.

The model allows derive the decay curve of non dimensional shear modulus. For the interpolation of data  $(\gamma, \bar{G})$ , apply a linear relationship of the model so that the experimental points, plotted on a bi-logarithmic scale graph, can be interpolated with a straight line that provides the settings parameters of the model.

$$\gamma(\bar{G})^{R-1} = \frac{1 - \bar{G}}{C \cdot \bar{G}^R} \quad (7.22)$$

$$\gamma(\bar{G})^{R-1} \cdot C \cdot \bar{G}^R = 1 - \bar{G} \quad (7.23)$$

$$(R - 1) \log \gamma + \log C + R \log \bar{G} = \log(1 - \bar{G}) \quad (7.24)$$

$$\log[\gamma(1 - \bar{G})] = R \log(\gamma \cdot \bar{G}) + \log C \quad (7.25)$$

Replacing in (7.25):

$$Y = \log[\gamma(1 - \bar{G})] \quad (7.26)$$

$$X = R \log(\gamma \cdot \bar{G}) \quad (7.27)$$

We obtain a straight line equation

$$Y = a \cdot X + b \quad (7.28)$$

In which  $a = R$ ;  $b = \log C$

So from the values pairs  $(\gamma, \bar{G})$ , is possible to calculate the values of  $Y = \log[\gamma(1 - \bar{G})]$  e  $X = R \log(\gamma \cdot \bar{G})$ , by linearly interpolation is obtained the angular coefficient  $a$  and the intercept  $b$ , from which  $R = a$  e  $C = 10^b$ .

For the variation curve of damping the procedure is the same.

The Ramberg Osgood model with Masing criteria allows to derive a variation law  $D(\bar{G})$ :

$$D(\bar{G}) = \frac{n}{\pi} \cdot \frac{R-1}{R+1} \cdot (1 - \bar{G}) \quad (7.29)$$

In which  $R$  has the same value that in the corresponding curve  $\bar{G}(\gamma)$

$n$  is the calibration parameter of the curve. (Silvestri 1991)

The curve so obtained shows the values of  $D + D_0$ . In our case  $D_0 = 1.5\%$  as from the literature value of  $1\% < D_0 < 2\%$  for pozzolana. (Papa et al. 1988)

The results of interpolation are shown in the following (Figure 7.7).

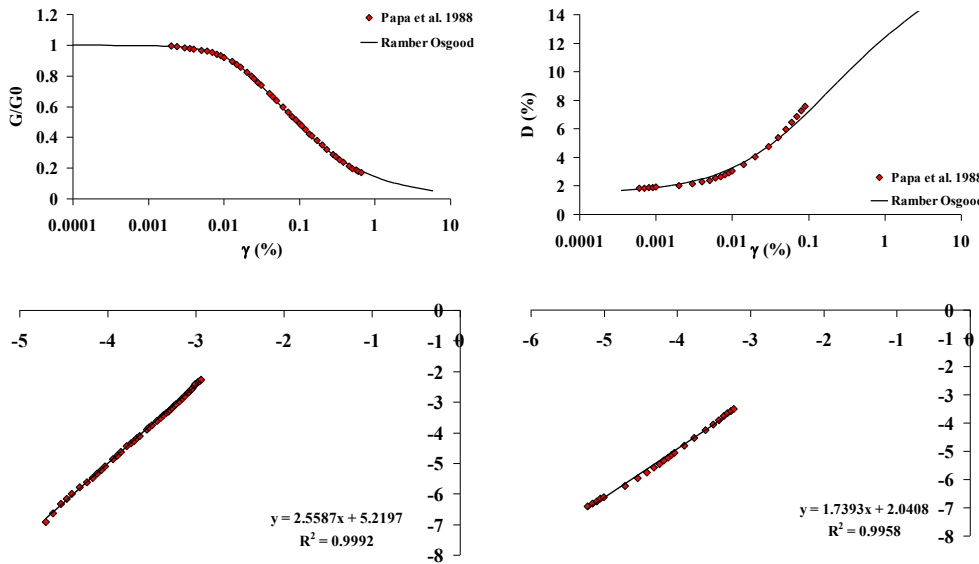


Figure 7.7 – Nondimensional shear stiffness modulus  $G(\gamma)/G_0$  and damping  $D(\gamma)$  curves fitted with Ramberg-Osgood method

## 7.5 ANALYZED CASES

Defined the characteristics of the reference model (case 0), as shown in the previous paragraph, different hypotheses of intervention were examined.

In the field of the gravity injective techniques treatment, acting on the constitution soil, were analyzed three different effects on the stiffness of the soil before and after intervention: two types of interventions that would increase the stiffness of the treated layer, and one that, instead reduce it. The treatment effect was expressed as the ratio  $E_V$  between the seismic wave velocity  $V_S$  of soil treated and not, according to the values in (tab. 4.2).

$$E_V = \frac{V_{S\text{treat}}}{V_{S0}} \quad (7.30)$$

For each type of treatment were considered to operate at different depths, for a total number of 9 analyzed cases. The description and characteristics of the analyzed cases are summarized in the following (Table 7.3).

*Table 7.3 – Analyzed cases*

				CASE	0	1	2	3
Rif.	Description	Thicknes of intervention	Depth of intervention (m)	Treated layer -	$V_S$ before (m/s)	$V_S$ after (m/s)		
<b>A</b>	The treatment is performed just below the plan of laying the foundations	1	1.8	1	219	110	330	650
<b>B</b>	The treatment is performed just above the first layer of lava	1	3.6	2	219			
<b>C</b>	The treatment is assumed in contact with the bedrock, in the layer of sand, which is the reverse of the profile of $V_S$	1.2	8.6	4	233			
				$E_V$	<b>1</b>	<b>0.5</b>	<b>1.4</b>	<b>3</b>

The following figures show the profiles of velocity and shear stiffness for each case.

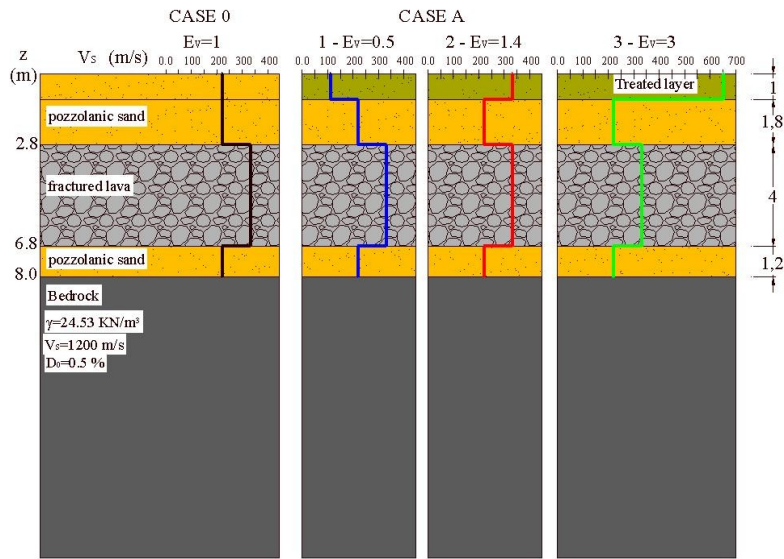


Figure 7.8 – Seismic wave velocity  $V_s$  profile for Case A: 1- $E_v=0.5$ ; 2- $E_v=1.4$ ; 3- $E_v=3$

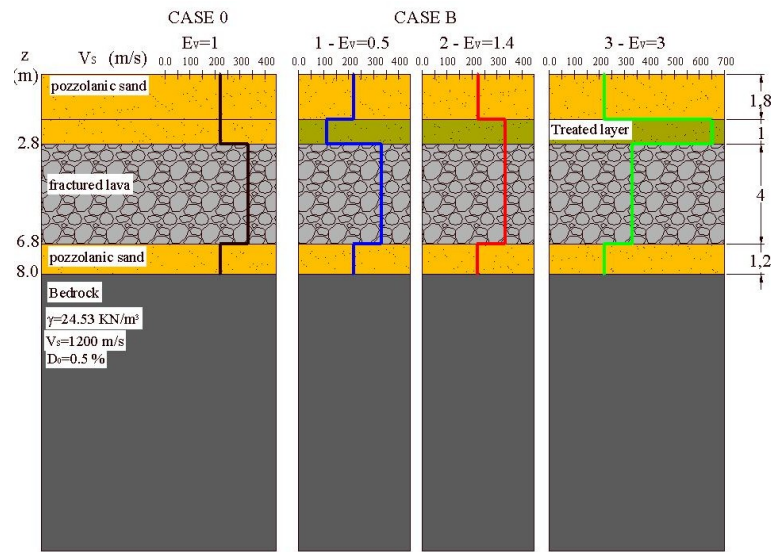
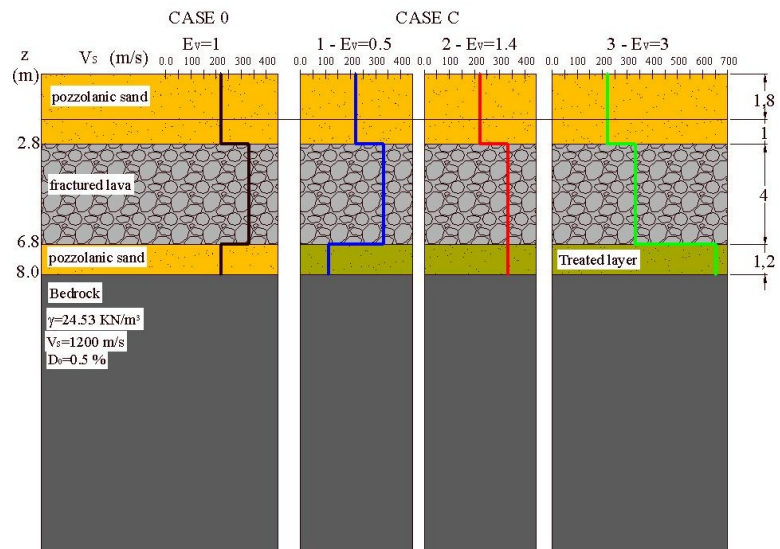


Figure 7.9 - Seismic wave velocity  $V_s$  profile for Case B: 1- $E_v=0.5$ ; 2- $E_v=1.4$ ; 3- $E_v=3$



The seismic input assigned to the numerical model for the analyses is defined and widely described in chapter 6.

For each case (10), analyzes were performed for each of the two limit states specified in chapter 6 (SLC-SLD) and for each of the selected accelerograms (7), for a total number of 140 analysis.

## 7.6 ANALYSIS RESULTS

The analysis results were expressed in terms of maximum acceleration, stress and strain profiles as a function of depth; of response spectra in acceleration and displacement in time domain and in terms of amplification function in frequencies domain.

### 7.6.1 Reference case before soil treatment :case 0

Figure 7.11-Figure 7.13 show the results of analysis relating to the reference case (case 0) for each limit state (SLD-SLC) and for all seven accelerograms input.

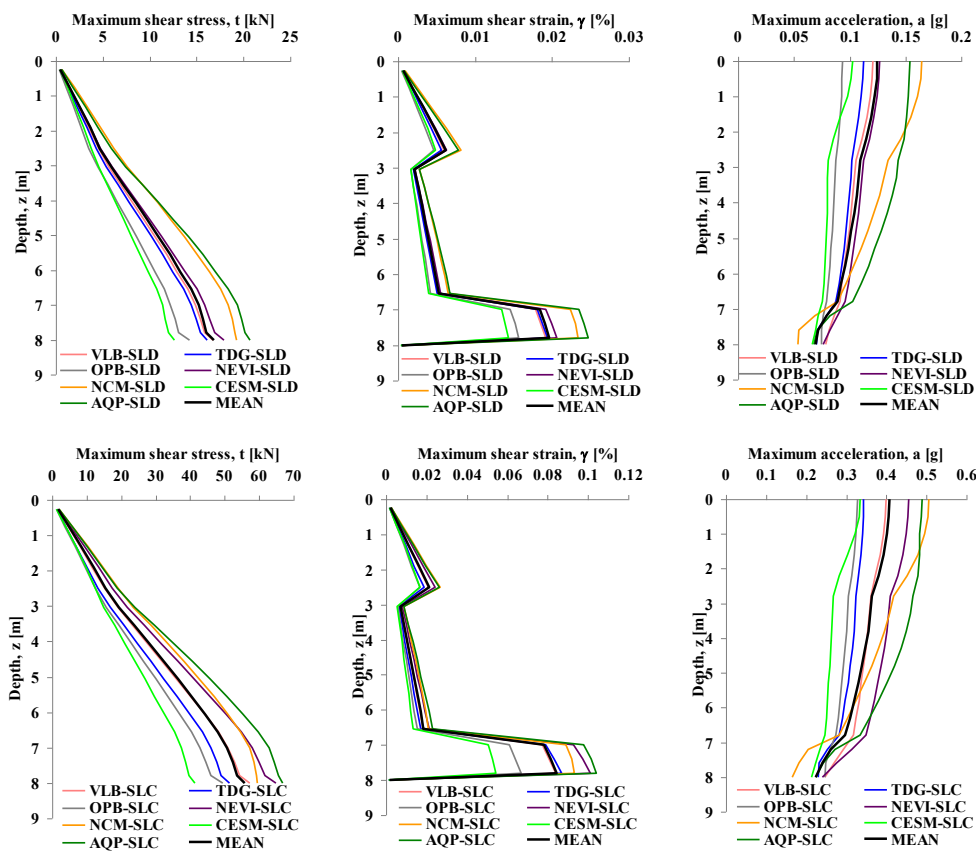


Figure 7.11 – Comparison between  $a_{max}$ ,  $\tau_{max}$ ,  $\gamma_{max}$  profiles for Case 0: SLD-SLC



In Figure 7.11 is possible to see that the relative behaviour between the different accelerometric input is the same in both limit states: the only difference is the amplitude of plotted parameters that for SLC is three times the values achieved in the SLD.

The same comparison is shown in terms of response spectra in Figure 7.12

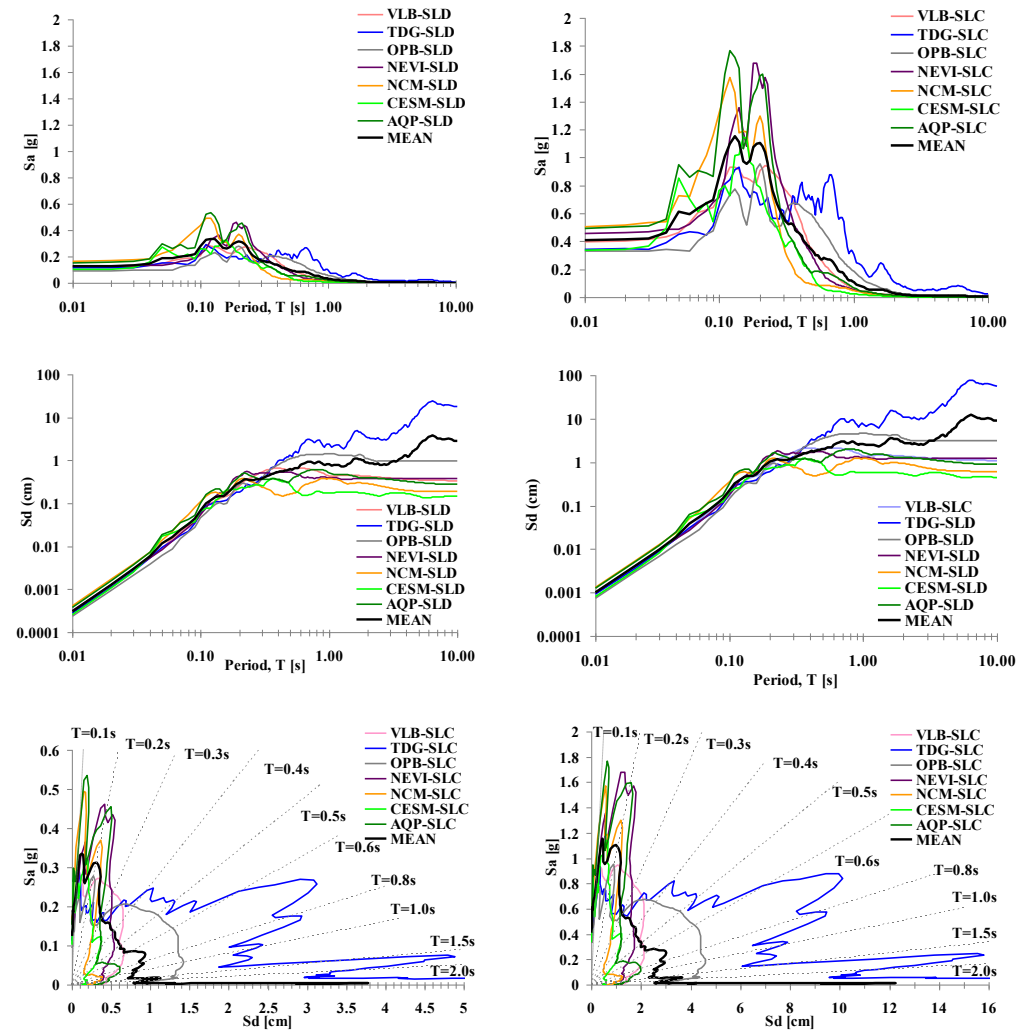


Figure 7.12 – Comparison between  $S_a(T)$ ;  $S_d(T)$ ,  $S_a(S_d(T))$  for Case 0: SLD-SLC

The considerations made for Figure 7.11 may recur even with regard to Figure 7.12. It is noted, however that the behavior in terms of spectral acceleration is similar for all selected events, while in terms of displacements the records corresponding to the high magnitude event ( $M=7$ ) (TDG and OPB) show significantly different behavior with displacements of size an order higher than the other signs of low magnitude ( $M = 4$ ).

Following Figure 13 show the amplification function of the deposit (Bedrock.free surface) and those partial related to each layer: the first is obtained from the product of the second.

It's evident that each layer amplifies differently: each will have one or more peaks of different amplitude and at different frequencies. The amplification function of each layer is also connected to the impedance ratio with the adjacent layers, so modify the characteristics of only one layer also means modifying the amplification functions of other layers and consequently that deposit.

Note also that the top layer has an amplification function almost constant throughout the frequency range and equal to unity, meaning that this layer does not contribute to the amplification of the earthquake. This is due to the unit value of impedance ratio of this layer with respect to the underlying layer 2 as well as the relatively thin layer ( $1\div1.8\text{m}$ ).

Conversely, in the intermediate layers 2 and 3, for the same reasons you look at the higher peaks of amplification: the layers are thicker ( $1.8\div4\text{m}$ ) and the impedance ratio with the adjacent layers is very different from the unity.

The two columns show the amplification functions relative to the input corresponding to two examined limit states (SLD, SLC): by comparison is seen as increasing the amplitude of the seismic input, the behaviour, essentially, remains the same, although more stress amplitude (SLC) will notice a slight difference between the amplification functions related to different records. This variation is undoubtedly related to the nonlinearity of the medium which involves  $G$  values corresponding to different strain values  $\gamma$  induced by the different input signals.

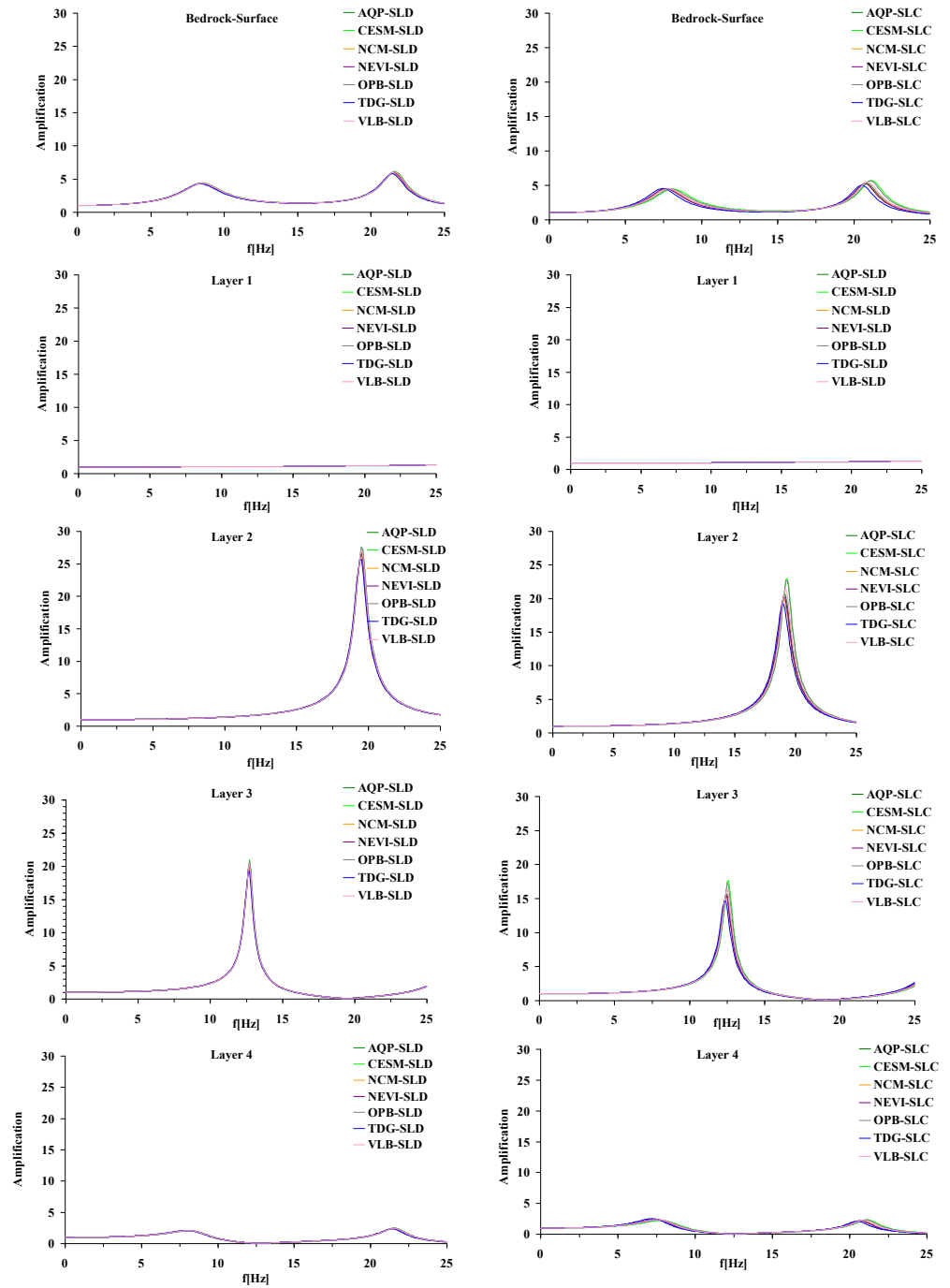


Figure 7.13 – Comparison  $A(f)$  for each layer in Case 0: SLD-SLC

### 7.6.2 Treated soil cases

For each case of treated soil the results are expressed as mean values of the seven input accelerograms applied.

In Figure 7.14-Figure 7.15, we compared the profiles of variation of maximum acceleration with depth in relation to each case for SLD and SLC: in the first row charts show the comparison for different values of  $E_v$  (1- $E_v=0.5$ , 2- $E_v=1.4$  and 3- $E_v=3$ ) with the same treated layer (A-layer 1, B-layer 2 or C-layer 4), in the second row profiles are compared respect the same  $E_v$  value varying the treated layer.

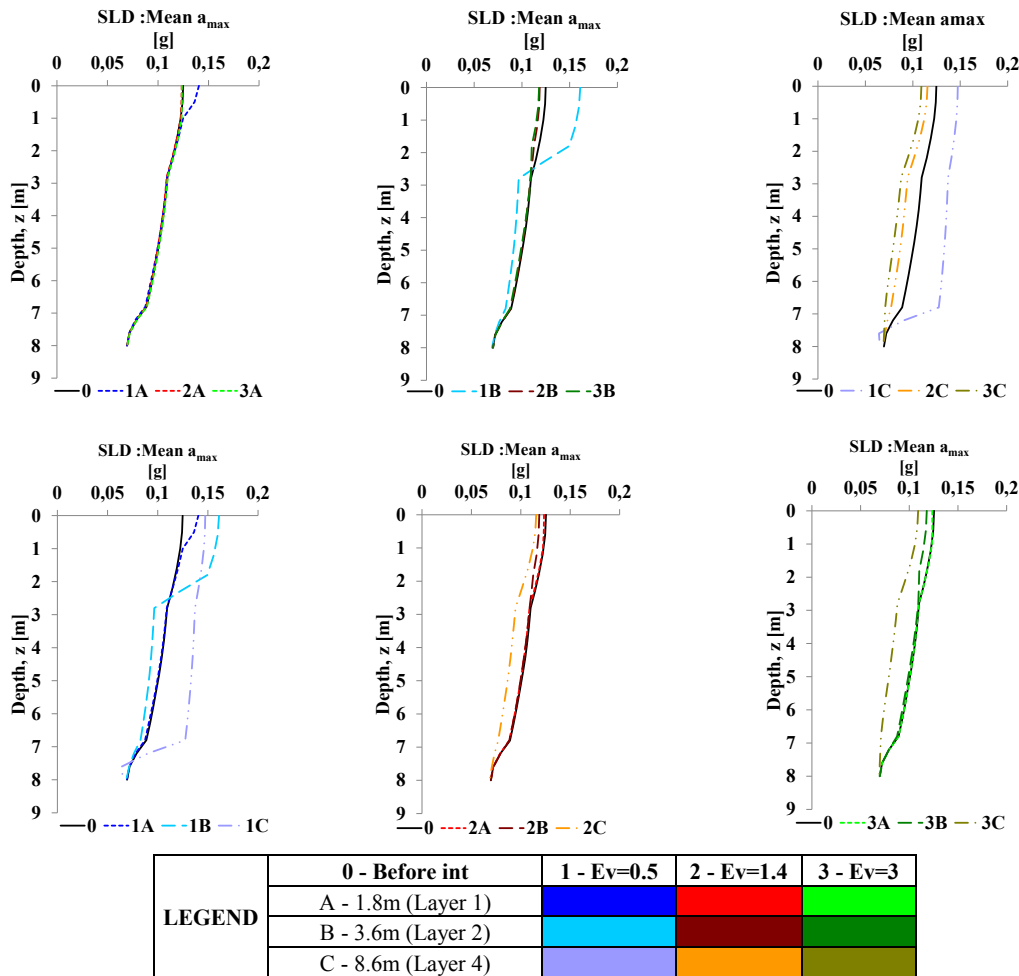


Figure 7.14 – Comparison of 9 analyzed cases:  $a_{max}(z)$  profile (SLD)

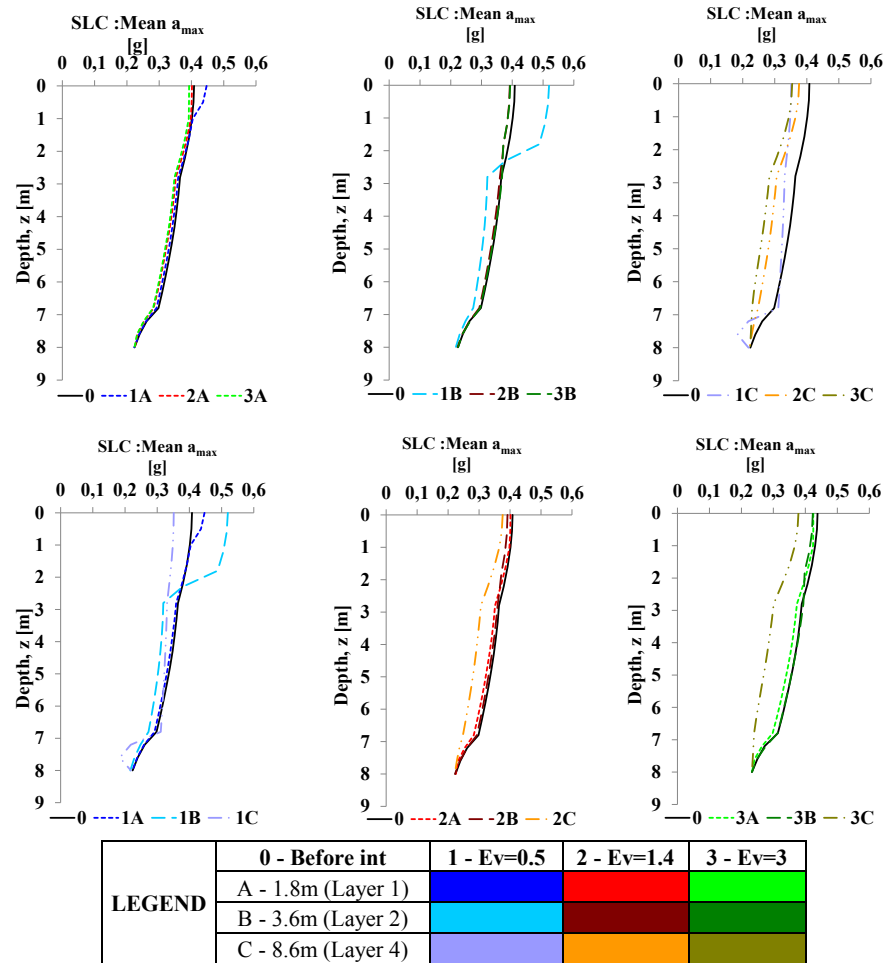


Figure 7.15 – Comparison of 9 analyzed cases:  $a_{max}(z)$  profile (SLC)

Comparisons above shown can be observed as in a surface treatment (Case A-Layer 1), stiffening the soil (CASE 2-3  $Ev > 1$ ) don't get any appreciable benefit in terms of reducing surface maximum acceleration compared to the reference case without treatment, while in the case of a reduction in stiffness (case 1  $Ev = 0.5$ ) is the intervention, although only slightly, even pejorative response surface. It should be remembered that this type of intervention could also result in problems from the static point of view, increasing the failure of the structure above.

When the intervention is performed deeper, layer 2 (Case B) and in layer 4 (case C) the difference in behaviour between an increase and a reduction in stiffness is even more pronounced. We note, again, that treatments increasing the stiffness of the layer treated does not reduce the surface amplification proportionally to the increase, or significant difference are obtained by applying the treatment to a layer or another. From this it is stated that, in the case study, stiffening above a certain value or beyond a certain depth would be an economic burden not justified by a greater benefit. It is, finally, to note that in the layers treated with the effect of reducing the stiffness we observe a "displacement", ie a sudden increase of accelerations, corresponding to an increase in shear strain  $\gamma$ . (Figure 7.16)

Increasing the amplitude of the input seismic, ie passing from SLD to SLC, we see essentially the same situation with the exception of the case 1C which is now the intervention of most benefit: lower maximum acceleration at the surface and no filler material stiffening. The explanation for this is related to the nonlinear behaviour of the soil, which implies that increasing the  $g$  value we have a shear modulus value  $G$  reduction, but contemporary the increase of the damping  $D$ : amplifying actions the nonlinearity effect became relevant than measures of SLD where the soil reached values of  $\gamma < 0.2$  SLC to the size of strain is 5 times higher. (Figure 7.17)

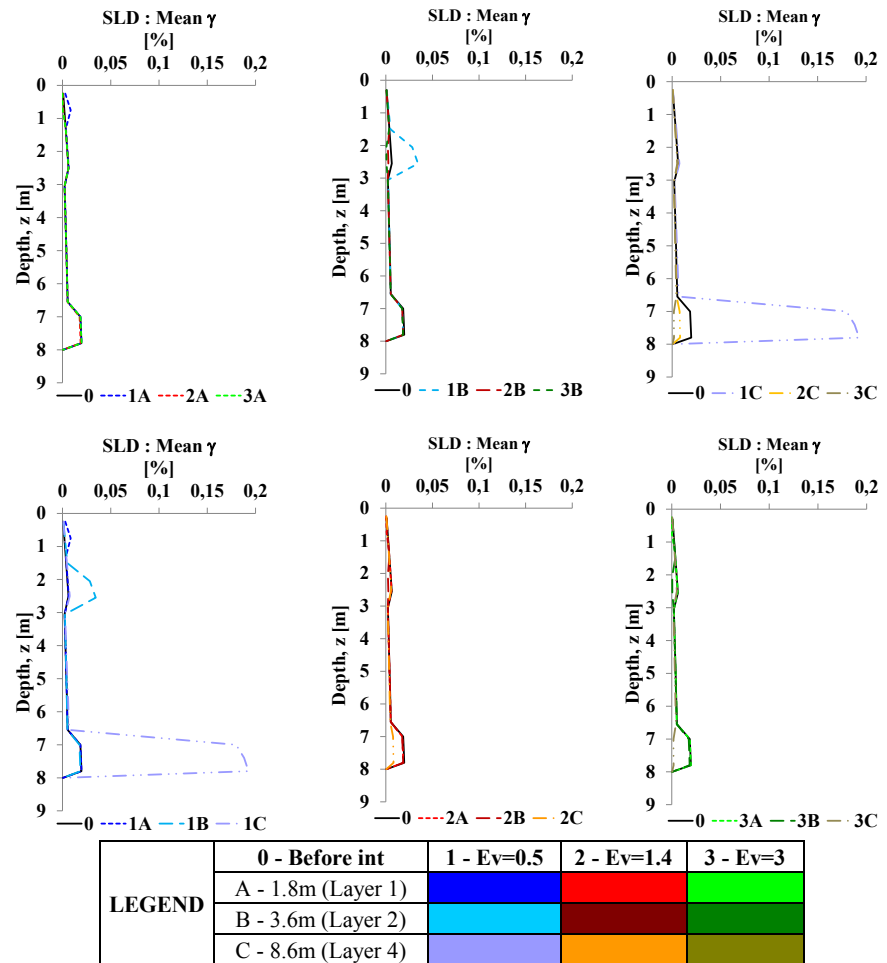


Figure 7.16 – Comparison of 9 analyzed cases:  $\gamma_{max}(z)$  profile (SLD)

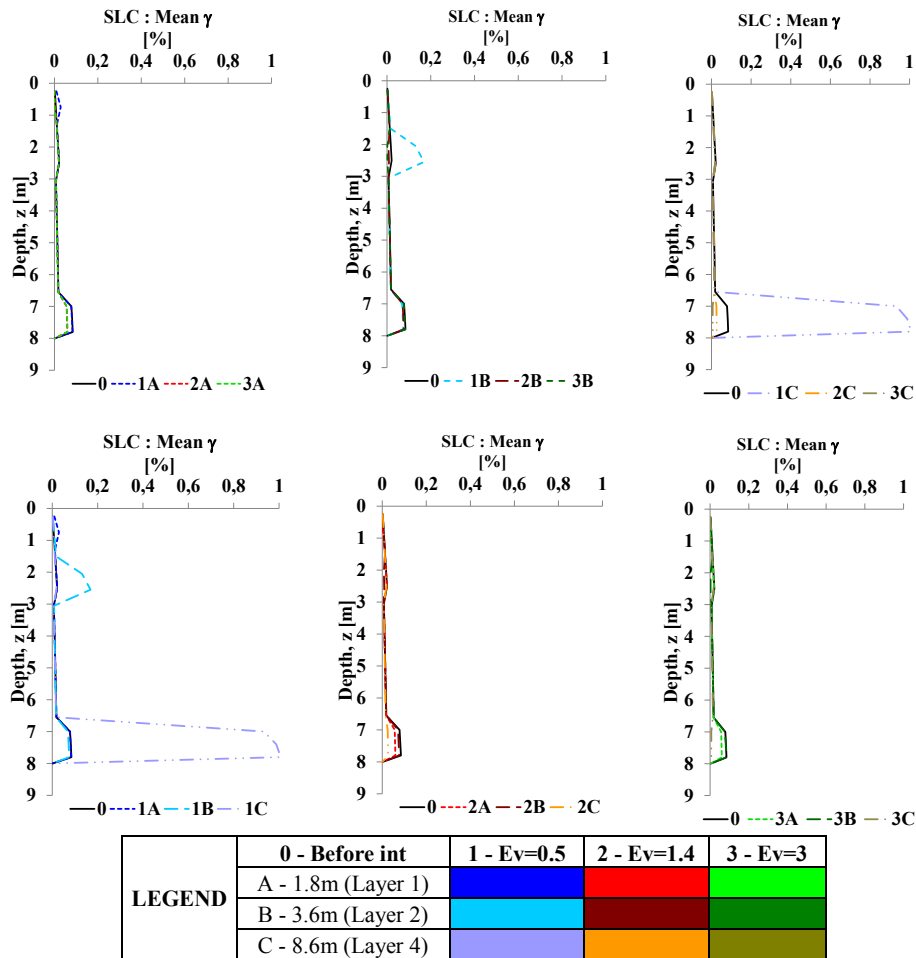


Figure 7.17 – Comparison of 9 analyzed cases:  $\gamma_{\max}(z)$  profile (SLC)

The following Figure 7.18-Figure 7.21 show the comparisons in terms of acceleration  $S_a(T)$  and displacement  $S_d(T)$  response spectra. From acceleration spectra  $S_a(T)$  confirms what has already highlighted in the comparison of profiles  $a_{\max}(z)$ , for actions of service (SLD) the maximum acceleration peaks are obtained for interventions reducing the stiffness ( $1-E_v=0.5$ ). In such cases, we note that the peak increases deepening the treated layer and simultaneously moves toward higher values of period remaining in the range (0.1-0.5s).



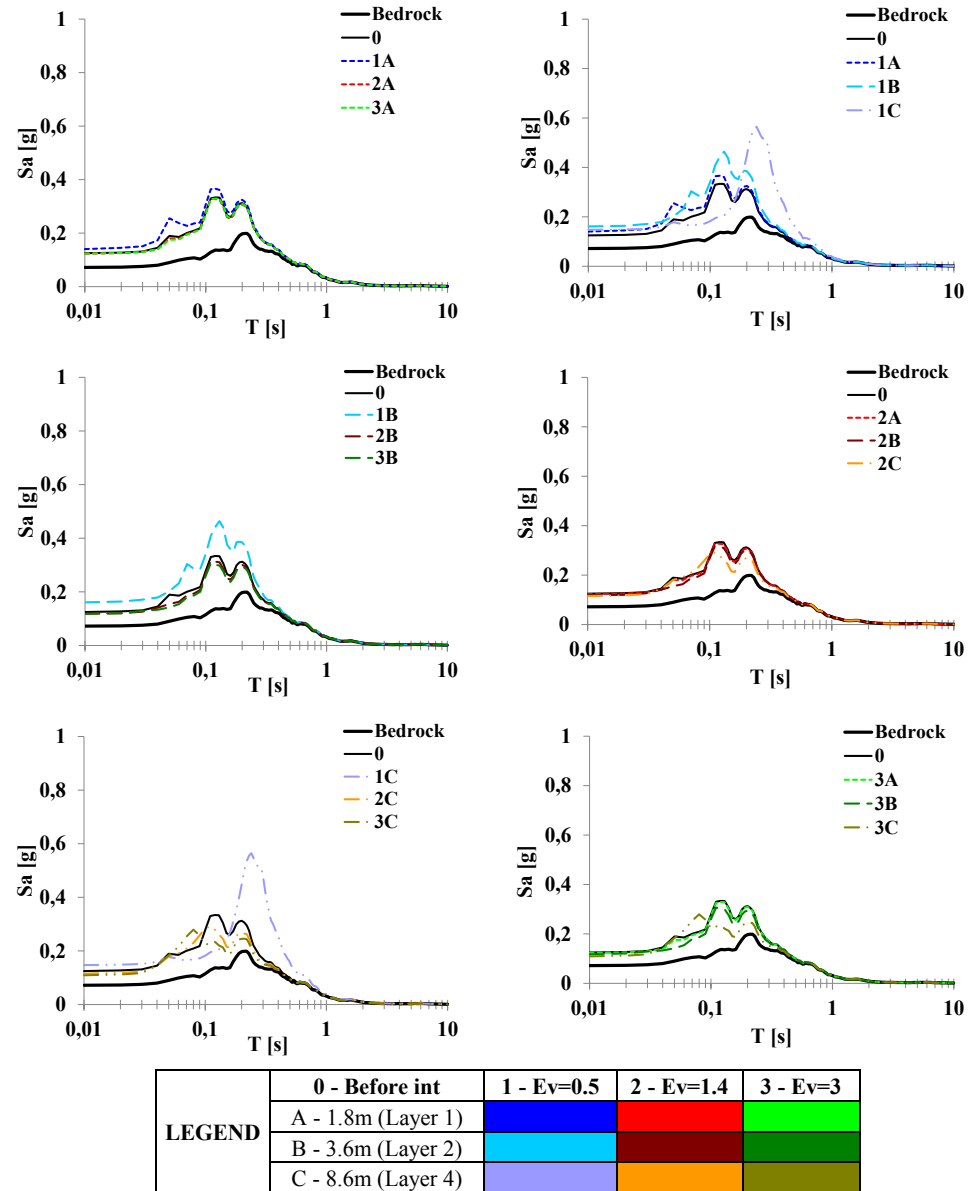


Figure 7.18 – Comparison of 9 analyzed cases:  $S_a(T)$  (SLD)

Collapse action (SLC) will once again have the situation highlighted by the comparisons of other parameters: the maximum reduction in acceleration is achieved by intervening in the deeper layer (C-Layer 4).

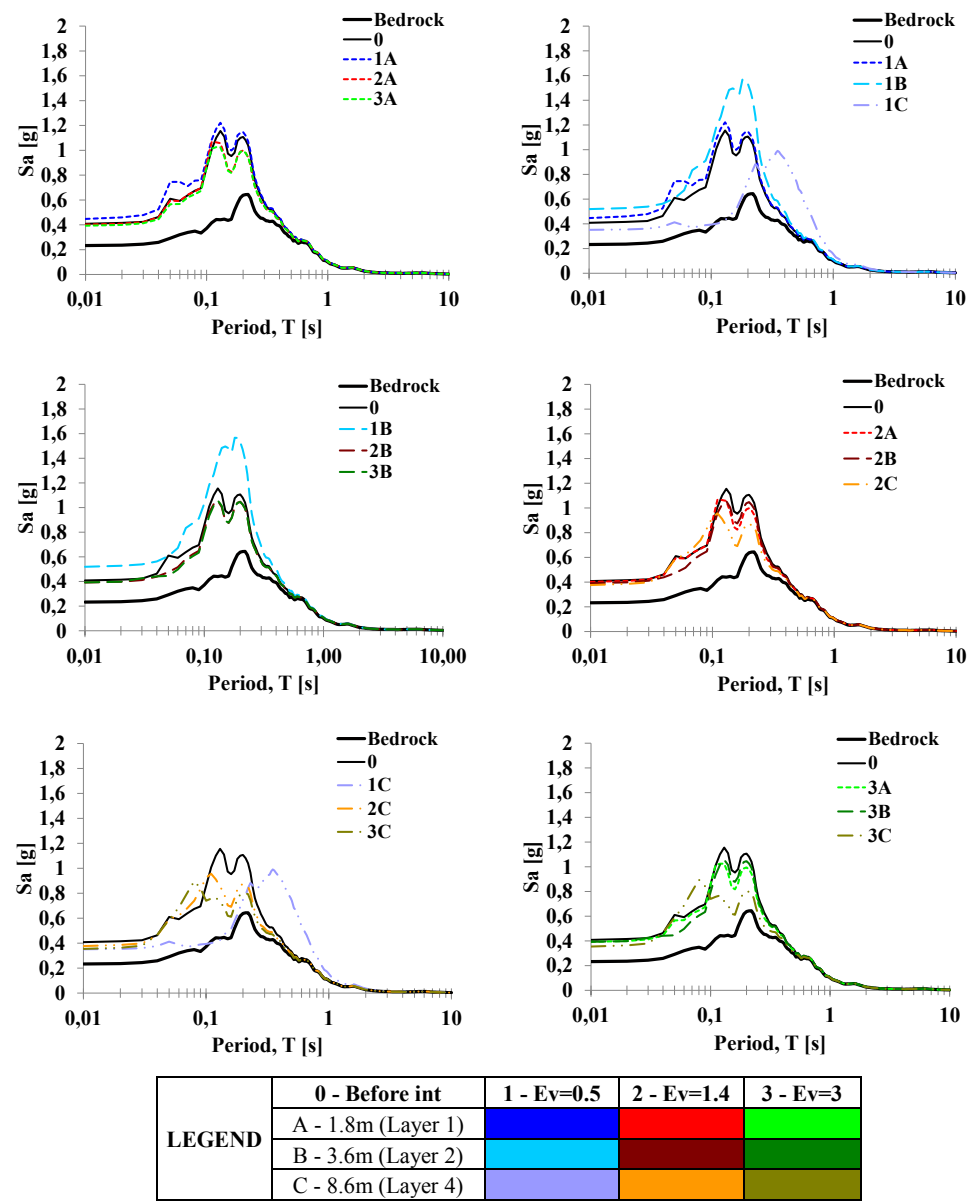


Figure 7.19 – Comparison of 9 analyzed cases: $S_d(T)$  (SLC)

In terms of spectral displacement  $S_d(T)$  the only case which shows some significant variation is 1C ( $E_v=0.5$ -layer 4), for which  $S_d(T)$  increase in all range of periods (0-2s) and comes to triple in some cases ( $T=0.3s$ ).

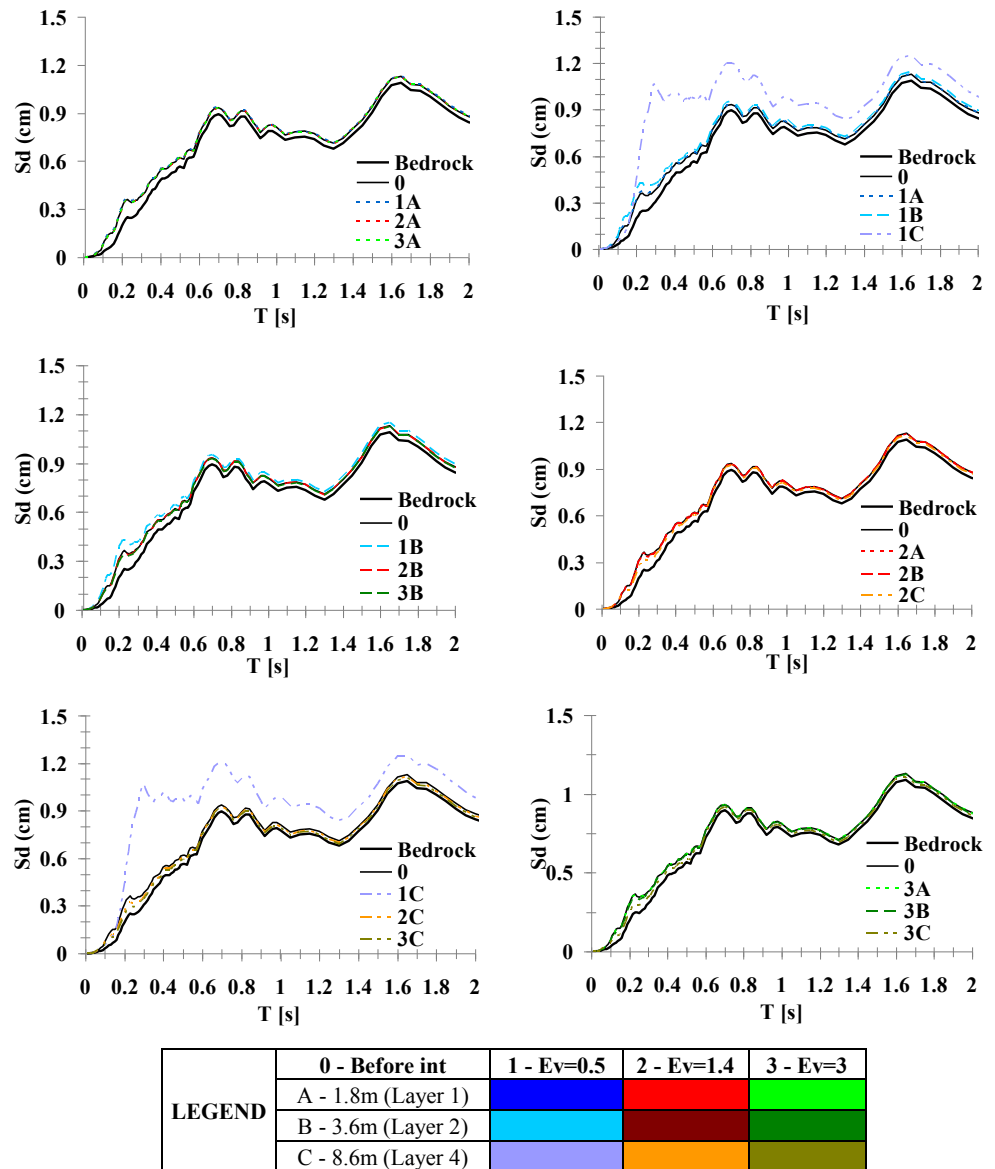


Figure 7.20 – Comparison of 9 analyzed cases:  $S_d(T)$  (SLD)

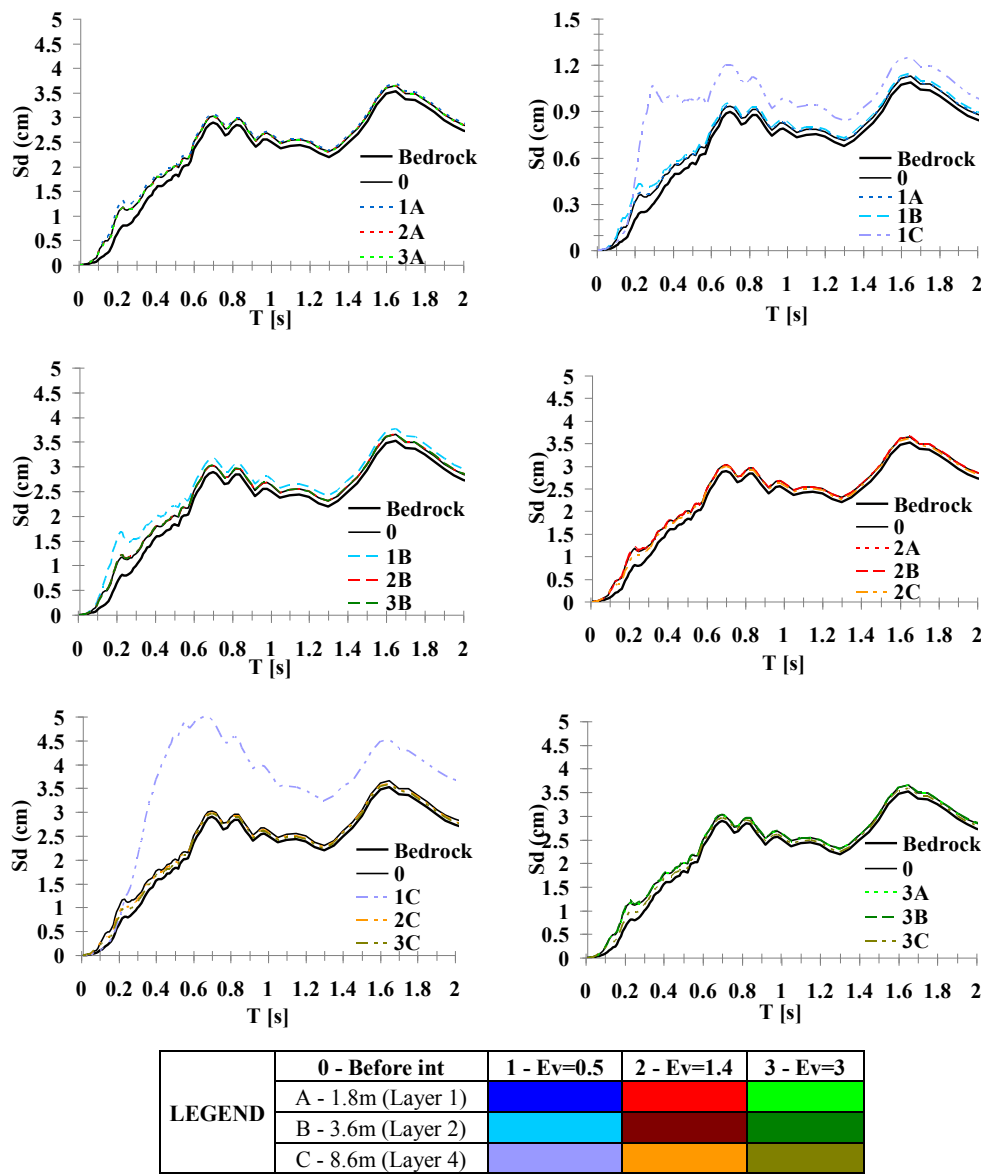


Figure 7.21 – Comparison of 9 analyzed cases: $S_d(T)$  (SLC)

Finally, composing the information obtained from  $S_a(T)$  and  $S_d(T)$  we obtain the diagrams of Fig 22-23, from which you can simply check as the same case of treatment for a certain period, may be the most worse in the terms of  $S_a$  but not in terms of  $S_d$ : from the graphs you can find the period or

range of periods for which different treatments are more convenient.

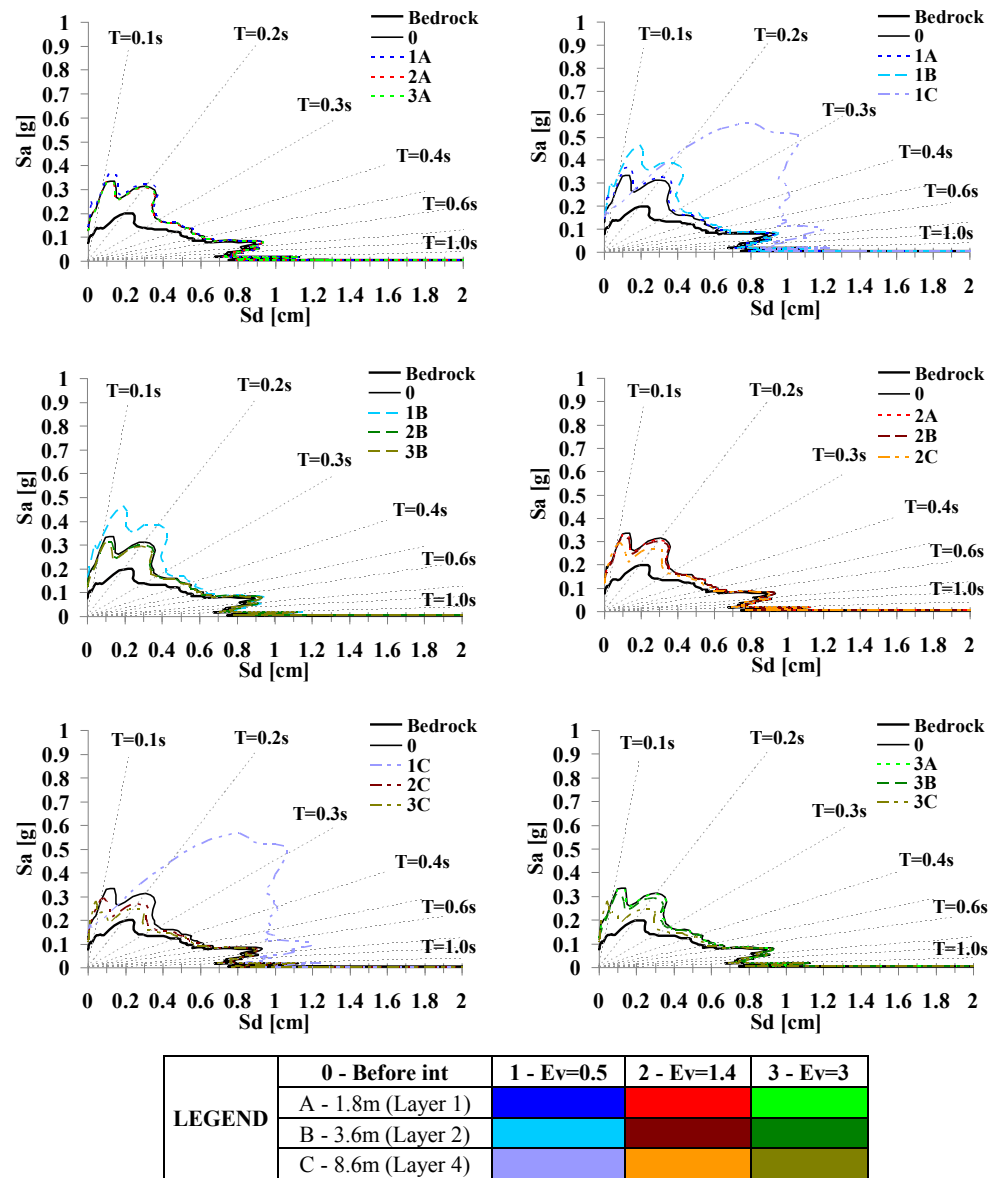


Figure 7.22 – Comparison of 9 analyzed cases:  $S_a[S_d(T)]$  (SLD)

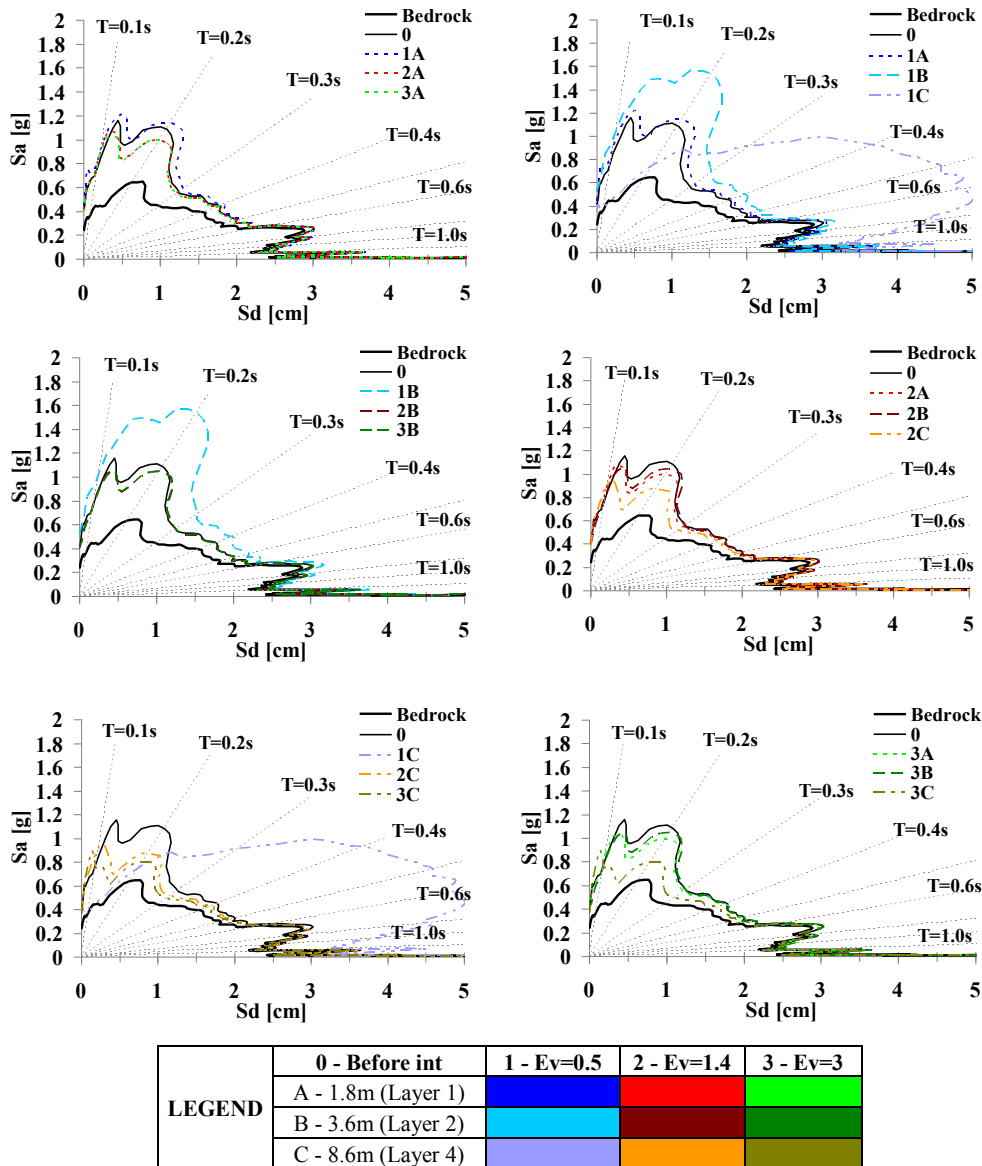


Figure 7.23 – Comparison of 9 analyzed cases:  $S_a[S_d(T)]$  (SLC)

The figures 7.24-7.26 compare the amplification functions in each treated layer (Case A-layer 1; B-layer 2 or C-layer 4) for different  $E_V$  values (1- $E_V=0.5$ ; 2- $E_V=1.4$  and  $E_V=3$ ). In each figure were marked in red graphs corresponding to the treated layer.

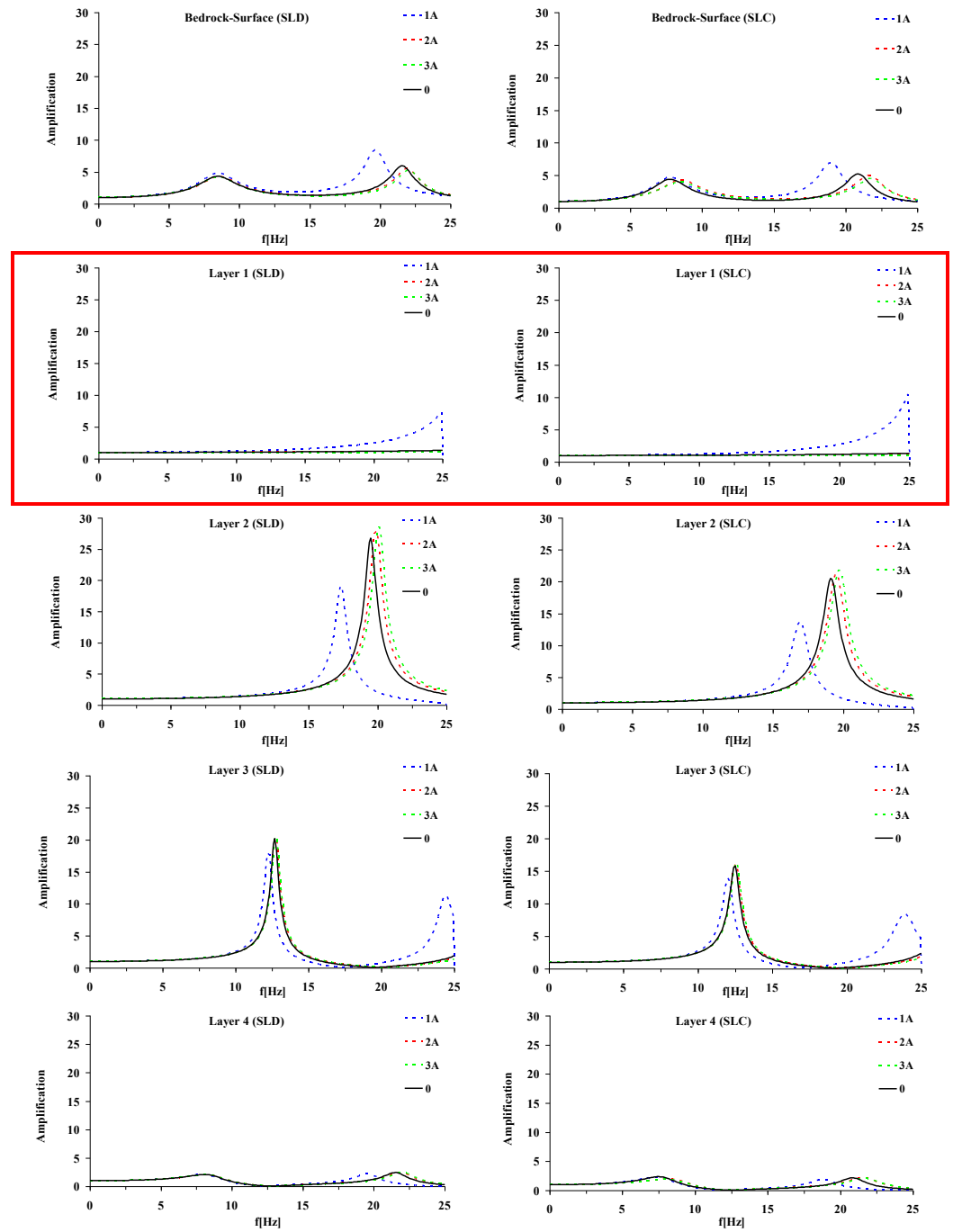


Figure 7.24 – Comparison of mean  $A(f)$  for each layer for different  $E_V$  Case A: SLD-SLC

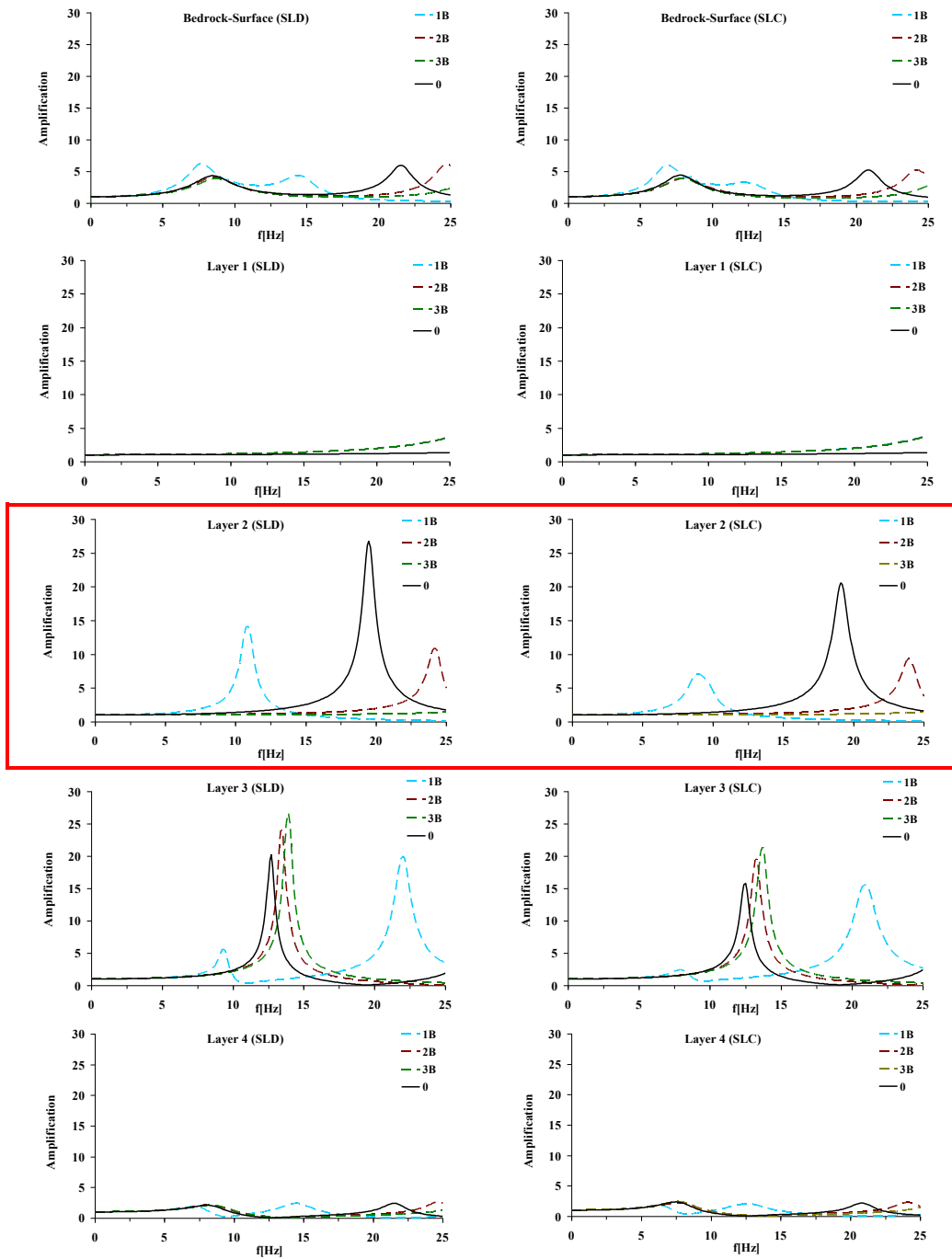


Figure 7.25 – Comparison of mean  $A(f)$  for each layer for different  $E_V$  Case B: SLD-SLC



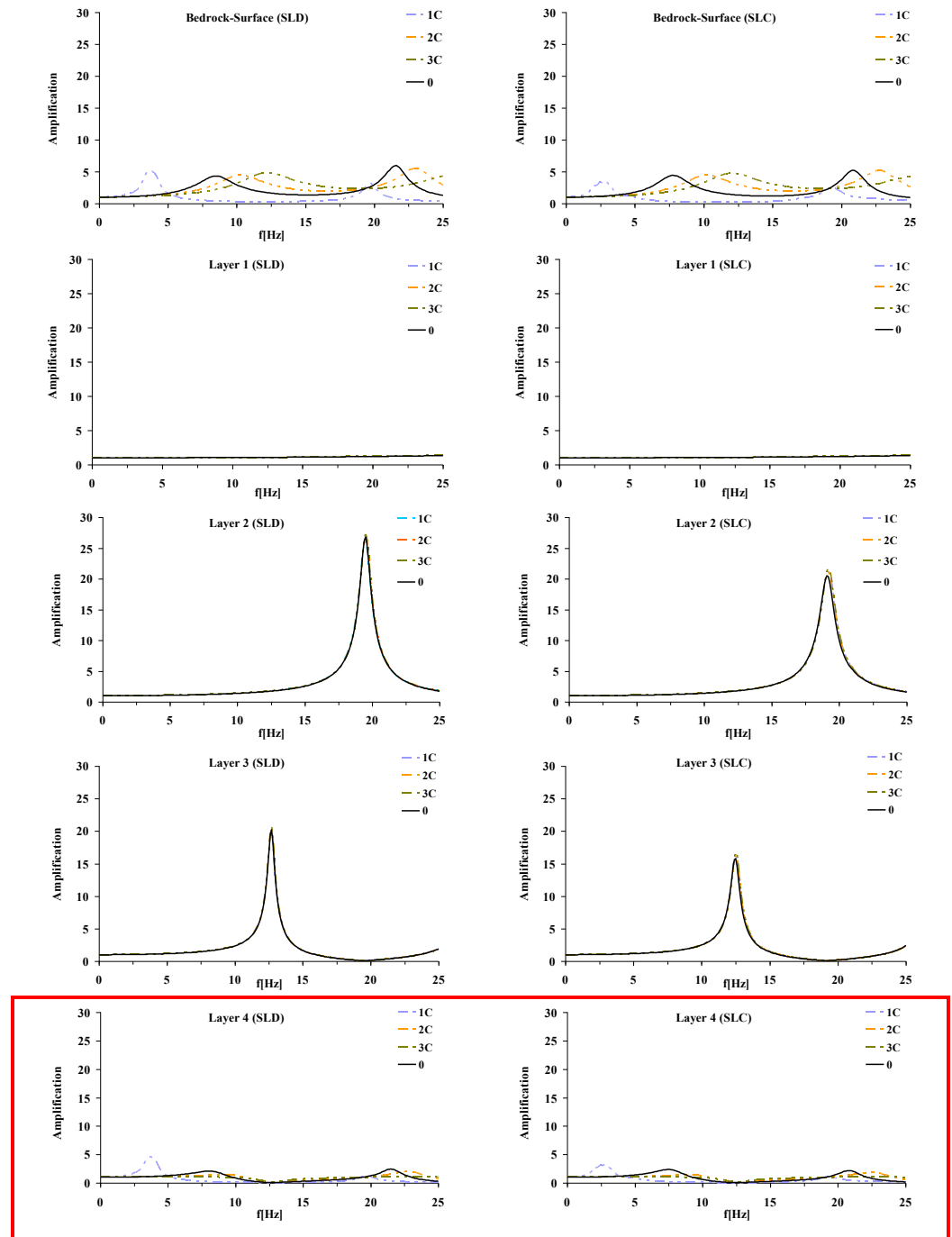


Figure 7.26 – Comparison of mean  $A(f)$  for each layer for different  $E_V$  Case C: SLD-SLC

For the case A corresponding to the treatment of the surface layer (layer 1) (Figura 7.24) can be deduced that the reduction of stiffness ( $1-E_v=0.5$ ), raising and moving toward lower frequencies, the peak of amplification connected to the second mode of vibration of the deposit, leaving unchanged the fundamental peak of amplification. An increase in stiffness ( $2-E_v=1.4$ ;  $3-E_v=3$ ), however, have no effect on amplification function.

For treatments in the layer 2 (case B) (figura 7.25) we see that reducing the stiffness the amplification peaks of different layers coming near and this would lead to significant amplification at the surface when arrived to overlap. We note, also, that the fundamental amplification peak increases and moves to the lower frequencies. Stiffening layer, however, once again you do not get appreciable changes in the surface compared to the reference case 0.

Finally, for the case C (treated Layer 4) (Figura 7.26) reducing the stiffness the peak frequency continues to decline, but in this case it also reduces the value of the amplitude. In particular, we wish to emphasize that only in this case (1C), the amplification function varies significantly in relation to the accelerogram input and the corresponding to seismic event characteristics. (figura 7.27)

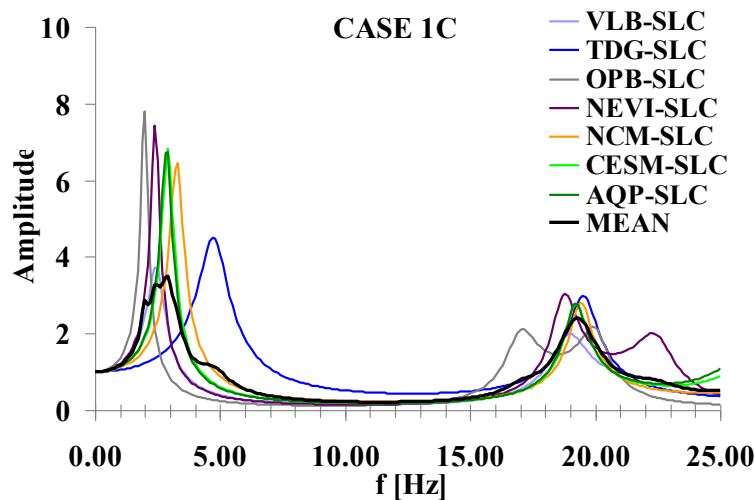


Figure 7.27 –  $A(f)$  for different seismic events SLC for case 1C ( $E_v=0.5$ -treated layer 4)

Reason of this difference is related, once again, the nonlinear behaviour of the soil, involving different strains for different input and consequently different values of stiffness  $G$  and damping  $D$ . (Figura 7.28)

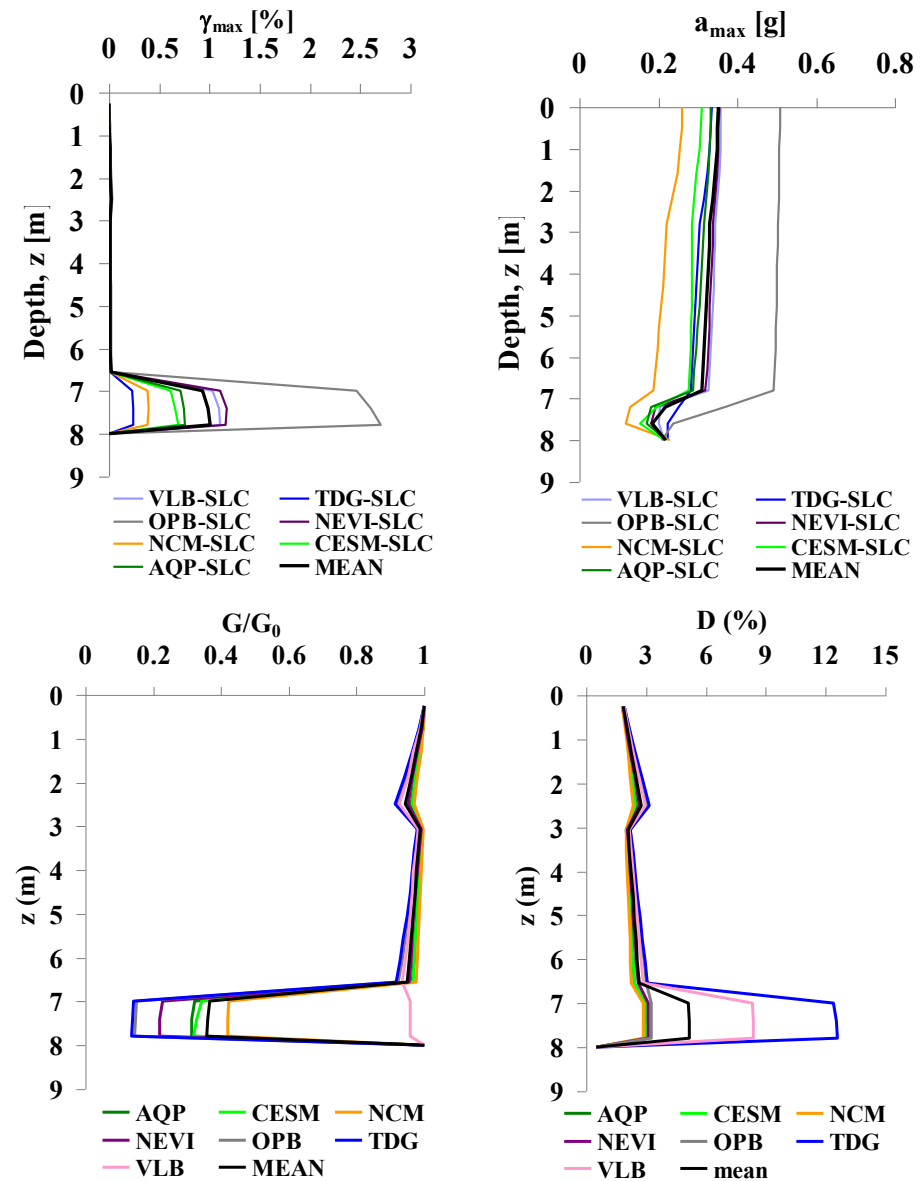


Figure 7.28 – Comparison of mean  $A(f)$  for different treated layer  $E_v=0.5$ : SLD-SLC

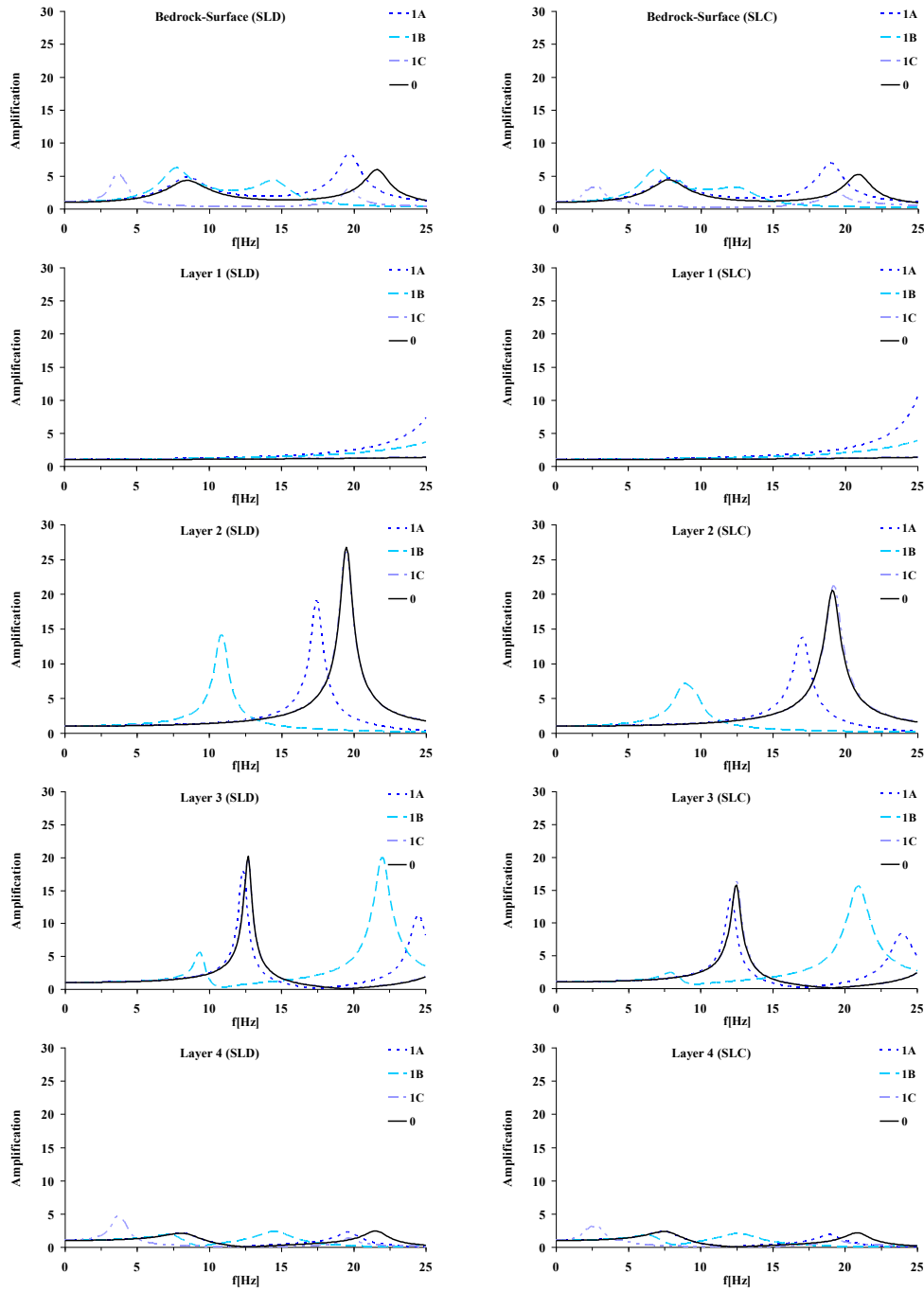


Figure 7.29 – Comparison of mean  $A(f)$  for different treated layer  $E_v=0.5$ : SLD-SLC

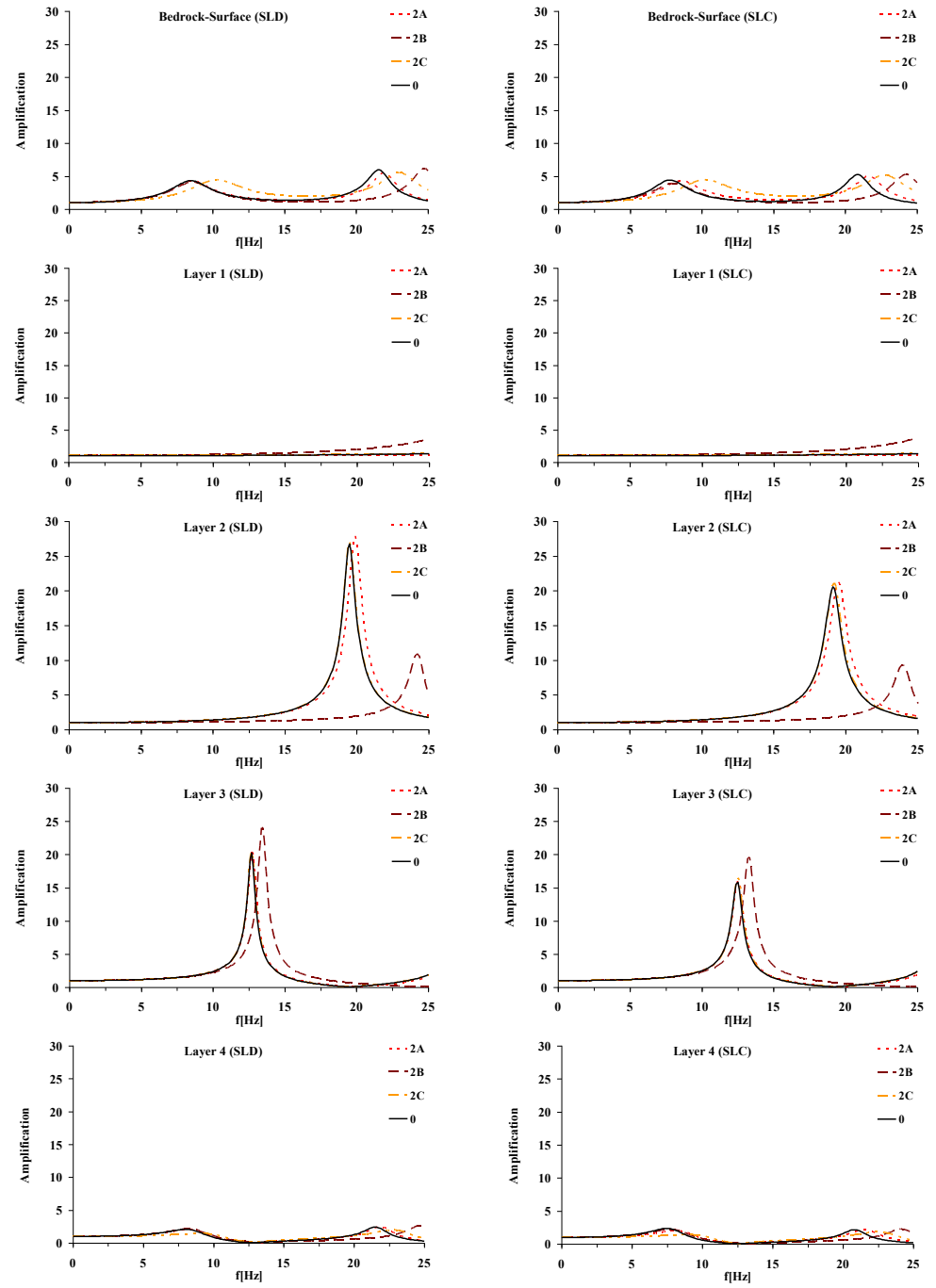


Figure 7.30 – Comparison of mean  $A(f)$  for different treated layer  $E_V=1.4$ : SLD-SLC

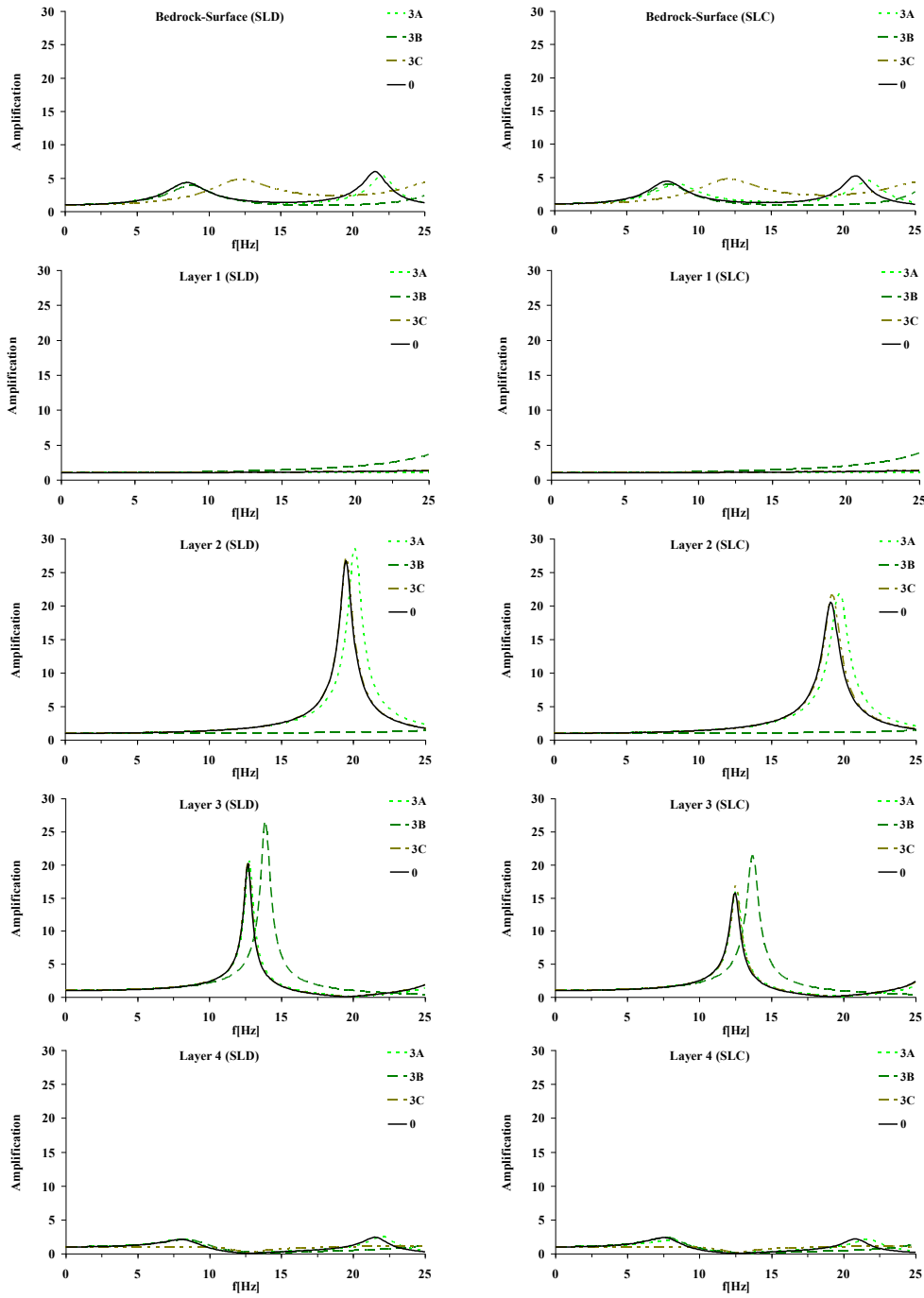


Figure 7.31 – Comparison of mean  $A(f)$  for different treated layer  $E_V=3$ : SLD-SLC

The graphs shown in Figure 7:29 to 7:31, compare cases of equal treatment to different layers. For  $E_v = 0.5$  (case 1) minor amplification is obtained by treatment in deeper layers (layer 4), for values of  $E_v = 1.4$  and  $E_v = 3$ , in which the layer stiffness after treatment increases the amplitude peaks remains unchanged, but moves to higher frequencies.

The numerical value of amplitude and frequency (A,f) corresponding the fundamental vibration mode of the deposit, for different cases ere reported in table 4-5.

Table 7.4 - Numerical value of amplification peak for different cases(SLD)

Intervention	1 - $E_v=0.5$			2 - $E_v=1.4$			3 - $E_v=3$		
	f [Hz]	T [s]	A -	F [Hz]	T [s]	A -	f [Hz]	T [s]	A -
<b>0 - Senza int</b>	8.50	0.12	4.32	8.50	0.12	4.32	8.50	0.12	4.32
<b>A - 1.8</b>	8.50	0.12	4.82	8.60	0.12	4.26	8.50	0.12	4.26
<b>B - 3.6</b>	7.70	0.13	6.19	8.70	0.11	4.03	8.70	0.11	3.86
<b>C - 8.6</b>	3.70	0.27	5.17	10.00	0.10	4.38	10.00	0.10	3.15

Table 7.5 - Numerical value of amplification peak for different cases(SLC)

Intervention	1 - $E_v=0.5$			2 - $E_v=1.4$			3 - $E_v=3$		
	f [Hz]	T [s]	A -	F [Hz]	T [s]	A -	f [Hz]	T [s]	A -
<b>0 - Senza int</b>	7.80	0.13	4.41	7.80	0.13	4.41	7.80	0.13	4.41
<b>A - 1.8</b>	7.80	0.13	4.69	8.60	0.12	4.27	8.50	0.12	3.99
<b>B - 3.6</b>	6.90	0.14	5.89	8.00	0.13	3.88	7.90	0.13	3.94
<b>C - 8.6</b>	2.90	0.34	3.50	10.00	0.10	4.39	10.00	0.10	3.25

This page is, intentionally, left blank



## BIBLIOGRAPHY

AGI (2005). Aspetti geotecnici della progettazione sismica, Linee guida AGI

Bardet JP, Ichii K, Lin CH (2000) EERA a Computer Program for Equivalent-linear Earthquake site Response Analyses of Layered Soil Deposits. Univ. of Southern California

Idriss, I. M. and Sun, J. I. (1992). User's Manual for SHAKE91, Center for Geotechnical Modeling, Department of Civil Engineering, University of California, Davis.

Kuhlmeyer R.L, Lysmer J. (1973). Finite Element Method Accuracy for Wave Propagation Problems, *Journal of the Soil Mechanics and Foundation Division*, 99 n.5, pp. 421-427

Lanzano G. (2008). Physical and analytical modelling of tunnels under dynamic loadings, PhD dissertation, Università di Napoli Federico II

Lanzo G., Silvestri F. (1999). Risposta sismica locale – Teoria ed esperienze. *Hevelius edizioni*.

Lanzo G. (2005), Soluzioni analitiche approssimate per il calcolo del moto sismico in superficie, Aspetti geotecnici della progettazione sismica, Linee guida AGI

Papa V., Silvestri F., Vinale F., (1988). Analisi delle proprietà di un tipico terreno piroclastico mediante prove dinamiche di taglio semplice. I Convegno GNCSIG. Monselice (PD).

Ramberg W., Osgood W. R. (1943). Description of stress-strain curves by three parameters. Technical Note No. 902, National Advisory Committee For Aeronautics, Washington DC

Sanò T. (2008). Le Analisi Numeriche per la Valutazione della Risposta Sismica Locale. SERM-SEismic Risk Management, Università degli Studi di Udine

Seed H.B., Idriss I.M. (1970). Soil moduli and damping factors for dynamic response analysis. Report No. EERC70-10, Earthquake Engineering Research Center, Univ. of California, Berkeley, (California)

Schnabel, P. B., Lysmer, J., and Seed, H. B. (1972). SHAKE: A Computer Program for Earthquake Response Analysis of Horizontally Layered Sites, *Report No. UCB/EERC-72/12*, Earthquake Engineering Research Center, University of California, Berkeley, December, 102p.

Silvestri F. (1991). Analisi del comportamento dei terreni naturali in prove cicliche e dinamiche di taglio torsionale. PhD dissertation. Università di Napoli Federico II

---

## *Chapter 8*

# Study case: house of mosaics in Villa Favorita sea park

## **8.1 INTRODUCTION**

This chapter presents the historical and monumental building under study: the Palazzina of the mosaics.

The first part is devoted to the historical and territorial context in which the same fits. And It's led, then, a rapid excursus of the architectural characteristics and styles of the time, found within the complex of villas of which the building is a part.

We move, then, to a more detailed historical description of the park where the Palazzina is located and to the architectural, dimensional and structural description of Palazzina under consideration. For this purpose, a detailed geometric and photographic survey are carrier out on the palazzina. Subsequently, a thorough investigation of the works carried out over the decades on the structure, was conducted; thanks to the content made available from the Ente per le Ville Vesuviane archive. Finally, with the information previously obtained, an inspection conducted on the building showed, in an expeditious way, what might be its criticality.

The knowledge of the building, reached in this chapter is the basis on which, in chapter 9, will made the modelling and analysis of its seismic vulnerability.

## 8.2 HISTORICAL BACKGROUND: GOLDEN MILE VILLAS

With the resurgence of the independent Kingdom of Naples and the designation of the city as the capital, the Sovereign Court, following the impetus that the construction of Versailles by Louis XIV had spread throughout Europe, built places princely resort and recreational. The king of Naples Charles III of Borbone (1734-1759) in Naples could not find an adequate royal palace so he and his consort Princess Maria Amalia of Saxony, favourably impressed with the area of Portici when they visited the villa of Emmanuel Maurice d'Elbeuf, the Duke of Elbeuf there in 1738 ordered the construction of a palace in Portici that would act, not only as a private residence, but as a place to receive foreign officials travelling to the kingdom.

The new royal palace stimulated the construction of numerous other holiday residences in the neighborhood, 122 of which are now known as the Vesuvian Villas, as the palace was not large enough to accommodate the entire court.

Therefore during the course of the eighteenth century, despite the continuous eruptions, many villas were built and others were restored, transforming the area into a place rich in architectural and historical heritage (Alterio et al. 2010). Consequently the main road that connects Naples to Torre Annunziata (also called road of Calabrie) was called "Golden Mile", because, along the director, the Neapolitan aristocracy built beautiful villas electing this area as a summer residence for proximity to the palace. (PA.CO. s.r.l. 1990-A1)

On the other hand, the Vesuvian coast home to the summer residences of two centuries before the construction of the royal palace of Portici induce the Neapolitan aristocracy to build villas near the sea palace of Charles of Bourbon. The Romans, in fact, with the construction of many suburban villas, showed their appreciation for the landscape of that area, the goodness of the climate and the proximity to the sea that facilitated trade and commerce (PA.CO. s.r.l. 1990-A1).

In Roman times there is, therefore, a real process of agricultural colonization that wins the slopes of the volcano and goes into the northern side. The lava flow generated by the eruption of Vesuvius in 79 A.D. was transformed over the centuries in which a forest cover, covering the slopes of

the mountain to the coast, was kept intact until the eruption of 1631. Later it was slowly transformed into arable land by a more modern agricultural colonization closely related to the birth and flowering of many suburban residences. In these houses appear spacious lodges, courtyards for the carriages, the main floor features a refined furniture and decorations outside the strict sixteenth century residences. (Cardarelli et al.)

Was treated differently, however, the northern slope free from eruptions whose lava flows were directed mainly towards the sea, through the obstacle consists of a set sum. There were formed new villages including San Nastagio (now St. Anastasia) Pollenatrocchia, and other less consistency.

The villas built along the slopes of Vesuvius differ from those located on the coast, as rustic homes linked to the cultivation of agricultural land. Unlike traditional elegance of the "ville di delizia ", these are farms, villas, retreats more than places to stay mundane, in which prevails a function of production, which results mainly in the cultivation of fruit, wine and silk, favored by Vesuvius very fertile country.

These villas are real farms, home of country squires, arranged so that the main house has a view of the bay and one on the mountain, thanks to the opening of windows, lodges and terraces.

A typical feature of such buildings is the rustic courtyard around which are distributed to other buildings: the main, willing to multi-story and wanted by the architectural point of view, the secondary one, formed by the service areas and storage of food and agricultural tools from stables from the homes of servitude, sometimes topped by a panoramic terrace connected to the master, and finally the rustic courtyard, access channel for the home. In some cases, these villas were accompanied by a green area used as a fenced garden, which communicated with the court.

The Vesuvian area and in particular the coastal strip was therefore chosen as the privileged place of residence of the nobility and magnificence of court life, providing its villas scattered, also from a functional standpoint, a beautiful setting in which no permanent residence but only for short periods.

The various building typologies, in fact, don't show any privacy but at the contrary they have a direct facing on a large course, designed and widespread during the Baroque era for the movement of the carriages for pleasure. This reflects an overlooking conception of the whole outer life in the villa. Another facing, toward the mountains or the sea, was realized through open doorways, usually leaning over huge gardens and sea landings (PA.CO. s.r.l., 1990-A1)

### 8.3 TERRITORIAL DISTRIBUTION OF THE VILLAS

Figure 8.1 and the Table 5.1-8.6 shows the spatial distribution of the villas in the Vesuvian town.



Figure 8.1- 8The localization of the Golden Mile villas in Vesuvian Area. (Alterio et al. 2010)

Table 8.18 - The 19 villas located in Torre del Greco

Villa Cardinale	Villa Maria	Villa Prota	Villa Fienga
Villa Solimena	Villa Ercole	Villa Guerra	Villa Ginestre
Villa San Gennariello	Villa Macrina	Palazzo Petrella	Villa Mennella
Palazzo del Salvatore	Villa Caramiello	Palazzo Chicchella	Villa Vallelonga
Masseria Donna Chiara	Villa Bruno Prota	Villa delle Ginestre	

*Table 8.2 - The 22 villas located in Ercolano*

Villa Arena	Palazzo Correale	Villa Lucia
Villa Favorita	Palazzo Tarascone	Villa Aprile
Villa Durante	Villa Mannes Rossi	Villa Passaro
Villa Campolieto	Villa Giulio de la Ville	Villa Ruggiero
Palazzo Capracotta	Villa Tosti di Valminuta	Villa Consiglio
Villa Vargas Macchucca	Villa Principe di Migliano	Villa De Liguroro
Villa Signorini (Via Roma)	Villa De Bisogno Casaluce	Palazzo Municipale
Villa Signorini (Corso Resina)		

*Table 8.3 - The 31 villas located in Portici*

Villa Nava	Villa Maltese	Villa Zelo	
Villa Starita	Villa d'Elboeuf	Villa Gallo	
Palazzo Valle	Villa Ragozzino	Villa Meola	
Palazzo di Fiore	Palazzo Evidente	Villa Emilia	
Esedra(ex Villa Buono)	Palazzo Amoretti	Villa Menna	
Palazzo Serra di Cassano	Collegio Landriani	Villa Aversa	
Palazzo Lauro Lancellotti	Palazzo Moscabruno	Villa Sorvillo	
Palazzo, Corso Garibaldi n.40	Palazzo Ruffo di Bagnara	Palazzo Reale	
Palazzo, Corso Garibaldi n.100	Palazzo, Corso Garibaldi n.28	Villa Mascolo	
Palazzo Capuano (ora Villa Materi)	Rudere in C.so Garibaldi n.316	Villa d'Amore	
Palazzo, Corso Garibaldi n.101/111			

*Table 8.4 - The 30 villas located in San Giorgio a Cremano*

Villa Bruno	Villa Jesu	Villa Marulli	
Villa Galante, via Pessina	Villa Carsana	Villa Leone	
Villa Giulia o De Marchi	Villa Menale	Villa Olimpia	
Villa Tufarelli di Sotto	Villa Bonocore	Villa Cerbone	
Villa Carafa Percuoco	Villa Tanucci	Villa Lignola	
Villa Caracciolo di Forino	Villa Marullier	Villa Sinicopri	
Villa Pignatelli di Montecalvo	Villa Borrelli	Villa Vannuchi	
Villa Galante, via Buozzi	Villa Pizzicato	Villa Salvatella	
Villa Giarrusso e Maria	Villa Righi	Villa Ummarino	
Villa Avallone ora Tufarelli	Villa Cosenza	Villa Zampaglione	

*Table 8.5 - The 9 villas located in Barra*

Villa Nasti ora Letizia	Villa Amalia	Villa Salvetti	
Villa Pignatelli di Monteleone	Palazzo Bisignano	Villa Filomena	
Villa Giuli o De Gregorio di Sant'Elia	Villa Spinelli di Scalea	Villa Sant'Anna	

*Table 8.6 - The 11 villas located in San Giovanni a Teduccio*

I Villa Volpicelli	Villa Vittoria	Villa Papa	Villa Faraone
Palazzo Procacciani	Villa Cristina	Villa Vignola	Villa Percuoco
Villa Raiola Scarinzi	Villa Paudice	II Villa Volpicelli	

## 8.4 FEATURES AND ARCHITECTURAL STYLES OF THE VILLAS

All eighteenth-century Vesuvian Villas have, despite the wide variety of architectural forms, aspects constant. These include the duplicity of the configuration on the front and back, ie that the adoption of a compact prospect on the road, aligned to the edge of the surrounding buildings, as if it were an urban building, a former town mansion or a palace, and On the contrary, the articulation of a prospect completely different, much more lively at the back, is where this second statement is articulated to the sea and in the event that it is instead facing Vesuvius or the campaign. There is thus a singular contrast between the theme of 'urban' and the true character of outer suburban villa that we find inside, once past the hallway, closed the heavy door is often dominated by carved wooden rose.

Another constant feature in all the villas is the layout plan, almost always symmetrical, characterized by an axial way, covered / uncovered, which connects the internal park to the building through the sequence portal-atrium-courtyard-esedra - garden-. On this optical axis main gear, then, other episodes transverse or diagonal. Beautiful elliptical courtyards or scenic esedre, once adorned with statues, are found in many villas, including Villa Bruno, Bisignano Palace, Villa Pignatelli di Montecalvo, Villa Ruggiero, the Cardinal's villa, Villa Bruno Protta. Other villas are extruded with descending terraces towards the sea as Leo Villa, Villa Vannucchi, Lauro Villa Lancellotti.

Once in the park runs a number of avenues whose track was often suggested by soil degradation to the beach or to the planting of green areas, so you can see, over the gardens, on the one hand Vesuvius and the other a blue strip of sea.

Particular importance, as is always in Neapolitan contemporary architecture, take the stairs, usually grafted atrium, most often symmetrical, with a clear shot of the theme of urban capital of Bourbon, where the open staircase with flying buttresses on the courtyard is a constant feature, solved with singular variety of solutions, specific both in terms of morphological and dimensional aspect.



The skilful use of optical effects, associated with the experience of scenographic technique of the Baroque era, the famous theme of the ephemeral, in which all operators of the time were particularly versed, is completed through the unconventional mix of architectural styles encoded by Vignola, but used in a purely decorative rather than metric-proportionale, use perfectly allowed by the architectural climate of the Neapolitan Rococo.

Turning to the analysis of interior spaces, there is flexibility and freedom of spatial coupling, so that the typical solutions of salt for official use, if they accompany other more intimate spaces for privacy. Great attention is given to the first floor, decorated with frescoes and terraces, suggesting often the same scenery visible from the outside; through the frequent perspective to the key elements of the landscape, or the use of individual insights into 'natural pictures' suggested by the beauty of the site.

These buildings are therefore characterized by an interdependence between artistic expression and technique, between architecture and applied art, scenographic style of representation and precious furniture. There the rational floor plan, set to axis of symmetry, in contrast with the liberal interpretation of the ornamental forms that deny the building tradition of the Renaissance. They thus represent the image of a taste of real research inspired by nature. (PA.CO. s.r.l. 1990-A1)

The typical typologies of the Vesuvian villas are three: in the first, the building is surrounded by the garden, and the only contact with the street is a portal; in the second, the garden is on a side of the villa, and in the third, the build overlooks the street get the double benefit of direct contact with the district, through the balconies of the main facade, quiet and cool in the rear buildings and gardens. (PA.CO. s.r.l. 1990-A1)

The predominant architectural styles in the City of Golden Mile is certainly the Baroque and Rococo: All architectural and ornamental features found in the villas fit perfectly in the dictates of these two styles. Baroque elements are evident in the villas of the first half of the eighteenth century, whereas in the second half of the century a Rococò style predominates.

It must be pointed out that an important aspect of the architecture of the Vesuvian villas is the context and the relationship with the natural features of the area: the architecture of the villa was designed from time to time depending on the nature of the place leaving us so well with the architectural a huge wealth of botanical rarities.

In conclusion, we can say that the rich architectural heritage of the eighteenth century Vesuvius show a greater variety and especially freedom of composition in contrast to contemporary urban factories, most often influenced by more rigid geometry or the road layout of the city. Remarkable is, therefore, the contribution to the history of the Vesuvian of Neapolitan eighteenth century architecture, both for the extensive number of examples of spatial solutions, and for the delighted environment, unique and unrepeatable opportunity to unleash a wealth of inventive resources elsewhere mortified.

Information on the architects of the villas is, only partially, available from historical documents, but a significant number of important architects were engaged in their design. The list of architects includes:

a) in the first half of the eighteenth century:

*Solimena* who, in 1744, painted frescoes in his villa in Barra;

*SanFelice*, whose work can be found in Villa d'Elboeuf in Portici; Villa Granito of Bel Monte-Signorini in Ercolano; Palazzo Tarascone in Ercolano; Villa Durant who is credited production designer courtyard with a chapel and a staircase triangular shelves; Villa Pignatelli di Montecalvo in San Giorgio a Cremano; Villa Pignatelli di Montecalvo in Barra with typical sanfeliciano portal, portico and coffee-house in Villa Torre in Portici . Probably sanfelician school seem to be Palazzo Vallelonga in torre del greco, Villa Salvador in the same municipality and the facade of Palazzo Petrella.

*Domenico Antonio Vaccaro* work is remarkable in the symmetric double staircase with a portico and vaults on rampant in the back of the courtyard and typical rococo stuccos in Villa d'Anza then Meola, and the work in Villa Caravita today Maltese at Portici; Villa Signorini at Herculaneum .

*Muzio Nauclerio or Anaclerio* to which they attribute Villa d'Amendola, after named Menna, in Portici and the scale of the Villa Lignola.

*Antonio Canevari* for Villa Reale of Portici.

*Giuseppe Astarita*, whose work can be seen in Villa Cardinale with Esedra probably Nauclerio, frescoes by Giuseppe and Gaetano Magri Villa Magra and in the the Duke of Serra Cassano villa.

*Ignazio Cuomo*, who worked at the Palazzo Cuomo Giuseppe Maria di Lecce then Orsini of Gravina.

*Nicola Tagliacozzi Canale* in 1750 built the unidentified Villas for gentlemen Antonio Filomarino and Morcaldi.

*Giuseppe Pollio*, finally, he worked at Villa Domenico Viola.

b) in the *second* half of the eighteenth century:

*Mario Gioffredo* designed and directed the work of Villa Campolieto at Herculaneum, until 1761, then from 1760 supported by the Royal Engineers Carlo Zoccoli and Giovannai Amitrano.

*Michelangelo Giustiniani*, as a Royal Engineer, from 1761 to 1762 he worked at the completion of Gioffredo's work in Campolieto Villa at Herculaneum. Giustiniani idea is the new facade along the way, advancing six meters.

*Luigi Vanvitelli* work from 1763 to 1773 in Villa Campolieto at Herculaneum, by doing the work of consolidation of the structure, defining a new solution for the scale and the portico on this one yield elliptical

rather than circular. There you can see the resumption of some themes already developed by Vanvitelli in Caserta: the perspective view, the ramps of the staircase, and the memory of Versailles-in-porch Esedra. He also worked at the villa De Gregorio of St. Elias in San Giorgio a Cremano and at Villa Pignatelli di Monteleone in Barra.

*Carlo Vanvitelli* was responsible for the care of the interiors and furnishings of Villa Campolieto; niches exedra enclosure of Villa De Gregorio St. Elias. We find, then, his contributions in Villa D'Amorites in Portici, in the Villas and Passaro Cecere at Herculaneum and in Villa Mennella at Torre del Greco.

*Ferdinando Fuga* to which is credited with designing the Villa Favorita at Herculaneum and Villa Maria in Torre del greco.

*Pompeo Schiantarelli* worked on Villa Lancellotti.

*Tommaso Saluzzi* which can be attributed to Royal stables of Charles of Bourbon at Portici.

## 8.5 SEA PARK OF VILLA FAVORITA

### 8.5.1 *Villa Favorita: historical background*

The Villa "Favorita" among the most famous and popular of the Vesuvian ranks 700 in the second when, from the '751 states the roman school of Luigi Vanvitelli.

The Villa Favorita planimetric arrangement differs from other patterns in eighteenth-century villas in the area, all built around the courtyard space, usually prelude to the garden, that is visible from the street. Here, the structuring is different because of the curtain wall that don't allows a direct perspective communication from the street, through the building, with the park to which the central body, inaccessible by road, stretches to the sea. The building, in this way isolated from the external traffic, was conceived, rather than as the residence of a great noble family, to offer favorable conditions for a short summer vacation, hunting and the sumptuous feasts of the court. In opposition to the "uniform plan" face on the road, the front overlooking the garden has a great variety.

According to documents, the villa was built by Ferdinando Fuga, known in Naples as the official architect of Royal Court in 1750, with minors Ignatius Cuomo, Giuseppe Astarita, and others, for Beretta family, Dukes of Simari and Marquis of Mesa; and later purchased by the Prince of Jaci and Campofiorito, Stefano Reggio Gravina, general arms of Charles of Bourbon.

Other witnesses, however, confirm that "Fuga performed for the Prince Jaci a very considerable villa on the deligthfu Resina's site, at Portici" (Militia 1792) and that "in 1768, his most magnificent master Jaci, could give in it a sumptuous feast" at the arrival of Queen Maria Carolina of Austria, wife of Ferdinand IV and that on that occasion, "features the magnificence, the vagueness of the lighting ... The abundance and the delicacy of refreshments" (Celano 1792), so it deserves by Sovereign of the name of "Favorita" in memory of Schonbrunn Palace.

Also in the "Map of the city and its boundaries" by G. Carafa, Duke of Noja (1775) (Figure 8.2) is marked as the villa "of estate and casino Jaci Prince" and is presented in accordance with the planimetric disposition corresponding to the current one: in fact, you can see the two open courtyards at the end of central body that develops in depth to the garden. It appears very clearly also the layout of the avenues of the park: two at the side of the yards, ending with two small buildings. Observable is, also, the central body that stretches up to the semi-circular terrace from which you could get off the beach, where two symmetrical sides of a gate corresponded to two rooms, places of shady siesta and coffee, overlooking the marina and to which accessed by external stairs. Maps are also visible in the chapel, the house of mosaics (then Zezza little house) and the building called "Montagne russe".

The originality of Fuga's work is also demonstrated by an engraving by Francesco Sicuro of 1775 and therefore prior to the additions and rebuilding made to run by Ferdinand IV in the period immediately following. (Figure 8.3-Figure 8.4)

In the Sicuro's engraving we can see the front of the Villa facing the street and in the background there is the long path that leads to the sea and the garden on both sides. We can enter the house from the street by going through a huge yard which leads to the stables. The yard is limited by some columns topped by trophies. In the other Sicuro's engraving, the Villa is seen from the sea.

When the Prince of Jaci died, the Villa according to the last will and testament of the Prince, returned back to the King, who transferred here Academy of Navy officers.

Between 1787 and 1797, Ferdinand IV had again furnish the building, renovate and expand the park by purchasing the cottage and the farm of Zezza, thus further extending the gardens towards the sea, that in the additions to Celano (1792) are described as follows:

“ripartiti per gli stradoni tutti sparsi di mezzi busti di marmo e con spalliere di agrumi e con giouchi di mortelle e di bosso, si veggono più caffè con tutte sorti di comodi pel riposo e il divertimento; si estende questo fino al mare ve n'è non si dunque e oltre alla molta terra destinata alle delizie un'altra coltivabile formando un tutto che ha da queste parti uguale in ampiezza”

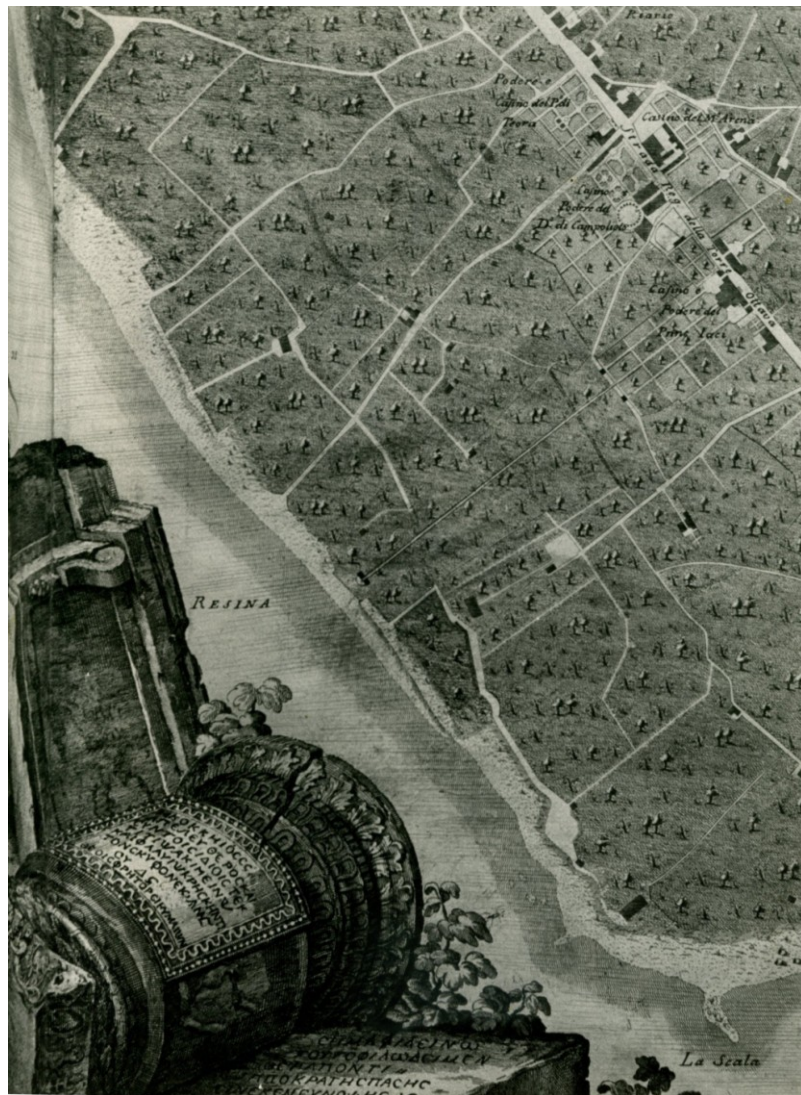


Figure 8.2 - Map of the city and its boundaries "by G. Carafa, Duke of Noja



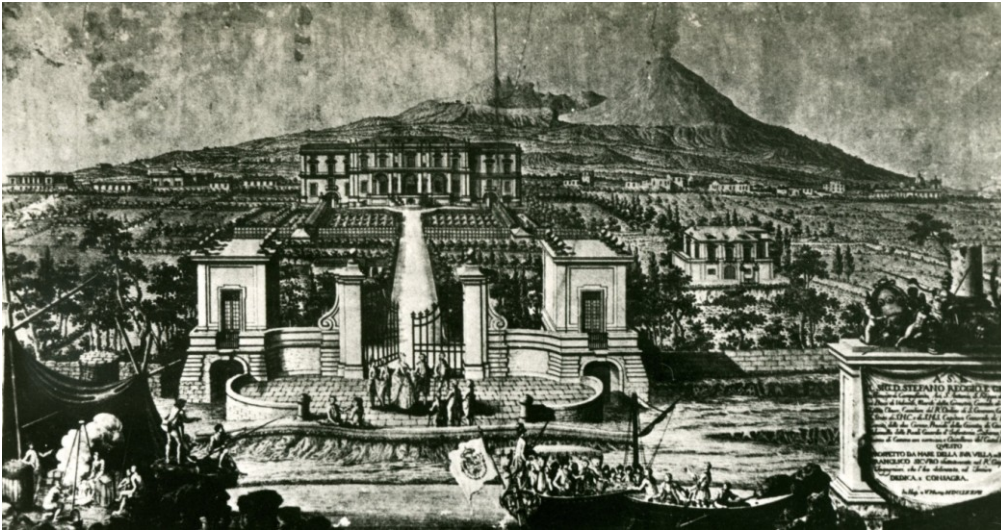


Figure 8.3- Etching by Francesco Sicuro, Second Lieutenant of the Royal Corps of engineers, dedicated to Stefano Reggio and Gravina - view from the sea – (Museum of S. Martino)

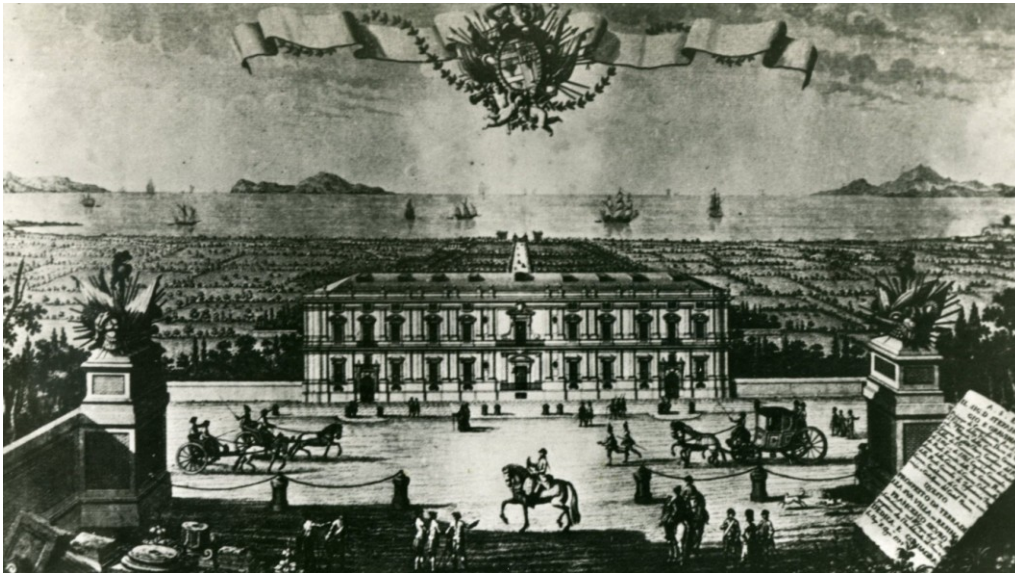


Figure 8.4- Etching by Francesco Sicuro, Second Lieutenant of the Royal Corps of engineers, dedicated to Stefano Reggio and Gravina– main front on the road – (Museum of S. Martino)



This was the heyday for the "Favorita", in which the villa was the site of entertainment and festivities of the court and was host of the Guard Marine Academy, founded by Charles III for young noblemen who remained there until the Revolution of 1799.

In 1799 the villa was restored: the decoration of some interiors was remade, the park was expanded with the purchase of cottage Zezza at the sea and the port was built to reach it more easily so here Ferdinand landed June 27 1802, after the reconquest of the Kingdom by Cardinal Ruffo.

After the historical events of those years, in 1802, Ferdinand re-landed here and the "Favorita" was, therefore, "riacconciata a regia dimora". (Del Pezzo, 1893).

Dates back to 1804 a detailed description of the villa and its furnishings from the drama author Kotzebue, who's admiration decreases when he speaks of the garden:

"se non avrebbe alcun pregio: e storti ed i vigneti sono per giunta i giardini piccoli, poveri e senza non fosse in riva al mare gli alberi d'arancio piccoli assai più belli in campagna sono pieni di edificiucci gusto a lor volta riempiti delle più brutte statue e busti".

Afterwards, the King donated the Villa to his second son Leopoldo, Prince of Salerno, who further embellished it by committing architect Pietro Bianchi to build in the park a residence for guests, new stables and a playground. On bank holidays, the Villa was open to the public and people used to come from all over the Kingdom to enjoy orchestras, whirls, horse shaped swings and roller coasters. Still today, we can see in the park some elements of the playground such as the big wheel, the elegant roller-coasters building flanked by high towers.

In 1836, the villa was intended at a military establishment that used it as living quarters for military families themselves, and then to a military boarding school orphanage run by the Salesians.

When Leopoldo died, in 1851, Villa Favorita was given back to Ferdinando II, King of the two Sicilies, who, committed architect Enrico Alvino to restore it once again by embellishing the holm oak wood with kiosks, an aquarium and a Chinese pagoda, surrounded by maritime pine trees. "spendendovi 80.000 ducati" e reopening it for the people. In the event of the kingdom of Italy the new dynasty had inherited too many royal palaces and villas to preserve all decorated and "La Favorita" was one of those abandoned and stripped of its furnishings, which went to the State sold the house to the sea and the garden on a private villa thereby denying the exit to the sea.

In 1879 the villa housed Pasha Khedive of Egypt, famous for the opening of the Suez Canal and who spent together with his court the period of exile, during which changed the building with additions and arab decorations regaining its owner the building towards the sea which is destined to house the Principles in its wake.

In 1889, Villa back to the State that he exhibited at public auction for 391 lire, but the sale was stopped only in 1893 and was purchased by Princess Santobuono, Emilia Cito that reopened the chapel to the cult. Shortly after the huge cost of maintaining the Princess forced to sell it to the State.

The park and the little house *Zezza* were sold to a private.

Until recently hosted a barracks for the armored units of the police, was later home to a school for prison guards and much of the park, specifically, the part that goes from Via D'Annunzio at the Golden Mile and is enclosed and adjacent to the barracks.

For most of the XX century villa with its huge park has degenerated into a state of total abandonment and neglect, to say nothing of the kiosks and smaller buildings in them, now reduced to the state of ruins. This long-standing condition lasted until 1990, when the local authority for the care of the Vesuvian Villas, announced a contract competition for the restoration and consolidation of the lower park of Villa Favorita and for the buildings in it.

### ***8.5.2 The House of mosaics: architectural, dimensional and structural characteristics***

In lower park of Villa Favorita there are seven small buildings that, at the time of construction, were used for recreational or leisure functions: the building of the Mosaic, the Chapel, the Coffee House, the building known as the "Rollercoaster", the laundry, and two houses.

The most interesting building in terms of both architectural and decorative is certainly the house of mosaics. This is centrally located with respect to the park with the main facade facing east towards Villa Favorita.

The building have a compact and smooth form that is developed on two floors with a volume of about 6,800 cubic meters. The rectangular plan have dimension 31.20m x 20.95m. The height of first interstorey is variable the minimum is 5.10m whereas the maximun is 5.60m; on the first floor height stands at 4.90m and then fall to 3.75 in the attic ,for a total height of 14.30 m.

The main façade has an extremely balance and symmetry to the point that some openings are present only in respect of the design, whilst not being functionally justified its existence (Figure 8.5).



*Figure 8.5 – Mosaics Palace: Main Facade*

The main facade has finishes of particular value as the corinthian capitals that crown the great arched portal entrance.(Figure 8.6)

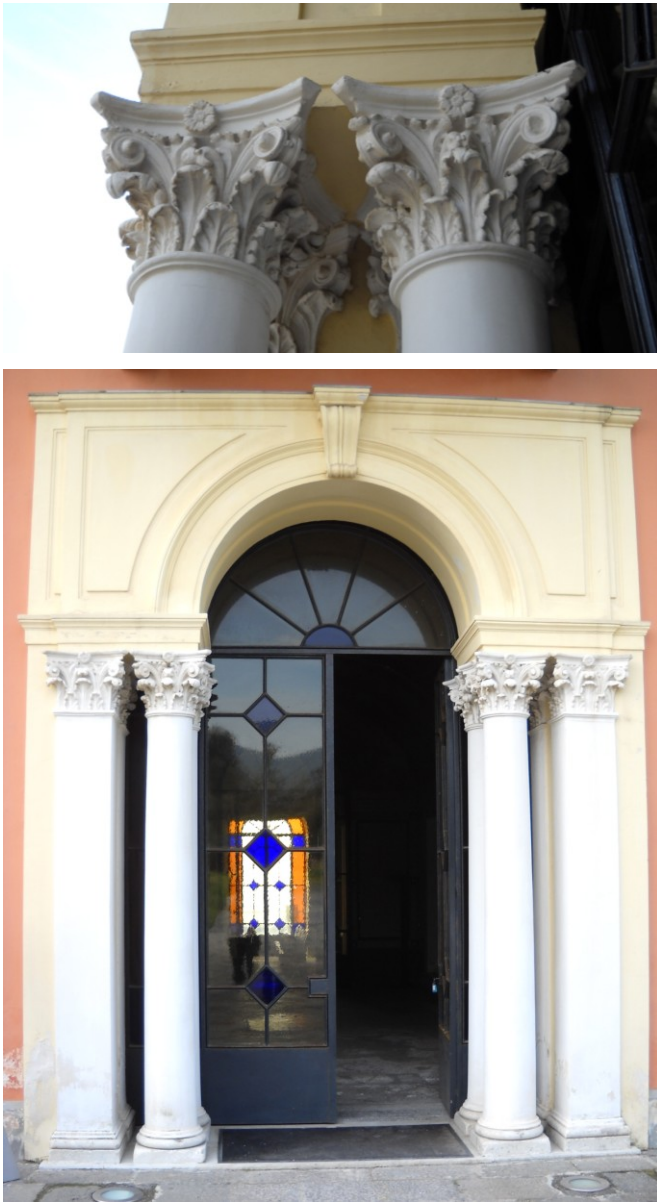


*Figure 8.6 – Entrance by main facade*

On the ground floor (Figure 8.7) at the entrance, there is a large vaulted atrium (Figure 8.8), which, according to an east-west axis, dividing the building into two equal portions and leads to the great hall of the mosaic to the sea.

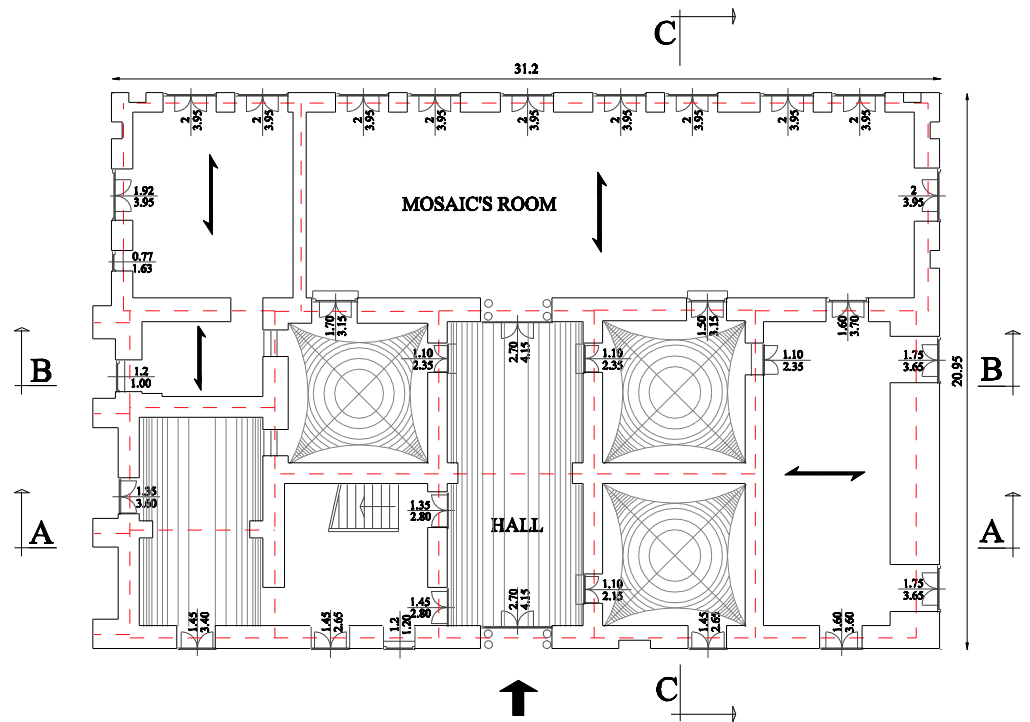


Figure 8.7- Mosaics Palace: ground floor plan

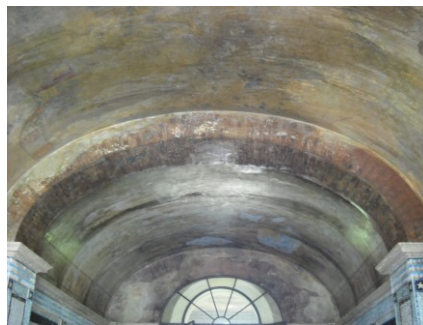


Figure 8.8– Vaulted atrium at ground floor

Mosaic's room, so named due to the presence of fine decorative glass tiles in the walls (Figure 8.9), has the ceiling completely painted (Figure 8.9) and arched windows delimit the front to the west (Figure 8.10).



*Figure 8.9– Mosaic's room: a) Decoration's wall; b) ceiling paint*



*Figure 8.10– Mosaic's palace: facade on the sea*



Same type of mosaic is also present in the hall. (Figure 8.11)



*Figure 8.11– Mosaics decoration in the hall*

The other rooms are partially covered by brick vaults, barrel or sail, and partially covered by flat slabs. (Figure 8.12)



*Figure 8.12 – Vault of room on the ground floor along the southern side*

All the rooms have similar dimensions except the room along the north side that is wider since it is made from the merger of two: on the walls is possible to see an interesting example of the classic Neapolitan red-yellow wall paint (Figure 8.13), second a drawing frames and find more or less on all the interior walls of the building.



*Figure 8.13- Example of the classic neapolitan red-yellow wall paint in house of mosaics*



The pavement of this room, as in the atrium, is made by mosaic floral motifs. (Figure 8.14)



*Figure 8.14– Mosaic floral motifs in a House of mosaics' room*

In the southern portion of the building in contact with the atrium is a valuable scale for flying buttresses. (Figure 8.15)

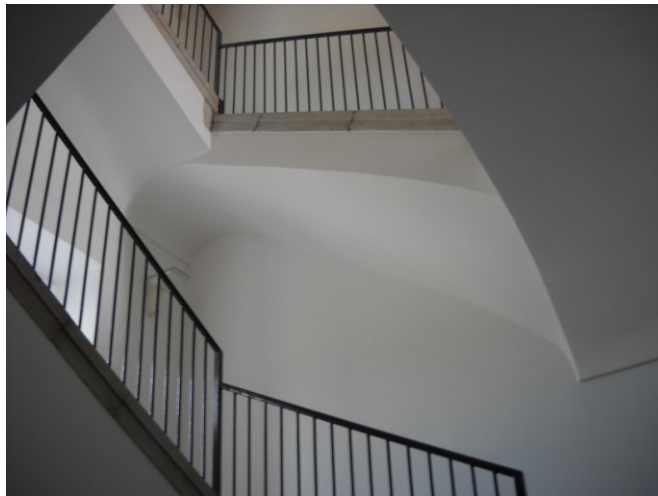


*Figure 8.15– House of mosaics: stairs for flying buttress*



Finally, you reach the attic floor, consisting of one room with dormer windows on all four sides of the building. (Figure 8.17)

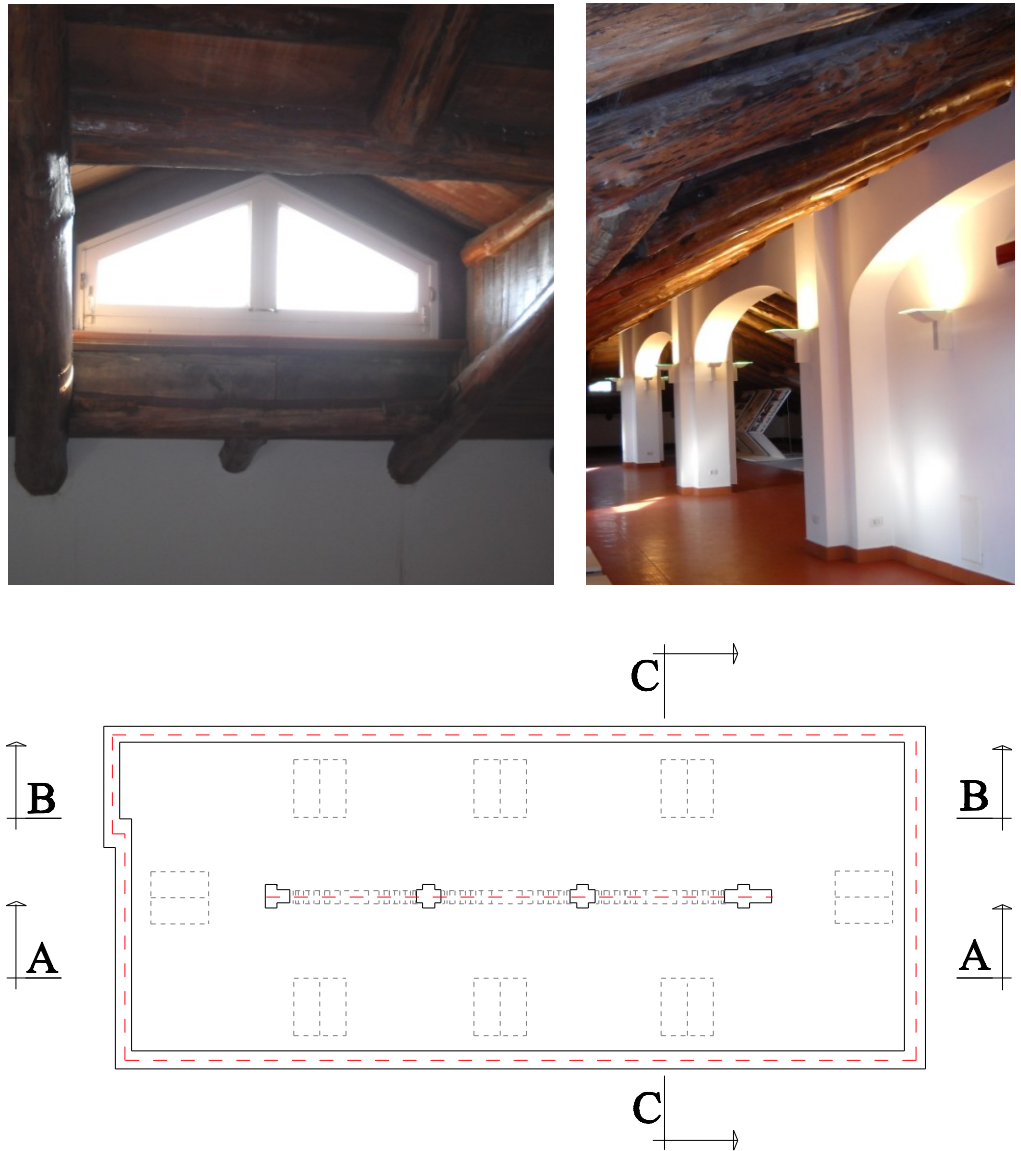


Figure 8.17 – House of mosaics: attic floor plan and details

The cover is made of four-foot wooden truss rafter spacing to 29 x 22 cm "i" equal to 200 cm and 12 x 15cm purlins at intervals of 100cm. The frame of the truss is the Piemontese type where the rafters, arranged according to the pitch of the roof, lean at the top on the wall of the spine and inferiorly on the curbs of the perimeter walls. (Figure 8.18) The purlins, typical in this type of warping, are arranged in parallel with eaves and supported on rafters.



*Figure 8.18 – Roof structure details*

Third and final part of the roof structure is the small warping, consisting of 5 x 6 cm joists at intervals of 50cm, tilted according to the slope of the roof and the horizontal section 3x5cm strips, placed at intervals of 30cm in parallel with eaves. Finally, the cover is made of tiles and tiles. (Figure 8.19)

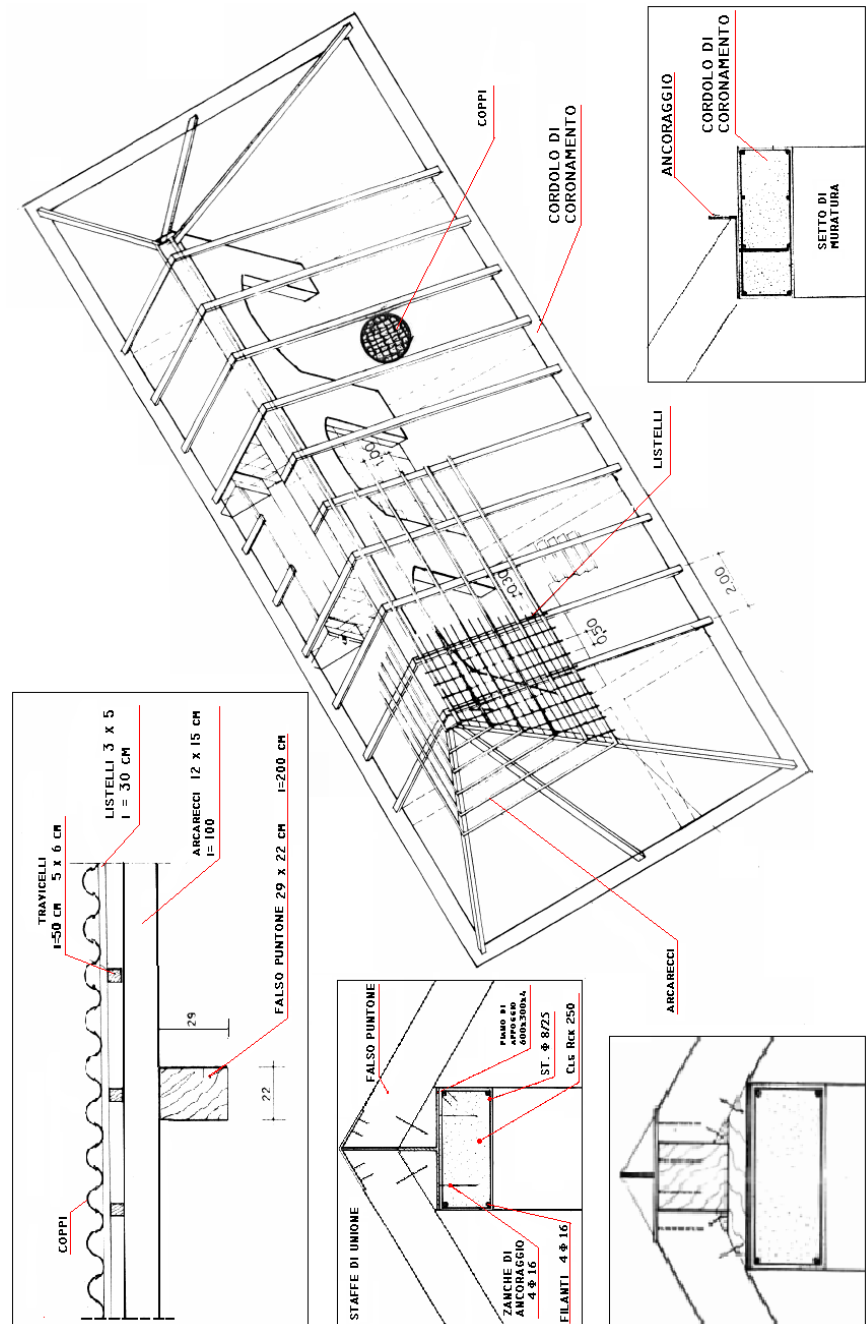


Figure 8.19 – Roof structure and construction details (redrafted from an design table by Ente Ville Vesuviane Archive)

With regards the structural characteristics the villas is in sack masonry, made by external framework in yellow Neapolitan tuff and an inner core with disordered structure filled by lava fragments.

The primary horizontal structures are constituted of plane steel floors, except, as mentioned above, some ground floor rooms. The binder used is composed of pozzolana and lime mortar.

The information retrieved from the archive of institution of the Vesuvian Villas report that the foundations continuous and direct, is in stone. Their depth of the laying is never less than 1.5 m under the ground surface and their thickness is the same of the wall in elevation, being completely absent every cut away. (Diotiguardi - R3)

The portals, the skirting boards, the thresholds of the balconies are made of Vesuvian stone, as well as some parts of the decorative fountain in one of the palace facade. (Figure 8.20)



*Figure 8.20 – House of mosaics: west façade*

As mentioned previously, the palace, together with all the lower park of Villa Favorita, has been the subject in 1990 of a comprehensive rehabilitation intervention. Upon such action the state of conservation of the structure appeared to be quite precarious.



### 8.5.3 *Palazzina Mosaic's condition at the time of restoration in 1990*

Many walls, especially those without plaster, had the external face, (A3 report) with obvious signs of erosion due to wind and marine agents. The conservation status of the mortar was good in most cases, particularly those walls still covered with plaster. Instead, when the floors collapsed were the mortar has lost consistency especially in the older ages. (Figure 8.21)

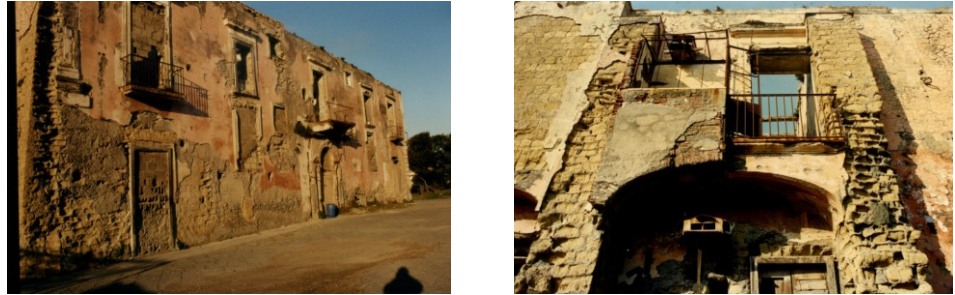


Figure 8.21 – Erosion of bearing walls in 1990 (Lodig R3-by Ente Ville Vesuviane Archive)

Regarding the horizontal structures, most of the original wooden floors were collapsed, and where still present, wooden beams (usually of chestnut) and panconcelle were crumbling to the infiltration of water with the consequent deterioration of mechanical properties of wood. Add to this the blunt dissection of the supports due to seismic activities occurred over the years. (Figure 8.22)



Figure 8.22 – Condition of wooden floors in 1990 (Lod R3-by Ente Ville Vesuviane Archive)

- a) The iron beams making up the remaining floor plans presented themselves highly oxidized and therefore not best placed to withstand the accidental overload in the expected reuse of the building. The brick vaults, where they had not collapsed, had however, a crack pattern that has allowed the recovery by way of consolidation. The stairs were total state of decay with incipient collapse in almost all rampant. (Figure 8.23)



a)



b)

*Figure 8.23 – Condition of the stairs in 1990 (Lod R3-by Ente Ville Vesuviane Archive)*

The attic floor, and the coverage, was demolished in 1962 because it was unsafe, due to the significant disruptions of the building. (Figure 8.24)



*Figure 8.24 – Building without attic floor in 1990 (Lod R3-by Ente Ville Vesuviane Archive)*



Unfortunately, stuccos and decorative paintings were greatly damaged, as well as the "oriental" mosaic decorations that characterized the great hall and the atrium. Some remains of the mosaic, however, were still found in the flooring. (Figure 8.25)



*Figure 8.25 – Stuccos, mosaics and paintings' damaging in 1990 (Lod R3-by Ente Ville Vesuvian Archive)*

The foundation had a condition deemed suitable for transmission of loads resulting from its own weight and the new overloads that would be a burden on them during operation of the facilities.

#### 8.5.4 Palazzina Mosaic's consolidation intervention in 1990

The consolidation interventions were made in order to recover the original static scheme of the building without altering the characteristics of the bearing elements, which, where possible, were recovered rather than replaced.(PA.CO, 1990-A3)

Figure 8.26 shows the distribution and the type realized on the walls:

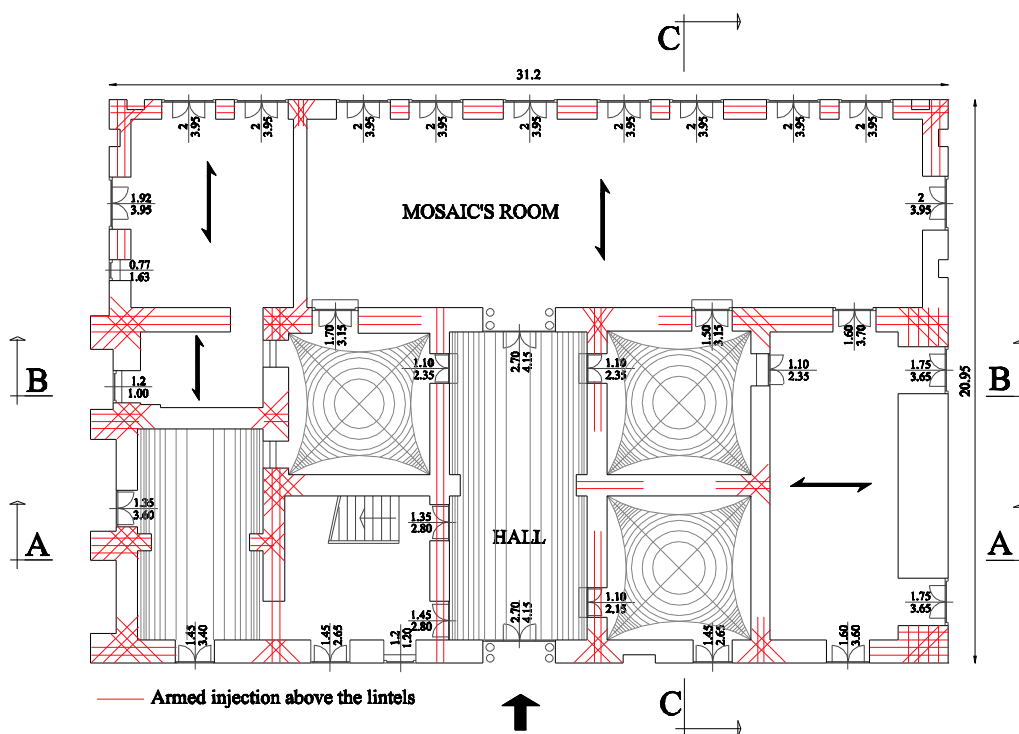


Figure 8.26 – Intervention on the walls

- a) Armed Injections in order to restore the detachable in cantonal, made with rotary drilling diameter of  $\Phi 30$  and armor made of rods  $\Phi 16$  drowned in reoplastic mortar shrinkage. The injections, in order to safeguard, where present fresco or plaster of particular artistic value, were made after washing the wall with water under pressure and according to the plans of heading.
- b) Injections not armed to strengthen the walls whit degraded mortar, in order to restore the static operation of wall. Were performed 4 injections in 1 mq surface to be restored, made in rolling diameter holes  $\Phi 30$ . The execution took place in two phases: the first at low pressure (up to 2 atm), after washing the wall and a second stage pressure of 4 atm.
- c) Reconstruction of partial collapse or excessively damaged walls by the technique of "Sewing and Undoing" using stone in square blocks of tuff and willing bound by lime mortar. Where the external face was deeply eroded by wind, the stone was replaced and then injected to ensure complete coverage in order to have the restoration of the initial thickness of the wall.
- d) Lintels made of steel profiles UPN tied together by threaded rods  $\Phi 16$  and finishing with cement concrete. The arc compartments opening were restored by armed injection properly arranged (Figure 8.27).

*Figure 8.27 – Executive details of the lintels restoration (by Ente Ville Vesuviane Archive)*



brick and casting concrete and finished with welded steel mesh  $\Phi$  8/20. The connections to the walls of the floors were secured by suitable anchors to "dovetail" as well as in graphs and also to curb internal armed perimeter (Figure 8.29).

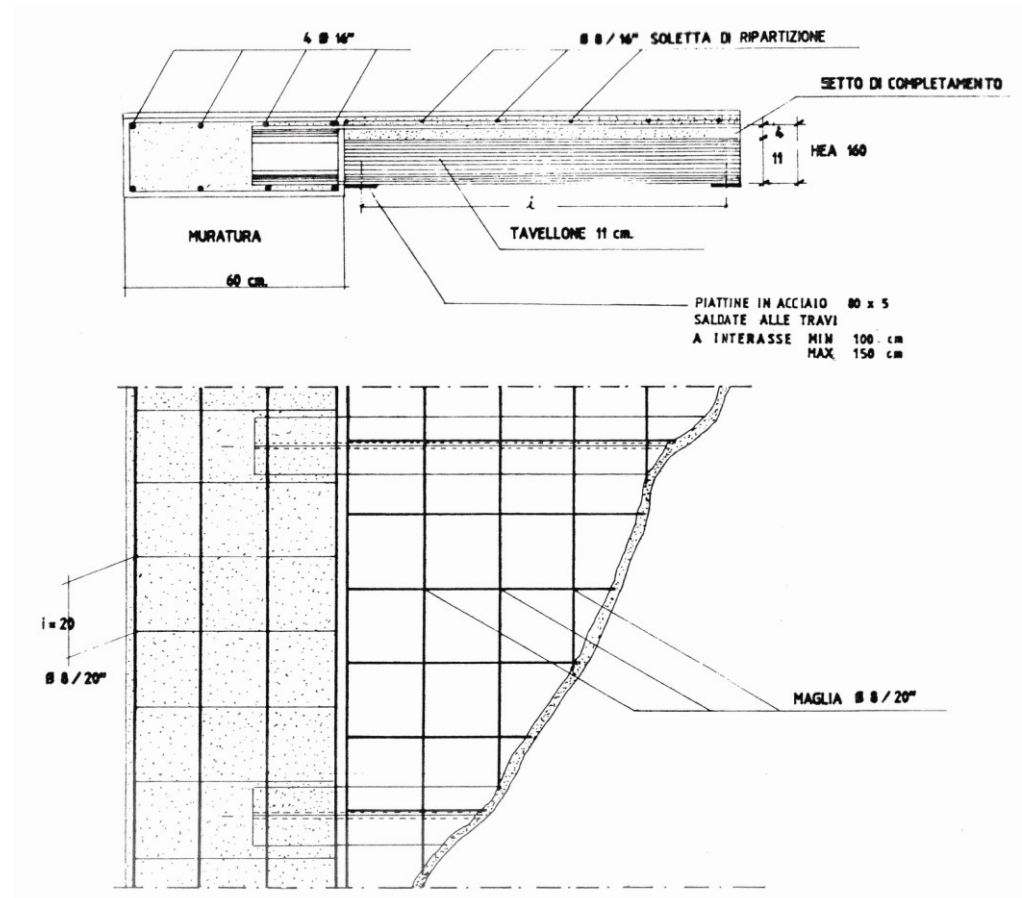


Figure 8.29 – Executive design of new floor in steel beams and brick (by Ente Ville Vesuviane Archive)

- c) The only existing slab steel was to cover the great hall of the Mosaic, which, however, despite being severely damaged by leaks, it was impossible to replace, presenting a valuable fresco soffit, so the new floor has been set at a level slightly higher than the existing. (Figure 8.30)

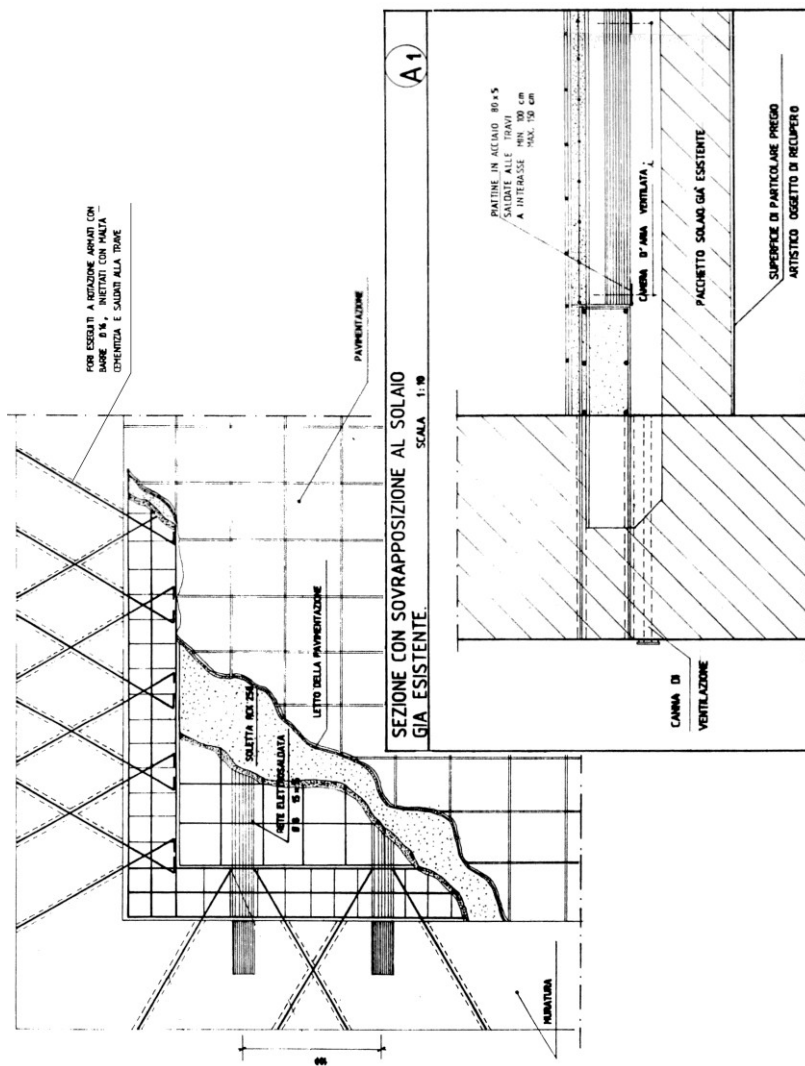


Figure 8.30 – Executive design of new slab on Mosaic's room (by Ente Ville Vesuviane Archive)

- d) The vaults, still in good status, were recovered by removing the upper filling, cleaning extrados, wedges of wood and reinforced concrete slab is anchored to the upper walls with armed properly placed injections. (Figure 8.31)

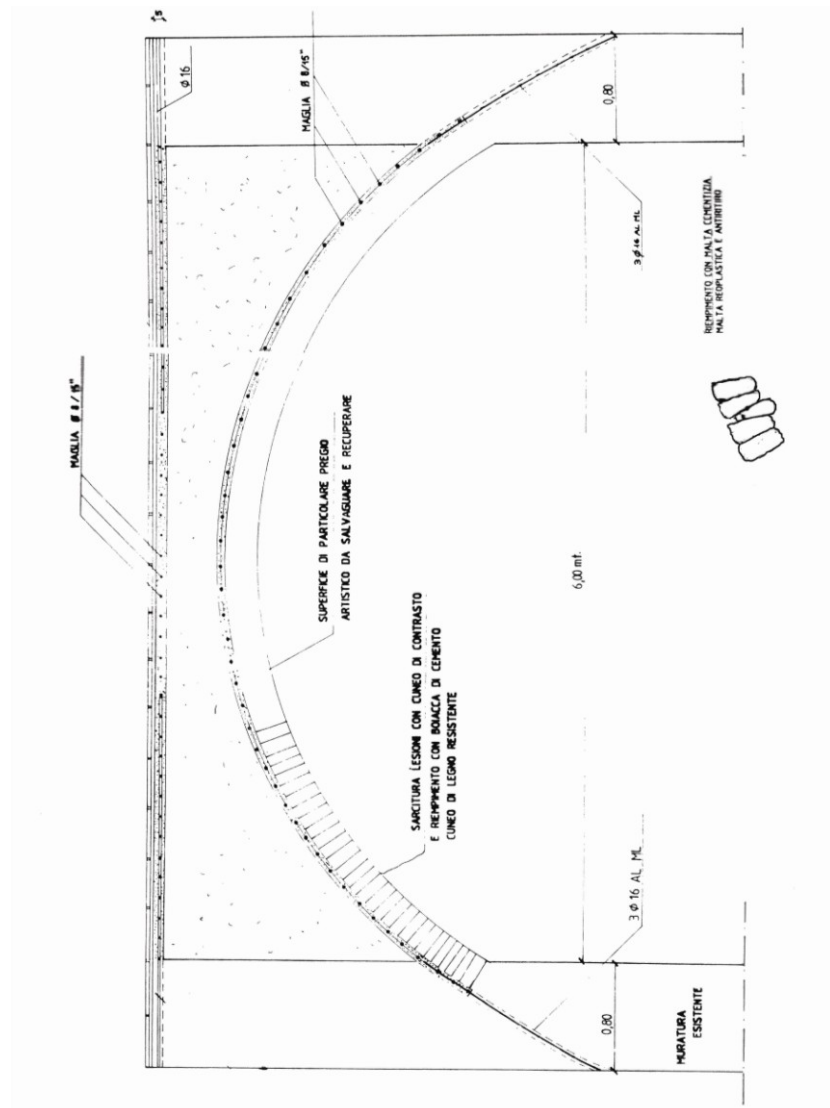


Figure 8.31 – Technical design of consolidation of the vaults (by Ente Ville Vesuviane Archive)

- e) Totally renovation of the stairs. (Figure 8.32)



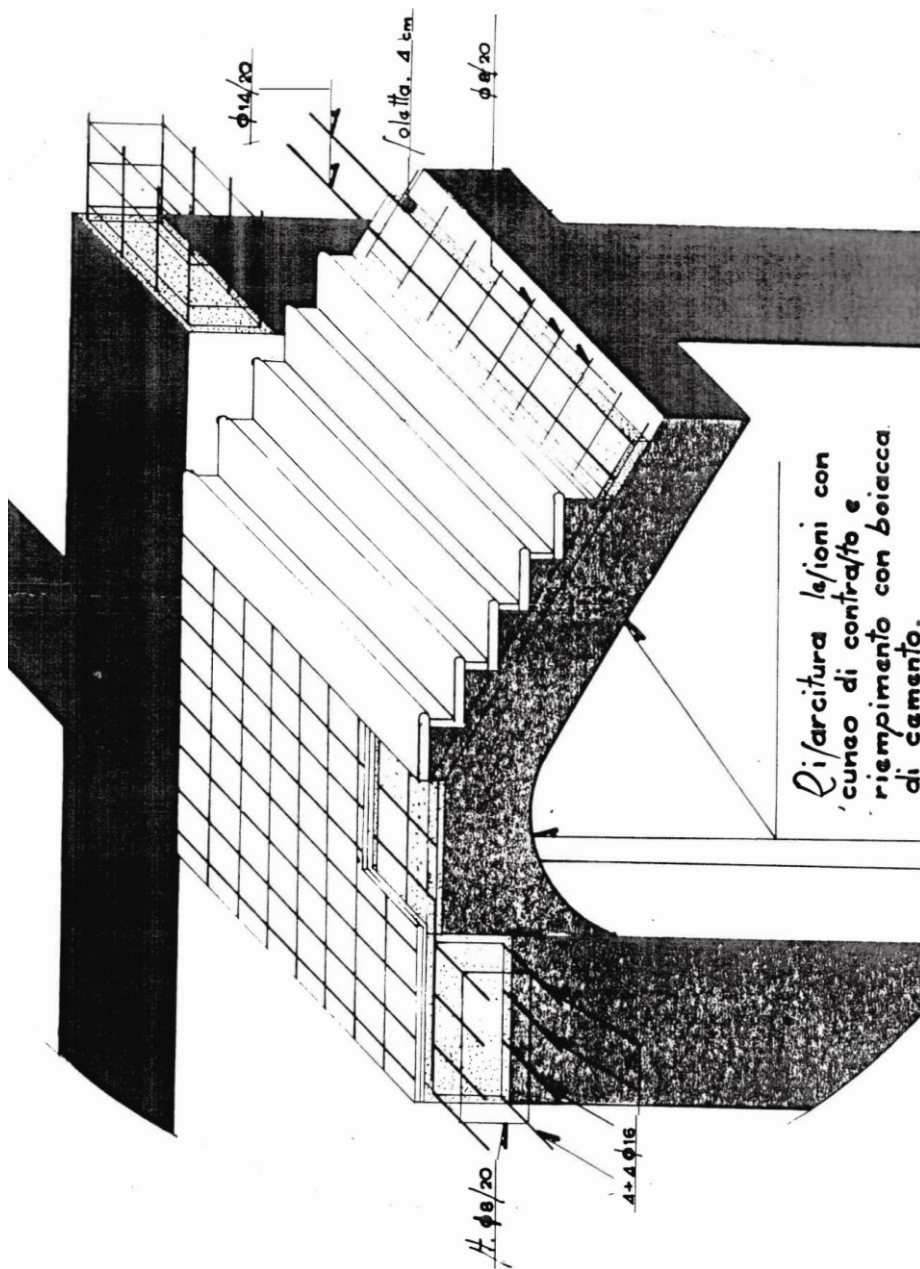


Figure 8.32 – Technical design of the renovation of the stairs (by Ente Ville Vesuviane Archive)



Finally, as regards the preservation work on the finishes were restored picture frames, moldings and decorative elements damaged: when these were not recoverable have been reinstated in the same shape and size as the original.

The materials used in the above mentioned works of consolidation and reconstruction are:

- For ceilings, floors, lintels concrete  $R_{ck}$  250 kg/cm<sup>2</sup>;
- Steel Feb38k for reinforcement rod;
- For metal structures steel type Fe360 having breaking stress greater than 360 N/mm<sup>2</sup> and yield stress greater than 235 N/mm<sup>2</sup>;
- The welds were made, using coated electrodes with approved type E44 UNI 5132-74 class;
- Finally the mortar for anchoring and cement type shrinkage reoplastic, with allowable stress greater than 85 kg/cm, while injecting cement grout used was type 425.

#### **8.5.5 *Palazzina Mosaic's recent survey activities***

Into the topics of the EU COST Action C26 ("Urban Habitat Constructions under Catastrophic Events"), a case study on Vesuvius has been developed. (Alterio et al. 2010)

One important activity has been the in situ survey for the seismic and volcanic vulnerability assessment on different construction typologies, such as residential and historical buildings, school buildings and monumental villas, located in areas exposed to volcanic hazard.

During this activity, the buildings vulnerability elements to seismic and volcanic actions has been identified through a visual investigation, aided by an ad hoc form developed by PLINIVS Centre. (*COST Action C26 report, 2009; Mazzolani et al., 2010*)

The survey activity was aimed also to identify, due to the high artistic value monuments of the villas, appropriate methods of protection from exceptional actions, taking into account the characteristics and structural deficiencies and the same site.

To investigate the seismic vulnerability elements of the villa was used the MEDEA methodology and form. (*F. Papa, G. Zuccaro* Manual on damage and practicability of ordinary masonry building).

Table 8.7 summarize the survey's results.

*Table 8.7 – Vulnerability elements according to MEDEA form*

V. E.	Description	
1.	Absence of connection between orthogonal walls and/or tie-beams or stringcourse at different levels	●
2.	Presence of stringcourses in breccia on masonries with double facings	●
3.	Any floors badly connected with the walls	□
4.	Masonry of low-quality, reduced resistant area along one or both directions	●
5.	High percentage of openings	●
6.	Foundations inadequate to resist the vertical load increment due to the earthquake	□
7.	Different consistencies of the foundation soils, presence of landslide or liquefaction	□
8.	Presence of added buildings with different stiffness and/or with localized connections	□
9.	Variation of the structural system at upper levels	□
10.	Presence of a raising and/or a stiff and badly connected roof structure	□
11.	Presence of staggered levels	□
12.	Excessive distance between bracing walls	●
13.	Pushing structure and/or absence of connection between the wall and the roof	●
14.	Presence of lintel with reduced bending stiffness or with inadequate support length	□
15.	Presence of lowered arches or inadequate support of lintel	□
16.	Local reduction of the masonry section (presence of flues, niches, etc.)	●
17.	Local discontinuities (filling of old openings, bad realization of masonry sewing, etc.)	●
18.	Presence of ridge beam of considerable sizes	●
19.	Presence of openings in the proximity of the roof ridge	●

● = Yes; □ = No; — = I don't know

All highlighted items prevent a “box” behaviour of the structure in case of an earthquake, with the probable consequence of global or partial mechanism.

In the Palazzina of mosaics was found a percentage of openings between 25-50%, which, as evident, especially in the facade facing the sea, involves the presence of masonry walls very thin. The presence of niches and arches involves localized weakening of the masonry shell, resulting in the presence of horizontal cracks in masonry walls adjacent to them.

It's also clear erosion of the plaster in several places due to wind and marine environment. (Figure 8.33 - Figure 8.34 )



*Figure 8.33 – Crack pattern of the façade on the sea*



*Figure 8.34 – Crack pattern of the east facade*

Finally, infiltrations were found in the upper terrace where the result was the splitting of the arcs of the rooms below. Also in this façade is evident the local weakness of masonry walls at the niches. (Figure 8.35)

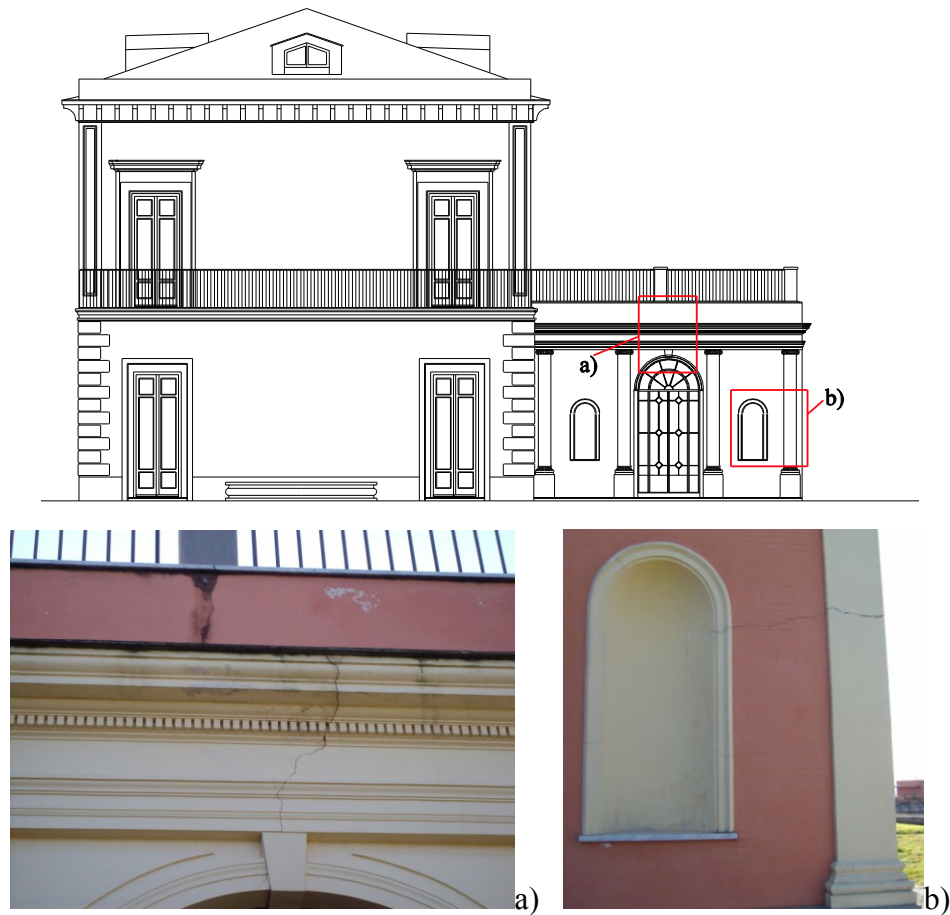


*Figure 8.35 – Crack pattern on the west facade*

On the basis of the vulnerability and the points above, the second part of the MEDEA form was compiled. In this regard, it is necessary to point out that in the form, only the possible collapse mechanism, have been reported. These were not necessarily based on the crack pattern (Figure 8.33 - Figure 8.34 - Figure 8.35), even because the Palazzina investigated had been recently repaired.

The probable mechanisms recorded in the investigation are reported in Table 8.8.

*Table 8.8 – Damage Mechanism of Palazzina of mosaics*

D. M.	Description	
1	Storey shear mechanism	●
2	Storey shear mechanism (upper storeys)	—
3	Whole wall overturning	●
4	Partial wall overturning	●
5	Vertical instability of the wall	—
6	Wall bending rupture	—
7	Horizontal sliding failure	●
8	Foundation subsidence	—
9	Irregularity between adjacent structures	●
10	Floor and roof beam unthreading	●
11	Lintel or masonry arch failure	●
12	Material irregularity, local weakness	●
13	Roof gable wall overturning	—
14	Corner overturning in the upper part	—
15	Overturning of the wall supporting the roof	●
16	Vault and arch overturning	●
17	Other	●

● = Possible; — = Improbable

Is important to notice that the global or local mechanism identified in Table 8.8 are possible mechanisms, and consistent with the structural characteristics of the villas.

## BIBLIOGRAPHY

Alterio L, De Gregorio D., Faggiano B, Di Feo P., Flori G., Formisano A., Mazzolani F.M., Cacace F., Zuccaro G., Borg R.P., Coelho C., Indirli M., Leonidas Kouris, Victoria Sword-Daniels. Survey activity for the seismic and volcanic vulnerability assessment in the vesuvian area: the golden mile villas. *Proceeding of the International Conference COST Action C26 Urban habitat constructions under catastrophic events*, Naples, Italy, 16-18 September 2010

Cardarelli U., Romanello P., Venditti A.. Ville Vesuviane. Progetto per un patrimonio settecentesco di urbanistica e architettura. *Electa Napoli*. pp.39-46,75-76,81-96

Celano C. (1792). Notizie del bello dell'antico e del curioso della città di Napoli. Rev. dal Cav. G. B. Chiarini (1856). Stamperia Florianiana, Napoli

Del Pezzo N. (1893). Napoli Nobilissima

Diotiguardi s.p.a (1990). Relazione geologica e geotecnica, comunicazione personale

Mazzolani F.M., Faggiano B., Formisano A., De Gregorio D., Indirli M. and Zuccaro, G. 2010. Survey activity for the volcanic vulnerability assessment in the Vesuvian area: the 'quick' methodology and the survey *Proceeding of the International Conference COST Action C26 Urban habitat constructions under catastrophic events*, Naples, Italy, 16-18 September 2010.

PA.CO srl (1990)-A1. Opere di consolidamento e restauro della villa Favorita-Parco Inferiore (Ercolano). Relazione Tecnica Generale, comunicazione personale.

PA.CO srl (1990)-A3. Opere di consolidamento e restauro della villa Favorita-Parco Inferiore (Ercolano). Progetto di verifica strutturale, comunicazione personale.

---

Papa F., Zuccaro G. Manual on damage and practicability of ordinary masonry building (MEDEA)



---

*Chapter 9*

# Numerical modelling and pushover analysis of a vesuvian villa

## 9.1 INTRODUCTION

This chapter presents the numerical modelling and evaluation of seismic vulnerability of the House of mosaics carried out with reference to the methods proposed by the *Linee Guida per la valutazione eriduzione del rischio sismico del patrimonio culturale* intengracting in the evaluation procedure the results obtained in Chap. 7: in particular was performed a non-linear static analysis (pushover) according to the provisions of section 7.3.4.1 of the DM 14/01/2008 and to the point C8.7.1.4 of Circular n.617 of 02/02/2009 which is derived from the capacity curve of the building. The curve was then compared, both in terms of acceleration, which displacement with the spectra obtained from the analysis of seismic site response, in relation to each of the treatments identified. To implement the numerical model was used Tremuri software (Galasco et al. 2001), which operates in three dimensions using the equivalent frame approach. The characteristics of the model have been based on knowledge achieved through the investigation of the structure shown in Chap. 8. The current condition of the building, as a result of the consolidation works realized over the year, are such as to exclude the possibility of activation of local mechanisms. For this reason, in this study, checks on the individual kinematics of collapse have not been developed.

## 9.2 KNOWLEDGE OF THE STRUCTURE

The knowledge of a building of historical value is the prerequisite order to perform the evaluation of seismic safety of it is reliable. The path of knowledge of the building in question was conducted investigating different aspects in order to define a model able to interpret adequately, both in qualitative and quantitative terms, the structural behavior of the same. The degree of reliability will be clearly linked to the level of detail and the available data: it was not possible, for this regard, to run a campaign of research, particularly in terms of material, complete and exhaustive as it would be too invasive.

The steps of this process are:

- a first phase of general identification of the building, its location and its valuable elements,
- the geometric survey of the current state of the building, taking care to carefully determine the crack: for each level was measured geometry of all the wall elements, and the thickness profile of the time and the floors, the type and the warping coverage and scales, as well as the possible presence, location and extent of niches, cavities or openings that represent points of closed reduction of the section of load bearing walls.
- understanding the evolution of the structure over the centuries to reflect the consolidation of operations where the building has been the subject;
- precise identification of the body strong, and every element of connection between them: taxes have been identified for the support of these horizons and the bearing walls, was conducted a careful analysis of the loads, so as to define the constraints and the loads imposed on each element of the walls,
- identification of the materials, their degradation and their mechanical properties,
- knowledge of the subsoil, foundation structures while taking into account the changes occurred over time.

The detailed description of each of the aspects listed above and the results of surveys on the building have been extensively outlined in chapter 8.

### 9.2.1 Knowledge level and confidence factor

Once we have identified the building in relation to the deepening of the performed investigation was calculate the confidence factor  $F_c$ . The above mentioned factor is a coefficient applied to the properties of the materials by reducing their resistance, in order to take into account the model uncertainties, linked to a greater or lesser level of knowledge of the structure.  $F_c$  was obtained through the relation:

$$F_c = 1 + \sum_{k=1}^4 F_{ck} \quad (9.1)$$

in which  $F_{CK}$  (with  $K = 1,2,3,4$ ) are the factors associated with partial confidence to the four categories of investigation and level of detail achieved in them, as defined in paragraph 4.2 of the guidelines .... In particular the numerical values assigned to them are shown in Table 1.1: it is assumed for each of them, more conservative value of those proposed by the above mentioned guidelines, it was not possible to deepen, as well as a first level, the crack surveys, the construction phases, building material and geotechnical.

Table 9.1 – Definition of partial factors of confidence

Category of investigation	Level of detail	$F_{CK}$
Geometric survey	Complete geometric survey	$F_{C1}=0.05$
Identification of historical and constructive specificities of the building	hypothetical construction phases based on a limited survey of material and structural components associated with the understanding of the transformation events (documentary surveys and thematic one)	$F_{C2}=0.12$
Mechanical properties of materials	mechanical parameters derived from data already available	$F_{C3}=0.12$
Soil and foundation	limited investigations on the ground and foundations, in the absence of geotechnical data and availability of information on foundations.	$F_{C4}=0.06$

The confidence factor is assumed, thus, equal to 1.35

On the basis of this value has been reduced strength properties of materials: in particular, the mechanical parameters of materials used for the evaluation of seismic safety, were derived from those raised by the table C8.A.2.1 of the Circular 02/02/2009, N. 617, in relation to different types of masonry found in the construction, assuming mean values of the ranges proposed and

multiplying them, where may occur, for the improvement coefficients provided by the Circular itself. The description of the types of masonry used, the improvement coefficients and the resulting values of mechanical properties is shown in the following Table 9.2.

Table 9.2 – Mechanical properties of material used in the model

N	Masonry tipology	Improvement coefficients	E [N/mm <sup>2</sup> ]	G [N/mm <sup>2</sup> ]	W [kN/m <sup>3</sup> ]	f <sub>m</sub> [N/cm <sup>2</sup> ]	τ <sub>0</sub> [N/cm <sup>2</sup> ]
1	Sack masonry of rough-hewn blocks masonry, with elements of limited thickness and inner core	Thin joints <10mm (f=1.2) Poor and/or large core (f=0.8)	1,180.8	393.60	20	142.22	2.28
2	Sack masonry of rough-hewn blocks masonry, with elements of limited thickness and inner core + injection	Thin joints <10mm (f=1.2) Poor and/or large core (f=0.8) Consolidation with injection of binders mixture (f=1.5)	2,007.4	669.12	20	241.78	3.87
3	Tuff masonry	Thin joints <10mm (f=1.2)	1,080.0	360.00	16	103.70	2.07

The different materials were then associated with each wall in relation to the content of the graphics of the consolidation works performed on the construction. The Figure 1.1- Figure 9.3 show the scheme of the resistant elements for each level, and materials associated with them.

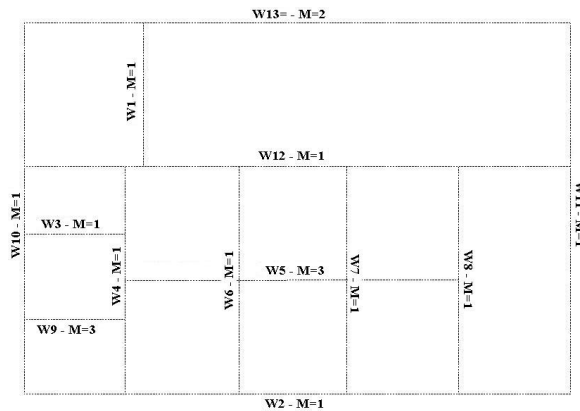


Figure 9.1 – Palazzina of mosaics: sheme axis of resistant wall with indication of assigned material (first floor)

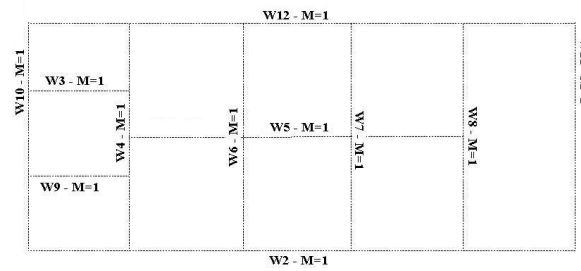


Figure 9.2 - Palazzina of mosaics: sheme axis of resistant wall with indication of assigned material (second floor)

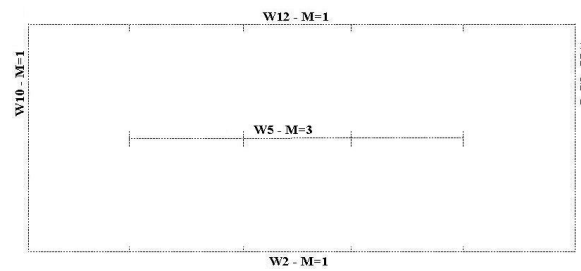


Figure 9.3 - Palazzina of mosaics: sheme axis of resistant wall with indication of assigned material (attic floor)

In particular, please note that the attic was completely rebuilt with new walls in tuff stone ( $M = 3$ ) and each wall wall is topped by concrete curbs, which are shown the materials and their mechanical properties in Table 9.3 .

Table 9.3 – Mechanical properties of material used for the reinforced concrete curbs on the attic floor

Material	Category	E [N/mm <sup>2</sup> ]	G [N/mm <sup>2</sup> ]	W [kN/m <sup>3</sup> ]	f <sub>m</sub> [N/cm <sup>2</sup> ]	f <sub>k</sub> [N/cm <sup>2</sup> ]
Concrete	C20/25	29,962.00	12,484.00	2500	28.00	20
Seel	Feb 38k	210,000.00	80,769.00	79	296.30	375

### 9.3 TREMURI® SOFTWARE (Galasco et al 2002)

Software Tremuri, used for the numerical modelling of the building under study, working with three-dimensional approach to frame equivalent. The theoretical model on which the calculation code is based is defined macro-elements: its theoretical formulation of and is derived directly from observation and from experimental test of masonry behaviour in buildings under the action of the earthquake.

#### 9.3.1 Non-linear macro-element model

The non-linear macro-element model, representative of a whole masonry panel, proposed by Gambarotta and Lagomarsino (1997), permits, with a limited number of degrees of freedom (8), to represent the two main in-plane masonry failure modes, bending-rocking and shear-sliding (with friction) mechanisms, on the basis of mechanical assumptions.(Figure 9.4)



Figure 9.4 – Masonry failure modes: a) shear b) Bending-rocking

This model considers, by means of internal variables, the shear-sliding damage evolution, which controls the strength deterioration (softening) and the stiffness degradation.

Figure 9.5 shows the three sub-structures in which a macro element is divided: two layers, inferior ① and superior ③, in which the bending and axial effects are concentrated. Finally, the central part ② suffers shear-deformations and presents no evidence of axial or bending deformations. A complete 2D kinematic model should take into account the three degrees of freedom for each node “i” and “j” on the extremities: axial displacement  $w$ , horizontal displacement  $u$  and rotation  $\varphi$ .

There are two degrees of freedom for the central zone: axial displacement  $\delta$  and rotation  $\phi$  (Figure 9.5).

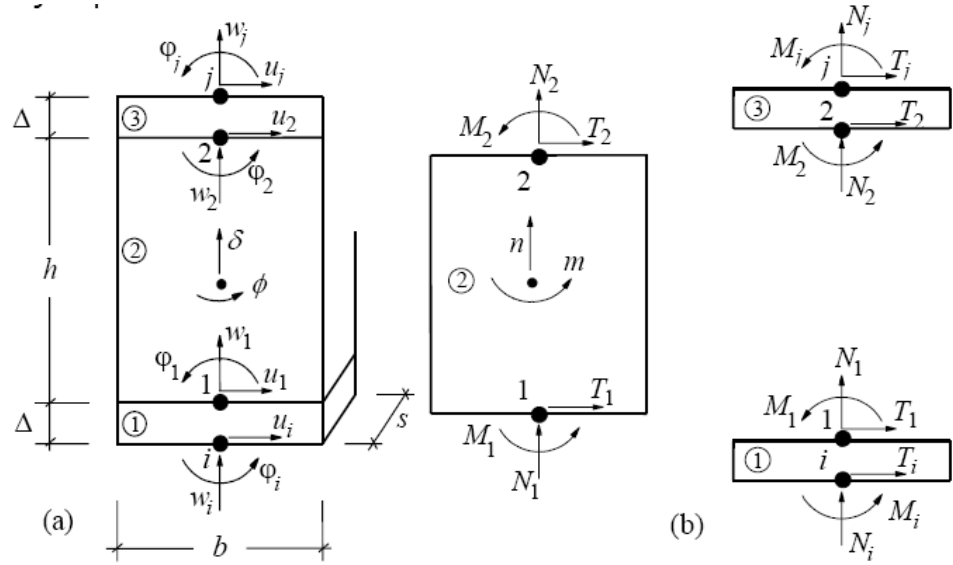


Figure 9.5 – Kinematic model for the macro-element (Penna et al 2004)

Thus, the kinematics is described by an eight degree freedom vector,  $\mathbf{a}^T = \{u_i \ w_i \ \phi_i \ u_j \ w_j \ \phi_j \ \delta \ \phi\}$ , which is obtained for each macro-element. It is assumed that the extremities have an infinitesimal thickness ( $\Delta \rightarrow 0$ ).

The overturning mechanism, which happens because the material does not show tensile strength, is modeled by a mono-lateral elastic contact between ① and ③ interfaces. The constitutive equations between the kinematic variables  $w$ ,  $j$  and the correspondent static quantities  $n$  and  $m$  are uncoupled until the limit condition  $|m/n| \leq b/6$  for which the partialization effect begins to develop in the section.

The panel shear response is expressed considering a uniform shear deformation distribution  $\gamma = \Phi + (u_i - u_j)/h$  in the central part ② and imposing a relationship between the kinematic quantities  $u_i$ ,  $u_j$  and  $\Phi$ , and the shear stress  $T_i = -T_j$

The model described above is completed including a collapse mechanism (Figure 9.6): in the case of non-linear static analysis, the maximum deformation (drift) acceptable for the panel, are:

$$\delta_m^{DL} = \frac{\Delta_m}{h_m} = \delta_u \begin{cases} 0.4\% - \text{shear} \\ 0.6\% - \text{bending} \end{cases} \quad (9.2)$$

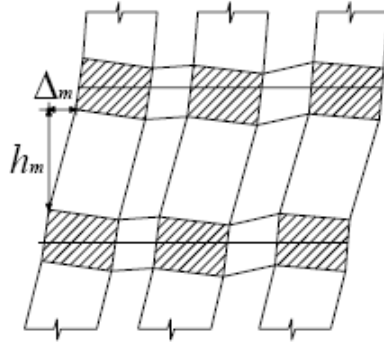


Figure 9.6 – Collapse mechanism relative to maximum drift

If these values are exceeded, the panel is not considered able to withstand horizontal actions, that there is a total loss of bending strength and shear panel, which retains even a small axial stiffness (thus becomes a connecting rod).

The cracking damage is usually located on the diagonal, where the displacement take place along the joints and is represented by an inelastic deformation component, which is activated when the Coulomb's limit friction condition is reached.

The macro-element shear model is a macroscopic representation of a continuous model (Gambarotta a & Lagomarsino 1997), in which the parameters are directly correlated to the mechanical properties of the masonry elements. The macro-element parameters should be considered as representative of an average behaviour. In addition to its geometrical characteristics, the macro-element is defined by six parameters: the shear module  $G$ , the axial stiffness  $K$ , the shear strength  $f_{vq0}$  of the masonry, the nondimensional coefficient  $c$  that controls the inelastic deformation, the global friction coefficient  $f$  and the  $b$  factor, that controls the softening phase.



### 9.3.2 Crushing and compressive damage model

The macro-element used in the program to assemble the wall model keeps also into account the effect (especially in bending-rocking mechanisms) of the limited compressive strength of masonry (Penna 2002). Toe crushing effect is modelled by means of phenomenological non-linear constitutive law with stiffness deterioration in compression: the effect of this modellization on the cyclic vertical displacement-rotation interaction is represented in Figure 9.7.

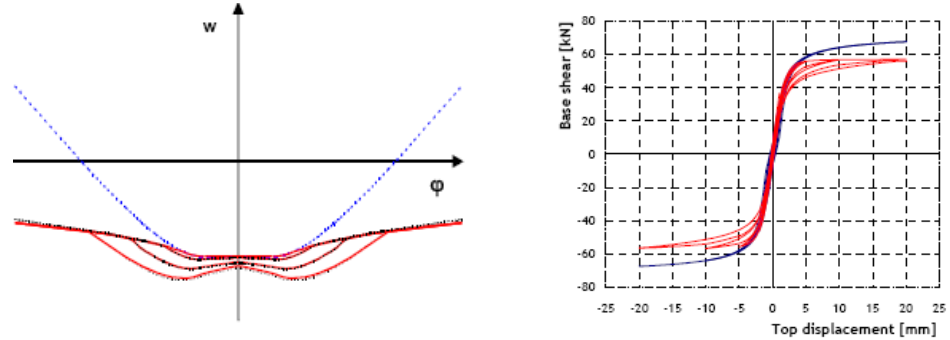


Figure 9.7 - (a) Cyclic vertical displacement-rotation interaction with (red line) and w/o toe crushing (blue dots) in Penna 2002; (b) Rocking panel with (red line) and without (blue line) crushing.

### 9.3.3 Three-dimensional masonry building model

The 3-dimensional modelling of a building starts from some hypotheses on their structural and seismic behaviour: the bearing structure, both referring to vertical and horizontal loads, is identified, inside the construction, with walls and floors (or vaults); the walls are the bearing elements, while the floors, apart from sharing vertical loads to the walls, are considered as planar stiffening elements (orthotropic 3-4 nodes membrane elements), on which the horizontal actions distribution between the walls depends; the local flexural behaviour of the floors and the walls out-of-plane response are not computed because they are considered negligible with respect to the global building response, which is governed by their inplane behaviour (a global seismic response is possible only if vertical and horizontal elements are properly connected).

A frame-type representation of the in-plane behaviour of masonry walls is adopted: each wall of the building is subdivided into piers and lintels (2 nodes macro-elements) connected by rigid areas (nodes) (Figure 9.8). Earthquake damage observation shows, in fact, that only rarely (very irregular geometry or very small openings) cracks appear in these areas of the wall: because of this, the deformation of these regions is assumed to be negligible, relatively to the macro-element non-linear deformations governing the seismic response. The presence of stringcourses (beam elements), tie-rods (non-compressive spar elements), previous damage, heterogeneous masonry portions, gaps and irregularities can be easily included in the structural model.

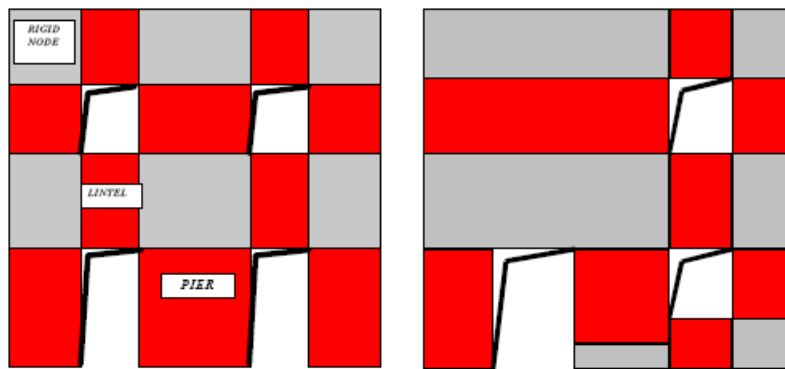


Figure 9.8 - Macro-element modelling of masonry walls

The non-linear macro-element model, representative of a whole masonry panel, is adopted for the 2-nodes elements representing piers and lintels. Rigid end offsets are used to transfer static and kinematic variables between element ends and nodes. A global Cartesian coordinate system ( $X, Y, Z$ ) is defined and the wall vertical planes are identified by the coordinates of one point and the angle formed with  $X$  axis. In this way, the walls can be modelled as planar frames in the local coordinate system and internal nodes can still be 2-D nodes with 3 d.o.f. The 3D nodes connecting different walls in corners and intersections need to have 5 d.o.f. in the global coordinate system ( $u_x, u_y, u_z, \text{rot}_x, \text{rot}_y$ ): the rotational degree of freedom around vertical  $Z$  axis can be neglected because of the membrane behaviour adopted for walls and floors.

These nodes can be obtained assembling 2D rigid nodes acting in each wall plane (Figure 9.9) and projecting the local degrees of freedom along global axes.

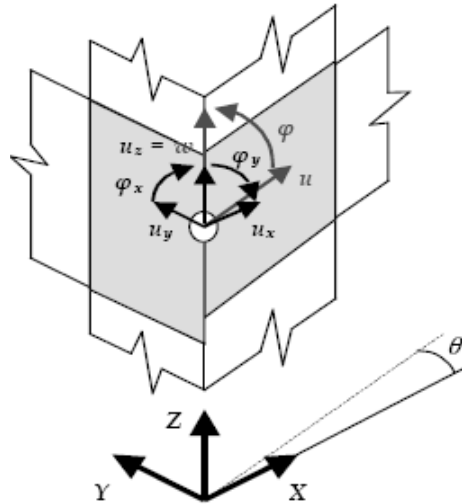


Figure 9.9 – Scheme of assembling 2D rigid nodes to obtain 3D nodes displacement

The relationships between the 5 components of displacement and rotation of a 3D node and 2D artificial node, belonging to a single wall, are, therefore:

$$\begin{cases} u = u_x \cos \theta + u_y \sin \theta \\ w = u_z \\ \phi = \phi_x \sin \theta - \phi_y \cos \theta \end{cases} \quad (9.3)$$

where  $u$ ,  $w$  and  $\phi$  are the 3 displacement components according to the d.o.f. of the artificial node belonging to the generic wall oriented at an angle  $\theta$  in plan.

Similarly, the forces applied to the 3D nodes are decomposed along the directions identified by the medium floor of the walls and applied to the macro-elements in their plan.

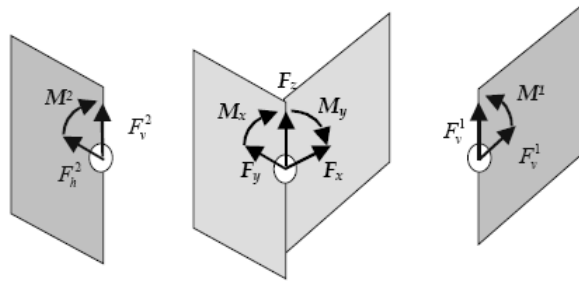


Figure 9.10 – Scheme of assembling 2D rigid nodes to obtain 3D nodes reaction

Having the 2D nodes no degrees of freedom along the orthogonal direction to the wall plane, in the calculation the nodal mass component related to out-of-plane degrees of freedom is shared to the corresponding dofs of the nearest 3D nodes of the same wall and floor according to the following relations (:

$$\begin{cases} M_x^I = M_x^I + m(1 - |\cos \alpha|) \frac{1-x}{1} \\ M_y^I = M_y^I + m(1 - |\sin \alpha|) \frac{1-x}{1} \end{cases} \quad (9.4)$$

where the meaning of the terms is shown in Figure 9.11.

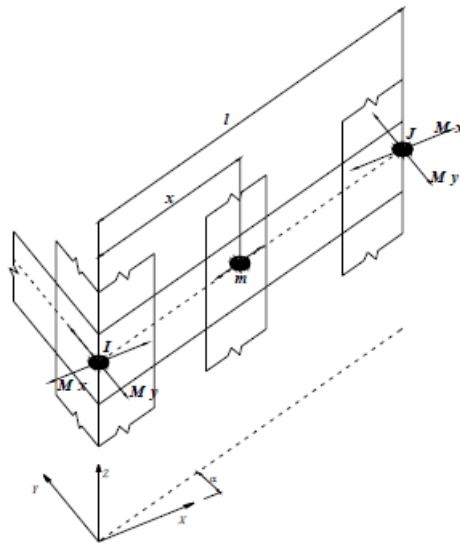


Figure 9.11 - Scheme of 3D and 2D nodes and out-of-plane mass sharing.

Finally, the floor elements, modelled as orthotropic membrane finite elements, with 3 or 4 nodes, are identified by a principal direction, with Young modulus  $E_1$ , while  $E_2$  is the Young modulus along the perpendicular direction,  $\nu$  is the Poisson ratio and  $G_{1,2}$  the shear modulus:  $E_1$  and  $E_2$  represent the wall connection degree due to the floors, by means also of stringcourses and tie-rods.  $G_{1,2}$  represents the inplane floor shear stiffness which governs the horizontal actions repartition between different walls.

This solution then permits the implementation of static analyses with 3 components of acceleration along the 3 principal directions and 3D dynamic analyses with 3 simultaneous input components, too.

#### 9.4 HOUSE OF MOSAICS MODEL

The model of the House of mosaics is shown in the following Figure 9.12- Figure 9.13: it is noted that the wooden roof, can not be directly modeled, was considered by applying discharges to the walls below.

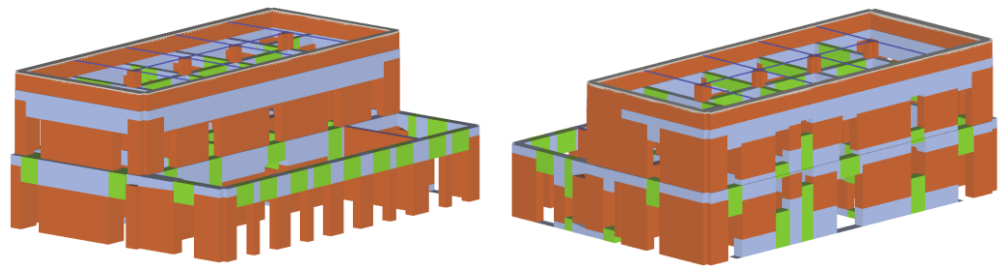


*Figure 9.12 – Axonometric view of 3D model of House of mosaics*

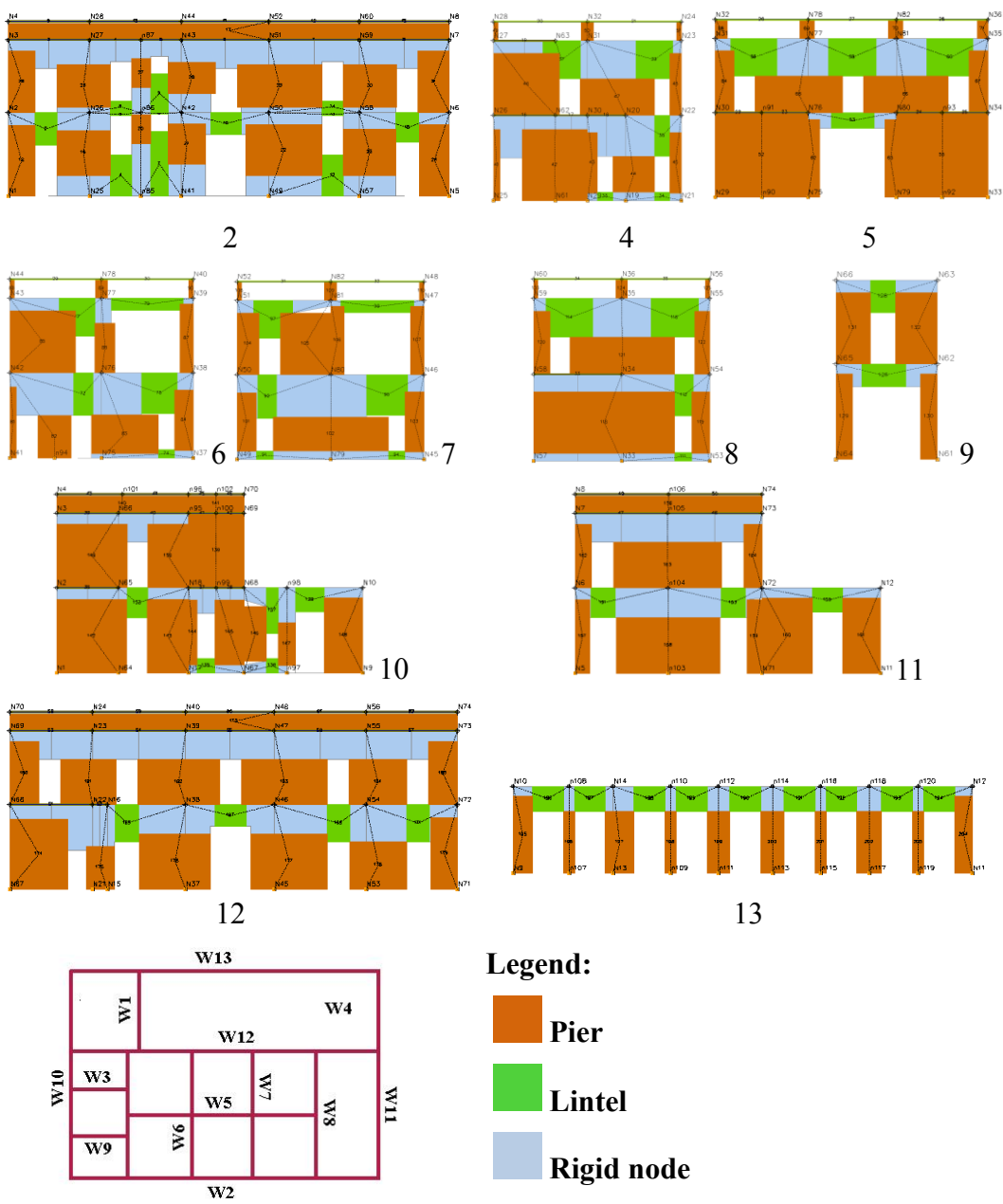


Figure 9.13 –House of mosaics resistant walls

## 9.5 STATIC NON LINEAR ANALYSIS (PUSHOVER)

In order to assess the vulnerability of the building in question, it has been subjected to a 'non-linear static analysis, so the ability to compare with the stress-strength due to the earthquake, as well as to see how varied the ratio between these two, in terms of Acceleration and displacement, according to the different treatments on the ground.

Nonlinear static analysis (pushover) apply, incrementally, to the model of the structure a special distributions horizontal loads, "pushing" it in the non-linear field, in order to take it to collapse.

The horizontal loads, during the analysis, are all scaled, maintaining the relationships between them relating to the various floors, so as to increase monotonically the horizontal displacement of a control point of the structure.

Must be considered two different horizontal loads distributions for each direction of the building:

- the first proportional to the masses,
- the second proportional to the product of the masses and the movement of the first mode of vibration.

This choice derives from the consideration that the lateral forces distribution should approximate the inertia forces distribution during an earthquake. Comparisons with non-linear dynamic analysis showed that distributions of strength proportional to the first vibration mode better capture the dynamic response until the structure remains within the elastic field, and when you reach the large deformation dynamic response can be better represented by forces distributed proportionally to the masses. These distributions are to be applied in two main directions of the building, but in separate analysis.

Analysis result is a curve, called capacity curve, which describes the displacement value of a control point of the structure  $d_c$  with increasing of base shear  $F_b$ .

The control point must be chosen so that its displacement is significant global behavior of the structure, typically is chosen the gravity center of the last floor. (Manfredi et al. 2007)

For verification, as mentioned, it is necessary to compare the capacity of the structure, represented by the capacity curve, with demand represented by

the action seismic. In order to achieve this, the behaviour of the structure to more degrees of freedom (M- d.o.f.) is reduced to that of an equivalent model with one degree of freedom (1-d.o.f.), as it allows to use the elastic response spectra, representing the stresses to which the structure must be able to resist for different limit states.

The 1-dof system is obtained dividing the abscissae and ordinates of M-d.o.f. capacity curves for the first mode participation factor  $\Gamma$ , expressed by the relation:

$$\Gamma = \frac{\sum m_i \cdot \Phi_i}{\sum m_i \cdot \Phi_i^2} \quad (9.5)$$

where  $\Phi_i$  is the  $i$ -th element of the first eigenvalue and  $m_i$  is the mass of the  $i$ -th floor.

Relations for the displacement and base shear of 1-d.o.f. equivalent system are provided in § C7.3.4.1 of the Ministerial Circular n.617 of 02/02/2009:

$$F^* = \frac{F_b}{\Gamma}; \quad d^* = \frac{d_c}{\Gamma} \quad (9.6)$$

The curve obtained is approximated with a bilinear (Figure 6.3.2) on the basis of the principle of equivalence of the areas between the diagrams of the real system and the equivalent to the point at the ultimate displacement, thus making the energy dissipation capacity in the non-linear 1-d.o.f. model is preserved in the bilinear equivalent.

The ultimate displacement  $d_{CU}$  of the curve is computed at the step which corresponds to a decay of 15% of the base shear compared to the peak value  $F_{bu}$ .

The yield strength of  $F_y^*$  and the final value of the displacement  $d_m^*$  are determined with relations (9.7):

$$F_y^* = \frac{F_{bu}}{\Gamma}; \quad d_m^* = \frac{d_{cu}}{\Gamma} \quad (9.7)$$



To determine fully the equivalent model is also necessary to know the displacement  $d_y^*$ . This displacement, as shown in Figure 9.14, represents the limit of linear behaviour and the origin of the tract of perfectly plastic model. To calculate  $d_y^*$  using the criterion of equality of the areas, which requires equality between the area of the trapezoid of vertices  $(0.0) - (d_m^*, 0) - (d_m^*, F_y^*) - (d_y^*, F_y^*)$ , and the area under the curve of capacity for 1-d.o.f. in the section between 0 and  $d_m^*$ . (Manfredi et al. 2007)

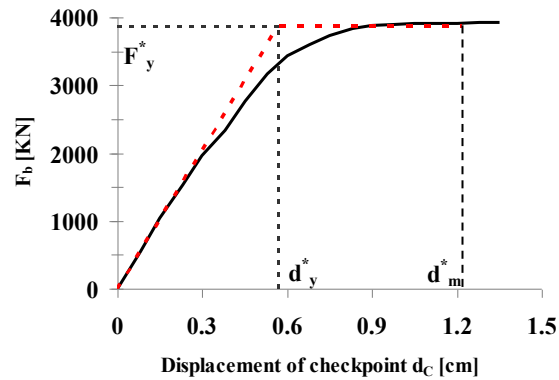


Figure 9.14 –Example of capacity curve and equivalent bilinear

The stiffness of the elastic stretch of the bilinear system equivalent to  $k^*$  can now be determined using the equation (9.8):

$$k^* = \frac{F_y^*}{d_y^*} \quad (9.8)$$

Finally, it is possible to determine the fundamental period of the system equivalent to 1-d.o.f.  $T^*$  through the formula (9.9):

$$T^* = 2\pi \sqrt{\frac{m^*}{k^*}} \quad (9.9)$$

In which  $m^* = \sum m_i \cdot \Phi_i$  is the mass of equivalent system

Known  $T^*$ , now, being a model with 1-d.o.f. is allowed to use the spectra in acceleration and displacement in order to identify the request associated with a given seismic action (limit state). We obtain, therefore, from the spectrum of each limit state, the displacement demand for the building at  $T^*$ .

The ultimate limit state (SLC) verification is to satisfy the inequality:

$$d_u^* \leq d_u \quad (9.10)$$

With  $q^* \leq 3$

The verification at service limit states (SLD), however, that:

$$d_{\max}^* \leq d_d \quad (9.11)$$

Where  $d_d$  is the minimum value between that corresponds to the maximum shear and that would exceed the maximum value of the storey drift (0.003).

In the analysis, as required by regulations (DM p.to 7.2.6 January 14, 2008), took into account the eccentricity of its structure as well as the result of misalignment of the center of gravity of the masses and that of stiffness, even a 'accidental eccentricity of the center of mass computed for each direction, such as 5% of the maximum size of the building in a direction perpendicular to the earthquake.

Finally there are 24 different analyses as consequence of the combination between the distribution of loads and direction and considered additional accidental eccentricity.

Table 9.4 report the summary data for the 24 analyses conducted on the building.

Table 9.4 – Pushover analyses carried out on the House of mosaics

		Load in X direction +											
Load Distr.	e	ID	$\Gamma$	w	m*	D <sub>u</sub> SLV	d* <sub>u</sub>	d* <sub>y</sub>	F* <sub>y</sub>	T*	D <sub>d</sub> SLD	PHA SLV	PHA SLD
	[cm]	-		[t]	[t]	[cm]	[cm]	[cm]	[KN]	[s]	[cm]	[m/s <sup>2</sup> ]	[m/s <sup>2</sup> ]
1°Mode	0	1				<b>1.80</b>	1.50	0.46	3754.61	0.322	<b>0.9</b>	2.18	1.22
	100.8	9				1.87	1.56	0.48	3757.61	0.329	1.35	2.18	1.8
	-100.8	10	1.2	3356.2	2132.42	1.80	1.50	0.46	3712.43	0.321	1.2	2.16	1.63
	0	2				2.32	1.93	0.51	3661.02	0.344	1.5	2.15	1.91
	100.8	11				2.40	2.00	0.51	3667.64	0.342	1.5	2.15	1.92
	-100.8	12				2.32	1.93	0.52	3643.82	0.345	1.42	2.15	1.81
		Load in X direction -											
1°Mode	0	3				1.95	1.63	0.44	3617.61	0.319	1.05	2.10	1.45
	100.8	13				2.03	1.69	0.44	3634.73	0.318	1.05	2.11	1.45
	-100.8	14	1.2	3356.2	2132.42	1.88	1.57	0.44	3610.51	0.319	1.05	2.10	1.44
	0	4				<b>1.73</b>	1.44	0.49	3503.77	0.344	1.58	2.06	2.01
	100.8	15				2.48	2.07	0.49	3517	0.344	1.5	2.07	1.91
	-100.8	16				2.33	1.94	0.49	3466.94	0.343	1.58	<b>2.04</b>	2.01
		Load in Y direction +											
	e	ID	$\Gamma$	w	m*	D <sub>u</sub> SLV	d* <sub>u</sub>	d* <sub>y</sub>	F* <sub>y</sub>	T*	D <sub>d</sub> SLD	PHA SLV	PHA SLD
	[cm]	-		[t]	[t]	[cm]	[cm]	[cm]	[KN]	[s]	[cm]	[m/s <sup>2</sup> ]	[m/s <sup>2</sup> ]
1°Mode	0	5				1.73	1.56	0.59	4185.04	0.316	1.28	2.43	1.93
	100.8	17				2.18	1.96	0.55	4079.48	0.308	1.43	2.84	2.24
	-100.8	18	1.11	3356.19	1779.31	1.65	1.49	0.59	3923.94	0.324	1.20	2.24	1.76
	0	6				1.80	1.62	0.59	3434.31	0.346	1.58	2.25	2.16
	100.8	19				<b>1.35</b>	1.22	0.57	3483.64	0.338	<b>1.35</b>	<b>1.73</b>	1.90
	-100.8	20				1.73	1.56	0.61	3395.16	0.355	1.58	2.11	2.11
		Load in Y direction -											
1°Mode	0	7				1.80	1.622	0.6	3770.96	0.333	0.97	2.35	1.39
	100.8	21				2.02	1.82	0.58	3855.8	0.325	<b>0.90</b>	2.69	<b>1.31</b>
	-100.8	22	1.11	3356.19	1179.31	<b>1.65</b>	1.486	0.58	3523.26	0.341	0.97	2.09	1.36
	0	8				1.72	1.55	0.58	3067.91	0.364	1.72	2.05	2.25
	100.8	23				1.50	1.351	0.56	3083.39	0.357	1.50	1.81	1.99
	-100.8	24				1.87	1.685	0.6	3008.19	0.373	1.80	2.17	2.29

show the capacity curve corresponding to each analyses.

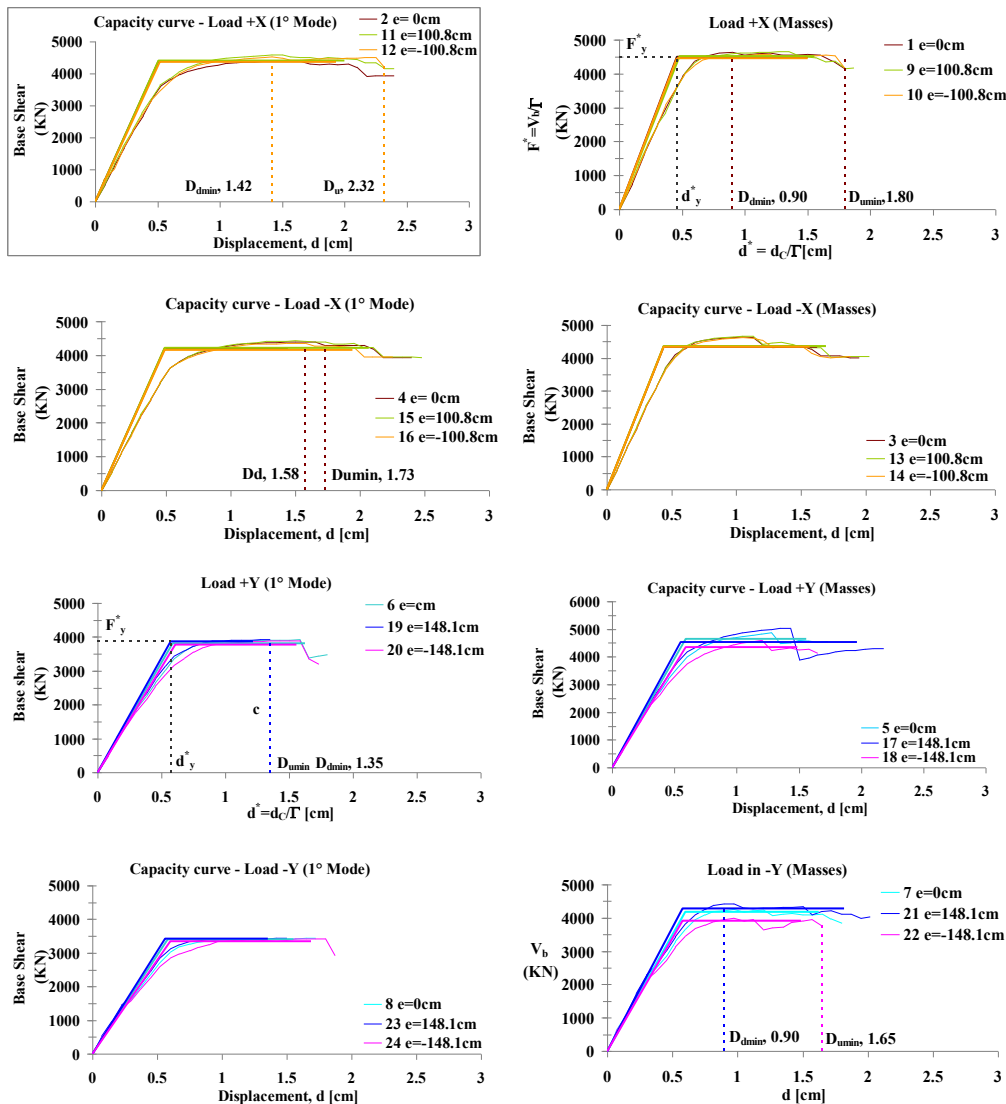


Figure 9.15 –Capacity curves

In many cases, the capacity curve is not regular show irregularities and localized. These irregularities are a symptom of failure of one or more significant structural elements that give rise to a sudden lack of resistance.

The results of the analyses show that the direction most weak is the transverse (y direction), where the area of resistant masonry is lower than the longitudinal direction (x direction) of the building. In terms of  $F_{bu}$ , the more severe analysis is the number 19, in terms of capacity displacement, both of damage  $D_{Cd}$  that ultimate  $D_{CU}$ , is the number 24: both relative to Y direction

In Figure 9.16 are shown the comparison between the capacity curve corresponding the minor value of  $F_{bu}$  of the building and the  $S_a$ - $S_d$  spectra for each case of soil treatment analyzed in chap. 7, for each limit state (SLD-SLC).

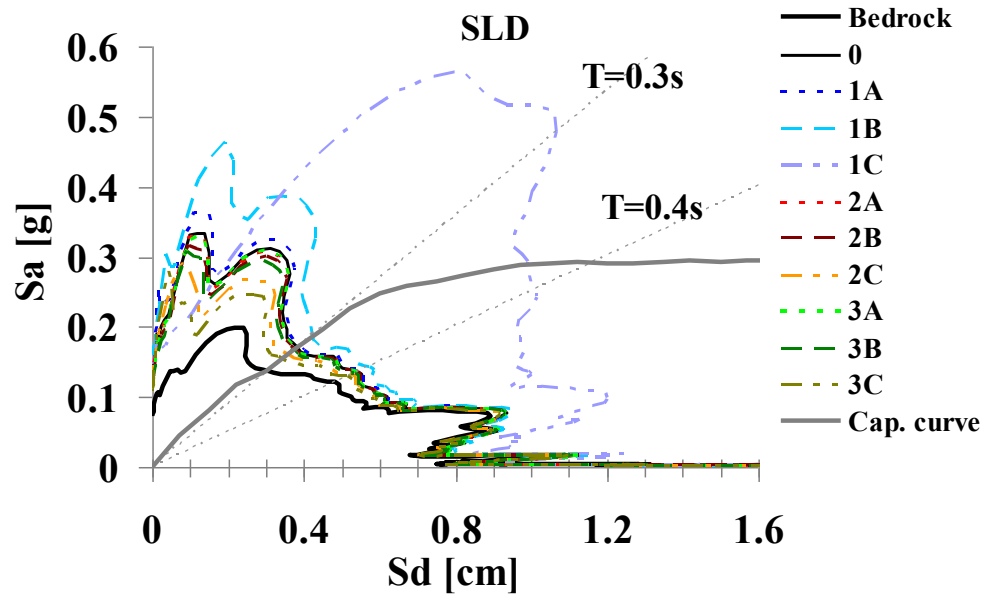


Figure 9.16 – Comparison between the capacity curve with the minor  $F_{bu}$  (analysis n. 24 y direction) and the  $S_a(S_d)$  spectrum for different soil treatments (SLD)

The numerical value corresponding the comparisons shown in are reported in the following table 9.5: have been reported only, in either direction, the results of the analysis more severe, ie those that showed the minor displacement value offered by the structure.

In blue are indicated the minor value of displacement (or acceleration), while in red the higher values.

Table 9.5 – Comparison between the capacity displacement of the building  $D_{dmim}$  and the demand displacement for each case of soil treatment analyzed for different pushover analyses

1 - Load +X (1°Masses); T*= 0.322 - Dd-SLD <D <sub>dmin</sub> =0.90cm					
	Depth of intervention (m)	CASO 0	CASO 1	CASO 2	CASO 3
		Ev=1	Ev=0.5	Ev=1.4	Ev=3
A	1.8	0.41	0.42	0.41	0.41
B	3.6		0.44	0.40	0.40
C	8.6		1.00	0.39	0.38

12 - Load +X (1°Mode); T*=0.345 Dd-SLD < D <sub>dmin</sub> =1.42cm					
	Depth of intervention (m)	CASO 0	CASO 1	CASO 2	CASO 3
		Ev=1	Ev=0.5	Ev=1.4	Ev=3
A	1.80	0.48	0.49	0.48	0.48
B	3.6		0.51	0.47	0.47
C	8.6		0.95	0.46	0.44

19 - Load +Y (1°Mode); T*= 0.338 - Dd-SLD <D <sub>dmin</sub> =1.35cm					
	Depth intervention (m)	CASO 0	CASO 1	CASO 2	CASO 3
		Ev=1	Ev=0.5	Ev=1.4	Ev=3
A	1.8	0.46	0.46	0.45	0.45
B	3.6		0.49	0.45	0.45
C	8.6		0.96	0.43	0.42

21 - Load -Y (1°Masses); T*= 0.325 - Dd-SLD <D <sub>dmin</sub> =0.90cm					
	Depth of intervention (m)	CASO 0	CASO 1	CASO 2	CASO 3
		Ev=1	Ev=0.5	Ev=1.4	Ev=3
A	1.80	0.43	0.43	0.43	0.43
B	3.6		0.46	0.42	0.42
C	8.6		0.99	0.41	0.39

Table 9.6 – Comparison between the capacity acceleration of the building  $D_{dmim}$  and the demand acceleration for each case of soil treatment analyzed for different pushover analyses

PGA <sub>C</sub> -SLD =0.12 g T <sub>R</sub> =219anni					
	Depth of intervention (m)	CASO 0	CASO 1	CASO 2	CASO 3
		Ev=1	Ev=0.5	Ev=1.4	Ev=3
A	1.8	0.16	0.16	0.16	0.16
B	3.6		0.17	0.16	0.15
C	8.6		0.33	0.15	0.15

Regard the SLD, the results show as the structure, in all cases analyzed, except in the case 1C ( $E_v = 0.$ , Layer 4), satisfies verification for displacement to damage limit. On the contrary verification terms of acceleration is never satisfied: the demand is always greater than the capacity offered by the structure. It will, however, point out that, regardless of the treated layer, the cases in which decreased the stiffness of the soil, always involves a worse response in terms of spectral acceleration and displacement, compared to the reference case of untreated soil, on the contrary of cases where the processing involves an increase in soil stiffness. Finally, it is noted that the minor value of demand displacement corresponds, for all analyses, to the case 3C; the worse to case 1C. The same comparison is operated, also, for seismic action relative to SLC.

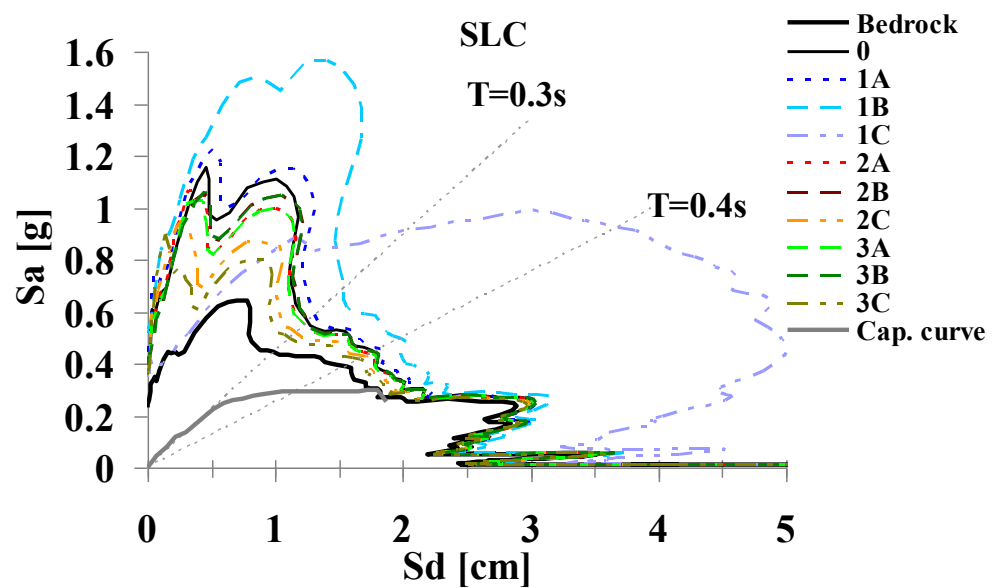


Figure 9.17—Comparison between the capacity curve with the minor  $F_{bu}$  (analysis n. 24 y direction) and the  $S_a(S_d)$  spectrum for different soil treatments (SLC)

Table 9.7 – Comparison between the capacity displacement of the building  $D_{dmim}$  and the demand displacement for each case of soil treatment analyzed for different pushover analyses

1 - Load +X (1°Masse); $T^*=0.322$ - Du-SLC < $D_{umin}=1.80\text{cm}$					
	Depth of intervention (m)	CASO 0	CASO 1	CASO 2	CASO 3
		Ev=1	Ev=0.5	Ev=1.4	Ev=3
A	1.8		1.39	1.32	1.32
B	3.6	1.32	1.56	1.33	1.34
C	8.6		2.40	1.26	1.22

4 - Load -X (1°Modo); $T^*=0.344$ - Du-SLC < $D_{umin}=1.73\text{cm}$					
	Depth of intervention (m)	CASO 0	CASO 1	CASO 2	CASO 3
		Ev=1	Ev=0.5	Ev=1.4	Ev=3
A	1.8		1.54	1.47	1.47
B	3.6	1.47	1.70	1.48	1.49
C	8.6		2.80	1.41	1.36

19 - Load +Y (1°Modo); $T^*=0.338$ Du-SLC < $D_{umin}=1.35\text{cm}$					
	Depth of intervention (m)	CASO 0	CASO 1	CASO 2	CASO 3
		Ev=1	Ev=0.5	Ev=1.4	Ev=3
A	1.8		1.54	1.47	1.47
B	3.6	1.47	1.70	1.48	1.49
C	8.6		2.80	1.41	1.36

22 - Load -Y (1°Masse); $T^*=0.341$ - Du-SLC < $D_{umin}=1.65\text{cm}$					
	Depth of intervention (m)	CASO 0	CASO 1	CASO 2	CASO 3
		Ev=1	Ev=0.5	Ev=1.4	Ev=3
A	1.8		1.54	1.47	1.47
B	3.6	1.47	1.70	1.48	1.49
C	8.6		2.80	1.41	1.36

Table 9.8 – Comparison between the capacity acceleration of the building  $D_{dmim}$  and the demand acceleration for each case of soil treatment analyzed for different pushover analyses

$\text{PGA}_{\text{C-SLC}}=0.22 \text{ m/s}^2$ - $T_R=1250$ anni					
	Depth of intervention (m)	CASO 0	CASO 1	CASO 2	CASO 3
		Ev=1	Ev=0.5	Ev=1.4	Ev=3
A	1.8		0.53	0.51	0.51
B	3.6	0.53	0.59	0.52	0.52
C	8.6		0.98	0.49	0.47

The findings limit state damage actions also proposes to limit state of collapse, with the difference that, now, for the analysis of more severe (19 - Y-direction) displacement verifications are never satisfied, even in the reference case (case 0) related to the current situation, without any treatment.



## BIBLIOGRAPHY

Circolare n. 617 del 2.II.2009. Istruzioni per l'applicazione delle nuove norme tecniche per le costruzioni. *Ministero delle infrastrutture e dei trasporti*

DM 14/1/2008. Norme Tecniche per le Costruzioni. S.O. n. 30 - *Gazzetta Ufficiale della Repubblica Italiana, No. 20 - 4/2/2008*

Linee Guida per la valutazione ed riduzione del rischio sismico del patrimonio culturale - Ministero per i Beni e le Attività Culturali – Circolare n. 26 del 2.12.2010

Galasco, A., Lagomarsino, S. and Penna, A. (2002). TREMURI Program: Seismic Analyser of 3D Masonry Buildings, *University of Genoa*

Gambarotta L. and Lagomarsino S. (1997). Damage models for the seismic response of brick masonry shear walls. Part II: the continuum model and its applications. *Earthquake Engineering and Structural Dynamics*, 26, 441-462

Manfredi G., Masi A., Pinho R., Verderame G. M., Vona M.(2007). Valutazione di edifici esistenti in cemento armato. *IUSS Press*

Penna A. (2002) A macro-element procedure for the nonlinear dynamic analysis of masonry buildings, *Ph.D.dissertation, Politecnico di Milano, Italy*

This page is, intentionally, left blank

---

## CONCLUSIONS

It's been addressed the problem of seismic vulnerability reduction of the built heritage in Italy, studying the possibility to obtain it through subsoil treatments, so to change a priori the seismic action induced on historical buildings. The study was motivated by the unsatisfactory situation in which no doubt, in respect of seismic risk, historic buildings are and inadequate pay and/or the inability to apply them criteria and methodologies that are widely used on the new construction. The issue has been addressed through a multidisciplinary approach. So the first part of the work is devoted to the analysis of literature relative each aspect of the studied question.

In the research was selected case study that showed the characteristics necessary for the same: a site where it was possible to adequately know the geology, stratigraphy, the mechanical properties of the soil through both the existing bibliographical material than non-destructive in situ tests and it was schematized in a one-dimensional domain such that its site effects were linked exclusively to the stratigraphy. On the site, also at the same time, that there was need of great historical architectural value factories and built adjacent to no other. The park on the sea Villa Favorita in Herculaneum had all the above mentioned characteristics.

The research was conducted through uncoupled numerical models: one relative to the site and the other regarding the structure in elevation. The two models were constructed with the use of two softwares: EERA for testing one-dimensional seismic response of local and TREMURI for nonlinear static analysis of the villa.

Propaedeutic to the implementation of models and numerical analysis was conducted a study of seismic hazard for the site and of selection criteria for proper seismic input that might be more representative of the same. For this purpose, on the basis of theoretical and bibliographic studies conducted on the topic, methodological procedure has been developed ad hoc. After the characterization of seismic input a large part is devoted to in-depth knowledge of the site and of the structure of interest: the Palazzina of the mosaics.

The seismic response analyses were conducted on different cases obtained: assuming the treatment of one soil layer identified in the stratigraphy. Have been hypothesized three different treatment situations, corresponding to three different values of the shear velocity of the treated layer: one in which the velocity, and thus the stiffness, was reduced, in order to investigate whether such a layer could lead to one reduction of the surface effects, similar to a mechanical disconnect, and two cases in which the stiffness was increased so that by checking how the variation of stiffness could influence seismic surface amplification. For each of the three situations described above, has been changed the position of the treated layer, passing from the top layer up to consider the treatment of a layer adjacent to the bedrock.

The following are the main conclusions were reached for each phase of work.

The study of the literature on soil treatments was possible to show that, because of the executive modalities of each of them, not all are suitable for be used on monuments. In addition, it should be noted, often an approach in the project of these interventions more empirical than effectively scientific, thus leaving a great uncertainty about the physical phenomena involved. It should also be kept in mind that these treatments are born and developed, and with them the related technologies and materials used for respond to static requirements. It should therefore develop new technologies or modified existing ones to calibrate, both materials and executive modalities that the equipment used, the needs of a seismic protection. A major benefit would, however, certainly to be able to operate without disturbing the above structure, a relatively low cost and consideration that they improve the soil conditions in the static field.

The subsequent search of the input to be used in seismic analysis has revealed several issues to date, still unresolved and debated in the scientific field. First among the others is the alignment between different tools such as hazard and disaggregation mapping with the regulatory update: the maps, in fact, is provided in connection only with regard to probability of exceedance in 50 years and not for a period as needed of the case. With regard, however, the selection of a set accelerometer, is to emphasize that, common practice once found records that satisfy the search parameters, is to use only one of the two components of the record, usually that with higher PHA, without considering that this parameters alone may not be significant to the physical characteristics of a seismic event. This choice is even more questionable if one takes into account the frequency content of the seismic signal, different for each component: neglect, therefore, a component of the registration would result in a lack of consideration of frequencies that may, however, be significant for the study of seismic response local site, and consequently for the structures analyzed above. In addition, the accelerograms are often improperly scaled with factors high ( $>4$ ) leading to energy content in-realistic in this regard also the software most commonly used for research and selection of the set accelerometer, have limitations in this regard. They do not restrict the scaling factor of each record individually, but allow give the maximum value only in average terms, thus leading to the selection of recordings with even higher scale factors.

In general there has been some difficulty to find at least 7 accelerograms whose average fell within the ranges of spectral compatibility dictated by the Code. The accelerometric set resulting from the procedure performed, in fact, shows that, for the site in question, although the spectra of reference (D.M 14.01.2008) in general overestimate the seismic action to be assigned, do not account for individual high peak values, corresponding to periods of significant structures (0.1-0.5s).

From the seismic site response analyses conduct on the study case in Chapter 7, it was possible to show that each layer amplifies differently: each will have one or more peaks of different amplitude and at different frequencies. The amplification function of each layer is also connected to the impedance ratio with the adjacent layers, so modify the characteristics of only one layer also means modifying the amplification functions of other layers and

consequently that deposit. Note also that the top layer has an amplification function almost constant throughout the frequency range and equal to unity, meaning that this layer does not contribute to the amplification of the earthquake.

From the comparison between the analyses of different cases is possible to see that for service limit state a surface treatment, stiffening the soil don't get any appreciable benefit in terms of reducing surface maximum acceleration compared to the reference case without treatment, while in the case of a reduction in stiffness is the intervention, although only slightly, even pejorative response surface. When the intervention is performed deeper, the difference in behaviour between an increase and a reduction in stiffness is even more pronounced. We note, again, that treatments increasing stiffness of the layer does not reduce the surface amplification proportionally to the increase, or significant difference is obtained by applying the treatment to a layer or another. From this it is stated that, in the case study, stiffening above a certain value or beyond a certain depth would be an economic burden not justified by a greater benefit.

Increasing the amplitude of the input seismic, ie passing from SLD to SLC, we see that intervention of reduction stiffness could lead a reduction of horizontal surface acceleration, exploiting the capacity of the material non-linear soil. This aspect must be, however, with more detailed studies on the variation that the damping of the soil suffers as a result of real treatments. This is, clearly, linked to many factors, rheological, mechanical and chemical for which laboratory and field application studies would be needed.

In case of high seismic action for treatment of the surface layer can be deduced that the reduction of stiffness, raising and moving toward lower frequencies, the peak of amplification connected to the second mode of vibration of the deposit, leaving unchanged the fundamental peak of amplification. An increase in stiffness, however, has no effect on amplification function. In, instead, the treated layer is deeper reducing the stiffness the peak frequency continues to decline, but in this case it also reduces the value of the amplitude.

In conclusion we can say that the effectiveness and efficiency of each treatment on the problem under study is strongly influenced by local

stratigraphic details: the surface seismic response of the deposit is, in fact, linked, not only the characteristics of the treated layer, but also those of the layers adjacent to it and the relative impedance ratios between them. This suggests, therefore, that while the method of operation can be easily applied to other cases, the conclusions are not easily generalizable. Furthermore, it is also necessary verify the effectiveness of each technique using more complex schematization of subsoil, and simultaneously more realistic, for example, through two-dimensional models, which take into account the real development of treatments within the subsoil.

From the knowledge process, conduct on the palazzina of mosaics derives that the current condition of the building, as a result of the consolidation works realized over the year, are such as to exclude the possibility of activation of local mechanisms. And statically the factory is not particularly suffering, on the contrary if it analyzed in the dynamic field, because of the material and geometrical irregularity, local weakness for the presence of niches, possible vault and arch overturning, high percentage of openings.

Finally, from the vulnerability analysis of the palazzina, through the 24 pushover analysis conducted on it, results that in many cases, the capacity curve is not regular because of the localized irregularities above mentioned. These irregularities are a symptom of failure of one or more significant structural elements that give rise to a sudden lack of resistance. The results of the analyses show that the most weak direction for the construction is the transversal one (y direction), where the area of resistant masonry is lower than the longitudinal direction (x direction). Comparing the capacity curve of the structure with Sa-Sd spectra obtained for each case of soil treatment analyzed in chapter 7, for each limit state results that for damage limit state (i.e. for service action), in terms of displacements the capacity is major than the demand, except in the case of reduction stiffness in the layer most deep. On the contrary verification in terms of acceleration is never satisfied: the demand is always greater than the capacity offered by the structure. It will, however, point out that, regardless of the treated layer, the cases in which decreased the stiffness of the soil, always involves a worse response in terms of spectral acceleration and displacement, compared to the reference case of untreated

soil, on the contrary of cases where the processing involves an increase in soil stiffness. Finally, it is noted that the minor value of demand displacement corresponds, for all analyses, to the case of soil reinforcement in the deeper layer; the worse to case at the same layer operate a stiffness reduction. The same comparisons operated, also, for seismic action relative to SLC shows that displacement verifications are never satisfied, even in the reference case (case 0) related to the current situation, without any treatment: the structure is therefore, unable, to resist earthquakes of high magnitude.

It should be noted that, while not allowing the structure to fully satisfy the verification of regulation, the reinforcement treatment of the mechanical soil properties, however, involve a reduction in terms of demand, leading to the possibility of reducing the improvements intervention on the building, which would certainly very invasive.